Pacific Northwest National Laboratory
Operated by Battelle for the
U.S. Department of Energy

Effect of Geochemical and Physical Heterogeneity on the Hanford 100 D Area In Situ Redox Manipulation Barrier Longevity

J. E. Szecsody   V. R. Vermeul
J. S. Fruchter   M. D. Williams
J. L. Phillips   B. J. Devary
M. L. Rockhold   Y. Liu

November 2005

DISCLAIMER

This report was prepared as an account of work sponsored by an agency of the United States Government. Neither the United States Government nor any agency thereof, nor Battelle Memorial Institute, nor any of their employees, makes **any warranty, express or implied, or assumes any legal liability or responsibility for the accuracy, completeness, or usefulness of any information, apparatus, product, or process disclosed, or represents that its use would not infringe privately owned rights**. Reference herein to any specific commercial product, process, or service by trade name, trademark, manufacturer, or otherwise does not necessarily constitute or imply its endorsement, recommendation, or favoring by the United States Government or any agency thereof, or Battelle Memorial Institute. The views and opinions of authors expressed herein do not necessarily state or reflect those of the United States Government or any agency thereof.

PACIFIC NORTHWEST NATIONAL LABORATORY
operated by
BATTELLE
for the
UNITED STATES DEPARTMENT OF ENERGY
under Contract DE-AC05-76RLO 1830

Printed in the United States of America

**Available to DOE and DOE contractors from the
Office of Scientific and Technical Information, P.O. Box 62, Oak Ridge, TN 37831;
prices available from (615) 576-8401.**

**Available to the public from the National Technical Information Service,
U.S. Department of Commerce, 5285 Port Royal Rd., Springfield, VA 22161**

This document was printed on recycled paper.

Effect of Geochemical and Physical Heterogeneity on the Hanford 100 D Area In Situ Redox Manipulation Barrier Longevity

J. E. Szecsody   V. R. Vermeul
J. S. Fruchter   M. D. Williams
J. L. Phillips   B. J. Devary
M. L. Rockhold   Y. Liu

November 2005

Executive Summary

The purpose of this study was to quantify the influence of physical and/or geochemical heterogeneities in the Hanford 100D area In Situ Redox Manipulation (ISRM) barrier that may be contributing to the discontinuous chromate breakthrough locations along the 65-well (2,300-ft-long) barrier. Chromate breakthrough has been observed in as many as 17 of the 70 ISRM injection wells. Breakthrough has occurred at various locations along the barrier length with, in many cases, adjacent wells indicating good barrier performance. In addition to this spatial variability, observed chromate concentrations over the degraded sections of the barrier also vary seasonally. There is widespread nitrate upgradient of the ISRM barrier (60 mg/L) and lower nitrate concentrations downgradient. A recent nitrate study showed that, while the presence of nitrate will decrease barrier longevity uniformly, it cannot account for specific locations of chromate breakthrough.

Possible causes of chromate breakthrough that were investigated during this study include:

- high hydraulic conductivity zones

- zones of low reducible iron

- high hydraulic conductivity zones with low reducible iron.

This laboratory-scale investigation used geochemical and physical characterization data collected at 0.5- to 1-ft intervals from four borehole locations. The four characterization borings were 10 to 12 ft up- and downgradient of two existing ISRM injection wells that have seen high chromate breakthrough concentrations. Additional data collected over the past few years pertaining to the ISRM barrier were also used to interpret both redox and flow conditions and the lateral extent of these hydrogeologic and geochemical properties. Supplemental data used in this interpretation included electromagnetic borehole flow meter data, multilevel sampler data, core pictures, and previous reductive capacity measurements.

Results of this laboratory study did not provide definitive support for any of the proposed hypotheses for explaining chromate breakthrough at the Hanford 100D Area ISRM barrier. While site characterization data indicate a significant degree of vertical variability in both physical and geochemical properties in the four boreholes investigated, lateral continuity of high-conductivity/low-reductive capacity zones was not observed. The one exception was at the water table, where there was some indication of low reductive capacity at all four boreholes, three of which also showed high-K zones near the water table. A lack of 1-D column data near the water table for two of the four boreholes made characterization of this effect at these locations less certain. If physical heterogeneity alone strongly influenced barrier oxidation (hypothesis 1), there should be an inverse correlation between zones of high hydraulic conductivity and the field reductive capacity, which was generally not supported by the data except at the water table and, to a lesser extent, isolated locations deeper in the profile. The average saturated hydraulic conductivity of the aquifer for all four boreholes, based on sediment textural data, was 0.0348 ± 0.0498 cm/s ($n = 59$). Although these data showed considerable variability with depth, that variability was not well correlated with field reductive capacity (correlation coefficient, $r = 0.07$). In addition, although electromagnetic borehole flow meter (EBF) data from 25 wells indicated high-K channels in half the wells, there was no strong indication that high-K zones were laterally continuous (at a 35-ft distance) between adjacent barrier wells.

Based on results from this laboratory study, variability in the vertical distribution of field reductive capacity can be best explained by 1) proximity to the water table, 2) the effects of preferential flow in higher permeability materials (hypothesis 1, best illustrated near the water table), and 3) total reducible iron content (hypothesis 2). The observed loss in reductive capacity near the water table is most likely due to water level fluctuation, resulting in oxidation of the reduced sediment and, to a lesser extent, the potential for elevated dissolved oxygen, chromate, and nitrate concentrations near the water table. In addition to the water table region, there were several examples of intervals deeper in the formation that showed some degree of loss in reductive capacity. The average field reductive capacity for these four 2005 boreholes (13.64 ± 7.79 µmol/g, n = 37; 1-D column oxidation) was slightly greater than previous values (10.6 ± 6.6 µmol/g in 2002; 11.2 ± 7.4 µmol/g in 1999). These data indicate that the barrier in the vicinity of the two locations investigated has not been fully reoxidized (i.e., the bulk of the sediments tested still show significant reductive capacity). The total iron oxide concentration of the sediment was considerable (145 ± 16.7 µmol/g), and there was a fair correlation (r = 0.58) between the total iron oxides and the resulting field reductive capacity. There were no zones of low total iron oxide content. The combination of total iron oxides and hydraulic conductivity (hypothesis 3) was a poor predictor (r = 0.40) of the field reductive capacity.

Laterally continuous high permeability zones that contain oxic sediment near the water table are the most likely explanation for high-concentration chromium breakthrough responses observed at various locations along the barrier. A mechanism that could explain partial chromate breakthrough in the ISRM barrier is the relationship between the field reductive capacity and the *rate of chromate oxidation*. Sub-surface zones with low reductive capacity still have sufficient ferrous iron mass to reduce considerable chromate, but the *rate* of chromate reduction slows by 1 to 2 orders of magnitude relative to sediments with moderate to high reductive capacity. While there should be no chromate breakthrough in the ISRM barrier under average groundwater flow (1 ft/day) or even at 3 ft/day, there could be 5% chromate break-through in a worst-case scenario of 10 ft/day flow (10 times the average) combined with a low reductive capacity (4 µmol/g). A scenario that could explain high chromate breakthrough in wells D4-26 and D4-37 is high flow (i.e., 80% of groundwater) in oxic sediments at the water table (that have no reductive capacity).

The original barrier longevity estimate of 160 pore volumes for homogeneous reduced sediment, or approximately 20 years (with 5 mg/L dissolved oxygen and 2 ppm chromate), is reduced to 85 pore volumes (10 years) when the widespread 60-ppm nitrate plume is included in the calculation. However, this reduction in barrier lifetime is not as great for high-permeability channels because there is not enough time to reduce nitrate (and consume ferrous iron). If the cause of laterally discontinuous breakthrough of chromate along the ISRM barrier is due to oxic transport of chromate near the water table, additional dithionite treatment in these zones will not be effective. Treatment near the water table with a technology that emplaces considerable reductive capacity is needed, such as injectable zero valence iron.

Contents

Figures

# Tables

1.0   Introduction

The in situ redox manipulation (ISRM) groundwater barrier in the Hanford 100D Area was designed to prevent migration of a chromate plume through the groundwater into the Columbia River. This ISRM barrier consists of 65 wells spaced across a 2300-ft section of the chromate plume (Figure 1.1). In the presence of < 2 mg/L chromate (maximum detected) and dissolved oxygen in water, the longevity of the barrier is approximately 180 pore volumes or 15 to 20 years, depending on the groundwater flow rate. The presence of a widespread groundwater plume of 60 mg/L nitrate reduces barrier longevity by roughly half—to 90 pore volumes (7 to 10 years).

Barrier performance has been mixed. Characterization data in the majority of wells indicate that reducing conditions have been maintained and chromate is being reduced. However, specific wells (primarily in the eastern half of the barrier) show chromate breakthrough while in some cases adjacent wells remain anoxic (with no chromate breakthrough), as shown in Figure 1.2. In addition, chromate trend plots (Figure 1.3) show a strong seasonal response, with the highest concentrations observed during seasonal low-river-stage conditions when groundwater velocities through the barrier are at their highest. While the presence of nitrate will decrease barrier longevity uniformly, it cannot account for specific locations of chromate breakthrough. Possible causes of chromate breakthrough in specific well locations include the following:

- Thin natural high hydraulic-conductivity zones in the 15- to 30-ft-thick aquifer have greater groundwater flow and are oxidized more rapidly; these zones could be natural or enhanced by the air rotary drilling used to install some ISRM wells (physical heterogeneity, hypothesis 1).

- Some natural zones have low reducible iron (i.e., geochemical heterogeneity, hypothesis 2).

- Natural high hydraulic-conductivity zones may have lower reducible iron oxide content (an inverse correlation between physical and geochemical heterogeneity, hypothesis 3).

In addition to the potential influence of the specific type of physical or geochemical heterogeneities, the scale (size) of the heterogeneities also affects barrier longevity. Small (< 10-ft lateral extent along groundwater flow path) high-flow and/or low iron oxide zones would not result in contaminant break-through of the ~40-ft-wide barrier. However, a high-flow zone with large lateral extent would result in more rapid oxidation in a specific aquifer section.

This laboratory investigation was initiated in the spring of 2005 by collecting aquifer cores in four boreholes up- and downgradient of boreholes D4-26 and D4-37 (two wells exhibiting premature chromate breakthrough) (Figure 1.2). To address physical hydraulic conductivity variability with depth, half the cores were used for sieve/hydrometer analysis with calculation of the saturated hydraulic conductivity (a total 78 of analyses in four boreholes at ~1 ft intervals). To address vertical spatial variability of iron oxides, iron extractions for ferrous, ferric, and total natural iron oxides were measured at 1-ft intervals. To address the vertical spatial variability of the field reductive capacity, 1-D column oxidation studies and ferrous iron extractions were measured at 1-ft or 0.5-ft intervals (total 51 column experiments, 165 iron extractions). These results were also used to develop any correlations between hydraulic conductivity and geochemical properties. In addition, 161 pictures were taken of the cores at 0.5-ft intervals for a qualitative correlation of grain size and reduction extent. These laboratory results are compared with previous reductive capacity measurements determined in 2002, 1999, and 1997.
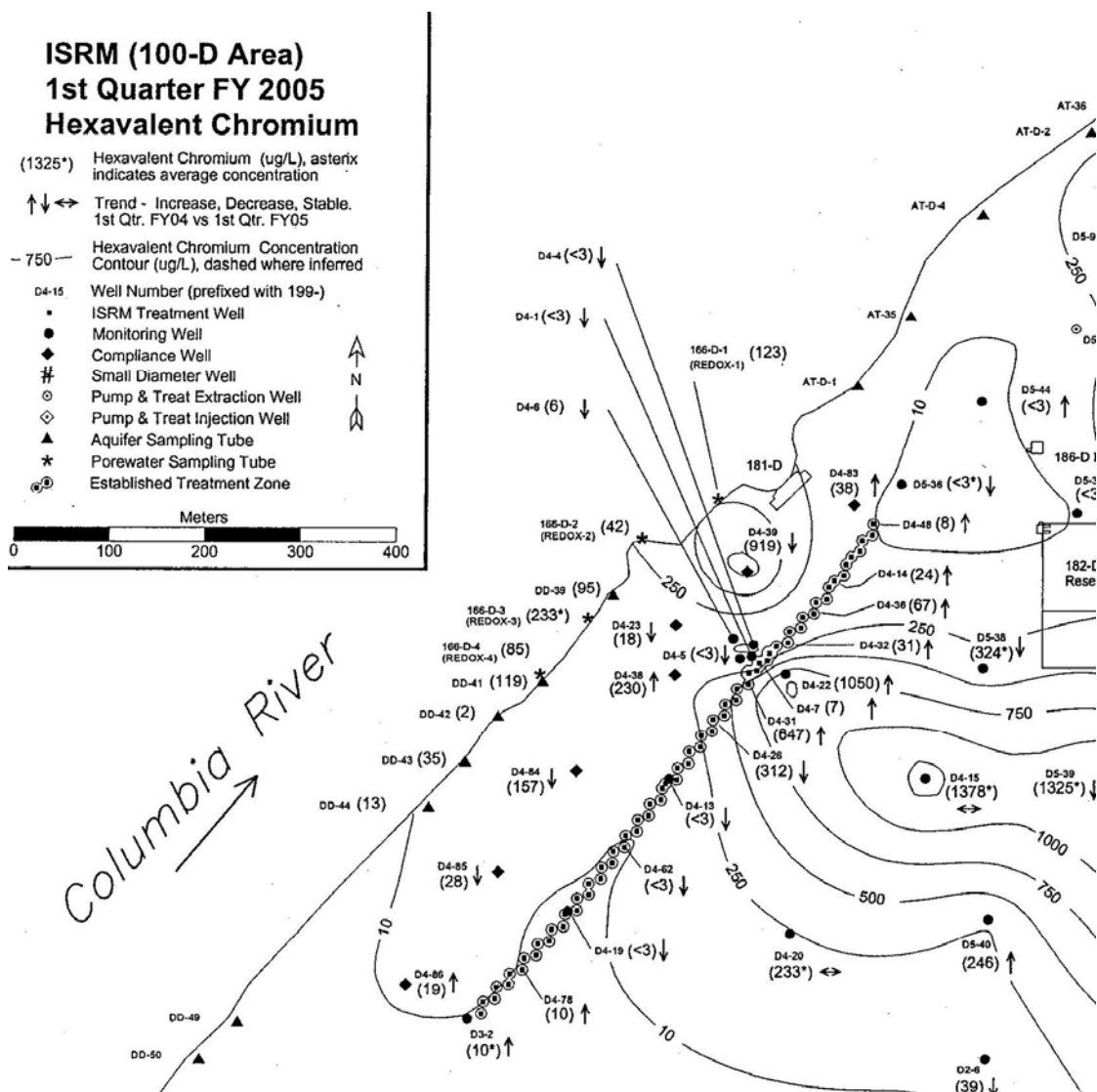
Figure 1.1. 100D ISRM Barrier Location and Chromate Plume

The purpose of this study was to determine whether physical and geochemical heterogeneities are causing ISRM barrier breakdown in specific areas. There may be limitations in the applicability of laboratory results to the field because of the small scale of the core samples used in the physical or geochemical analysis (4-inch diameter) and the limited number of spatially distributed locations where the data were collected. Therefore, data from other field scale studies conducted on the ISRM barrier are also used in this report, including electromagnetic borehole flow meter (EBF) data collected in 2002 and multilevel sampler (MLS) data collected in 2002 and 2004.
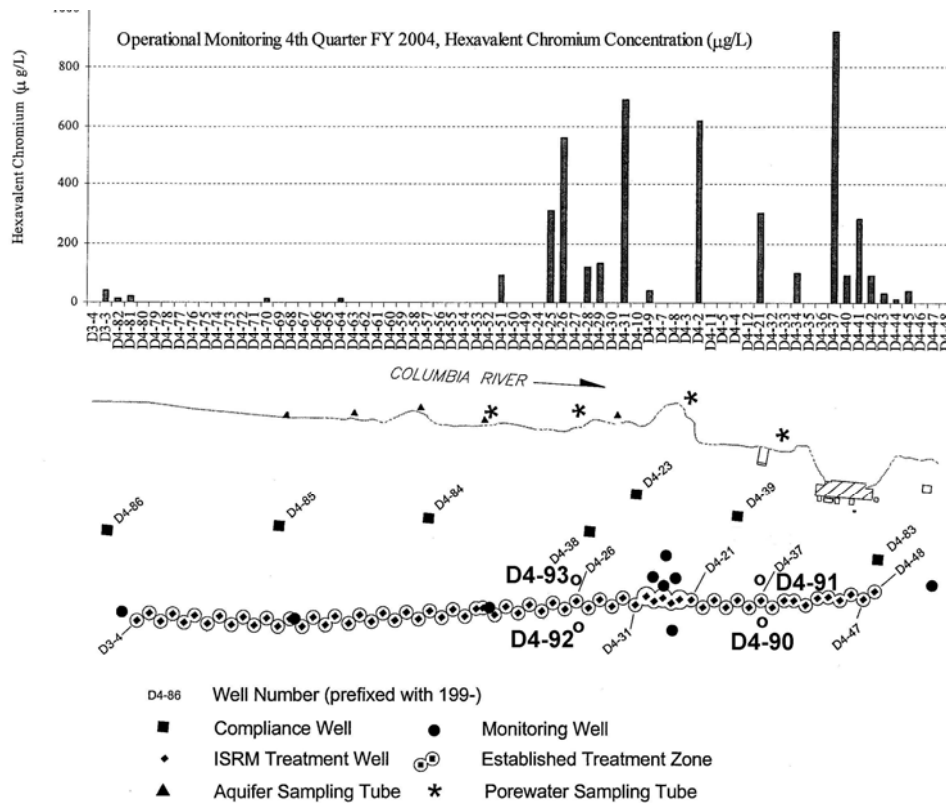
Figure 1.2. 100 D ISRM Well Chromate Concentrations (12/2004) and Borehole Locations for This Study (up- and downgradient 10 to 12 ft of D4-26 and D4-37)
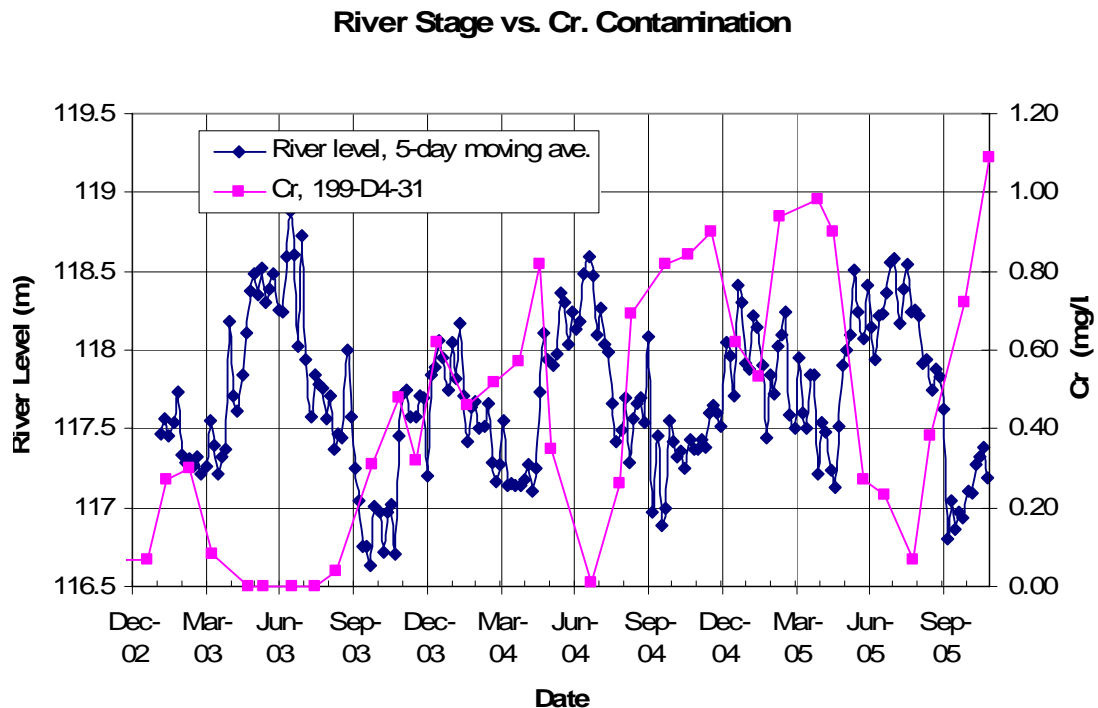
Figure 1.3. Comparison of Seasonal Chromate Trend Plot at Well 199-D4-31 with Columbia River Stage

1.3

2.0   Background: Sediment Reduction and Oxidation Reactions

2.1   Sediment Reduction Mechanism

The ISRM approach involves creating a permeable treatment zone downstream of a contaminant plume or contaminant source by injecting a chemical reducing agent to alter the redox potential of aquifer fluids and sediments (Fruchter et al. 1994, 2000; Vermeul et al. 2002; Szecsody et al. 2004b, 2005b). Redox-sensitive contaminants migrating through this treatment zone are immobilized (metals) or destroyed (organic solvents). Injected reagents create the zone through reactions that reduce iron naturally present in aquifer sediments from Fe(III) to Fe(II). The reducing agent used in these field and laboratory tests is sodium dithionite ($Na_2S_2O_4$). Sodium dithionite is a strong reducing agent that has several desirable characteristics for this type of application, including instability in the natural environment (~ days) with reaction and degradation products, which ultimately oxidize to sulfate. A potassium carbonate/bicarbonate pH buffer is also added to the injection solution to enhance the stability of dithionite during the reduction of available iron.

The dithionite chemical treatment dissolves and reduces amorphous and some crystalline Fe(III) oxides (Szecsody et al. 2004b) and 2:1 smectite clays (Stucki et al. 1984). The reduced Fe(II) created by the dithionite chemical treatment appears to be present in several different Fe(II) phases: adsorbed Fe(II), Fe(II)-carbonate (siderite), and FeS (iron sulfite), although adsorbed Fe(II) appears to be the dominant Fe(II) phase. There may be other unidentified Fe(II) mineral phases produced. Although more than one iron (III) phase is likely reduced in a natural sediment, it can be useful to determine how simple a chemical model is needed to generally describe the observations. Equation 1 is the reaction that describes a single phase of iron reduced by sodium dithionite:

$$S_2O_4^{-2} + 2 \equiv Fe^{3+} + 2H_2O \Leftrightarrow 2 \equiv\equiv Fe^{2+} + 2SO_3^{-2} + 4H^+ \tag{1}$$

shows that the forward rate is a function of the dithionite concentration and the square of the reducible iron concentration (rate is overall a third-order function of concentration). 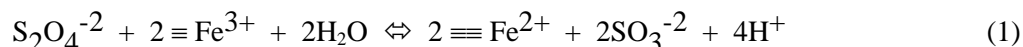The aqueous Fe(II) produced has a high affinity for surfaces so is quickly adsorbed. Therefore, Fe(II) mobility in mid- to high-pH, low ionic-strength groundwater is extremely limited, and iron is not expected to leach from sediments during the dithionite treatment. Aqueous iron measurements in previous studies have shown < 1% iron leaching even after 600 pore volumes of groundwater through a sediment column (Szecsody et al. 2004b). Corresponding solid iron measurements of sediments used in these columns showed 4–10% loss of iron. Iron mobility is somewhat higher during the actual dithionite injection because, at high ionic strength (~0.3 mol/L in this case), other cations compete for the same adsorption sites as Fe^{2+}, resulting in some Fe^{2+} desorption. If the number of slowly reducing sites is small and the mass of iron is far in excess of the dithionite, reaction (1) can be reduced to a first-order reaction in which Fe^{3+} remains constant. Another reaction occurs in the system, which describes the disproportionation of dithionite in contact with sediment:

$$2S_2O_4^{-2} + H_2O \Leftrightarrow S_2O_3^{-2} + 2HSO_3^- \tag{2}$$

This reaction accounts for the mass loss of dithionite that cannot be used for iron reduction. Previous studies have shown that this reaction has a half-life of ~27 hr (basaltic sediments). The consequence of this reaction is to limit how slowly dithionite can be reacted with sediment in the field (i.e., minimum injection rate). If dithionite is injected too slowly, a significant amount of the mass is lost to dispropor-tionation. Although iron(III) phases are the most significant to react with dithionite, other mineral phases present in natural sediments may also be reduced and use some of the dithionite. Previous studies have shown that some Mn reduction occurs as a result of the dithionite treatment of Hanford sediment, although reduced Mn^{II} phases were only 3 to 4% relative to reduced iron phases. Ferrous iron associated with iron oxides also appears to act as a semiconducting surface that facilitates electron transfer, which is more effective than simple electron transfer from aqueous ferrous iron alone (Balko and Tratnyek 1998; Scherer et al. 1999, Wehrli 1992).

2.2 Sediment Oxidation by Dissolved Oxygen, Chromate, and Nitrate

The oxidation of the adsorbed and structural Fe(II) in the sediments of the permeable redox barrier occurs naturally by the inflow of dissolved oxygen and other contaminants such as chromate, nitrate, uranium, technetium, trichloroethylene, carbon tetrachloride, and other electron acceptors. If redox equilibrium completely defined the mechanism (i.e., no effects from activation energies or surface catalysis), and the following contaminants were present in equal molar concentrations, they would be reduced in the following order:

$$\text{Chromate} > \text{dissolved oxygen} > \text{nitrate} > \text{uranium} > \text{pertechnetate} > \text{TCE} \tag{3}$$
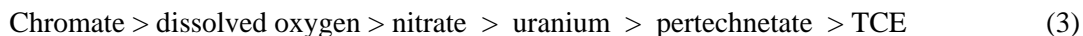
In most aquifers, dissolved oxygen in water is the dominant oxidant of reduced iron species because contaminants are generally present in lower molar concentrations relative to dissolved oxygen. Chromate reduction should not be influenced by the presence of dissolved oxygen (assuming sufficient reductant is present), but nitrate reduction should occur more slowly in the presence of dissolved oxygen (i.e., dis-solved oxygen is reduced first, then the nitrate). The oxidation of reduced iron in pure mineral phases is described by the following reactions for dissolved oxygen and chromium. Fe(II) species that are known to exist in the dithionite-reduced sediments include adsorbed Fe(II) and siderite [$Fe(II)CO_3$]. A single mole of electrons is consumed as a mole of these species is oxidized:

$$Fe^{2+} \Leftrightarrow Fe^{3+} + e^- \quad \text{Eh} = \text{-0.771 v} \tag{4}$$

$$FeCO_3(s) + 3H_2O \Leftrightarrow Fe(OH)_3(s) + 2H^+ + HCO_3^- + e^- \tag{5}$$

The use of dissolved oxygen as an oxidant is generally divided into two electron sequences, which combined,

$$O_2 + 4H^+ + 4e^- \Leftrightarrow H_2O, \quad \text{Eh} = \text{1.23 v} \tag{6}$$
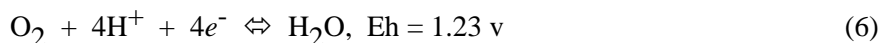
show that 4 moles of electrons are needed per mole of O_2 consumed. The rate of reaction (6) has generally been observed to be first order at fixed pH, and the rate increases 100-fold for a unit increase in pH (Pratt et al. 1997, Blowes et al. 1997). Experimental evidence during iron oxidation experiments

indicates that two reduced iron species are present, adsorbed ferrous iron and siderite. Combining the two iron oxidation half reactions with oxygen reduction,

$$4 \equiv Fe^{2+} + O_2 + 4H^+ \Leftrightarrow 4 \equiv Fe^{3+} + H_2O \quad Eh = -1.85 \text{ v} \quad (7)$$

$$4 \equiv FeCO_3(s) + O_2 + 4H^+ \Leftrightarrow 4 \equiv Fe^{3+} + 2 H_2O + 4CO_3^2 \quad (8)$$
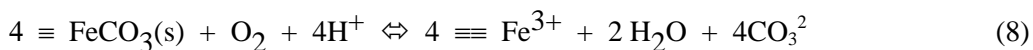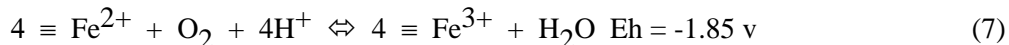
yields 4 moles of Fe(II) oxidized and 4 moles of electrons transferred per mole of O_2 consumed. At oxygen-saturated conditions (8.4 mg L^{-1} O_2, 1 atm, 25°C), 1.05 mmol L^{-1} Fe(II) is consumed. Experimental evidence indicates that the oxygenation of Fe(II) in solutions (pH >5) is generally found to be first order with respect to Fe(II) and O_2 concentration and second order with respect to OH⁻. The rate of oxidation of aqueous Fe^{2+} by oxygen at pH 8 is a few minutes (Eary and Rai 1988, Buerge and Hug 1997). In contrast, the oxidation rate (as a half-life) observed in natural sediments [surface Fe(II) phases mainly adsorbed Fe(II) and Fe(II)CO₃] was found to be 0.3 to 1.1 hr (Szecsody et al. 2000, 2004b). The Hanford 100D area aquifer is generally about half-saturated with respect to oxygen (about 4–5 mg L^{-1}).

The reduction rate of Cr(VI) species by ferrous iron has been extensively studied under various geochemical conditions. For chromate,

$$CrO_4- + 4H_2O + 3e^- \Leftrightarrow Cr(OH)_3 + 5OH- \quad Eh = -0.13 \text{ v} \quad (9)$$

3 moles of electrons are consumed per mole of chromate reduced. Because the reduction potential of this half-reaction (9) per electron is greater than that for oxygen (7), chromate reduction would proceed before oxygen and more rapidly in the presence of ferrous iron if present in equimolar concentrations with dissolved oxygen (and activation energy did not affect the reaction rat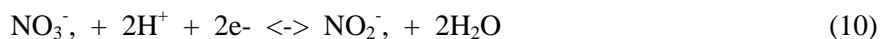e). The reduction of one mole of chromate oxidizes three moles of Fe(II), or 41 mg L^{-1} chromate is needed to oxidize the equivalent mass of Fe(II) as water saturated with dissolved oxygen [1.05 mmol L^{-1} Fe(II)].

Chromate at the Hanford aquifer pH of 7.7 to 8.3 exhibits essentially no adsorption (Zachara et al. 1987), whereas at low pH, considerable chromate adsorption has been observed (Jardine et al. 1999, Seaman et al. 1999). Although reaction (9) is written as a Cr(III) hydroxide, in actuality, mixed (Fe, Cr) hydroxide phases precipitate. With excess iron to Cr, the solubility of these mixed phase precipitates is orders of magnitude less than $Cr(OH)_3$ (Sass and Rai 1986, Blowes et al. 1997, Boursiquot et al. 2002), which makes the reduced sediment concept for immobilization of chromate ideal under alkaline pH conditions. Interestingly, although chromate reduction does occur at low pH, several Cr(III) species are formed and some are mobile (aqueous). In addition, ferrous iron that is adsorbed under alkaline conditions is mobile under acidic conditions. Reduced sediment barriers can still be effective even under highly acidic conditions (pH 4.3) (Loyaux-Lawniczak et al. 2000, 2001; Jardine et al. 1999; Anderson et al. 1994) because immobile ferrous iron from 2:1 smectite clays or iron sulfides are the electron donors not adsorbed ferrous iron (Kim et al. 2001, Patterson and Fendorf 1997).

Nitrate reduction reactions of significance include

$$NO_3-, + 2H^+ + 2e- \; <-> \; NO_2-, + 2H_2O \quad (10)$$

$$2NO_2^-, \ + \ 4H^+ \ + \ 4e\text{-} \ <\text{->} \ N_2^{2-}, \ + \ 2H_2O \qquad\qquad (11)$$

$$NO_2^-, \ + \ 8H^+ \ + \ 6e\text{-} \ <\text{->} \ NH_4^+, \ + \ 2H_2O \qquad\qquad (12)$$
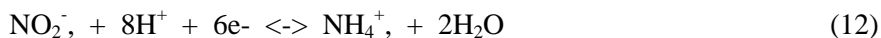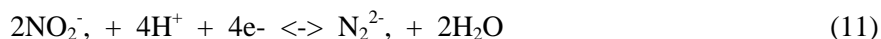
which indicate that the conversion of one mole of nitrate to nitrite consumes two moles of electrons; one mole of nitrate to N_2 consumes four moles of electrons, and one mole of nitrate to ammonia consumes eight moles of electrons. So the reduced sediment barrier longevity can be significantly less with greater reduction of the nitrate. Results of a recent laboratory-scale study on the nitrate reduction mechanism (Szecsody et al. 2005a) showed that the presence of 60 ppm nitrate in the 100D groundwater will reduce the barrier capacity by half. There is a widespread groundwater plume of 60 mg/L nitrate upgradient of the ISRM barrier and lower nitrate concentrations downgradient, suggestive of nitrate reduction. Batch and 1-D column experiments in that study showed that nitrate is being slowly reduced to nitrite and ammonia. These nitrate reduction reactions are predominantly abiotic because experiments with and without bactericides showed no difference in nitrate degradation rates. Nitrogen species transformation rates that were determined in experiments covered a range of ferrous iron/nitrate ratios such that the data can be used to predict rates in field-scale conditions. Field-scale reaction rate estimates for 100% reduced sediment (16^oC) are

- nitrate degradation = 202 ± 50 hr (half-life)

- nitrite production = 850 ± 300 hr

- ammonia production = 650 ± 300 hr.

The influence of dissolved oxygen, chromate, and nitrate reduction on the barrier capacity is described in Section 2.3.

2.3 Calculation of ISRM Barrier Longevity

The longevity of a dithionite-reduced zone can be determined from the ratio of ferrous iron phases (electron donor) in the sediments to the electron acceptors in the aquifer (dissolved oxygen, chromate, nitrate) that flow through the reduced zone. Several studies were done in the Hanford 100D area to determine the mass of ferrous iron in the ISRM barrier. The "laboratory (maximum) reductive capacity" refers to 120 hr of 0.09 mol/L dithionite treatment in a small laboratory column (excess dithionite/ reducible iron for 5 days), so it represents a maximum amount. The "field reductive capacity" refers to sediment cores taken after field dithionite treatment and can be comparable to the laboratory reductive capacity if the core location was near an injection well and in a zone that receives effective treatment, or significantly less than the laboratory reductive capacity if the core location was far from an injection well and/or located in a zone that received ineffective treatment.

In the 1997 study, the reductive capacity averaged 11.0 ± 3.0 µmol Fe^{II}/g of sediment for 18 samples reduced in the laboratory, not with excess dithionite but with a concentration (0.023 mol/L) to be used in the field. In the 1999 study, the field reductive capacity averaged 11.2 ± 7.4 µmol Fe^{II}/g for 8 field-reduced samples. The mean capacity was the same, but the standard deviation was greater for the field-reduced samples because field-scale injections do not treat the sediment uniformly (likely due to flow heterogeneities). In the 2002 study, the field reductive capacity averaged 10.6 ± 7.5 µmol Fe^{II}/g for 16

field-reduced samples, and the laboratory (maximum) reductive capacity averaged 40.0 ± 15.0 μmol Fe^{II}/g for seven samples. The 2002 study used cores from three boreholes (D4-87, D4-88, and D4-89).

Calculation of the ISRM barrier longevity in pore volumes (nondimensional) or in years is the ratio of the electron donor to acceptors using field-scale sediment physical parameters. The mass of electron donor (i.e., Fe(II) and other reduced transition metals) can be calculated per unit volume of water (i.e., pore space) in packed porous media as follows:

- Electron donor: moles of electrons per cm^3 liquid from the Fe(II):

$$(11.2 \text{ μmol } Fe^{2+}/g)(1 \text{ } e^-/Fe^{2+})(2.3 \text{ g sed.}/cm^3)(cm^3/0.14 \text{ } cm^3 \text{ liquid})(mol/10^6 \text{ μmol})(10^3 \text{ } cm^3/L)$$
$$= 0.184 \text{ mol } e^-/L \text{ liquid (using field bulk density and porosity)}$$

- Electron acceptors: moles of electrons per cm^3 liquid from dissolved oxygen and other redox-reactive species (CrO_4^{2-}, TCE, RDX, NO_3^-…):

$$(5.1 \text{ mg/L } O_2)(g/1{,}000 \text{ mg})(mol \text{ } O_2/32 \text{ g}) (4 \text{ mol } e^-/mol \text{ } O_2)$$
$$= 6.38 \text{ x } 10^{-4} \text{ mol } e^-/L \text{ from dissolved oxygen}$$

$$(1.0 \text{ mg/L } CrO_4^-)(g/1{,}000 \text{ mg})(mol \text{ } CrO_4^{2-}/117 \text{ g}) (3 \text{ mol } e^-/mol \text{ } CrO_4^{2-})$$
$$= 2.6 \text{ x } 10^{-5} \text{ mol } e^-/L \text{ from chromate}$$

$$(45.0 \text{ mg/L } NO_3^-)(g/1{,}000 \text{ mg})(mol \text{ } NO_3^{2-}/62 \text{ g}) (2 \text{ mol } e^-/mol \text{ } NO_3^{2-})$$
$$= 1.45 \text{ x } 10^{-3} \text{ mol } e^-/L \text{ from nitrate}$$
$$\text{Total electron acceptors} = 6.38 \text{ x } 10^{-4} + 2.6 \text{ x } 10^{-5} + 1.45 \text{ x } 10^{-3} = 2.1 \text{ x } 10^{-3} \text{ mol } e^-/L$$

- Barrier longevity: electron donors/electron acceptors (number of pore volumes barrier will last)

$$\textit{for } 5.1 \text{ mg/L } O_2, 1.0 \text{ mg/L } CrO_4^-, \text{ and } 45.0 \text{ mg/L } NO_3^{-2}$$
$$0.184 \text{ mol } e^-/L/2.1 \text{ x } 10^{-3} \text{ mol } e^-/L = 88 \text{ pore volumes}$$

$$\textit{for } 5.1 \text{ mg/L } O_2, \text{ and } 1.0 \text{ mg/L } CrO_4^-$$
$$0.184 \text{ mol } e^-/L/6.6 \text{ x } 10^{-4} \text{ mol } e^-/L = 277 \text{ pore volumes}$$

To determine the actual longevity in years, the average groundwater flow rate through that aquifer zone is needed. An estimated longevity in years based on a groundwater flow rate of 1 ft/day and an average reduced sediment barrier thickness of 40 ft is calculated as follows. A 40–ft-width was assumed with high reductive capacity, although there would be some additional capacity to a 50-ft width not accounted for.

$$(40 \text{ ft})(day/1 \text{ ft})(88 \text{ pore volumes})(year/365.25 \text{ days}) \quad = 9.6 \text{ years}$$
$$\textit{for } 5.1 \text{ mg/L } O_2, 1 \text{ mg/L } CrO_4^-, \text{ and } 45 \text{ mg/L } NO_3^{-2}$$

$$(40 \text{ ft})(day/1 \text{ ft})(277 \text{ pore volumes})(year/365.25 \text{ days}) \quad = 30 \text{ years}$$
$$\textit{for } 5.1 \text{ mg/L } O_2 \text{ and } 1 \text{ mg/L } CrO_4^-$$

These calculations assume a single, homogeneously reduced aquifer unit. At the 100D area, there are aquifer zones with differing flow rates and variations in both iron content and reductive capacity. Similar calculations can be made to approximate these differing characteristics to determine whether premature breakthrough is predicted to occur in high-flow zones.

Calculating the influence of nitrate reduction on the 100D Area reductive capacity requires consideration of mass balance (described above) and reaction rate effects. While dissolved oxygen and chromate reduction rates are rapid and essentially at equilibrium in the aquifer, nitrate transformation reactions are slow (hundreds of hours). During the estimated 40-day residence in the ISRM barrier, only a portion of the nitrate will be reduced, whereas dissolved oxygen and chromate are reduced to completion. With a groundwater velocity of 1 ft/day, it is estimated that the ISRM barrier reductive capacity is 277 pore volumes (with no nitrate), and 88 pore volumes if 60 mg/L nitrate is present. Due to the slow nitrate transformation reaction rates, zones with more rapid groundwater flow will be less influenced by nitrate reduction. For example, a zone with a groundwater velocity of 5 ft/day and 60 mg/L nitrate will have a reductive capacity of 135 pore volumes, as indicated in Figure 2.1 (for a 40-ft-wide barrier and a groundwater velocity of 5 ft/day, residence time within the barrier would be ~ 8 days, resulting in a reductive capacity of ~ 135 pore volumes). Conversely, aquifer locations with slower flow will provide sufficient additional residence time to consume additional ferrous iron (i.e., for the same barrier width and a groundwater velocity of 1 ft/d, residence time within the barrier would be ~ 40 days, resulting in a reductive capacity of ~ 75 pore volumes).
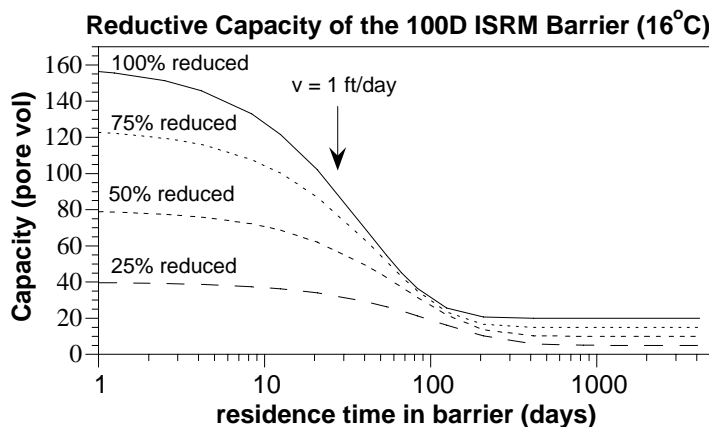
Figure 2.1.   Influence of Nitrate Reduction on 100D Area ISRM Barrier Longevity (60 mg/L nitrate assumed)

Long-term column experiments (Szecsody et al. 2005a) demonstrated the longevity of the reduced sediment barrier to reduce/immobilize 2 mg/L chromate in the presence of 8.4 mg/L dissolved oxygen (saturation), and 60 mg/L nitrate (maximums observed in the field). Initially the chromate reduction half-life was <0.1 hr. This reaction rate decreased to 2.4 hr by 120 pore volumes and 17 hr by 250 pore volumes. The chromate reduction rates are fast enough relative to the estimated 50-day average residence in the field for all chromate to be reduced/immobilized and the sediment completely oxidized (40 days equates to 56 half-lives of treatment at the lowest rate measured). Alternatively, for higher groundwater velocities in high-conductivity preferential flow paths (5 ft/day resulting in a residence time of 8 days), groundwater traveling through these zones is exposed to 11 half-lives of treatment at the lowest rate.

3.0 Laboratory Methods: Geochemical and Physical Characterization

## 3.1 100D Borehole Location and Sediment Collection

Four boreholes were drilled within the ISRM barrier during April and May 2005 to collect sediment for this study. Two boreholes were located up and downgradient of well D4-37 and two additional boreholes were located up and downgradient of well D4-26 (Figure 1.2). Borehole C4686 is 12.48 ft upgradient and borehole C4687 11.93 ft downgradient of well D4-37. Borehole C4688 is 10.15 ft up-gradient and borehole C4689 9.919 ft downgradient of well D4-26. Continuous cores were collected from a depth of ~75 ft bgs to the Ringold aquifer/confining unit contact (97- to 103-ft depth). The average water table is ~82 ft bgs and typically varies from 78.5 to 86.5 ft bgs annually. Sediment was collected using a 4-inch-diameter, 2-ft-long split spoon sampler fit with lexan liner material precut to 6-inch-long sections. The 2-ft core was split into 6-inch sections, two for sieve analysis and two for geo-chemical analysis. For the physical property analyses, the entire 6-inch section was used for conducting the sieve/hydrometer measurements. Geochemical cores were placed in anaerobic bags at the field site, argon gas was used to remove most of the air from the bag, and an oxygen scrubber and oxygen indicator were placed in each bag. The geochemical cores were kept anaerobic before, during, and after analysis. Sediment reductive capacity (1-D column oxidation experiments) and iron extractions (described below) were conducted on sediment taken at both ends of the 6-inch cores after first removing 1 inch of core material because these ends may have been exposed to air during core handling. As such, reductive capacity and iron extraction data are from a specific depth (for example, at 85.6 and 85.9 ft in the 85.5 to 86-ft deep core), whereas sieve analysis is from a depth range (for example, 86- to 86.5-ft deep).

3.2 Field Reductive Capacity by 1-D Column Oxidation

Sediments taken from field cores collected within the ISRM treatment zone were oxidized in con-trolled 1-D column experiments that consisted of injecting air-saturated water through the column at a constant rate for 300 to 700 hr until complete oxygen breakthrough had occurred. The mass of oxygen consumed over the entire experiment was used to stoichiometrically calculate the mass of ferrous iron present. While these experiments are time-consuming, cost is minimized by automation. This type of column oxidation experiment approximates field conditions well because sediment is oxidized slowly over a 2–4 week period (as opposed to the batch iron extractions described below). Laboratory results from these 1-D oxidation experiments are presented in Appendixes A through D. These column reductive capacity measurements are conducted by the same method as previous studies (2002, 1999, and 1997) of 100D sediments and enable direct comparison of field reductive capacity changes over time (see Appendix E).

The dissolved oxygen levels in the experiments were monitored at the column outlet by two in-line oxygen electrodes (20 μL flow-through volume, Microelectrodes, Inc.) with automated calibration every 6 hr (patent #6,706,527). This consists of two electrodes hooked up in a 6-way high-performance liquid chromatograph (HPLC) injection valve (Valco Industries) and 6-port Kloehn syringe pump, both controlled by a computer program (Figure 3.1). The program allows column effluent to flow through the

two electrodes, then at 6-hour intervals the electrodes are pulled off-line from the column, and oxygen-saturated water and oxygen-free water are injected through the electrodes (5 mL each). After a 1-minute equilibration time, oxygen data are recorded on a data logging board triggered by this program. Column effluent oxygen data were recorded twice per second and averaged over two minutes for a single value recorded every two minutes (data logging with a National Instruments DAK 500 card). A typical experiment then contained 1500 to 4000 data points of column effluent data and 20 to 50 oxygen-saturated water and oxygen-free water calibration points for each of two oxygen electrodes. The columns used in these experiments were 0.765 cm in diameter by 10 cm long, and the < 4 mm size fraction of sediment was packed into the column. The dry bulk density and porosity were calculated from dry and wet sediment weights and the column volume.
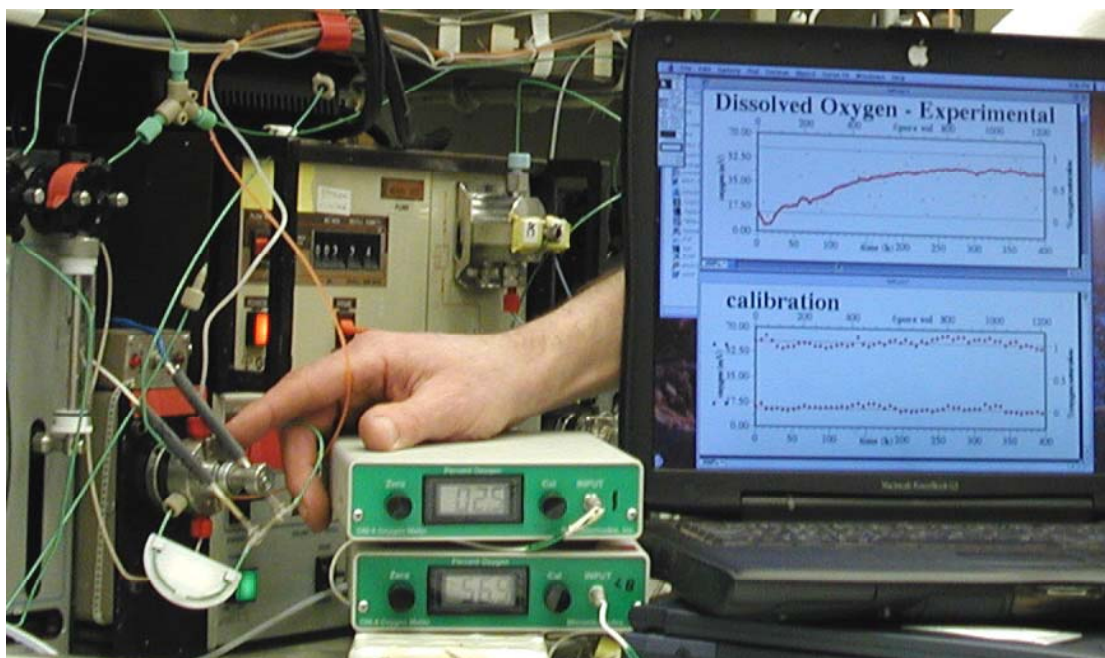
**Figure 3.1.** 1-D Column Oxidation System Used to Measure Sediment Reductive Capacity

3.3   Laboratory Reduction of 100D Sediments and Laboratory Reductive Capacity

The dithionite chemical treatment of sediment dissolves and reduces amorphous and some crystalline Fe(III) oxides (Szecsody et al. 2004a) and clays (Stucki et al. 1984). The reduced Fe(II) created by the dithionite chemical treatment appears to be present in several different Fe(II) phases: adsorbed Fe(II), Fe(II)-carbonate (siderite), and FeS (iron sulfide), although adsorbed Fe(II) appears to be the dominant Fe(II) phase. These reduction experiments consisted of injecting 0.09 mol/L dithionite and 0.36 mol/L K_2CO_3 for 120 hr at a constant flow rate with a 5-hr residence time to fully reduce the sediment Fe(III)-oxide and clay minerals (Szecsody et al. 2004b). The dry bulk density and porosity of the column was calculated from the dry and saturated column weight and column volume. The volumetric flow rate was calculated from the effluent volume and elapsed time. Seventy column reduction experiments were conducted.

After dithionite reduction, sediments were used in experiments to determine the laboratory (or maximum) reductive capacity. The two methods used consisted of a 1-D column experiment to oxidize the sediment over several weeks (previous section) and a 1-hr, 0.5-M HCl extraction (described below). Reduced sediment was stored in glass vials under water with no headspace and 1-cm-thick septa. These glass septa top vials are then stored in a refrigerator. This "laboratory-reduced" 100D sediment represents a maximum amount of reduction that can be achieved. Field-scale reduction is typically equal to or less than this maximum value, depending on the effectiveness of field-scale treatment at the specific location.

In the field, the reduction achieved at an aquifer location depends on the mass of dithionite and contact time that is achieved so that, in general, sediment is more reduced near the injection well and less reduced at a radial distance of 20 to 30 ft from the injection well. Laboratory experiments conducted with Fort Lewis, Washington sediment illustrate the sediment reductive capacity achieved is dependent on the amount of dithionite treatment (Figure 3.2). First, if the exact amount of dithionite is added to reduce the sediment (i.e., 2*di/Fe ratio = 1.0, one mole of dithionite reduces two moles of ferric iron), about 70% of the reductive capacity is achieved (Figure 3.2, solid triangles). If twice as much dithionite is added, the maximum capacity is achieved. Adding 30 times more dithionite than needed also achieves the maximum reductive capacity, but considerable dithionite is wasted. At dithionite/ iron ratios < 1, less reductive capacity is reached. The 1-D column oxidation method (solid triangles) of reductive capacity showed similar results as the 1-hr 0.5 M HCl iron extraction (open triangles and diamonds). There was also no difference between sediment reduced in batch systems (open triangles) and reduced in 1-D columns (open diamond). Thus, reductive capacity can be well predicted knowing the dithionite/iron ratio.
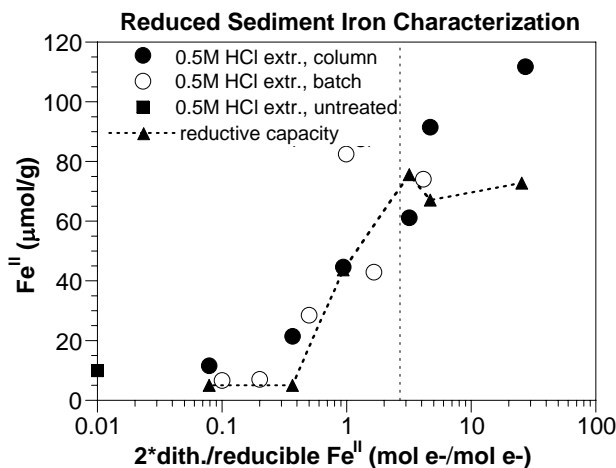

Figure 3.2. Amount of Dithionite Treatment and Resulting Reductive Capacity by Two Methods

3.4 Field Reductive Capacity by Ferrous Iron Extraction with 0.5 M HCl

A second method was used in this study to characterize the mass of ferrous iron in the 100D sediments that were reduced with dithionite in the field. This method consisted of an iron extraction technique using 0.5 M HCl, which slowly dissolves ferrous and ferric iron oxides over time. The 0.5 M HCl iron extraction (24 hr) is originally defined to extract the "total Fe(II) phases" as defined by Heron et al. (1994a, b). Although there was a positive correlation between the amount of dithionite treatment and the

0.5 M HCl extractable Fe(II) in 24 hr, the values were far greater. Time-course experiments conducted on a Strategic Environmental Research and Development Program project showed that a 1–2 hr contact time provided reductive capacity values similar to the 1-D column oxidation method for fully reduced sediment but was 40–60% low for partially reduced sediment (Figure 3.3). The sediment used in that study was from Fort Lewis, Washington. In this study, a 1-hr contact time was used for the 0.5-M HCl extraction. This acidic dissolution/ mobilization of ferrous iron is a very different mechanism than the slow (hundreds of hours) oxidation by mainly dissolved oxygen for reduced sediment in the field. As such, the HCl extraction method is in development, and results were compared with the 1-D column oxidation results. The 1-hr 0.5 M HCl extractions for ferrous iron were conducted at 1-ft or 6-inch intervals in the sediment. Each extraction consisted of using 20 g of field-reduced sediment that was packed into a 45-mL centrifuge tube from the core in an anaerobic chamber, then slow-mixed for 1 hr within the anaerobic chamber. The tube was then centrifuged, liquid extracted, filtered, and ferrous iron measured with a ferrozine colormetric method (Gibbs 1976).


Column Reduction/0.5M HCl Extraction
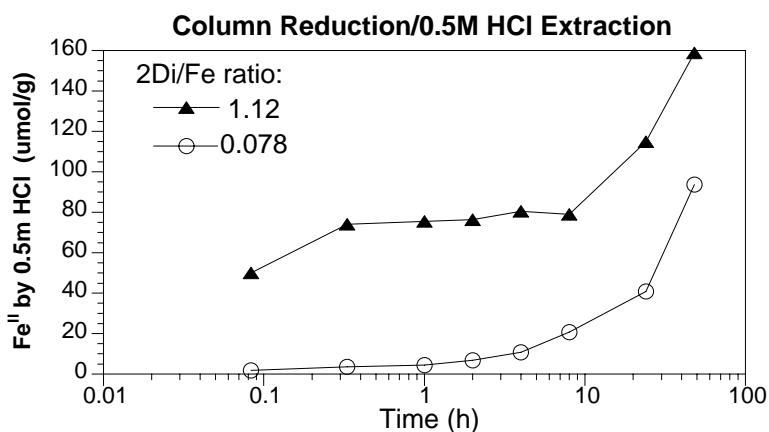
Figure 3.3. Influence of Contact Time on 0.5-M HCl Extraction for Ferrous Iron. Reductive capacity measured by 1-D column oxidation was 73 μmol/g for fully reduced sediment (triangles) and 10 μmol/g for partially reduced sediment (circles).

3.5 Iron Oxide Geochemical Characterization

Iron extractions were conducted to determine the total mass of ferric and ferrous iron in the sediment and to address spatial variability in the iron oxides that could cause low reduction zones during dithionite treatment. The process consisted of a 5 molar HCl extraction over two weeks (Heron et al. 1994a, b), with analyses of both ferrous and ferric iron. Aqueous Fe^{II} was quantified by ferrozine (Gibbs 1976). Fe_{total} extracted was also quantified by ferrozine, where Fe_{total} ($Fe^{II}+Fe^{III}$) was obtained by reducing aqueous Fe^{III} to Fe^{II} using 0.025 M NH_2OH, HCl. Extracted Fe^{III} is then computed as the difference between Fe_{total} and Fe^{II}. Each extraction was done in triplicate (previous standard deviations were ± 3.3 to 8.3%), with additional duplication for some samples. The following iron extractions conducted on 100D sediments in previous studies were not done in this study, though they provide additional information: 1) 1 M $CaCl_2$ (Fe^{II} ion exchangeable) (Heron et al. 1994a,b), 2) NH_2OH, HCl (amorphous iron oxides) (Chao and Zhou 1983), and 3) dithionite-citrate-bicarbonate (amorphous and crystalline iron oxides).

Pictures of Sediment Cores. Pictures of the 2005 sediment cores at 6-inch intervals (161 pictures, Appendix H) and the 2002 sediment cores at 1-ft intervals (74 pictures, Appendix I) provide a qualitative estimate of the grain size distribution and reductive capacity. While cobbles are obvious in some pictures because the hydraulic conductivity is controlled by the finer sediment fraction, pictures cannot be used for accurate flow determination. Grain size distributions (next section) were used for quantitative determination of the hydraulic conductivity. As sediment reacts with dithionite, resulting adsorbed ferrous iron (no color), siderite (grey), and FeS (black) change the color of the sediment. For a single sediment sample, the color can be used (Figure 3.4), but the observed color also changes with minerals present, grain size, and moisture content. Therefore, the color observed from pictures does not accurately reflect the reductive capacity.
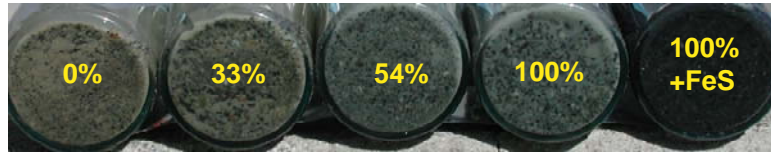
Figure 3.4. Dithionite Treatment (% dithionite/Fe) and Color

3.6 Sediment Grain Size Distribution and Calculation of Hydraulic Conductivity

Sieve and hydrometer analyses of sediment cores were conducted to determine the grain size distribution. Sediment in the entire 6-inch core was first dried at 45ºC and then subjected to sieve analysis (12 sieves, 50 to 0.053 mm). The < 0.07-mm size fraction was then subjected to hydrometer analysis to determine the silt/clay size fractions. The 78 sieve/hydrometer analyses conducted on the four boreholes are presented in Appendixes J–M.

Three methods were used to calculate the saturated hydraulic conductivity from the grain size distribution. The simplest empirical relation is Hazen's formula:

$$K_{sat} \text{ (cm/s)} = 1.0 \ (d_{10})^2 \tag{13}$$

where the 10% passing grain size (d_{10}) is in millimeters. This formula was originally determined for uniformly graded sands in the late 1800s. A "modified Hazen's formula" was empirically derived from the relationship between grain size distributions and measured saturated hydraulic conductivity measurements for various Hanford sediments:

$$K_{sat} \text{ (cm/s)} = 0.0961 \ (d_{25})^{1.6624} \tag{14}$$

where the 25% passing grain size (d_{25}) reflects some of the grain size mixture in Hanford sediments (as opposed to uniform porous media of the Hazen formula). The third empirical formula uses additional points of the grain size distribution, so more accurately reflects the influence of a range of grain sizes on flow. The modified Masch and Denny (1966) formula used in this study is

$$K_{sat} \text{ (cm/s)} = 0.0177 \ (d_{50}/ \ \sigma_{\phi})^{1.4319} \tag{15}$$

where

$$\sigma_\phi = [\phi_{16} - \phi_{84}]/4 + [\phi_5 - \phi_{95}]/6.6 \qquad (16)$$

and

$$\phi = -\log(mm)/\log(2)$$

is the grain size on the phi scale (Folk 1980). A mathematical model (van Genuchten function) was fit to the grain size data to generate a continuous distribution for calculating the grain size metrics used in Eq. (13) through (15). The values of K estimated from Eq. (14) and (15) correspond to the vertical direction because these regression equations were fit to data from vertically oriented core samples (Mark Rockhold, personal communication):

$$K_{sat} \ (cm/s) = 0.0961 \ (d_{25})^{1.6624} \qquad (14)$$

where the 25% passing grain size (d_{25}) reflects some of the grain size mixture in Hanford sediments (as opposed to uniform porous media of the Hazen formula). The third empirical formula uses additional points of the grain size distribution so more accurately reflects the influence of a range of grain sizes on flow. The modified Masch and Denny (1966) formula is used in this study:

$$K_{sat} \ (cm/s) = 0.0177 \ (d_{50}/std \ dev)^{1.4319} \qquad (15)$$

where $\qquad\qquad\qquad\qquad std \ dev = [d_{16} - d_{84}]/4 + [d_5 - d_{95}]/6.6$

where the standard deviation (std dev) of the grain size distribution was calculated using log (grain size, mm). A mathematical function (van Genuchten function) was used fit the log grain size distribution in order to accurately calculate the grain size percentages needed.

3.7 Multilevel Sampler Data–Field-Scale Vertical Aqueous Heterogeneity

The vertical aqueous stratification in the aquifer was characterized using an MLS and an EBF (described in Section 3.8). The MLS consists of a series of 30 mL bottles with filters on both top and bottom. The bottles are placed at discrete (approximately 1.1 ft) vertical intervals, as shown in Figure 3.5, and separated by rubber gaskets that limit vertical flow in the fully screened well. The sample bottles are filled with deionized water and left in place for several weeks so vial water equilibrates by diffusion with surrounding groundwater. The MLS was developed in Israel and has been used in many geochemical and microbial applications worldwide. Tests using a bromide solution in some bottles have shown, under ideal test conditions, that very little vertical flow occurs across the rubber gaskets (i.e., the data are representative of the vertical stratification in the groundwater). MLS were used in two wells (D4-7 and D4-9) in August 2002 (low groundwater flow) (see Appendix F) and in eight wells in March and April 2004 (high groundwater flow) (see Appendix G). Most installations were in 15-ft vertical sections (Figure 3.6).

Each MLS Well

~85' — 14.69'

sample bottle

baffle — 13.59'

— 12.27'

— 11.15'

0.24' copuler

— 10.04'
~90' — 9.80'

— 8.70'

— 7.35'

— 6.83'

0.24' copuler

— 5.11'
~95' — 4.87'

— 3.70'

— 2.38'

— 1.26'

~100' — 0.15'

well bottom
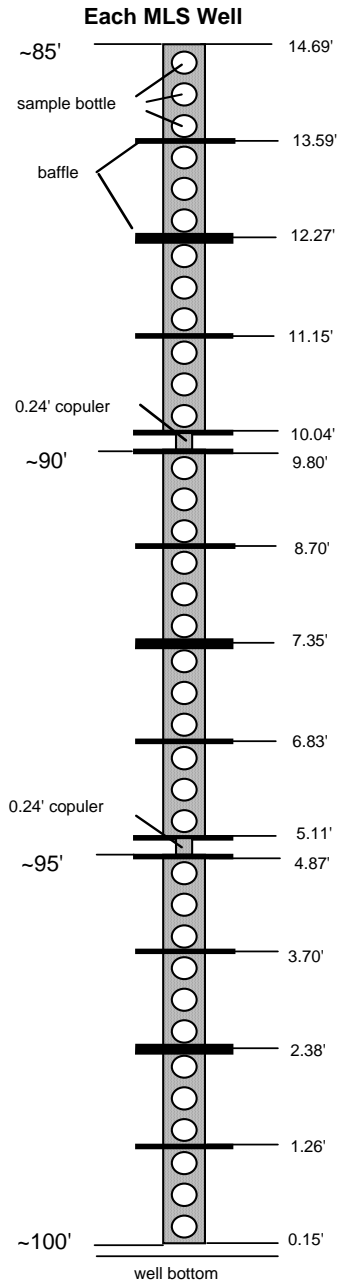
Figure 3.5.	MLS Configuration Used in 100D Wells

Figure 3.6.	Installation of an MLS in a 100D Area Well

3.8   Electromagnetic Borehole Flow Meter Data–Field-Scale Aquifer Flow Heterogeneity

The EBF method represents a reasonably simple approach for assessing the relative hydraulic conductivity in porous media or flow through fractured rock at discrete positions in a screened well or uncased borehole. The technique involves measuring vertical flow within a wellbore at arbitrarily selected intervals as water is transmitted through the well under ambient and induced pumping conditions.

These data can serve as the basis for computing the relative hydraulic conductivity at each interval. In principle, the flow meter method is very straightforward. When water is injected into or withdrawn from a well at a constant, relatively low rate, the water level inside the well will exhibit an initial pressure response, but after a few minutes will approach a quasi-equilibrium condition. At that time, water is flowing through the well screen at the same rate as stress is applied to the well. Water enters (or exits) the well horizontally throughout the screened interval and flows vertically within the well. The objective is to measure the vertical distribution of the horizontal flow through the well screen. The horizontal flow rate at each stratum is indicative of the hydraulic conductivity of those strata (Molz et al. 1994). Under ideal conditions, the probe is sealed to the wall such that any vertical flow must pass through the recording zone of the meter.

An EBF test is usually initiated by measuring ambient flow throughout the screened section of the well. This is typically initiated with the flow meter at the bottom of the screen where flow rates should be zero. The probe is then raised one increment. After any flow disturbance caused by the probe movement has subsided, the vertical flow at that station is recorded. This process is repeated throughout the entire screened interval. These ambient flows reveal the presence of vertical pressure gradients, positive or negative, between strata and provide a baseline for analyzing induced flow into the well during pumping. Once the ambient flow pattern has been recorded, the induced flow test is initiated by injecting into or withdrawing from the well at a relatively low, constant rate. The water surface is monitored to determine when equilibrium conditions have been achieved. At that time, the probe is systematically moved vertically with flow rates recorded at predetermined intervals throughout the well screen. Data at each depth are displayed on a digital readout and stored in a data file of a portable computer. The lateral inflow from each stratum is calculated by successively subtracting the cumulative flow measured at the selected strata from the cumulative flow recorded at the level immediately below. Hydraulic conductivity can be calculated for each depth discrete point by using the Cooper-Jacob formula for horizontal flow to a well. The ratio of local hydraulic conductivity K_i to average K_{ave} for each well is computed using (Eq. 7) (Molz and Young 1993):

$$K_i / K_{ave} = ((\text{Delta } Q_i - \text{Delta } q_i) / \text{Delta } z) / (Q_{pump} / b) \; ; \; i = 1,2, \ldots n$$

where Delta Q_i = flow from the ith layer in the well; Delta q_i = ambient flow from the ith layer of the well; Delta z = ith layer thickness; Q_{pump} = flow rate pumped from the well during the induced flow test; and b = aquifer thickness.

4.0   Results

4.1   Field Reductive Capacity

The field reductive capacity of the 100D sediments from the four boreholes showed variation with depth within boreholes and differences in capacity with nearby boreholes. This reductive capacity measured on sediments reduced in the field reflects 1) differences in initial reduction achieved by dithionite injection due to geochemical and flow heterogeneities at the field scale and 2) differences in oxidation with depth if high flow regions are present. The field reductive capacity was measured by two methods, oxidation of sediments in 1-D columns with air-saturated water (Tables 4.1–4.5 and all column data in Appendixes A–D) and a 1-hr, 0.5-M HCl iron extraction (see Appendix E). Although the 1-D column oxidation method is an idealized representation of groundwater flow, it does account for oxidation of the ferrous iron phases present on the sediment surfaces that can occur at different rates because the 1-D column experiments were run for 2 to 4 weeks. The 1-hr ferrous iron extraction dissolves/mobilizes some of the ferrous iron phases but may not access all redox reactive phases.

The field reductive capacity near well D4-37 shows a relatively uniform upgradient capacity but a greater downgradient capacity (18% average), especially in the lower half of the aquifer (Figure 4.1). The 1-hr iron extraction data were ~25 to 50% of the 1-D column reductive capacity and did not reflect the extremes in the trends (possibly due to the short contact time). As described in Section 4.3.2, greater hydraulic conductivity is generally indicated at 93–97-ft depth in both up- and downgradient boreholes. The trends observed may indicate that the 93–97-ft depth initially had greater reductive capacity (due to more dithionite flow into this region), but this region is also being oxidized more rapidly (the upgradient well shows lower capacity at this depth). Although the upgradient well may have been oxidized and the downgradient well is not oxidized (yet), an alternative interpretation is that even though high hydraulic conductivity is observed in both wells at this depth, it may not be a laterally continuous feature.

Lower reductive capacity was observed near the water table in the downgradient borehole. The upgradient borehole may exhibit a small amount of degradation associated with the water table boundary (though this is hard to quantify due to a lack of shallow column data at this location), but this effect is much more pronounced in the downgradient borehole. Physical property data for sediments within this interval indicate relatively high hydraulic conductivity. This region could have low reductive capacity because of the combination of water table fluctuation; higher concentrations of dissolved oxygen, chromate, and nitrate at the top of the aquifer; and higher flow. The MLS data for well D4-37 for April 2004 (see Appendix G) show no change in dissolved oxygen, electrical conductivity, and chromate (no high-flow zones are indicated). However, there was some concern about whether the rubber seals that separate vertical zones in the MLS were functioning (could be significant vertical mixing in the well).

The reductive capacity near well D4-26 (Figure 4.2) shows significant variation vertically in both up- and downgradient wells but also a 70% greater average capacity downgradient. There is a low-capacity region at 92 to 93 ft in both up- and downgradient wells. There is also lower reductive capacity at the 97–101-ft depth, which does correspond to a higher-flow region. The 1-hr iron extraction shows some of the trends observed in the 1-D column oxidation results but not the large trends so does not seem to be useful.

Table 4.1. Iron Data for D4-90, C4686 (upgradient of D4-37)

depth (ft)	mass fraction < 4 mm	field reductive capacity* 1h 0.5M HCl (μmol/g)	field reductive capacity* column O₂ ox. (μmol/g)	maximum reductive capacity* 1h 0.5M HCl (μmol/g)	maximum reductive capacity* column O₂ ox. (μmol/g)	ratio capacity O₂/HCl	reduced fraction field/maximum 1h 0.5M HCl	reduced fraction field/maximum average column O₂ ox.	total iron oxides* Fe^II 2 wk 5M HCl (μmol/g)	total iron oxides* Fe^{II+III} 2 wk 5M HCl (μmol/g)
79.1	0.549	0.066					0.006		78.1	231
81.6	0.583	0.01		14.2			0.001		54.1	140
82.6	0.352	0.36	water 83.5'	8.80			0.032		38.2	97.4
83.6	0.482	0.48		10.2			0.042		37.9	92.6
85.1	0.357	1.53	8.20	8.63		5.37	0.134	0.197	36.7	85.4
86.1	0.406	1.82	8.72	10.7		4.80	0.159	0.209	31.7	77.3
87.6	0.490	3.55	10.42	14.1		2.93	0.312	0.250	57.0	120.3
87.9	0.490	3.57					0.313			
88.6	0.509	3.31	11.4	7.33	47.9	3.45	0.290	0.274	72.0	136.3
88.9	0.634	4.77	14.26	26.7		6.53	0.419	0.342		
90.6	0.634	0.57	8.96	11.4		15.81	0.050	0.215	34.0	88.2
90.6	0.634	0.56					0.049		31.9	83.9
90.9	0.503	0.77					0.068			
92.1	0.503	0.93	11.0		30.6	11.85	0.082	0.265	23.4	56.6
92.4	0.503	1.70					0.149			
93.1	0.503	1.95	8.52	12.2		4.38	0.171	0.204	40.8	99.2
93.4	0.414	1.02					0.089			
94.6	0.414	0.51	8.08			15.79	0.045	0.194		
94.9	0.414	0.51		8.34			0.045		43.4	101
95.6	0.414	2.83	2.01	12.4	26.2	0.71	0.248	0.048	48.6	137
95.9	0.784	5.19				2.11	0.455			
95.9	0.784	4.99				2.11	0.437		88.8	243
96.6	0.784	6.51		23.1			0.571		70.6	164
mean ± std dev:		2.35 ± 1.87	9.16 ± 3.16	13.2 ± 6.17	34.9 ± 11.5	6.32 ± 5.26	0.206 ± 0.164	0.220 ± 0.092	49.2 ± 19.1	122 ± 52.6

for the full grain size distribution

** ratio of maximum reductive capacity (0₂ / 0.5M HCl)

Table 4.2. Iron Data for D4-91, C4687 (downgradient of D4-37)

depth (ft)	mass fraction < 4 mm	field reductive capacity* 1h 0.5M HCl (µmol/g)	field reductive capacity* column O_2 ox. (µmol/g)	maximum reductive capacity* 1h 0.5M HCl (µmol/g)	maximum reductive capacity* column O_2 ox. (µmol/g)	ratio capacity (O_2 / HCl)	reduced fraction field/maximum average 1h 0.5M HCl	reduced fraction field/maximum average column O_2 ox.	total iron oxides* Fe^{II} 2 wk 5M HCl (µmol/g)	total iron oxides* Fe^{II+III} 2 wk 5M HCl (µmol/g)
79.1	0.549	0.038							71.4	150
80.6	0.549	0.005				4.09**			32.5	101
81.6	0.583	0.01				2.01**			30.7	76
83.1	0.352	0.66	3.12	12.9	water 83.5'	3.95**	0.058	0.075	39.4	98.7
84.1	0.482	0.04	2.60	15.4		0.97	0.003	0.062	54.7	155
85.1	0.357	1.08	3.81	10.3		3.53	0.095	0.091	75.3	147
85.6	0.406	2.91	6.00	13.6		2.07	0.255	0.144	58.6	156
88.1	0.490	2.58	12.8	9.80	42.6	4.95	0.226	0.306	63.7	114
89.1	0.490	4.17	5.51			1.32	0.366	0.132		
90.6	0.509	3.21	9.29	11.2		2.89	0.282	0.223	29.5	69.1
91.6	0.634	5.29	6.90	12.8		1.30	0.464	0.165		
93.1	0.634	5.27	22.7	13.4	29.3	4.31	0.462	0.545	60.0	144
94.1	0.634	6.41	9.81			1.53	0.562	0.235	128.5	326
95.6	0.503	3.89	18.8			4.84	0.341	0.452	46.6	123
96.6	0.503	4.86	21.2	17.6	69.3	4.36	0.426	0.508	68.5	155
97.9	0.414	0.01	> 2000 psi	6.67					9.2	315
mean ± std dev:		3.97 ± 1.57	10.8 ± 7.10	12.4 ± 3.06	47.1 ± 20.4	2.92 ± 1.54	0.348 ± 0.138	0.280 ± 0.166	54.9 ± 28.5	152 ± 77.1

* for the full grain size distribution

** ratio of maximum reductive capacity (O_2 / 0.5M HCl)

Table 4.3. Iron Data for D4-92, C4688 (upgradient of D4-26)

depth (ft)	mass fraction < 4 mm	field reductive capacity* 1h 0.5M HCl (μmol/g)	field reductive capacity* column O_2 ox. (μmol/g)	maximum reductive capacity* 1h 0.5M HCl (μmol/g)	maximum reductive capacity* column O_2 ox. (μmol/g)	ratio capacity (O_2 / HCl)	reduced fraction field/maximum 1h 0.5M HCl	reduced fraction field/maximum average column O_2 ox.	total iron oxides* Fe^{II} 2 wk 5M HCl (μmol/g)	total iron oxides* Fe^{II+III} 2 wk 5M HCl (μmol/g)
78.1	0.496	4.30					0.377		79.6	150
80.6	0.471	2.21					0.194		54.7	110
82.6	0.379	0.32	water 83.5'	8.14			0.028		42.3	89.5
83.6	0.402	0.44		9.90			0.039		53.5	113
85.1	0.361	0.41	4.25	7.40		10.4	0.036	0.102	55.5	91.3
85.4	0.390	2.84					0.249			
86.1	0.390	2.30	6.54	8.93		2.85	0.202	0.157	41.0	85.2
87.4	0.608	3.69	12.63	13.7		3.42	0.324	0.303	76.0	143
87.6	0.608	6.02					0.528			
87.9	0.545	5.46					0.479			
88.6	0.545	5.78	10.59	13.7		1.83	0.507	0.254	71.0	146
88.9	0.545	4.33					0.380			
90.1	0.997	10.6	28.95		35.6	2.73	0.930	0.694	165	287
90.4	0.437	4.28				2.92	0.375			
91.6	0.444	3.80	8.96	11.3		2.36	0.334	0.215	60.6	123
91.6	0.444	3.71					0.326		60.1	124
91.9	0.459	5.31					0.466			
92.6	0.459	4.53	6.40	13.2		1.41	0.397	0.154	50.3	113
94.1	0.431	4.89		11.6			0.429		49.6	102
95.1	0.503	6.78	26.78	14.7	26.7	3.95	0.595	0.642	95.9	193
96.6	0.572	5.19		19.9		1.82	0.455		60.3	129
97.6	0.584	5.20	15.28	21.3		2.94	0.456	0.366	84.4	222
99.6	0.421	1.28		3.75			0.112		62.7	167
100.6	0.379	6.95	21.99	6.56	41.6	3.16	0.610	0.527	58.7	132
102.1	0.379	0.01				6.34	0.000		5.65	142
mean ± std dev:		4.26 ± 2.46	14.2 ± 8.81	12.0 ± 4.97	34.6 ± 7.50	2.98 ± 1.28	0.392 ± 0.204	0.341 ± 0.211	65.6 ± 33.0	144 ± 52.0

* for the full grain size distribution

** ratio of maximum reductive capacity (0_2 / 0.5M HCl)

Table 4.4. Iron Data for D4-93, C4689 (upgradient of D4-26)

depth (ft)	mass fraction < 4 mm	field reductive capacity* 1h 0.5M HCl (µmol/g)	field reductive capacity* column O_2 ox. (µmol/g)	maximum reductive capacity* 1h 0.5M HCl (µmol/g)	maximum reductive capacity* column O_2 ox. (µmol/g)	ratio capacity (O_2 / HCl)	reduced fraction field/maximum 1h 0.5M HCl	reduced fraction average column O_2 ox.	total iron oxides* Fe^{II} 2 wk 5M HCl (µmol/g)	total iron oxides* Fe^{II+III} 2 wk 5M HCl (µmol/g)
79.1	0.507	1.62					0.142		74.5	149
80.6	0.450	1.42					0.124		64.5	126
81.6	0.418	0.19					0.016		40.3	95.2
81.6	0.418	0.17	water 82.5'				0.015		41.9	125
82.9	0.521	2.19		12.45			0.192		86.5	169
84.1	0.409	0.72		9.04			0.064		50.2	97.4
85.6	0.958	4.63		18.82			0.406		132	260
86.6	0.401	0.85		5.49			0.074		47.9	96.0
88.1	0.737	5.28	17.78		53.8	3.37	0.463	0.426	98.9	163
89.1	0.491	4.38		12.18		6.72	0.384		58.2	113
91.1	0.671	5.59	35.95	16.85	58.1	6.43	0.490	0.862	111	203
93.1	0.476	3.68				3.45	0.323		62.8	145
93.1	0.476	3.63	16.88			4.65	0.318	0.405	66.9	153
94.1	0.404	2.64	failed	5.09			0.232		114	170
95.6	0.660	0.83	34.75	12.59		6.59	0.073	0.833	88.9	267
96.6	0.342	5.27	14.47	13.62	38.6	2.75	0.462	0.347	73.0	175
98.6	0.417	1.42				4.83	0.124		62.8	165
100.1	0.344	0.19					0.016		37.4	87.5
100.9	0.360	0.00					0.000		5.30	150
mean ± std dev:		2.75 ± 2.00	24.0 ± 10.5	11.8 ± 4.63	50.2 ± 10.2	4.80 ± 1.34	0.242 ± 0.176	0.575 ± 0.251	73.0 ± 32.9	161 ± 53.0

for the full grain size distribution

** ratio of maximum reductive capacity (0_2 / 0.5M HCl)

Table 4.5. Iron Data Summary for All Four Boreholes

borehole	field reductive capacity* 1h 0.5M HCl (μmol/g)	column O$_2$ ox. (μmol/g)	maximum reductive capacity* 1h 0.5M HCl (μmol/g)	column O$_2$ ox. (μmol/g)	ratio capacity (O$_2$ / HCl)	reduced fraction field/maximum average 1h 0.5M HCl	column O$_2$ ox.	total iron oxides* Fe^{II} 2 wk 5M HCl (μmol/g)	Fe^{II+III} 2 wk 5M HCl (μmol/g)
Up and down gradient of D4-37:									
D4-90, C4686 (up)	2.35 ± 1.87	9.16 ± 3.16	13.2 ± 6.17	34.9 ± 11.5	6.32 ± 5.26	0.190 ± 0.151	0.249 ± 0.112	49.2 ± 19.1	122 ± 52.6
D4-91, C4687 (dn)	3.97 ± 1.57	10.8 ± 7.10	12.4 ± 3.06	47.1 ± 20.4	2.92 ± 1.54	0.318 ± 0.126	0.300 ± 0.178	54.9 ± 28.5	152 ± 77.1
Up and down gradient of D4-26:									
D4-92, C4688 (up)	4.26 ± 2.46	14.2 ± 8.81	12.0 ± 4.97	34.6 ± 7.50	2.98 ± 1.28	0.358 ± 0.186	0.366 ± 0.227	65.6 ± 33.0	144 ± 52.0
D4-93, C4689 (dn)	2.75 ± 2.00	24.0 ± 10.5	8.00 ± 3.36	50.2 ± 10.2	4.80 ± 1.34	0.221 ± 0.161	0.477 ± 0.209	73.0 ± 32.9	161 ± 53.0
all wells	3.33 ± 0.93	14.54 ± 6.65	11.4 ± 2.32	41.7 ± 8.12	4.26 ± 1.63	0.272 ± 0.079	0.348 ± 0.098	60.7 ± 10.7	145 ± 16.7
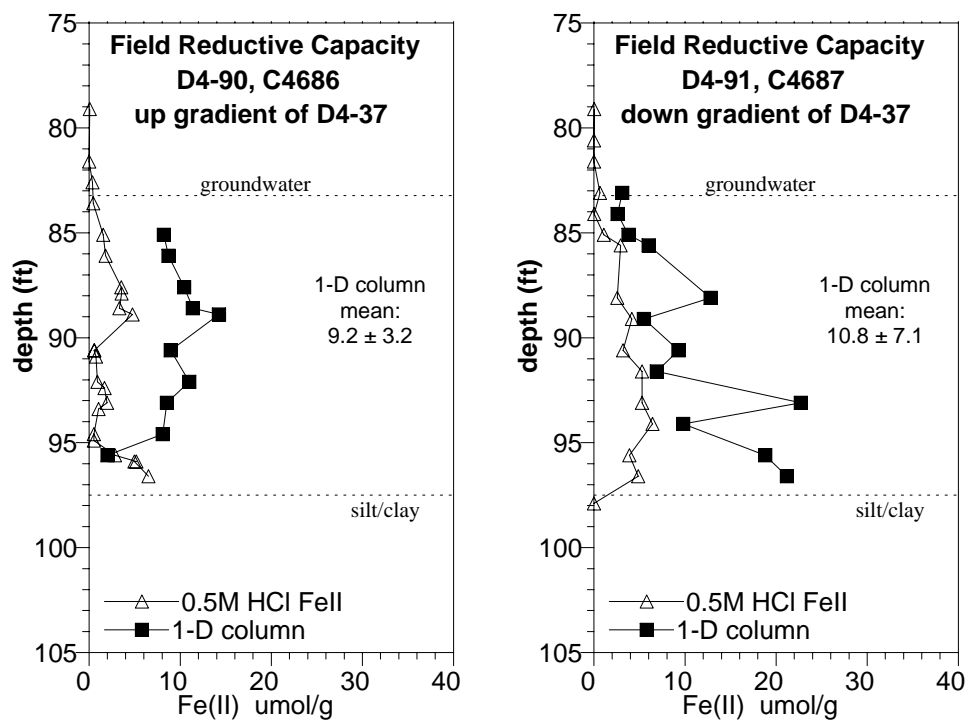
Figure 4.1.   Field Reductive Capacity in Boreholes C4686 and C4687 (up- and downgradient of well D4-37)
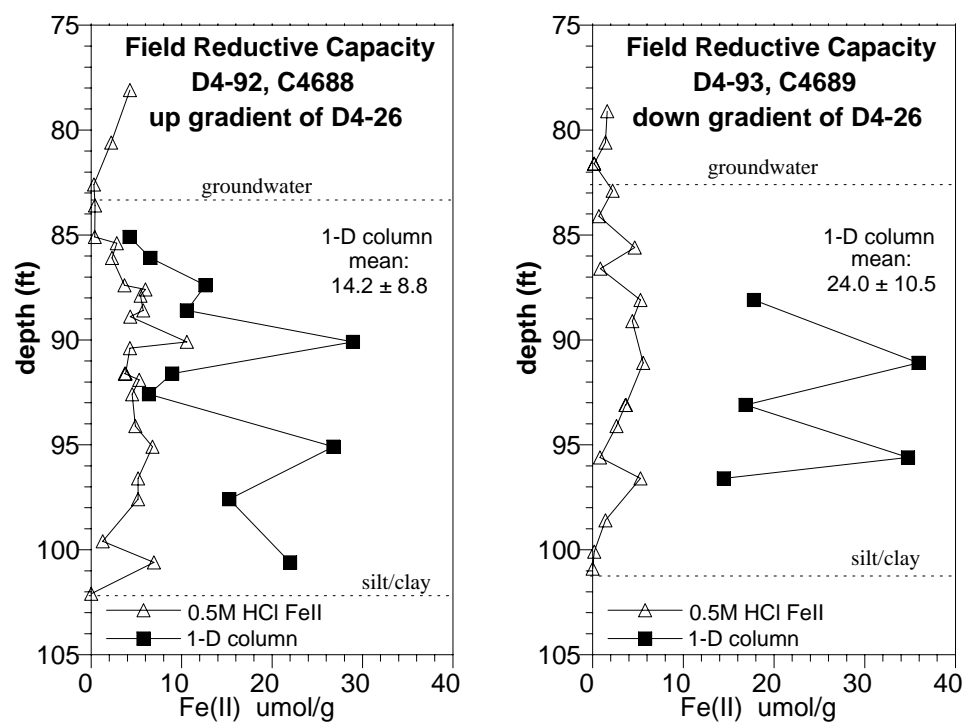
Figure 4.2.   Field Reductive Capacity in Boreholes C4688 and C4689 (up- and downgradient of well D4-26)

4.2   Maximum (Laboratory) Reductive Capacity

The 100D sediment cores that were reduced with excess dithionite for 5 days to achieve a maximum reduction showed 2 to 3 times more reductive capacity than field-reduced sediments. The laboratory reductive capacities of 35 µmol/g near well D4-37 (upgradient well C4686, shown in Figure 4.3) and 47 µmol/g (downgradient, well C4687) were about four times greater than the field-reductive capacity. There were only three 1-D column oxidations conducted per borehole but significant variability in lab-oratory reductive capacities, which indicates variability in the reducible iron mass because the dithionite treatment was uniform. The 1-hr ferrous iron extractions showed little variability with depth and no apparent trends. Comparing the 1-D column oxidation in upgradient borehole C4686 field-reduced (Figure 4.1a) with laboratory reduced (Figure 4.3a) sediment shows higher values at 89 ft and lower values at 96 ft, likely reflecting some differences in reducible iron content with depth. Comparing the 1-D column oxidation in downgradient borehole C4687 field-reduced (Figure 4.1b) and laboratory-reduced (Figure 4.3b) sediments also shows similarities, with a low value at 94 ft and high at 97 ft.
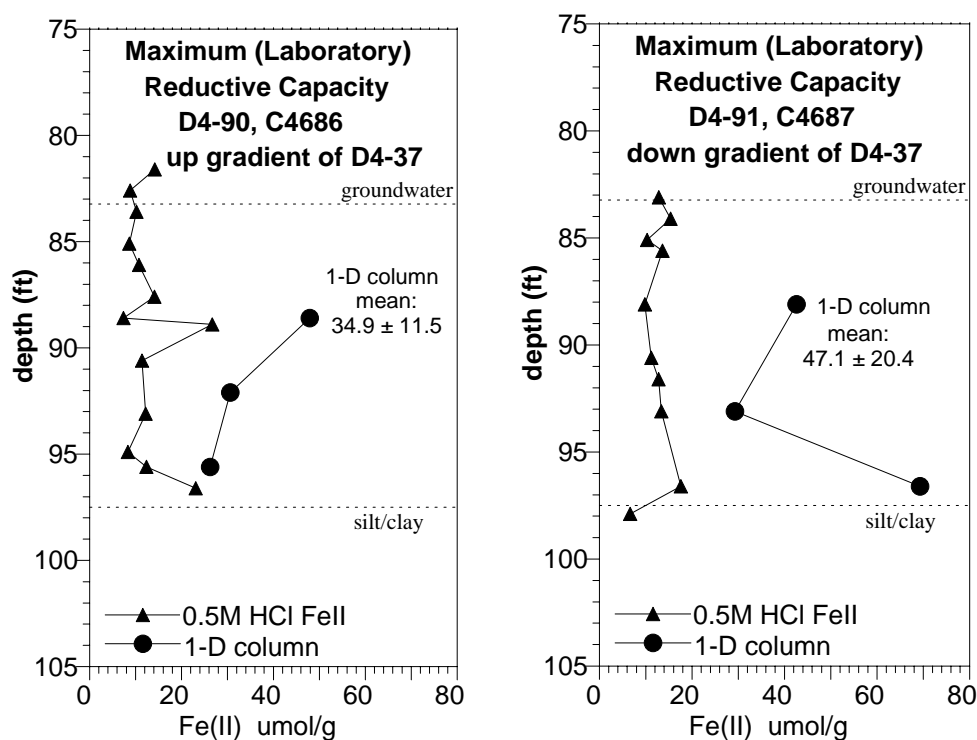
Figure 4.3.   Maximum (lab-reduced) Reductive Capacity in Boreholes C4686 and C4687 (up- and downgradient of well D4-37)

The laboratory reductive capacity of 35 µmol/g near well D4-26 (upgradient well C4688) (Figure 4.4) and 50 µmol/g (downgradient well C4689) were also about four times greater than the field reductive capacity (same trend observed near well D4-37). Comparing the 1-D column oxidation in upgradient borehole C4688 in field-reduced (Figure 4.2a) and laboratory reduced (Figure 4.4a) sediment showed one similarity. There were high field and laboratory reductive capacities at 101 ft, but the 92-ft depth, with a low trend in field reductive capacity, was not measured for laboratory reductive capacity.
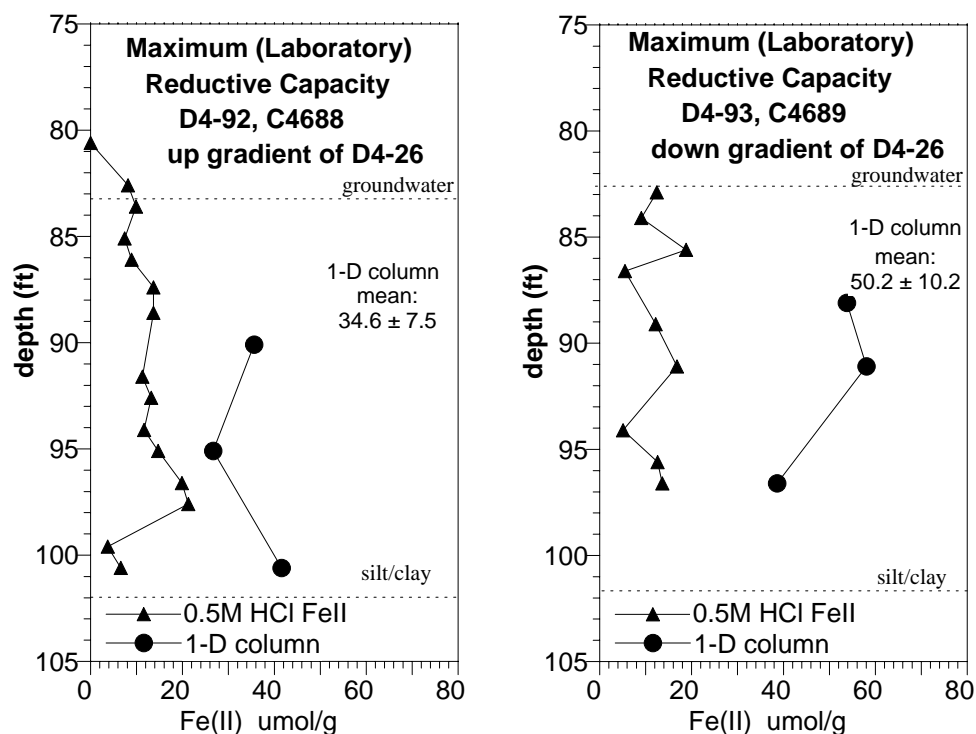
Figure 4.4. Maximum (laboratory-reduced) Reductive Capacity in Boreholes C4688 and C4689 (up- and downgradient of well D4-26)

Comparing the 1-D column oxidation in downgradient borehole C4689 in field- (Figure 4.2b) and laboratory-reduced (Figure 4.4b) sediments showed similarities, with a high reductive capacity at 91 ft and low at 97 ft. The ferrous iron extraction again showed few trends and was thus of little use.

4.3 Total Iron Oxides in Sediment

Total iron oxides measured in all sediment cores with a 5 M HCl extraction for 2 weeks showed the presence of a significant mass of iron oxides and some depth trends as well. The average ferrous and ferric iron oxide content of 145 ± 16.7 μmol/g in four boreholes (68 values) was about 10 times the average field reductive capacity (14.5 ± 6.65 μmol/g) and about 3 times the laboratory/maximum reductive capacity (41.7 ± 8.12 μmol/g). In other words, about 10% of the iron oxides were being dissolved or reduced by the dithionite treatment at the field scale, which is consistent with the trend observed previously for this sediment and three others (Fort Lewis and Vancouver, WA; Moffet Field near San Francisco) (Szecsody et al. 2004b). The fact that there were no large differences in iron oxide content with depth indicates, at least geochemically, that dithionite treatment could be an effective remediation technology. However, this statement assumes that hydraulically all sediments can be contacted and thus reduced, and there are no significant high-flow channels that are laterally extensive.

Trends in total iron oxides with depth reflected geochemical heterogeneity (i.e., no additional complications due to dithionite treatment). Near well D4-37, both up- and downgradient boreholes (C4686 and C4687 in Figure 4.5) showed high iron oxide content at >95 ft and low content at 90 to 92 ft.
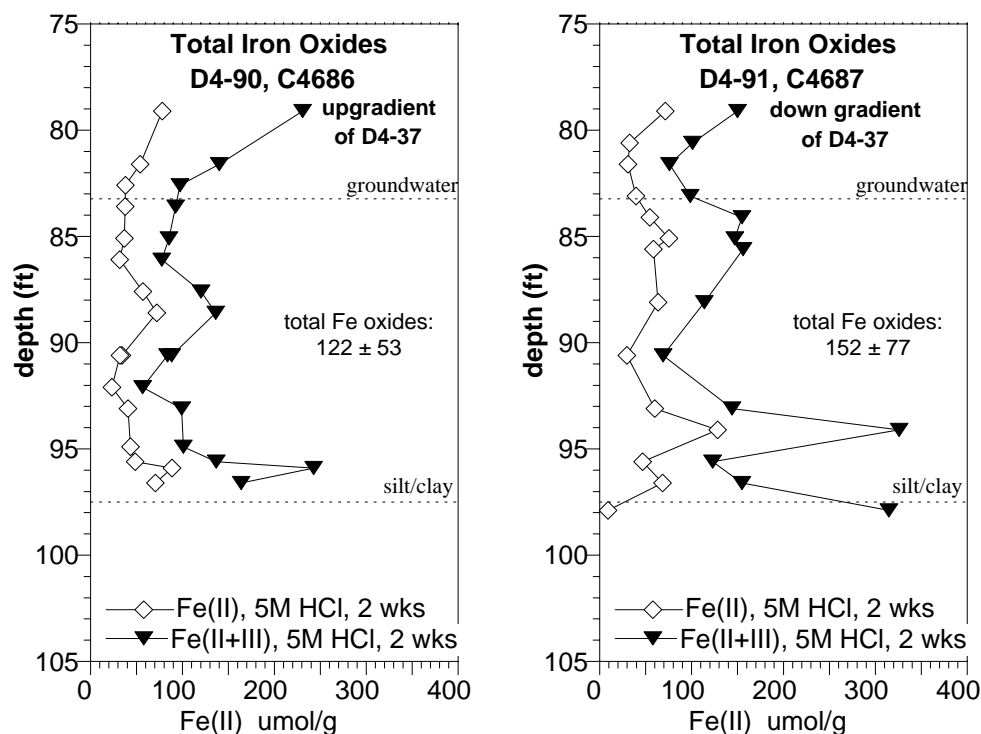
Figure 4.5. Total Ferric and Ferrous Oxides Extractable with 5 M HCl in Boreholes C4686 and C4687 (up- and downgradient of well D4-37)

There is a somewhat higher hydraulic conductivity at the 95-ft depth and low values at the 88–91 ft depth. This does not support the hypothesis that high-flow regions may have lower iron oxide content (in fact, the opposite is observed). Additional correlations between geochemical and physical depth data are presented in Section 5.

Near well D4-26, up- and downgradient boreholes (C4688, C4689) (see Figure 4.6) showed high iron oxide content at the 95–97-ft depth and low iron oxide content at the 84–85-ft depth. Additional high values in individual wells were not correlated between the two boreholes (90-ft depth for C4688, 86-ft depth for C4689).

4.3.1 Comparison of the Reductive Capacity Measurement Methods

The field and laboratory reductive capacities measured by a 1-D column oxidation method (used in 1997, 1999, and 2002 studies) and a 1-hr ferrous iron extraction using 0.5-M HCl show significant differences. As described in Section 3, these methods are significantly different, but studies with a Fort Lewis, Washington subsurface sediment (separate study) showed similar reduction values for fully reduced sediment and lower values for the 1-hr iron extraction relative to the column oxidation method for partially reduced sediment. Results in this study with Hanford 100D sediments show significant differences in the two measurement methods (Table 4.1). Trends in field reductive capacity (Figures 4.1 and 4.2) and laboratory reductive capacity (Figures 4.3 and 4.4) show significant vertical variability with the column oxidation method that is not apparent in the 1-hr iron extraction. Trends in the 2-week total
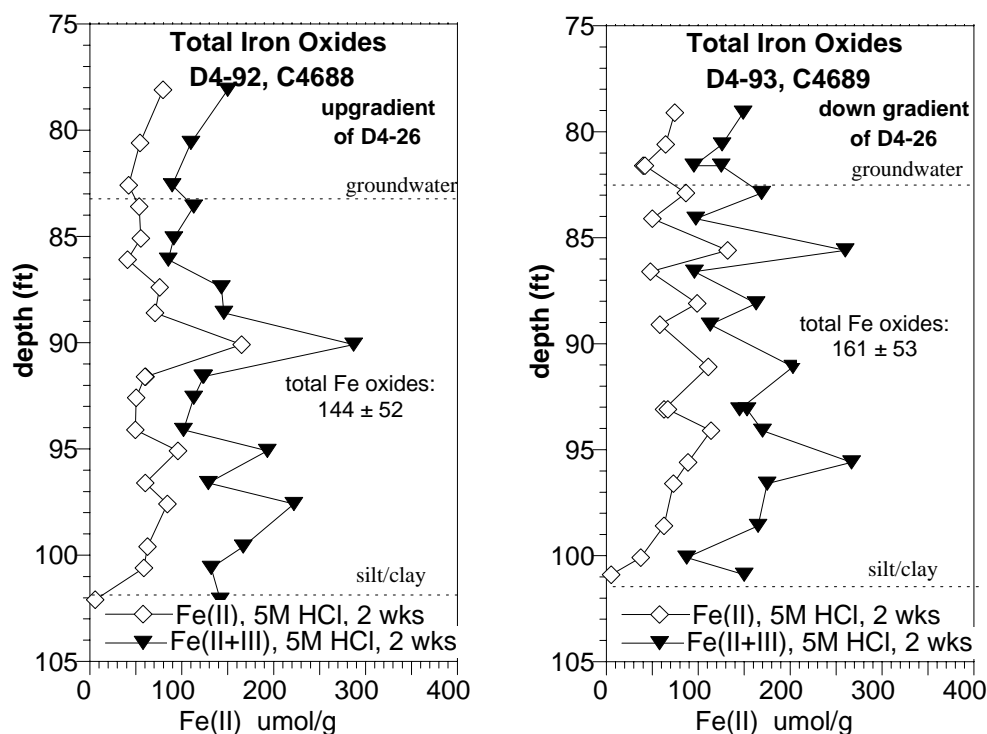
Figure 4.6. Total Ferric and Ferrous Oxides Extractable with 5 M HCl in Boreholes C4688 and C4689 (up- and downgradient of well D4-26)

iron extraction with 5 M HCl (Figures 4.5 and 4.6) show significant vertical variability, which correlates to some of the trends in reductive capacity (column oxidation method). Thus, it appears that longer contact times in experiments (e.g., 2 to 4 weeks for column oxidation or 2 weeks for the 5-M HCl total iron extraction) may access reactive sites that short contact-time experiments (1-hr, 0.5-M HCl iron extraction) do not. This may include reductive sites in microfractures (accessed by aqueous diffusion, which could take tens to hundreds of hours), iron oxides covered by other Fe/Al/Mn oxides (additional surface diffusion time needed to access sites), or redox-reactive ferrous phases within minerals such as 2:1 smectite clays. Given the hundreds to thousands of hours of contact time at the field scale, laboratory experiments with longer contact times are more likely to reflect field-scale conditions. Thus, the vertical trends in reductive capacity in each borehole indicated by the column oxidation method are considered to represent field-scale conditions more accurately than the 1-hr iron extraction by 0.5-M HCl.

A quantitative comparison of reductive capacities made of the column oxidation and 1-hr iron extraction methods also showed that 1-hr iron extraction was not representative. Each borehole had 8 to 22 data points on the same sediment sample (both methods). The ratio of reductive capacity obtained by column oxidation to 1-hr HCl extraction (Table 4.5, "ratio capacity" column) showed the averages for each borehole (6.3, 2.9, 3.0, 4.8) that are statistically different (95% confidence level). A plot of reductive capacity by the two methods on the same sediment samples (Figure 4.7) shows only a fair trend (R = 0.75). Histograms of this ratio of capacity also (Figure 4.8) show no similarities between boreholes (which would be observed if 1-hr iron extraction had the same trend as column oxidation).
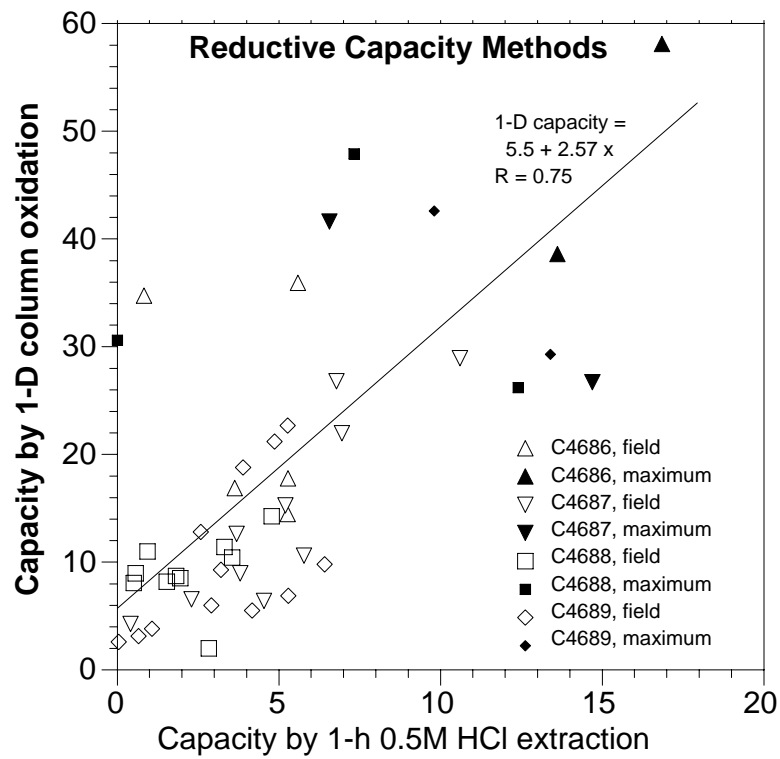
Figure 4.7. Reductive Capacity Measurement Comparison: 1-D Column Oxidation and 1-hr Iron Extraction with 0.5 M HCl
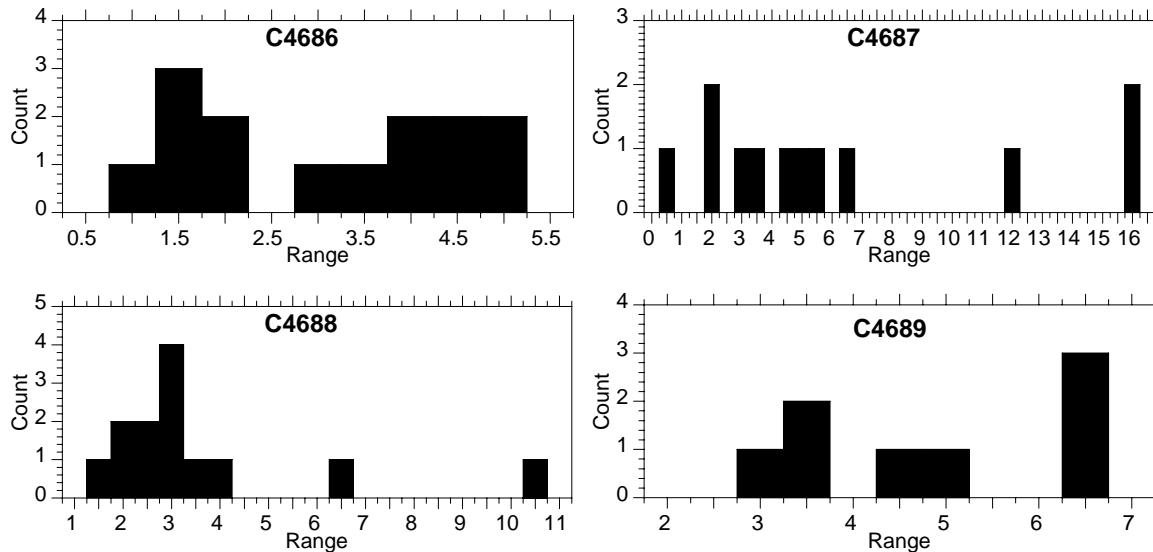
Figure 4.8. Histograms of the Ratio of Reductive Capacity by 1-D Column Oxidation to 1-hr Iron Extraction by 0.5 M HCl for Each of the Four Boreholes

4.3.2 Saturated Hydraulic Conductivity

The calculated saturated hydraulic conductivity (K_{sat}) from the 78 sieve/hydrometer analysis (see Appendixes J through M) indicated both high and low hydraulic conductivity zones. Boreholes C4686 and C4687 (up- and downgradient of D4-37) (Figure 4.9) both showed a higher conductivity zone near the water table (83 to 86 ft), a low conductivity zone at 88 to 92 ft, and a high-conductivity zone at the bottom of the aquifer (93 to 97 ft). Pictures of the cores at 6-inch intervals (see Appendix H) show some features indicated by the calculated hydraulic conductivity. Borehole C4686 has mixed gravel/sand and sand/gravel from 75 to 85 ft (some pictures are predominantly sand, some gravel), which accounts for the variation in K_{sat}. Borehole C4687 pictures show predominantly sand for the 75 to 82-ft depth and relatively uniform K_{sat} values. Below 85 ft, the sediment changes from tan to gray, indicating some dithionite treatment. The 1 to 2 order of magnitude decrease in hydraulic conductivity from 85 to 88 ft can be qualitatively observed in pictures from the change from sand/gravel to increasing silt/clay.

Of the three methods to calculate saturated hydraulic conductivity from the grain size distributions, the modified Hazen and Masch and Denny formulas produced similar results, but the Hazen results showed some differences. The Hazen formula, originally developed using uniform sands, relies only on the 10% passing grain size so does not accurately distinguish between uniform and poorly sorted distributions that have the same 10% grain size but likely different hydraulic conductivity. The modified Hazen formula is an empirical relationship between the 25% passing grain diameter and measured hydraulic conductivity values for several Hanford sediments (i.e., a Hanford-specific empirical relationship). The modified Masch and Denny formula uses the mean grain size and the standard deviation, so it accounts for the uniformity of grain sizes and is considered more accurate.
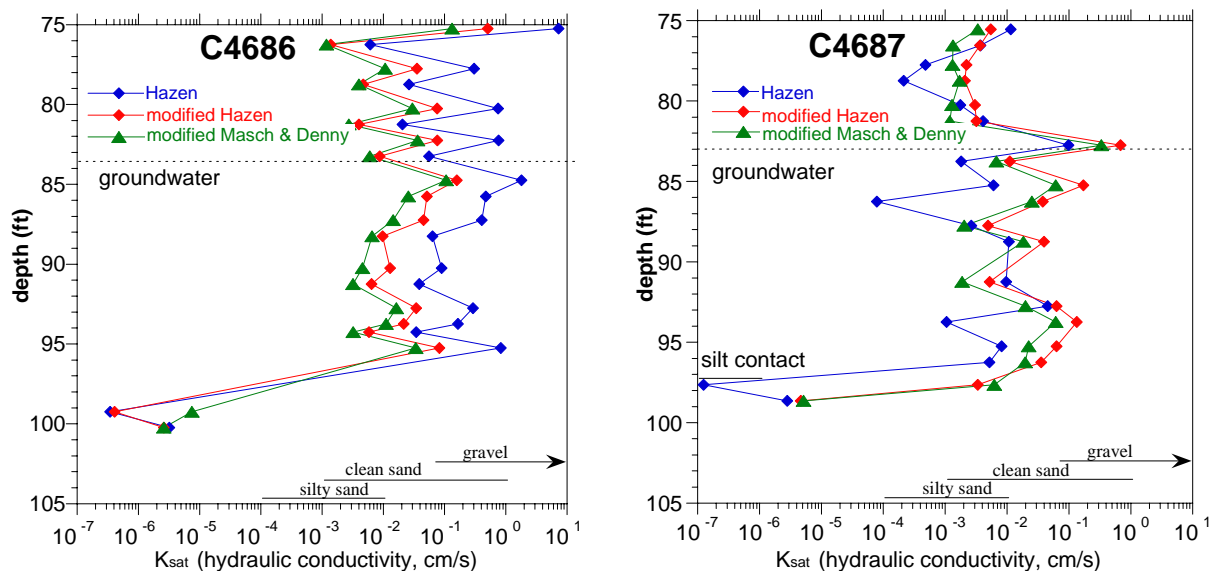
Figure 4.9. Calculated Saturated Hydraulic Conductivity (3 methods) from Sieve/Hydrometer Distributions for Boreholes C4686 and C4687 (up- and downgradient of well D4-37)

4.13

The calculated saturated hydraulic conductivity for boreholes C4688 and C4689 (up- and down-gradient of D4-26) (Figure 4.10) show some similar trends, including a high-conductivity zone near the water table (82- to 86-ft depth), a low-conductivity zone at 95 to 96 ft, and a high conductivity zone at 97 to 101 ft, next to the silt contact. There are additional high- and low-flow zones that are different in the two boreholes. Pictures clearly show the presence of gravel in the high-flow zone at 97 to 101 ft (see Appendix H). Other high- and low-flow zones are unclear from the pictures, which also show evidence of reduction below 85.5 ft, as described in Section 4.4.
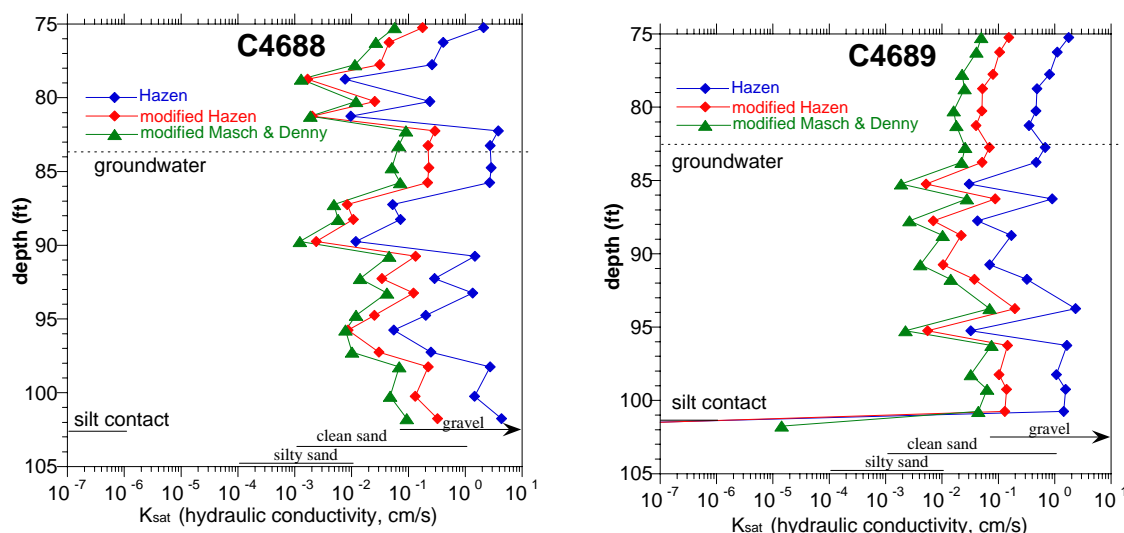
Figure 4.10. Calculated Saturated Hydraulic Conductivity (3 methods) from Sieve/Hydrometer Distributions for Boreholes C4688 and C4689 (up- and downgradient of well D4-26)

4.4 Core Pictures

High-resolution (2 MB) pictures were taken of each end of the 6-inch-long by 4-inch-diameter cores that were used for geochemical analysis (see Appendix H). As described in Section 4.3, gravel and sand grain sizes are apparent in the pictures, so a qualitative estimate of the hydraulic conductivity is possible, though percent silt/clay cannot be determined. In the absence of differences in sediment size and mineralogy, there is a general color change associated with increasing dithionite treatment, as described in Section 3 (Figure 3.1, different treatments on the same sediment sample). Differences in color for the core pictures were due to changes in dithionite treatment, grain size, mineralogy, and photography. Considerable effort was made to color balance pictures by using a rainbow-colored strip (in each picture, to the side of the core) and digitally altering each strip to a standard. This was only partially successful.

Inspection of the 161 pictures from the four boreholes clearly show tan sediments above the water table (~83 ft, known to be oxic), brown (moist) colored sediments from 83 to 85.5 ft (still appear to be oxic), then either brown or gray sediments at greater depth (some sediments appear reduced, some appear oxic). Pictures are useful in noting some dithionite treatment characteristics. While the aquifer zone is gray, the underlying aquitard (silt/clay unit) is tan. This interface may be mixed sand/silt, which can appear as spotty gray patches in brown sediment. This may be caused by dithionite traveling through higher flow zones (but not into silt/clay zones; see C4688, 102 ft, 5 inch depth) (see Appendix H).

A more careful comparison of the highly reduced zones, as defined by field-reductive capacity (by 1-D columns) (Figures 4.9 and 4.10) with the core pictures, does not show a clear correlation. In borehole C4686 (Figure 4.8a), there is a relatively uniform zone of low reduction from 85 to 95 ft, but pictures show gray sediment from 85 ft, 5 inches to 89 ft, then tan sediment below that. In borehole C4687, there is highly reduced sediment at 93 to 97 ft and moderate reduction at 88 ft (Figure 4.9b). Pictures at 93 to 97 ft are gray like the 88-ft picture. In borehole C4688, there is high reduction from 95 to 101 ft and a high point at 90 ft, and pictures are gray from 96 to 101 ft (and at 88.5 ft). In borehole C4689, highly reduced sediment exists at 91 and 96 ft, though the picture at 91 ft is gray/brown and at 96.5 ft dark gray.

5.0   Discussion

5.1   Reductive Capacity and Vertical Spatial Variability

The purpose of this laboratory investigation is to determine whether physical and/or geochemical heterogeneity in the aquifer is causing premature failure of the ISRM treatment zone; or, more specifically, whether there are high flow zones, low iron zones or a combination of high flow/low reduction zones that cause portions of the barrier to have limited reductive capacity. A comparison of the vertical distribution of field reductive capacity, saturated hydraulic conductivity, and total iron oxide in each borehole (see Figures 5.1 through 5.4) do show significant vertical variability. For each data set, the aquifer average ± standard deviation is listed on graphs, and zones are highlighted that are less or greater than 50% of the mean value.

For comparison, values for low and high field capacity, hydraulic conductivity, and iron oxide content are defined. Low capacity is defined as 1/3 the average field capacity of 11.2 µmol/g. The average field capacity has a longevity of ~85 pore volumes or 9.6 years (see Section 2) with 5.1 mg/L O_2, 2 mg/L Cr, and 60 mg/L NO_3, so low capacity is ~ 4 µmol/g with a longevity of 30 pore volumes or 3.4 years. Moderate field capacity is defined as 4 to 6 µmol/g. High field capacity is defined as 50% greater than the average or > 17 µmol/g. Given an average hydraulic conductivity of 0.035 cm/s, a low-K zone is 50% lower, or < 0.017 cm/s and a high-K zone is 50% higher, or > 0.05 cm/s. Given the average total iron oxide content of 145 µmol/g, a high Fe-oxide zone is 50% greater, or > 215 µmol/g, and a low Fe-oxide zone is 50% less, or < 72 µmol/g.

In borehole C4686 (upgradient of D4-37) (Figure 5.2), there appear to be high flow zones at 85 and 96 ft, with a corresponding low field reductive capacity near the water table (based on the less definitive iron extraction data shown in Figure 4.1) and at 95.5 ft. There is also a high iron oxide content at the 96-ft depth. Although vertical variability is low in this borehole compared with other boreholes, there may be a correlation between the high flow region and low field reductive capacity at 96 ft. In borehole C4687 (Figure 5.2, downgradient of D4-37), there is greater geochemical variability than in the upgradient borehole (C4686). There appear to be high conductivity zones at 82 to 87 ft (similar to C4686) and at 94 ft, with a corresponding low field reductive capacity zone near the water table (83 to 86 ft). There is also a high field reductive capacity zone at 93 to 97 ft with corresponding higher total iron oxide content. At a depth of 89 ft, there is a zone with moderate field capacity (6 µmol/g).

In borehole C4688 (upgradient of D4-26; Figure 5.3), high conductivity zones appear at 82 to 87 ft, 91 to 94 ft, and 98 to 102 ft, but only low field capacity at 85 ft (near the water table). There is a moderate field capacity at 93 ft (6 µmol/g) and high field capacity at 90 ft and 95 to 101 ft. Therefore, at the water table, high hydraulic conductivity and low field capacity are present, but at 90 ft, low-K and high capacity are present, and at 98 to 101 ft, high-K and high field capacity are present. In borehole C4689 (downgradient of D4-26) (Figure 5.4), a high-conductivity zone appears at 94 ft and from 96 to 101 ft, but there is no corresponding low field reductive capacity (values vary with depth, but all are relatively large). No 1-D column data were available near the water table at this borehole location, so the reductive capacity of this interval is not well characterized.
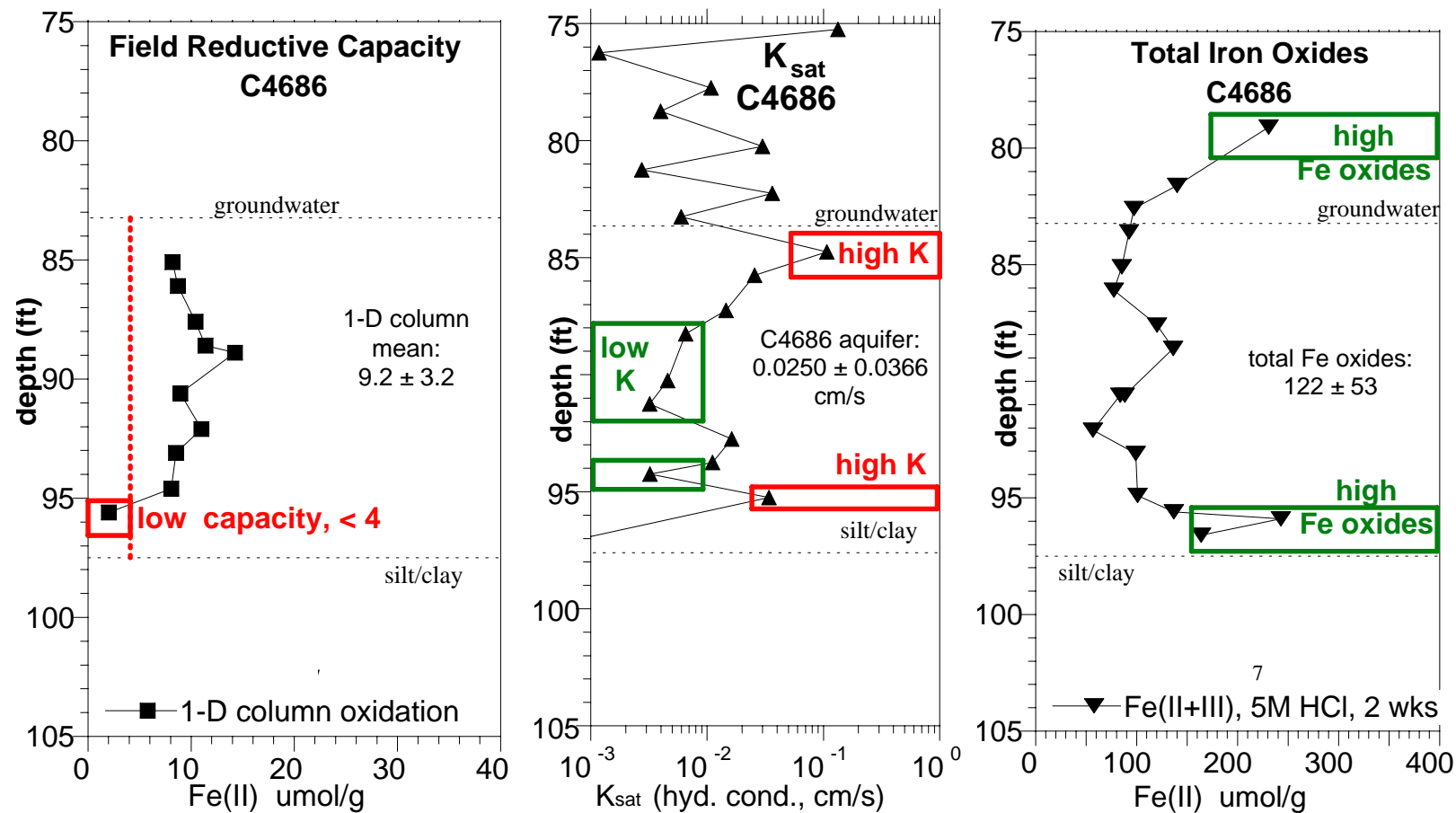
Figure 5.1. Comparison of Vertical Variability of a) Field Reductive Capacity, b) Saturated Hydraulic Conductivity, and c) Total Iron Oxides for Borehole C4686, D4-90 (upgradient of D4-37)
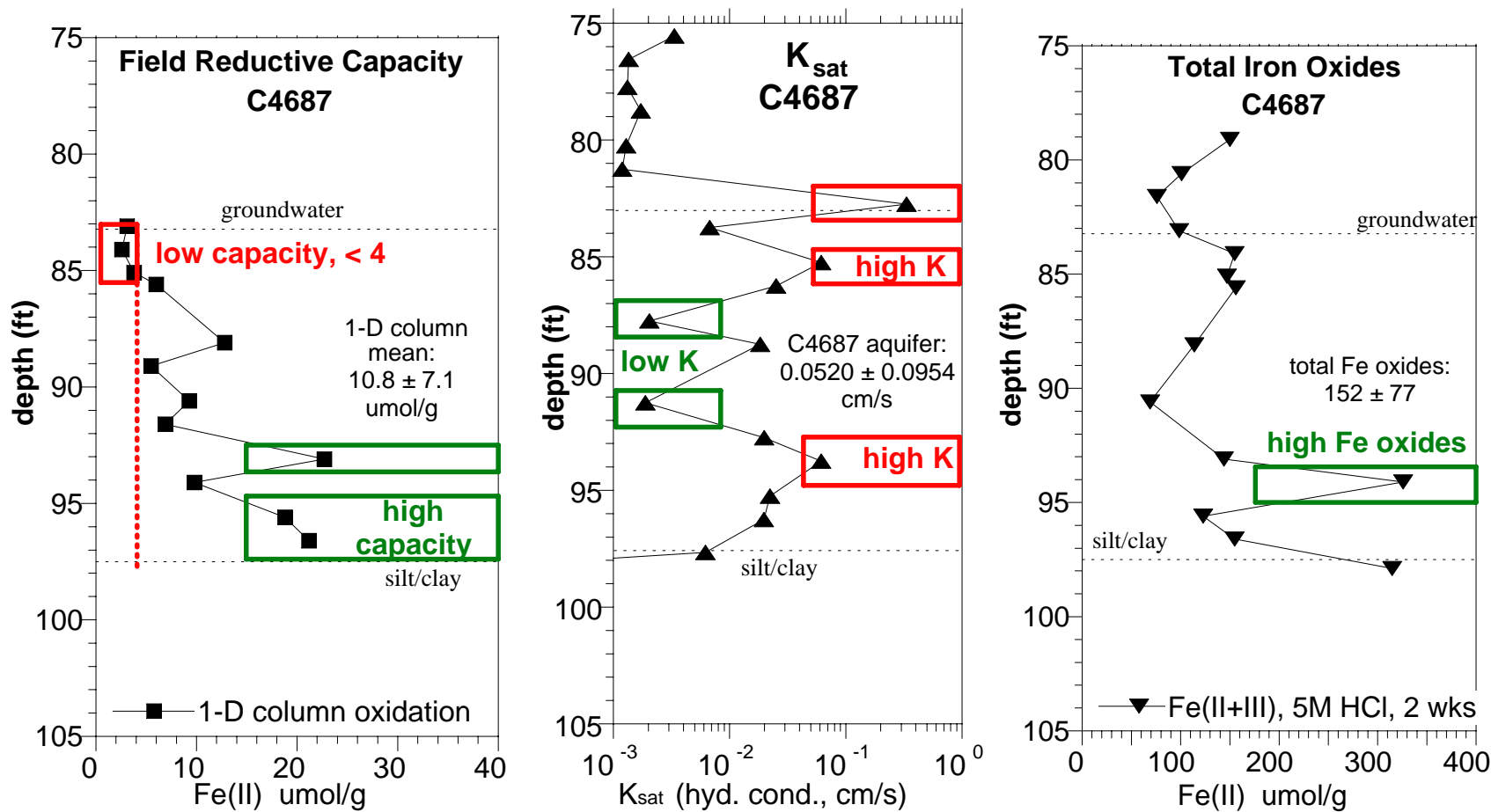
Figure 5.2. Comparison of Vertical Variability of a) Field Reductive Capacity, b) Saturated Hydraulic Conductivity, and c) Total Iron Oxides for Borehole C4687, D4-91 (downgradient of D4-37)
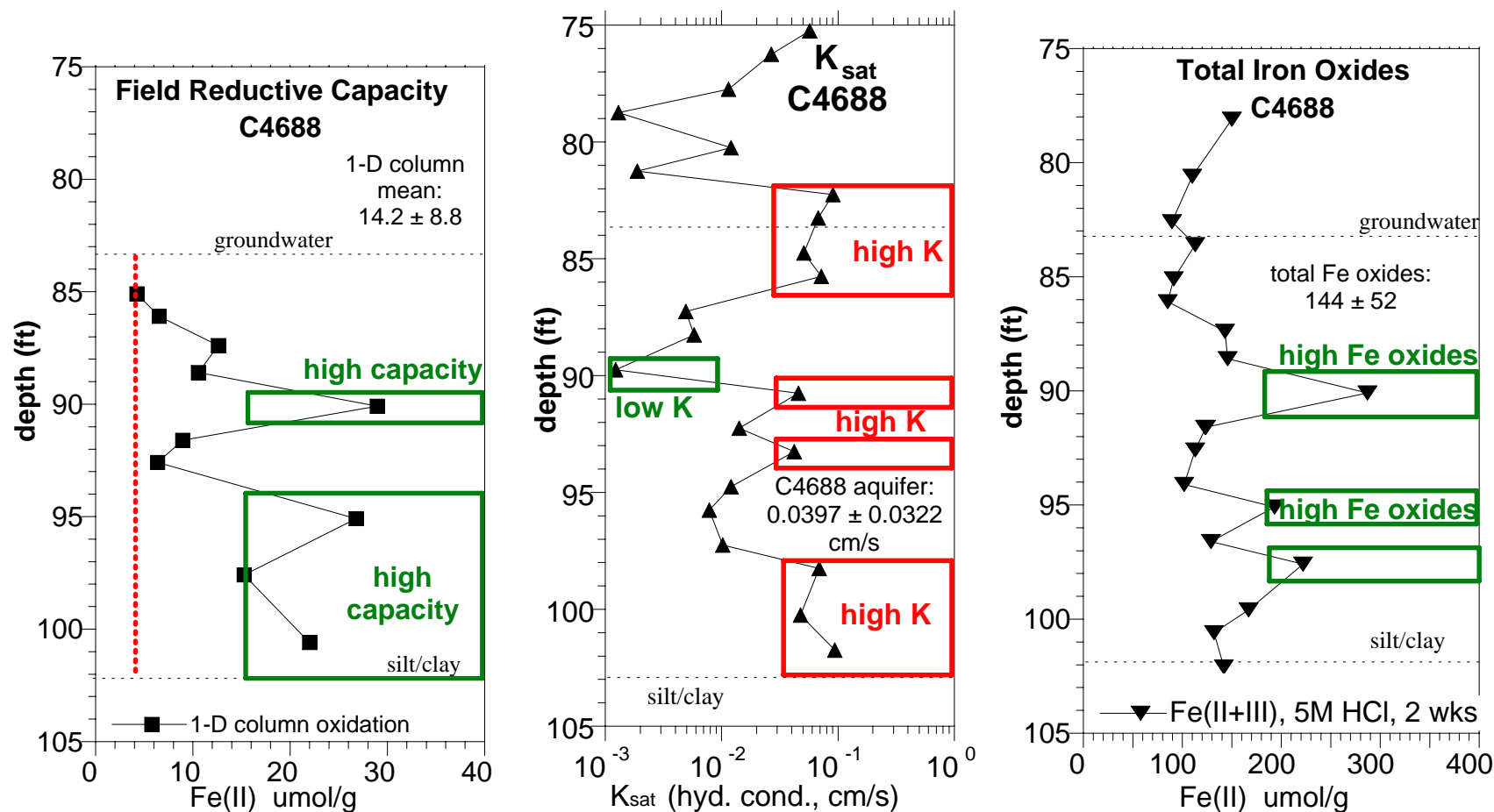
Figure 5.3. Comparison of Vertical Variability of a) Field Reductive Capacity, b) Saturated Hydraulic Conductivity, and c) Total Iron Oxides for Borehole C4688, D4-92 (upgradient of D4-26)
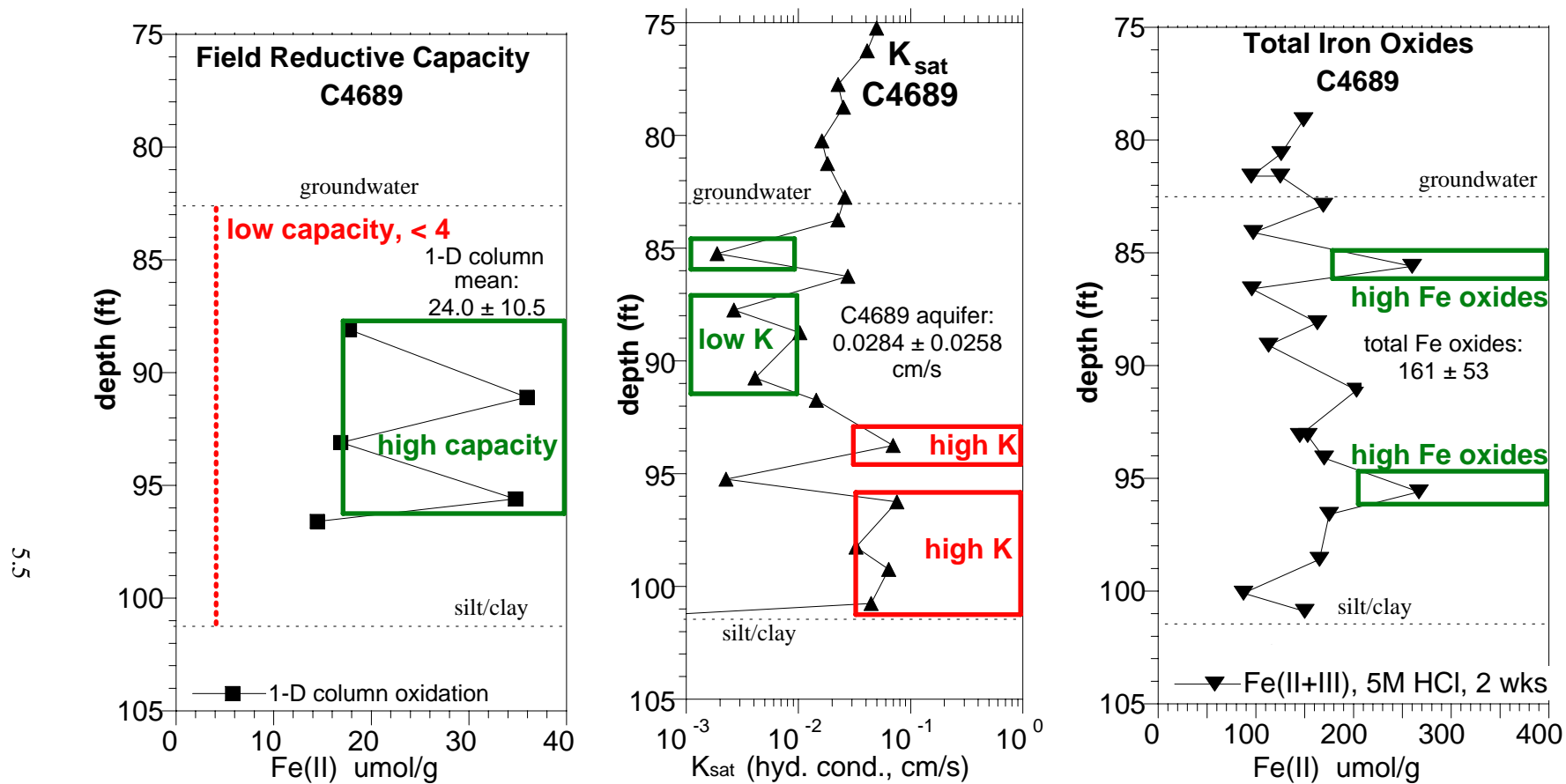
Figure 5.4. Comparison of Vertical Variability of a) Field Reductive Capacity, b) Saturated Hydraulic Conductivity, and c) Total Iron Oxides for Borehole C4689, D4-93 (downgradient of D4-26)

The average field reductive capacity was 13.64 ± 7.79 µmol/g (n = 37) for these four 2005 boreholes, determined by 1-D column oxidation, and the laboratory (maximum) reductive capacity was 41.7 ± 8.12 µmol/g. The average calculated saturated hydraulic conductivity of the aquifer for all four boreholes was 0.0348 ± 0.0498 cm/s (n = 59). For comparison, three boreholes cored in 2002 had an average field reduction of 10.6 ± 6.6 µmol/g and average laboratory (maximum) reductive capacity of 40 ± 15 µmol/g (Appendix F, Table F.3). Three boreholes cored in 1999 had average field reduction of 11.2 ± 7.4 µmol/g and average laboratory (maximum) reductive capacity of 17.4 ± 5.3 µmol/g (Appendix F, Table F.2). The original field-scale 100D area proof-of-principle test in 1997 had an average laboratory (maximum) reductive capacity of 24.3 ± 5.3 µmol/g. Therefore, the average amount of reduction in the 2005 boreholes corresponds well to previous averages and indicates that average in situ conditions near wells D4-26 and D4-37) still show significant reductive capacity.

The geochemical and geohydrologic data compiled in this report were collected to determine whether specific depths indicate low reductive capacities that result in premature chromate breakthrough at the 100D Area ISRM barrier. One generalization that can be made is that the field reductive capacity is low near the water table. In addition, data from three of the four boreholes indicate a high hydraulic conductivity near the water table. These conditions support the hypothesis that the observed barrier degradation is caused in part by reoxidation of sediments near the water table due to seasonal fluctuations in the water level and probable higher concentrations of dissolved oxygen, chromate, and nitrate contamination at the top of the aquifer. This hypothesis is also supported by MLS data that show correlations for three of eight wells with higher chromate levels near the water table with lower values at greater depth (Appendix G).

In addition to the treatment zone degradation observed near the water table, only one location deeper in the aquifer (C4686 at 96 ft) has low capacity (< 4 µmol/g) with corresponding high hydraulic conductivity. There are two additional locations depths with moderate capacity (<6 µmol/g; C4688 at 93 ft; C4687 at 89 ft), but these depths have low or average hydraulic conductivity. Zones of high field capacity exist in both high and low hydraulic conductivity zones (i.e., high capacity exists not only in low-K zones).

5.2 Physical Flow Control of Field Reductive Capacity

If preferential groundwater flow were the primary mechanism causing the observed barrier degradation at the 100D ISRM site (hypothesis 1), an inverse relationship between formation permeability and sediment reductive capacity should be observed (i.e., high hydraulic conductivity zones would correspond to low field reductive capacity). However, high conductivity zones may also receive more dithionite during treatment, so this hypothesis may be better observed when most of the sediment reductive capacity has been depleted in the field (i.e., there may be a better correlation in 10–15 years). A plot of the saturated hydraulic conductivity and the field reductive capacity for all four boreholes (Figure 5.5a) shows absolutely no correlation, implying that hypothesis 1 is not correct. Considering just the up-gradient boreholes, which should be more oxidized (Figure 5.5b), there is still no correlation. Therefore, although the calculated hydraulic conductivity and EBF indicate high flow zones, there are no corresponding low reductive capacity zones.
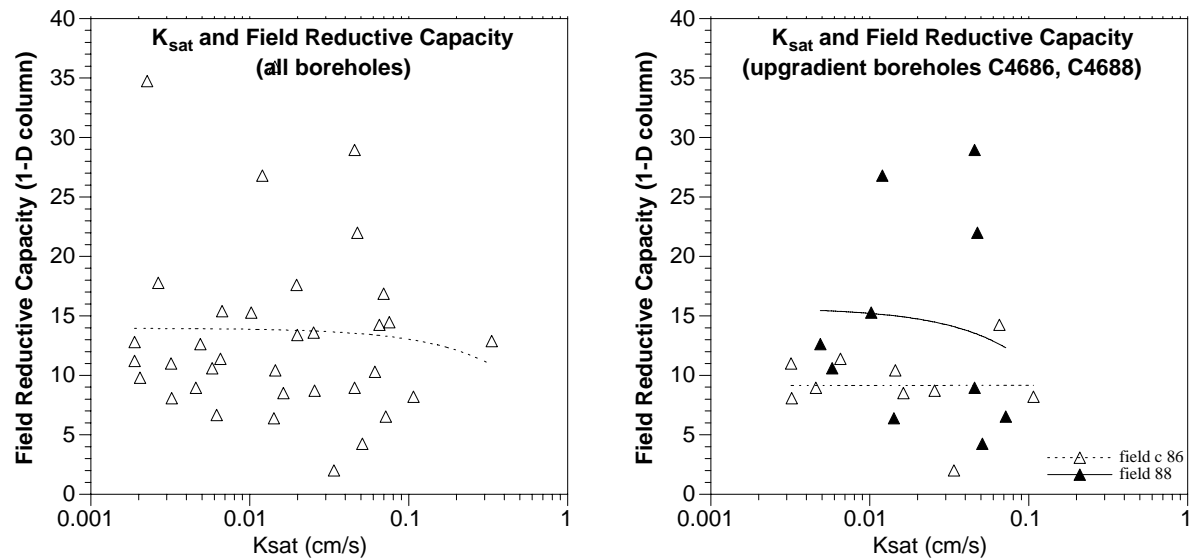
Figure 5.5. Correlation Between the Saturated Hydraulic Conductivity and Field Reductive Capacity for a) All Four Boreholes and b) Upgradient Boreholes C4686 and C4688

Data from an EBF for well D4-26 in 2002 indicate a high flow zone from 95 to 99 ft (Figure 5.6), a depth similar to that of a high flow zone indicated by up- (C4688 in Figure 5.3) and downgradient boreholes (C4689 in Figure 5.4). It is therefore likely that this high flow zone is laterally continuous for tens of feet. However, there is no corresponding low field reductive capacity associated with this zone. The upgradient borehole (C4688, Figure 4.1) shows high field reductive capacity in this zone, whereas the downgradient well (C4689, Figure 4.1) shows low reductive capacity in this zone. The EBF data for well D4-25 (35 ft from D4-26) show a significantly different profile overall profile (but high K zone ~96 to 98 ft), so it also indicates a lack of lateral continuity.
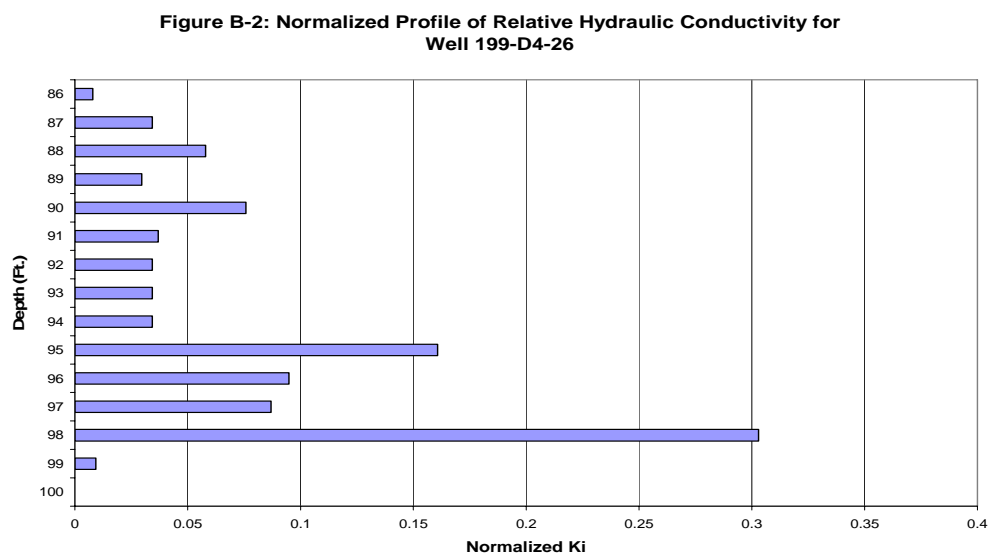
Figure 5.6. Relative Hydraulic Conductivity for D4-26 from EBF Data in 2002 (Appendix N)

A larger-scale measure of the existence of high-conductivity zones was determined by using the EBF tests on 25 wells in 2002 (Appendix N). The plots of normalized profiles show the relative hydraulic conductivity for 1-ft vertical intervals in the well. A well with "high flow zones" is defined by two 1-ft sections that have > 50% of the total flow in the well. Using this definition, 12 wells have high flow zones and 13 are relatively uniform. Further analysis of these data could be made to develop a standard deviation to compare with saturated hydraulic conductivity standard deviations to see if these values calculated from sieve analysis are representative of the vertical variation found at the field scale. These larger-scale EBF data indicate significant high-K channels at half of the wells tested. A second EBF testing campaign was conducted in 2004. However, due to data quality problems associated with induced turbulence in the well bore during these tests, results from this campaign are not included in this report.

Lateral continuity of high-K zones can be obtained by comparing EBF profiles in nearby wells, which are 35 to 40 ft apart. Although geostatistical analysis of these data would provide a more useful measure of connectivity, a rough indication of lateral correlation can be made by comparing adjacent wells. There were 16 pairs of wells (9/10, 10/11, 25/26, 62/63, 63/64, 64/65, 65/66, 66/67, 67/68, 68/69, 69/70, 70/71, 71/72, 72/73, 73/74, and 74/75) that all showed different profiles with the nearby well, and one pair (71/72, Appendix N) that showed a similar profile with a high-K zone at 93 ft. Additional correlations may exist if the elevations between wells are corrected and the possibility of dips in stratigraphy between locations is considered. Based on this rough approximation, 94% of the well pairs indicated that high-K zones were not laterally continuous at 40 ft. Thus, while there are significant high-K zones, the lateral continuity may be < 40 ft—or generally less than the 40- to 50-ft width of the ISRM barrier.

5.3 Geochemical Control of Field Reductive Capacity

If spatial variability in the total mass of iron oxides was the primary mechanism causing the observed barrier degradation at the 100D ISRM site (hypothesis 2) and there is little influence of preferential groundwater flow on the reductive capacity, there should be a positive correlation between the mass of iron oxides and the resulting reductive capacity. This implies that dithionite treatment is uniform (i.e., high flow zones do not receive additional dithionite treatment), which occurs in idealized 1-D laboratory columns but not at the field scale.

Considering just the high iron oxide zones indicated in the four boreholes (Figures 5.1 to 5.4), there is some correlation to high field reductive capacity (boreholes C4687, C4688). Perhaps a more important consideration is that there are no low iron oxide content zones. The total iron oxide content, which reflects geochemical variability only without the influence of dithionite or flow, is high in all four bore-holes (144 ± 72 μmol/g) with no zones of low iron oxide content. To address hypothesis 2, the total mass of iron oxides was plotted against the field reductive capacity for all four boreholes (Figure 5.7a); the plot showed a weak positive correlation ($R = 0.58$). Therefore, it appears that a zone with more iron oxides will have greater field reductive capacity. To eliminate the possible effects of flow during field scale reduction, the mass of iron oxides was plotted against the laboratory reductive capacity (Figure 5.7b) and unfortunately showed very little positive correlation. Nonetheless, a fair prediction of the field reductive capacity could be made given the total mass of iron oxides (field capacity = $2.73 + 0.76$ Fe_{total}, $R = 0.577$).

The amount of reduction in each borehole, while dependent on the total mass of iron oxides, was 20 to 30% of the maximum reductive capacity and only a small fraction of the total iron oxides. The average
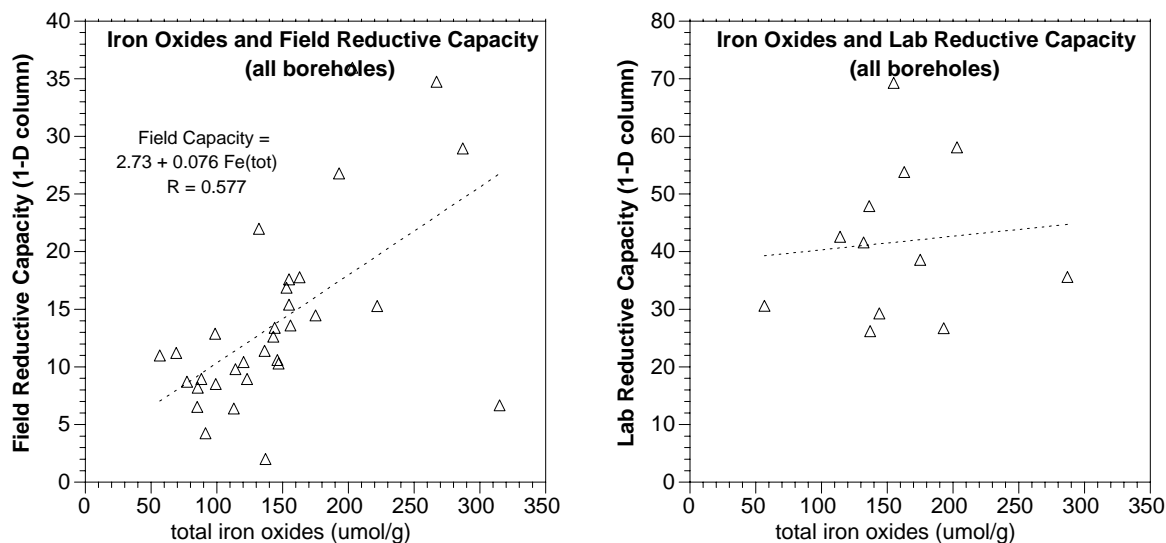
Figure 5.7. Correlation Between Total Iron Oxides and Reductive Capacity for a) Field-Reduced
Sediment and b) Laboratory-Reduced Sediment

percent reduction in each borehole was 22% (C4686), 26% (C4676), 34% (C4688), and 58% (C4689), an overall average of 35%. The up- and downgradient wells C4686/4687 near D4-37 had significantly lower reductive capacity than the wells near D4-26 (Table 4.5).

5.4 Coupled Geochemical and Physical Control of Field Reductive Capacity

If both the spatial variability in iron oxide content and preferential groundwater flow characteristics of a location were responsible for the observed loss of reductive capacity at a given location (hypothesis 3), there should be a positive correlation between the ratio of total iron oxides/saturated hydraulic conductivity and the field reductive capacity. This assumes that the saturated hydraulic conductivity measured in the 6-inch core corresponds to a laterally continuous layer from the injection well to that borehole location. A plot of this ratio (Figure 5.8) shows a poor correlation (R = 0.40) that is composed of the fair correlation of total iron to field reductive capacity (Figure 5.7a, R = 0.58) and the lack of any correlation of hydraulic conductivity to field reductive capacity (Figure 5.5a, R = 0.07). Based on results from core samples collected from the four borehole locations in this study, it appears that only the total iron content has a good correlation with the field reductive capacity (i.e., geochemical control apparently exerts the main influence on the field reductive capacity).

5.5 Rate of Ferrous Iron Oxidation and Influence on ISRM Barrier Performance

Field sediments that are analyzed for reductive capacity by 1-D column oxidation (with air-saturated water) provide the ferrous iron mass information and some additional ferrous iron oxidation rate information. All column experiments are run at a flow rate to achieve a 30-minute residence time
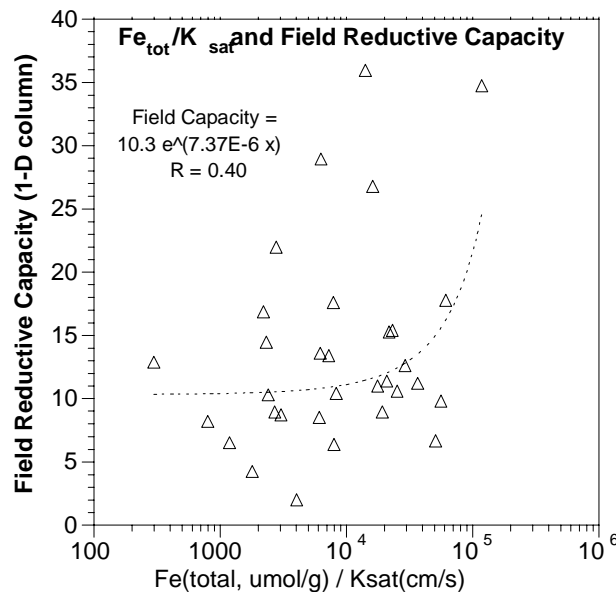
Figure 5.8. Correlation Between the Ratio of Total Iron Oxides/K_{sat} and the Field Reductive Capacity

(interstitial velocity 0.78 ft/hr), which is 30 times more rapid than the field average of 1 ft/day. A column experiment with reduced sediment showing a high reductive capacity (138 μmol/g) (Figure 5.9a) shows an oxygen breakthrough curve with complete oxygen consumption for the first 120 pore volumes, then a slow increase; but even at 1200 pore volumes there is still some oxygen consumption (i.e., effluent [black dots] does not equal influent [open circles above]). Iron extractions in other studies (Szecsody et al. 2004b) have shown that dithionite reduction of sediment results in more than one ferrous surface phase (i.e., adsorbed ferrous iron, reduced structural iron in clay, siderite, iron sulfide), which may oxidize at different rates when exposed to dissolved oxygen. It was hypothesized that adsorbed ferrous iron is rapidly oxidized, and siderite (second most common phase present) oxidizes more slowly. For the experiment with a high reductive capacity (Figure 5.8a), the oxidation rate was calculated at < 4 minutes for the first 120 pore volumes, then at 1.7 hr (half-life) from 600 to 1200 pore volumes. For a sediment with moderate reductive capacity (54 μmol/g) (Figure 5.9b), the same oxygen breakthrough shape is observed with both rapid and slowly oxidizing ferrous iron surface phases. However, for another sediment with moderate reductive capacity (46 μmol/g, Figure 5.9c), there are no rapidly oxidizing sites, so there is immediate partial oxygen breakthrough. For sediment with low oxidation capacity (27 μmol/g) (Figure 5.9d), there are only slowly oxidizing ferrous iron sites as well. Many of the 68 field reductive capacities (by 1-D column oxidation) in this 2005 study (Appendixes A–D) and 18 field reductive capacities in the 2002 study (table, Appendix E) show oxygen breakthrough curves that indicate the presence of only slowly oxidizing ferrous iron sites.

The significance of these changes in oxidation rate is in whether the slowly oxidizing ferrous iron sites have the ability to reduce chromate under field-scale conditions. In a recent 100D area nitrate study (Szecsody et al. 2005a), a long-term column experiment was conducted in which dissolved oxygen, chromate, and nitrate were injected through a dithionite-reduced sediment column for 100s of pore volumes (Figure 5.10). The oxygen breakthrough curve shape (Figure 5.10a, b) shows 60 pore volumes of removal of nearly all the dissolved oxygen, then slow increase in the dissolved oxygen concentration

5.10
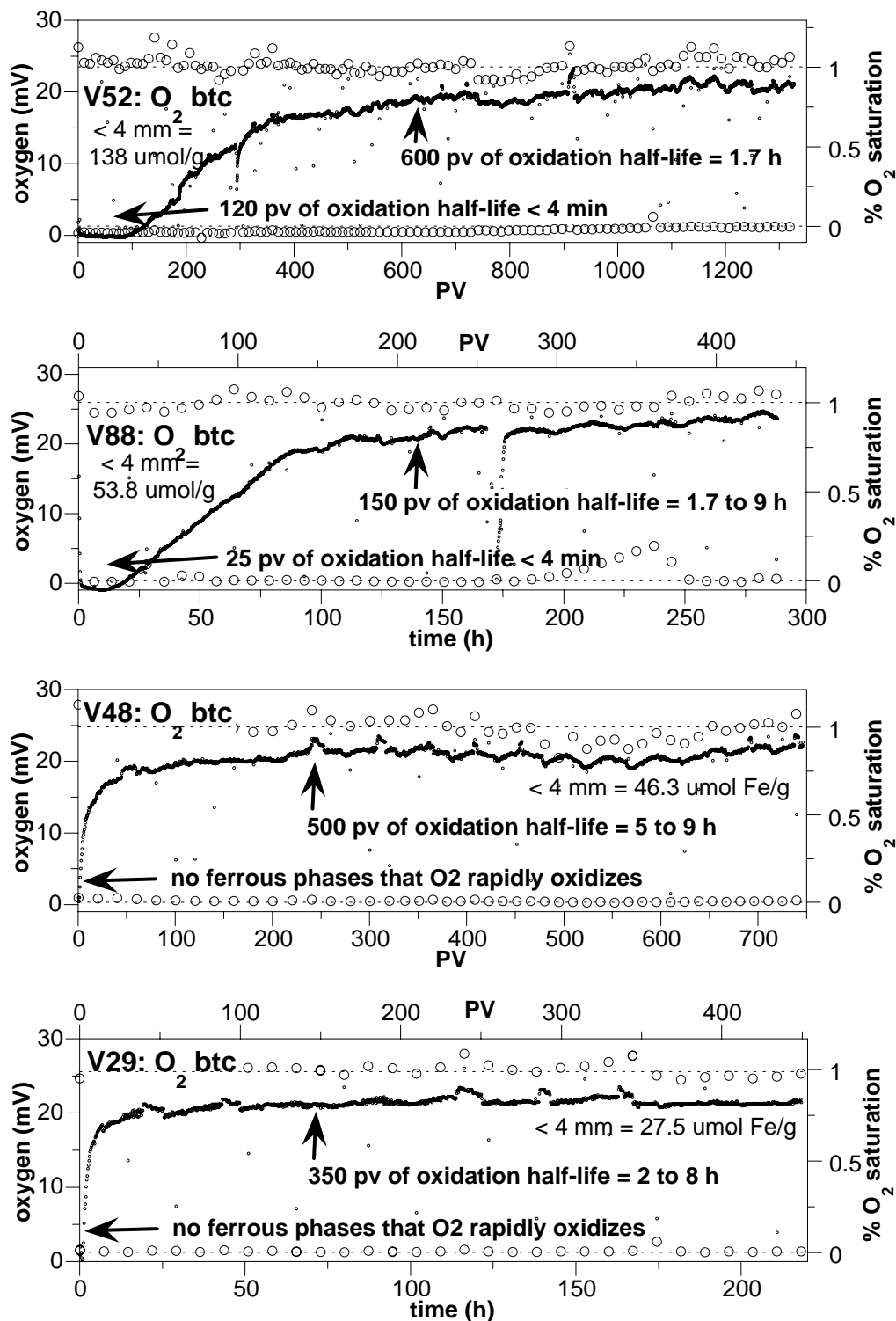
Figure 5.9. Oxidation of 100D Area Sediments Showing a) Lab-Reduced Sediment with High Capacity and Fast/Slow Oxidation Sites, b) Lab-Reduced Sediment with Moderate Capacity and Fast/Slow Oxidation Sites, c) Field-Reduced Sediment with Moderate Capacity but only Slow Oxidation Sites, and d) Field-Reduced Sediment with Low Capacity and Slow Oxidation Sites
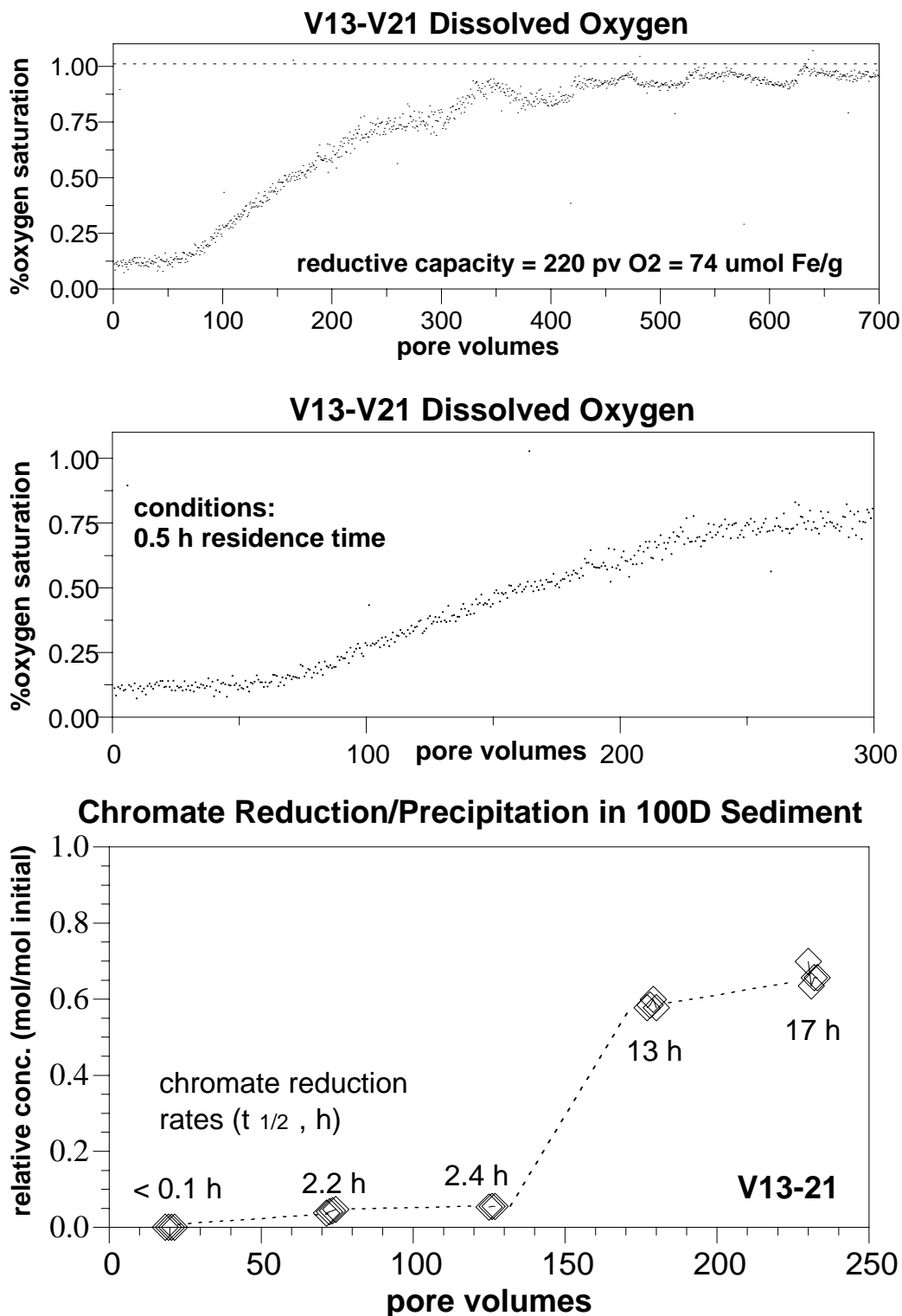
Figure 5.10. Long-Term Oxidation Column Experiment with a Reduced Sediment Column in Which 2 mg/L Chromate, 8.4 mg/L O_2, and 60 mg/L Nitrate Were Injected. Effluent concentration of dissolved oxygen (a, b), and chromate (c) are shown.

but not complete breakthrough) to 700 pore volumes. This corresponds to initial complete oxygen removal by the ferrous iron phases that are rapidly oxidized followed by slower removal by one or more different ferrous iron phases. Chromate removal was rapid for the first 120 pore volumes, then slower, with initial removal rates < 1 hr (half-life) to 17 hr by 250 pore volumes (Figure 5.10c). Many of the 2005 field reductive capacities (Appendixes A–D) breakthrough curves exhibit only slowly oxidizing sites even though there is sufficient capacity to remove dissolved oxygen and chromate, so it is likely that this partially reduced sediment can remove chromate at a slow rate (17-hr half-life). In a separate study of dithionite-reduced sediments in a Puchack, New Jersey aquifer (not shown), chromate continued to be reduced/ precipitated for >300 pore volumes, even though there was essentially no reductive capacity remaining (as defined by dissolved oxygen breakthrough).

The 17-hr half-life should be fast enough to remove all chromate in the estimated 40-day residence in the reduced sediment zone in the 100D area for homogeneous flow in the aquifer. However, if a zone were flowing 3 to 10 times faster (which is within reason given the EBF and saturated hydraulic conductivity data), the residence time in the reduced sediment zone is reduced significantly. At these more rapid flow rates (and a 17-hr half-life for chromate reduction), partial breakthrough of chromate is still not likely to occur. For a high-K zone with a velocity of 3 ft/day (3 times the average; 320 hr residence), the downgradient chromate concentration should be essentially zero (6E-3% of upgradient concentration). For a high-K zone with a velocity of 10 ft/day (10 times the average, 96 hr residence time), the downgradient chromate concentration would be 5.3% of the upgradient concentration. Therefore, the combination of high-K zones with a lateral continuity of ~40 ft (i.e., large enough to create a high-flow zone through the entire ISRM barrier) and partially reduced sediment (i.e., sediment with a low to moderate reductive capacity but still capable of a 17 hr half-life) is unlikely to cause high concentration chromate breakthrough.

6.0   Summary

The purpose of this study was to determine whether physical and/or geochemical heterogeneities are causing ISRM barrier failure and chromate breakthrough at specific locations along the 2300-ft ISRM barrier installed at Hanford's 100D Area. This laboratory-scale investigation of geochemical and physical properties used sediment samples collected from four boreholes drilled in April/May 2005 with continuous core from above the water table (~83 ft) to the aquifer/confining unit contact (97- to 103-ft deep). The four boreholes included C4686 and C4687 (12 ft up- and downgradient of well D4-37), and C4688 and C4689 (10 ft up- and downgradient of well D4-26).

Physical property analysis included sieve/hydrometer analysis at 1-ft vertical intervals to determine the particle size distribution of each sample and calculate the saturated hydraulic conductivity. Geochemical characterization included 1) the field reductive capacity by 1-D column oxidation and iron extraction (0.5-M HCl for 1 hr), 2) maximum (laboratory) reductive capacity by 1-D column oxidation and iron extraction, and 3) total ferric and ferrous iron oxides (5-M HCl for 2 weeks). The field reductive capacity by 1-D column oxidation was measured at 1-ft intervals in three wells and 2-ft intervals in one well. The field and laboratory reductive capacity by iron extraction and the total iron oxides were measured at 6-inch or 1-ft intervals in all four boreholes. Additional data collected over the past few years pertaining to the ISRM barrier were also used to interpret the redox or flow conditions and the lateral extent of these conditions; these data are included as appendixes to this report and include 161 pictures of the 2005 cores, 80 pictures of the 2002 cores, EBF data from 25 wells collected in 2002, MLS data collected in 11 wells (2002, 2004), and field reductive capacity measurements by column oxidation of cores collected in 2002, 1999, and 1997.

Chromate breakthrough has been observed in as many as 17 of the 70 ISRM injection wells. Breakthrough has occurred at various points along the barrier length with, in many cases, adjacent wells indicating good barrier performance. In addition to this spatial variability, observed chromate concentrations over the degraded sections of the barrier also vary seasonally. There is widespread nitrate upgradient of the ISRM barrier (60 mg/L) and lower nitrate concentrations downgradient. A recent nitrate study showed that, while the presence of nitrate will decrease barrier longevity uniformly, it cannot account for specific locations of chromate breakthrough. Possible causes of chromate breakthrough in specific well locations include:

- natural or anthropogenic high hydraulic conductivity zones (hypothesis 1)

- zones of low reducible iron (i.e., geochemical heterogeneity, hypothesis 2)

- high hydraulic conductivity zones with low reducible iron (coupled physical/geochemical heterogeneity, hypothesis 3).

Results from this study show that, while there is significant vertical physical and geochemical variability in the four boreholes investigated, lateral continuity of high-conductivity and low-reductive capacity zones was not observed, and subsequently none of these hypotheses alone is likely to explain barrier failure. The one exception was at the water table, where there was some indication of low reductive capacity at all four boreholes, three of which also showed high-K zones near the water table. A lack of 1-D column data near the water table for two of the four boreholes made characterization of this effect at these locations less certain. If physical heterogeneity alone strongly influenced barrier oxidation

(hypothesis 1), there should be an inverse correlation between zones of high hydraulic conductivity and the field reductive capacity that was not supported by the data (except at the water table). Of the six high-K zones noted in the four boreholes (excluding the water table), only two correlated with zones of low reductive capacity. A plot of all hydraulic conductivity values against the field reductive capacity indicated no correlation (correlation coefficient R = 0.07). The average saturated hydraulic conductivity of the aquifer for all four boreholes was 0.0348 ± 0.0498 cm/s (n = 59), showing considerable variability vertically. In addition, although EBF data from 25 wells indicated high-K channels in half of the wells, there was no strong indication that high-K zones were laterally continuous (at a 35-ft distance) between adjacent barrier wells. This observation does not rule out the possibility of laterally continuous higher-permeability channels that are oriented such that they are not sampled by the available well network, but it does make the likelihood of this scenario far less probable.

The vertical variability in the field reductive capacity could be explained by 1) proximity to the water table and 2) total reducible iron content (hypothesis 2). The observed loss in reductive capacity near the water table is most likely due to water level fluctuation, resulting in oxidation of the reduced sediment and, to a lesser extent, the potential for elevated dissolved oxygen, chromate, and nitrate concentrations near the water table. In addition to the water table region, there were several examples of intervals deeper in the formation that showed some degree of loss in reductive capacity. The average field reductive capacity for these four 2005 boreholes (13.64 ± 7.79 µmol/g, n = 37; 1-D column oxidation) was slightly greater than previous values (10.6 ± 6.6 µmol/g in 2002; 11.2 ± 7.4 in 1999). These data indicate that the barrier near the two locations investigated has not been fully reoxidized (i.e., the bulk of the sediments tested still show significant reductive capacity). The laboratory (maximum) reductive capacity was 41.7 ± 8.12 µmol/g for these four 2005 boreholes (also by 1-D column oxidation), which was similar to previous values (40.0 ± 15.0 µmol/g, 2002; 24.3 ± 5.3 µmol/g for 1997). The total iron oxide concentration of the sediment was considerable (145 ± 16.7 µmol/g) and there was a fair correlation (R = 0.58) between the total iron oxides and the resulting field reductive capacity. There were no zones of low total iron oxide content. The combination of total iron oxides and hydraulic conductivity (hypothesis 3) was only a poor predictor (R = 0.40) of field reductive capacity.

A mechanism that could explain partial chromate breakthrough in the ISRM barrier is the relationship between the field reductive capacity and the *rate of chromate oxidation* in combination with high-K channels. Based on K_{sat} and reductive capacity data alone, there should be no chromate breakthrough in most cases because there is sufficient reductive capacity at all depths to immobilize chromate for 100 to 200 pore volumes *assuming rapid chromate reduction*. However, recent data (Figure 5.10) show that initial chromate reduction is rapid (minutes) in sediments with moderate to high reductive capacity, but, as the sediment is oxidized, the remaining ferrous iron surface phases *reduce oxygen and chromate more slowly*. More specifically, the chromate reduction rate decreases two orders of magnitude from minutes to 17 hours (or greater) as the reductive capacity decreases to < 4 µmol/g. The importance of the chromate reduction rate is related to whether there is sufficient time in the reduced zone to reduce chromate.

With the average groundwater velocity of 1 ft/day in a 40-ft-wide barrier (960 hr residence within the reduced zone), there should be no chromate breakthrough, even in low-capacity sediments (Table 6.1). However, the worst-case scenario with 10 times greater flow (i.e., 10 ft/day) and low reductive capacity would show some (5%) chromate breakthrough. Therefore, laterally continuous high-K channels could support significant chromate breakthrough because those channels would be rapidly oxidized and have a

Table 6.1. Flow and Reductive Capacity Scenarios and Predicted Chromate Breakthrough

Aquifer Flow	Groundwater Flow (ft/d)	Reduction Capacity µmol/g	Chromate ox. Half-life (hr)	Predicted Chromate Breakthrough (%)[a]
Average	1.0	13.6 (average)	2.4	0.00
	1.0	6.8 950% low)	17	2×10^{-11}
High-K (3x avg.)	3.0	13.6 (average)	2.4	0.00
	3.0	6.8 (50% low)	17`	5.6×10^{-3}
High-K (10x avg)	10.0	13.6 (average)	2.4	9.3×10^{-8}
	10.0	6.8 (50% low)	17	5.3
(a) Percent of upgradient concentration.				

much slower (or no) chromate reduction rate. The calculated hydraulic conductivity and EBF data indicate that there are thin high-K channels in half of the wells that have up to 3 times (and some 10 times) more rapid flow than the average groundwater. These data also indicate that the high-K channels are generally not laterally continuous.

Based on evaluation of the sediments collected for this study, the most likely scenario causing chromate breakthrough in wells D4-26 and D4-37 is high flow in oxic sediments at the water table. Chromate concentrations in December 2004 in these two wells (Figure 1.2) of 0.6 and 1.0 ppm are near the estimated upgradient chromate plume concentration (Figure 1.1), so most (> 80%) of the groundwater would need to be flowing through sediments with essentially no reductive capacity to achieve this high chromate concentration at the wells. Because most depths in boreholes evaluated for this study have sufficient reductive capacity, a scenario that could explain the observed high chromate in D4-26 and D4-37 is that most groundwater is flowing through high-conductivity channels near the water table.

The original barrier longevity of 160 pore volumes for homogeneous reduced sediment or 20 years (considering the presence of only dissolved oxygen and 2 ppm chromate) is reduced to 85 pore volumes (10 years) with widespread 60-ppm nitrate. The barrier lifetime is greater than 85 pore volumes for high-K channels because there is not enough time to reduce nitrate and consume ferrous iron. Partial chromate breakthrough could occur if there were continuous high-K zones (10 ft/day) with low (to none) reductive capacity. The MLS, which collects depth-discrete aqueous chromate data in a fully screened well, should have addressed this question, but those data are suspect due to poor seals between vertical sampling sections. The observation of seasonal increasing chromate with higher groundwater flow is also consistent with high flow/low reduction zones resulting in partial chromate breakthrough because of 1) slow chromate reduction in zones of low reduction and 2) transport of chromate through oxic sediments near the water table. If the cause of laterally discontinuous breakthrough of chromate along the ISRM barrier is oxic transport of chromate near the water table, additional dithionite treatment in these zones will not be effective. Treatment near the water table with a technology that emplaces considerable reductive capacity is needed, such as injectable zero valent iron.

7.0   References

Anderson LD, DB Kent, and JA Davis. 1994. "Batch Experiments Characterizing the Reduction of Cr(VI) Using Suboxic Material from a Mildly Reducing Sand and Gravel Aquifer." *Environmental Science and Technology*, *28*(1):178–185.

Balko B and P Tratnyek. 1998. "Photoeffects on the Reduction of Carbon Tetrachloride by Zero-Valent Iron." *J. Physical Chemistry*, 102(8):1459–1465.

Blowes D, C Ptacek, and J Jambor. 1997. "In-situ Remediation of Cr(VI) Contaminated Groundwater Using Permeable Reactive Walls: Laboratory Studies." *Environmental Science and Technology*, 31(12):3348–3357.

Boursiquot S, M Mullet, and J Ehhrhardt. 2002. "XPS Study of the Reaction of Chromium (VI) with Mackinawite (FeS)." *Surface and Interface Analysis,* 34:293–297.

Buerge IJ and SJ Hug. 1997. "Kinetics and pH Dependence of Chromium(VI) Reduction by Iron(II). *Environmental Science and Technology*, 31(5):1426–1432.

Chao TT and L Zhou. 1983. "Extraction Techniques for Selective Dissolution of Amorphous Iron Oxides from Soils and Sediments." *Soil Science Society of America, Journal*, 47: 225–232.

Eary L and D Rai. 1988. "Chromate Removal from Aqueous Wastes by Reduction with Ferrous Ion." *Environmental Science and Technology*, 22: 972–977.

Folk RL. 1980. *Petrology of Sedimentary Rocks*, 2nd edition*.* Hemphill Publishing Co., Austin Texas.

Fruchter JS, FA Spane, JK Fredrickson, CR Cole, JE Amonette, JC Templeton, TO Stevens, DJ Holford, LE Eary, BN Bjornstad, GD Black, JM Zachara, and VR Vermeul. 1994. *Manipulation of Natural Subsurface Processes: Field Research and Validation*. PNL-10123, Pacific Northwest National Laboratory, Richland, Washington.

Fruchter J, C Cole, M Williams, V Vermeul, J Amonette, J Szecsody, J Istok, and M Humphrey. 2000. "Creation of a Subsurface Permeable Treatment Barrier Using In-Situ Redox Manipulation." *Ground-Water Monitoring Review*, 66–77.

Gibbs CR. 1976. "Characterization and Application of Ferrozine Iron Reagent as a Ferrous Iron Indicator." *Analytical Chemistry*, 48(8):1197–1200.

Heron G, TH Christensen, and JC Tjell. 1994a. "Oxidation Capacity of Aquifer Sediments." *Environmental Science and Technology*, 28:153–159.

Heron G, C Crouzet, AC Bourg, and TH Christensen. 1994b. "Speciation of Fe(II) and Fe(III) in Contaminated Aquifer Sediments Using Chemical Extraction Techniques." *Environmental Science and Technology*, 28:1698–1705.

Jardine PM, SE Fendorf, MA Mayes, IL Larsen, SC Brooks, and WB Bailey. 1999. "Fate and Transport of Hexavalent Chromium in Undisturbed Heterogeneous Soil." *Environmental Science and Technology*, 33(17):2939–2944.

Kim C, B Deng, E Thornton, and H Xu. 2001. "Chromium (VI) Reduction by Hydrogen Sulfide in Aqueous Media: Stoichiometry and Kinetics." *Environmental Science and Technology*, 35:2219–2225.

Loyaux-Lawniczak S, P Refait, JJ Ehrhardt, P Lacomte, and JR Genin. 2000. "Trapping of Cr by Formation of Ferrihydrite During the Reduction of Chromate Ions by Fe(II)-Fe(III) Hydroxysalt Green Rusts." *Environmental Science and Technology*, 34(3):438–443.

Loyaux-Lawniczak S, P Lecomte, and J Ehrhardt. 2001. "Behavior of Hexavalent Chromium in a Polluted Groundwater: Redox Processes and Immobilization in Soils." *Environmental Science and Technology*, *35*(7)1350–1357.

Masch FD and KJ Denny. 1966. "Grain size Distribution and its Effect on the Permeability of Unconsolidated Sand." *Water Resources Research*, 2(4):665– 667.

Molz FJ and SC Young. January-February 1993. "Development and Application of Borehole Flowmeters for Environmental Assessment." *The Log Analyst*, pp. 13-23.

Molz FJ, GK Boman, SC Young, and WR Waldrop. 1994. "Borehole Flowmeters: Field Applications and Data Analysis." *Journal of Hydrology*, 163:347-371.

Patterson RR and S Fendorf. 1997. "Reduction of Hexavalent Chromium by Amorphous Iron Sulfide." *Environmental Science and Technology*, 31-2039–2044.

Pratt A, D Blowes, and C Placek. 1997. "Products of Chromate Reduction on Proposed Subsurface Remediation Material." *Environmental Science and Technology*, 31(9):2492–2498.

Sass BM and D Rai. 1986. "Solubility of Amorphous Chromium(III)-Iron(III) Hydroxide Solid Solutions." *Inorganic Chemistry*, *26*(14):2228–2232.

Scherer MM, BA Balko, and PG Tratnyek. 1999. "The Role of Oxides in Reduction Reactions at the Metal-Water Interface." *ACS Symposium Series #715*, DL Sparks and T Grundl (Ed.), pp. 1–22.

Seaman JC, PM Bertsch, and L Schwallie. 1999. "In-situ Cr(VI) Reduction within Coarse-Textured, Oxide-Coated Soil and Aquifer Systems Using Fe(II) Solutions." *Environmental Science and Technology*, 33(6):938–944.

Stucki JW, DC Golden, and CB Roth. 1984. "Preparation and handling of dithionite-reduced smectite suspensions." *Clays and Clay Minerals*, 32(3):191–197.

Szecsody JE, MD Williams, JS Fruchter, VR Vermeul, and J Evans. 2000. "Influence of sediment reduction on TCE degradation, remediation of chlorinated and recalcitrant compounds." *Chemical Oxidation and Reactive Barriers*, G Wickramanayake (Ed.), p. 369–376.

Szecsody JE, B Devary, D Girvin, J Campbell, and M McKinley. 2004a. "Fate and Transport of the Explosive CL-20 in Soils and Subsurface Sediments." *Chemosphere*, 56:593-610.

Szecsody JE, MD Williams, JS Fruchter, VR Vermeul, and D Sklarew. 2004b. "In Situ Reduction of Aquifer Sediments: Enhancement of Reactive Iron Phases and TCE Dechlorination." *Environmental Science and Technology*, 38:4656-4663.

Szecsody J, J Phillips, V Vermeul, J Fruchter, and M Williams. 2005a. "Influence of Nitrate on the Hanford 100D Area In Situ Redox Manipulation Barrier Longevity." PNNL-15262, Pacific Northwest National Laboratory, Richland, Washington.

Szecsody JE, JS Fruchter, VR Vermeul, MD Williams, and BJ Devary. 2005b. "In Situ Reduction of Aquifer Sediments to Create a Permeable Reactive Barrier to Remediate Chromate: Bench-Scale Tests to Determine Barrier Longevity." Chapter 9, *Groundwater Remediation of Chromate*, J. Jacobs (Ed.). CRC Press, Boca Raton, Florida.

Vermeul VR, MD Williams, JE Szecsody, JS Fruchter, CR Cole, and JE Amonette. 2002. "Creation of a Subsurface." *Groundwater Remediation of Trace Metals, Radionuclides, and Nutrients, with Permeable Reactive Barriers.* Academic Press.

Wehrli B. 1992. "Redox Reactions of Metal Oxides at Mineral Surfaces." *Aquatic Chemical Kinetics*. W Stumm (Ed.). John Wiley and Sons, New York, pp. 311–337.

Zachara J, D Girvin, R Schmidt, and C Resch. 1987. "Chromate adsorption on amorphous iron oxyhydroxide in the presence of major groundwater ions." *Environmental Science and Technology*, 21:589–594.

Appendix A

1-D Oxidation of Field- and Laboratory-Reduced Sediments from 100D Area Borehole C4686 D4-90
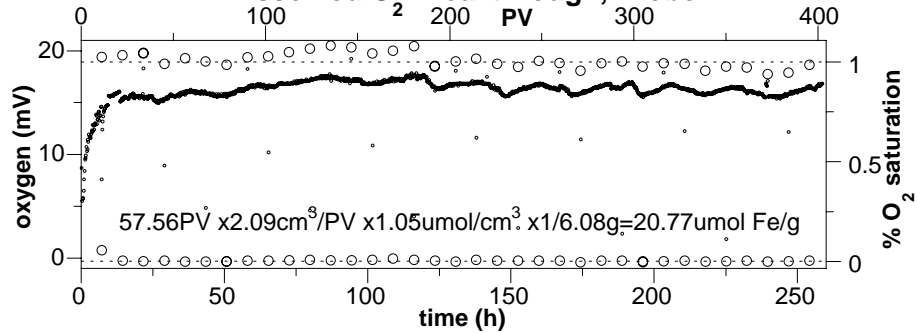
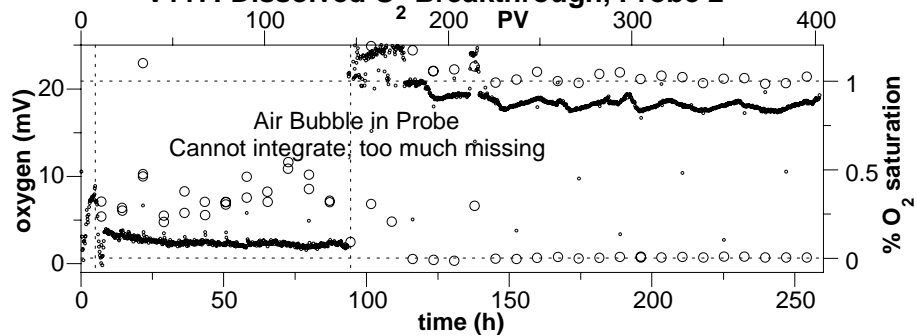# Appendix A - 1-D Oxidation of Field- and Laboratory-Reduced Sediments from 100D Area Borehole C4686 D4-90

100D Sediment Core (Field Reduced), C4686 D4-90, 85.1' bgs
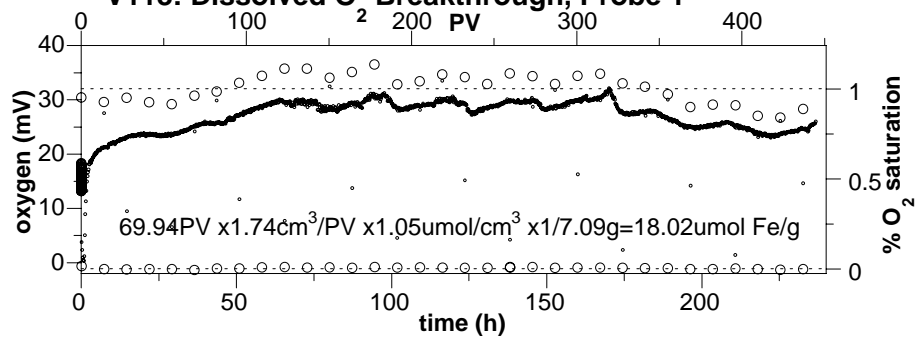**V122: Dissolved O$_2$ Breakthrough, Probe 1**

45.70PV x2.49cm^3/PV x1.05umol/cm^3 x1/5.20g=22.98umol Fe/g

V122: Dissolved O$_2$ Breakthrough, Probe 2

45.71PV x2.49cm^3/PV x1.05umol/cm^3 x1/5.20g=22.98umol Fe/g

100D Sediment Core (Field Reduced), C4686 D4-90, 86.1' bgs
V123: Dissolved O$_2$ Breakthrough, Probe 1

48.27PV x2.43cm^3/PV x1.05umol/cm^3 x1/6.42g=19.19umol Fe/g

V123: Dissolved O$_2$ Breakthrough, Probe 2

59.85PV x2.43cm^3/PV x1.05umol/cm^3 x1/6.42g=23.79umol Fe/g

A.1
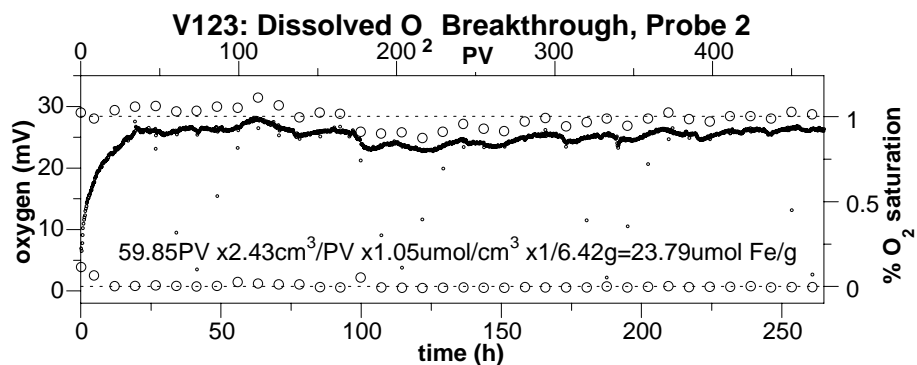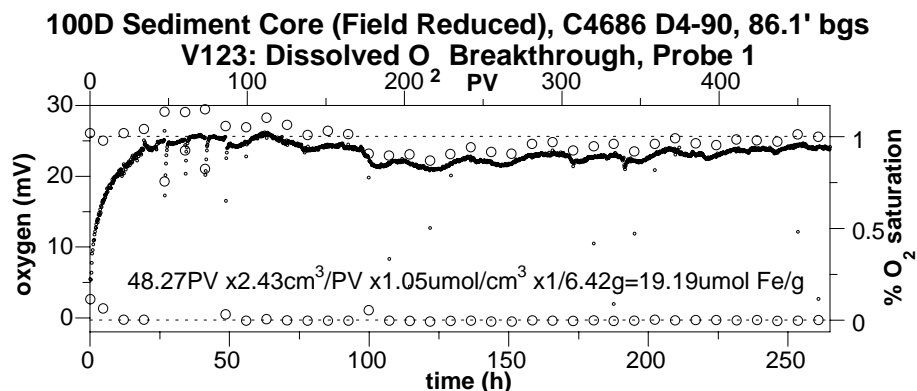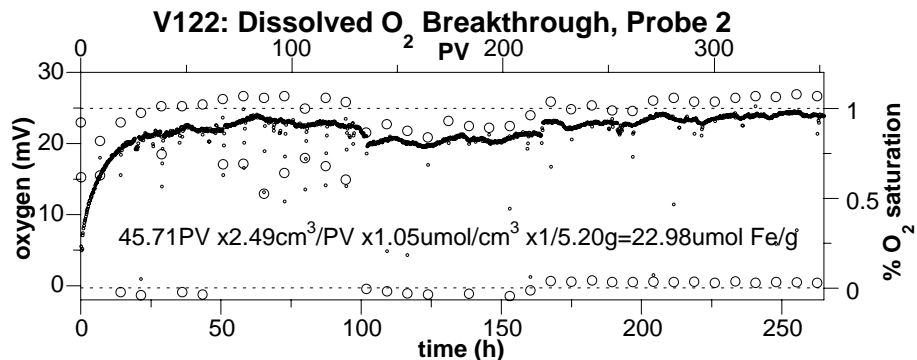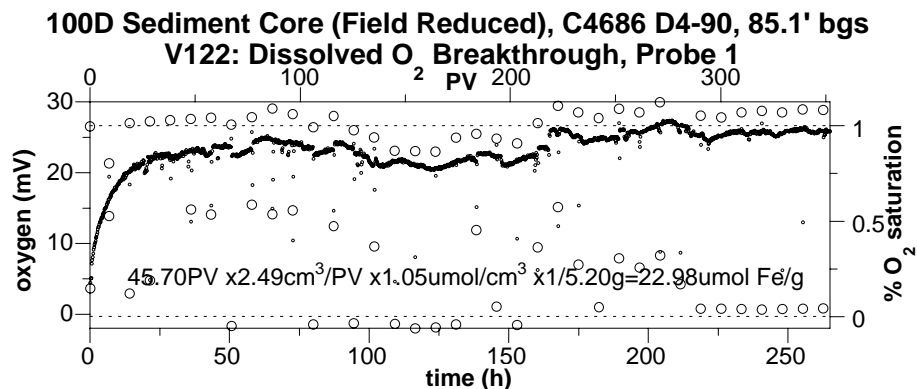
100D Sediment Core (Field Reduced), C4686 D4-90, 87.6' bgs
V124: Dissolved O₂ Breakthrough, Probe 1
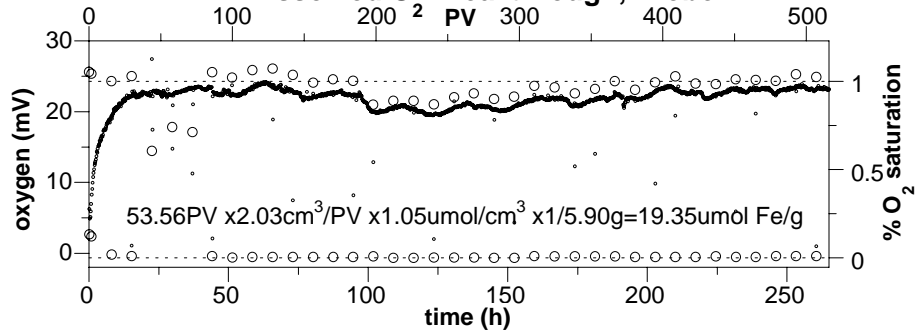
53.56PV x2.03cm^3/PV x1.05umol/cm^3 x1/5.90g=19.35umol Fe/g

V124: Dissolved O₂ Breakthrough, Probe 2

64.05PV x2.03cm^3/PV x1.05umol/cm^3 x1/5.90g=23.14umol Fe/g
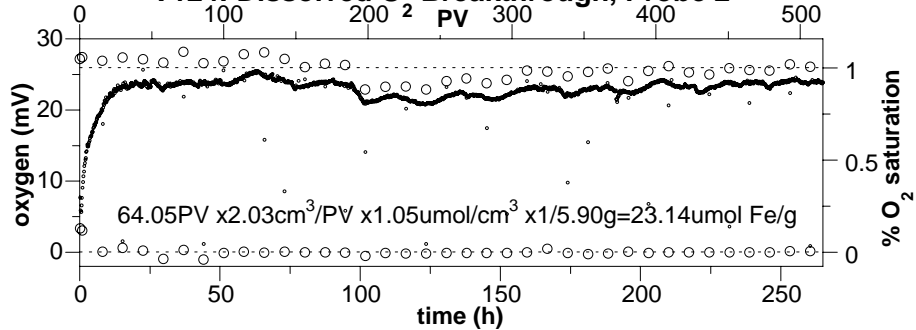
100D Sediment Core (Field Reduced), C4686 D4-90, 88.6' bgs
V125: Dissolved O₂ Breakthrough, Probe 1
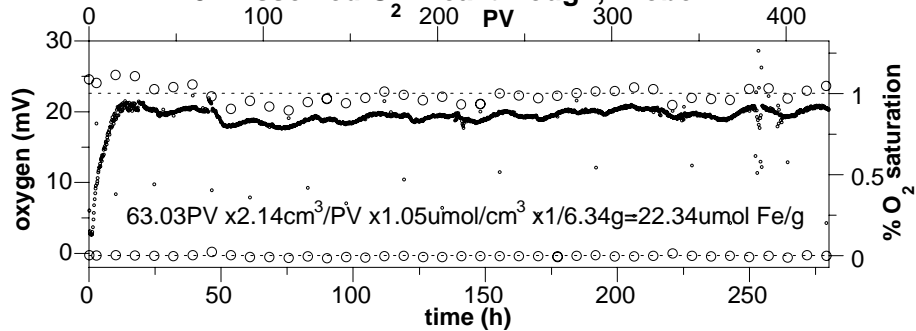
63.03PV x2.14cm^3/PV x1.05umol/cm^3 x1/6.34g=22.34umol Fe/g

V125: Dissolved O₂ Breakthrough, Probe 2

75.18PV x2.14cm^3/PV x1.05umol/cm^3 x1/6.34g=26.65umol Fe/g

A.2
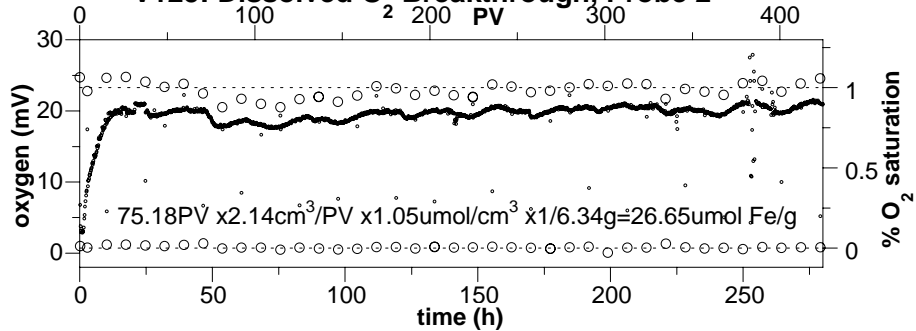
100D Sediment Core (Field Reduced), C4686 D4-90, 88.6' bgs
V54: Dissolved O$_2$ Breakthrough, Probe 1

oxygen (mV)

% O$_2$ saturation

Q_1=2.734 PV/h

Q_2=1.207 PV/h

88.6PV x1.85cm^3/PV x1.05umol/cm^3 x1/6.79g=25.35umol Fe/g

PV

V54: Dissolved O$_2$ Breakthrough, Probe 2

oxygen (mV)

% O$_2$ saturation

Q_1=2.734 PV/h

Q_2=1.207 PV/h

68.1PV x1.85cm^3/PV x1.05umol/cm^3 x1/6.79g=19.48umol Fe/g

PV
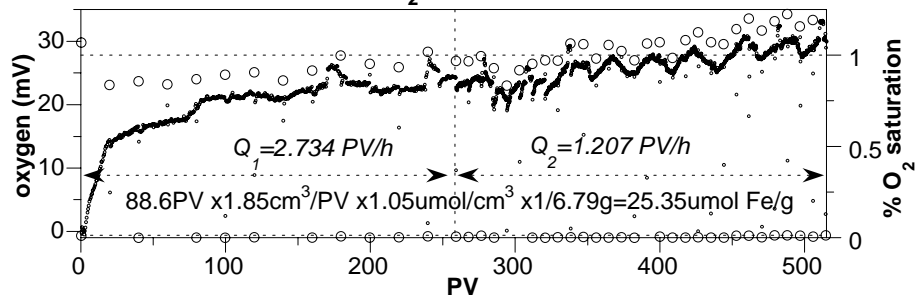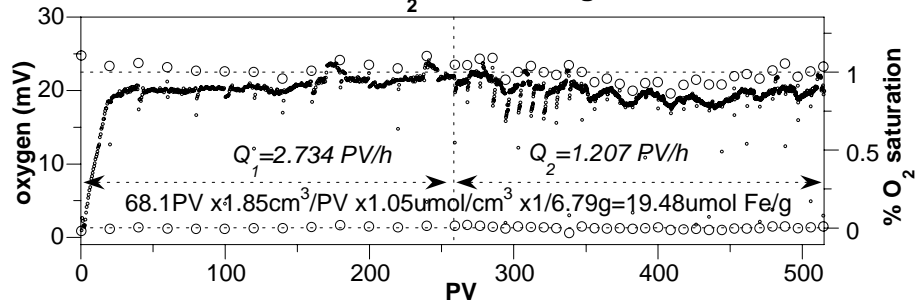
100D Sediment Core (Lab Reduced), C4686 D4-90, 88.6' bgs
V64: Dissolved O$_2$ Breakthrough, Probe 1

303 PV   374 PV   405 PV   604 PV

oxygen (mV)

% O$_2$ saturation

Q_1=0.928 PV/h

Q_2=1.268 PV/h

149.76PV x2.57cm^3/PV x1.05umol/cm^3 x1/5.28g=76.54umol Fe/g

PV

V64: Dissolved O$_2$ Breakthrough, Probe 2

184.16PV x2.57cm^3/PV x1.05umol/cm^3 x1/5.28g=94.12umol Fe/g

oxygen (mV)

% O$_2$ saturation

Q_1=0.928 PV/h

Q_2=1.268 PV/h

PV

A.3
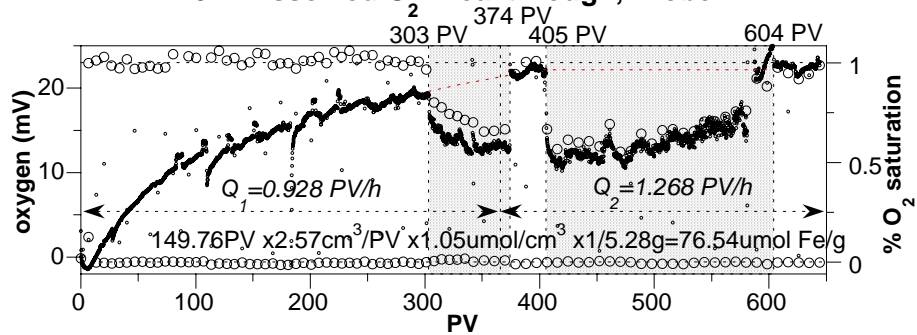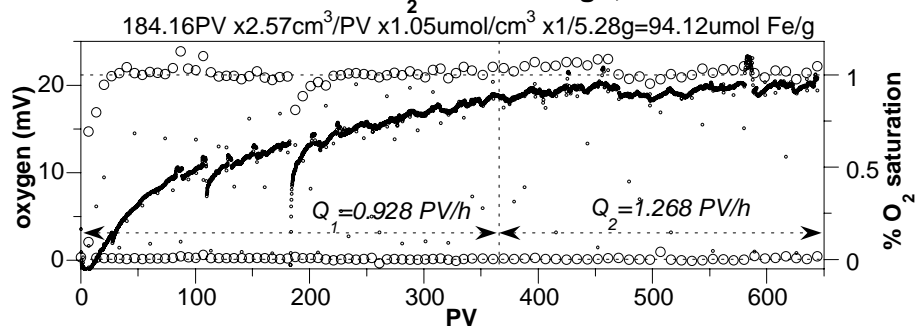
100D Sediment Core (Field Reduced), C4686 D4-90, 90.6' bgs
V126: Dissolved O$_2$ Breakthrough, Probe 1
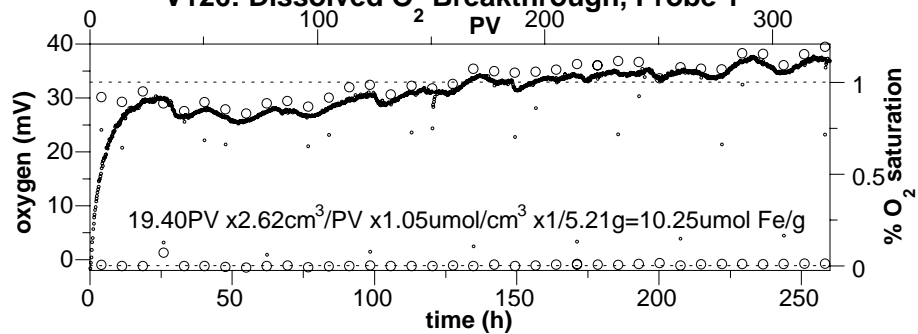
19.40PV x2.62cm^3/PV x1.05umol/cm^3 x1/5.21g=10.25umol Fe/g

V126: Dissolved O$_2$ Breakthrough, Probe 2

34.12PV x2.62cm^3/PV x1.05umol/cm^3 x1/5.21g=18.01umol Fe/g

A.4
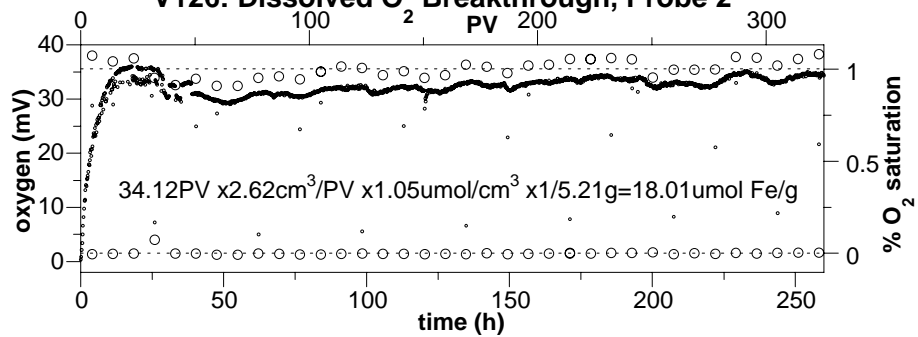
100D Sediment Core (Field Reduced), C4686 D4-90, 92.1' bgs
V55: Dissolved O$_2$ Breakthrough, Probe 1

Electrode Loop plugged (28-174PV), column flow not interrupted

Norm O$_2$; 0.908

Q_1=1.77 PV/h   **PV** Q_2=0.99 PV/h

V55: Dissolved O$_2$ Breakthrough, Probe 2

Electrode Loop plugged (28-174PV), column flow not interrupted

Norm O$_2$; 0.758
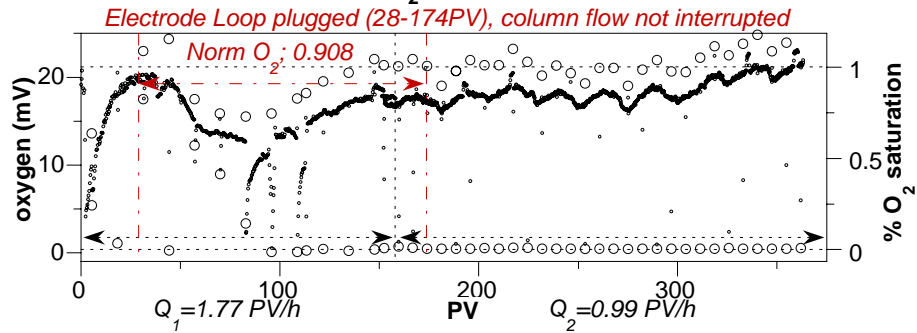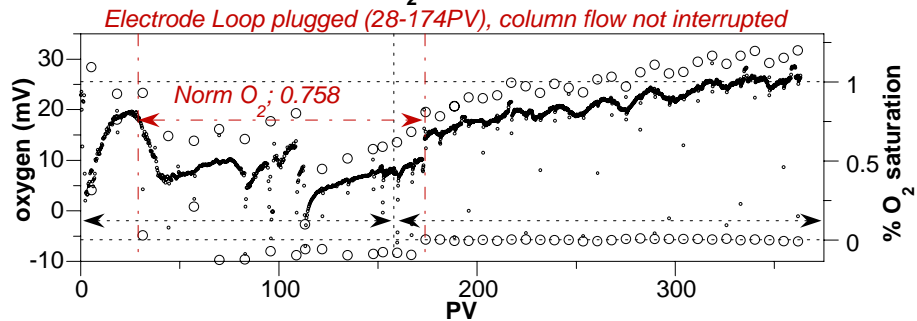
100D Sediment Core (Lab Reduced), C4686 D4-90, 92.1' bgs
V67: Dissolved O$_2$ Breakthrough, Probe 1

156.59PV x2.13cm^3/PV x1.05umol/cm^3
x1/5.74g=61.01umol Fe/g

V67: Dissolved O$_2$ Breakthrough, Probe 2

155.51PV x2.13cm^3/PV x1.05umol/cm^3
x1/5.74g=60.59umol Fe/g

Noise; 35-47 PV, 80-105 PV

A.5
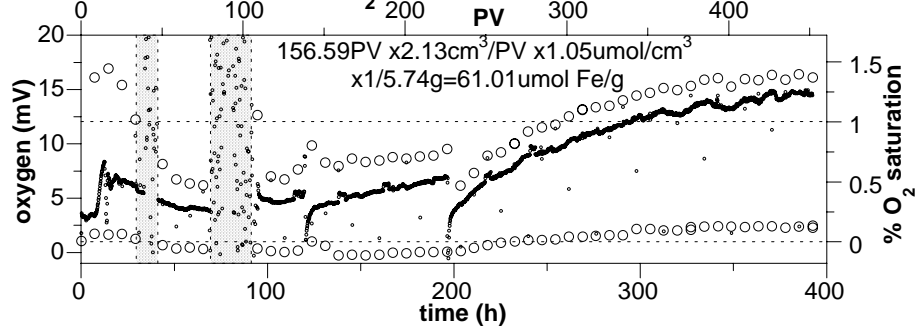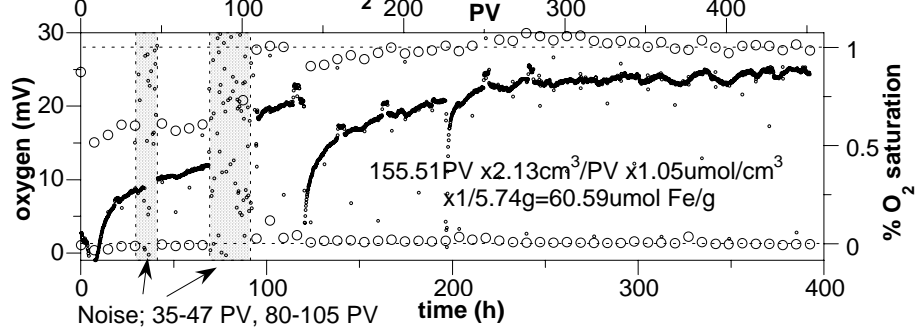
100D Sediment Core (Field Reduced), C4686 D4-90, 93.1' bgs
V127: Dissolved O₂ Breakthrough, Probe 1

$35.78PV \times 2.55cm^3/PV \times 1.05umol/cm^3 \times 1/5.55g = 17.26umol\ Fe/g$

V127: Dissolved O₂ Breakthrough, Probe 2

$34.40PV \times 2.55cm^3/PV \times 1.05umol/cm^3 \times 1/5.55g = 16.59umol\ Fe/g$
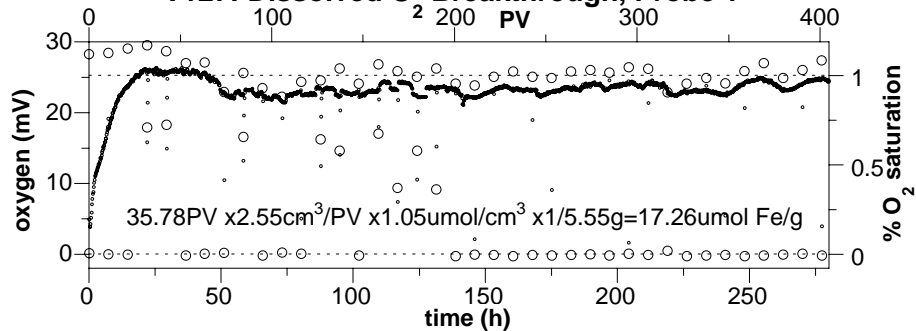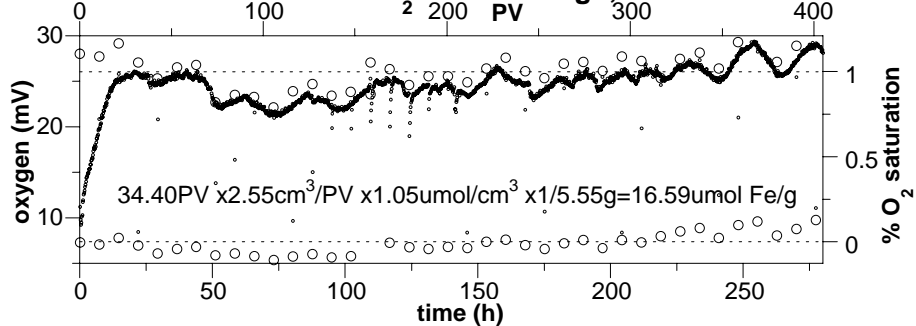
100D Sediment Core (Field Reduced), C4686 D4-90, 94.6' bgs
V128: Dissolved O₂ Breakthrough, Probe 1

$62.78PV \times 2.04cm^3/PV \times 1.05umol/cm^3 \times 1/6.37g = 21.11umol\ Fe/g$

V128: Dissolved O₂ Breakthrough, Probe 2

$53.50PV \times 2.04cm^3/PV \times 1.05umol/cm^3 \times 1/6.37g = 17.99umol\ Fe/g$

A.6
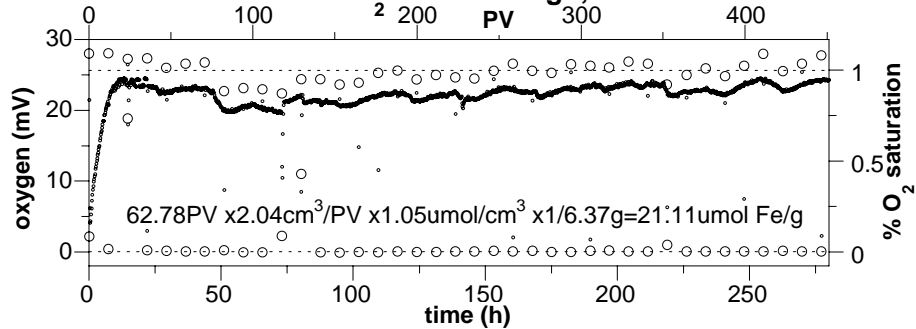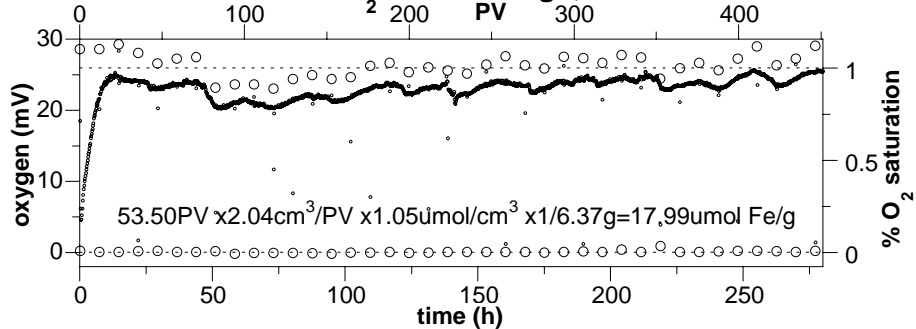
100D Sediment Core (Field Reduced), C4686 D4-90, 95.6' bgs
V56: Dissolved O$_2$ Breakthrough, Probe 1

11.90PV x2.13cm^3/PV x1.05umol/cm^3
x1/6.61g=4.03umol Fe/g

V56: Dissolved O$_2$ Breakthrough, Probe 2

14.33PV x2.13cm^3/PV x1.05umol/cm^3
x1/6.61g=4.85umol Fe/g
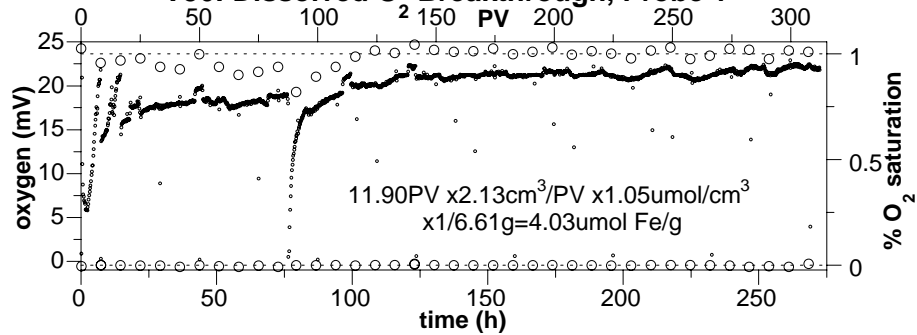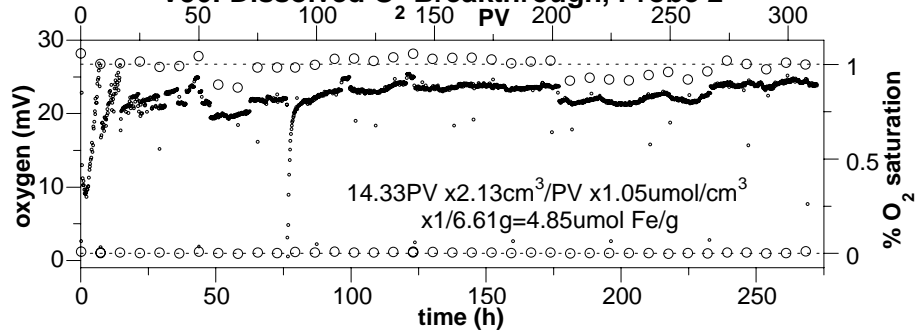
100D Sediment Core (Lab Reduced), C4686 D4-90, 92.1' bgs
V71: Dissolved O$_2$ Breakthrough, Probe 1
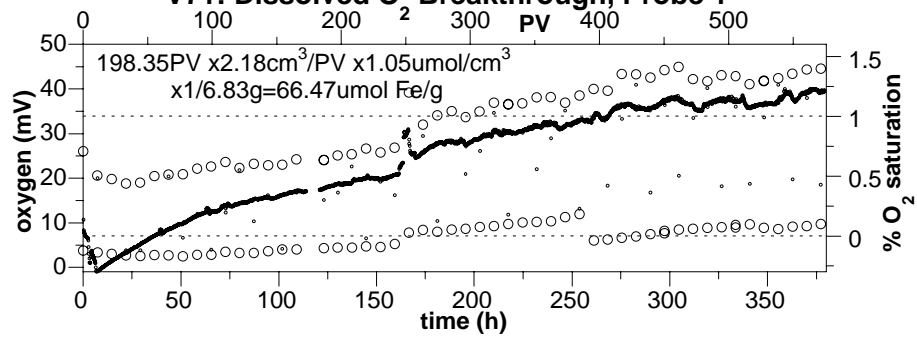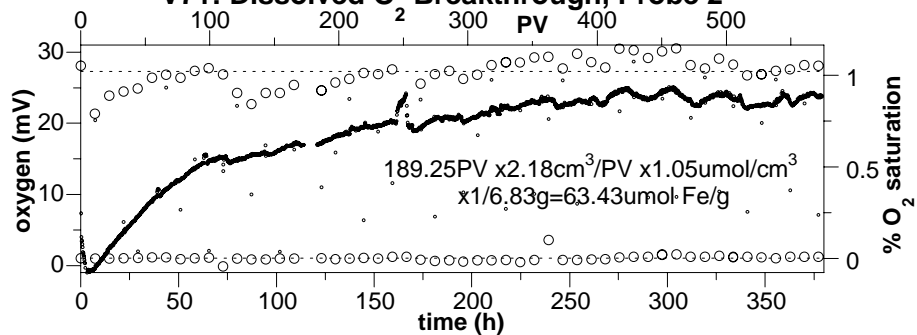
198.35PV x2.18cm^3/PV x1.05umol/cm^3
x1/6.83g=66.47umol Fe/g

V71: Dissolved O$_2$ Breakthrough, Probe 2

189.25PV x2.18cm^3/PV x1.05umol/cm^3
x1/6.83g=63.43umol Fe/g

A.7

Appendix B

1-D Oxidation of Field- and Laboratory- Reduced Sediments from 100D Area Borehole C4687 D4-91

Appendix B - 1-D Oxidation of Field- and Laboratory- Reduced Sediments from 100D Area Borehole C4687 D4-91

100D Sediment Core (Field Reduced), C4687 D4-91, 83.1' bgs
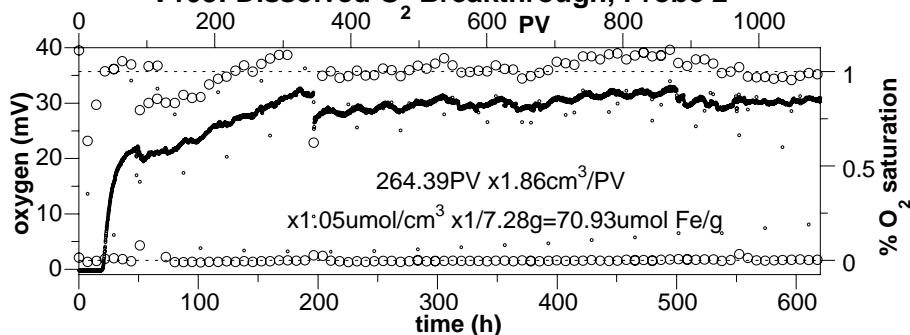**V25: Dissolved O$_2$ Breakthrough, Probe 1**

16.53PV x2.63cm^3/PV x1.05umol/cm^3 x1/5.81g=7.86umol Fe/g

V25: Dissolved O$_2$ Breakthrough, Probe 2

20.83PV x2.63cm^3/PV x1.05umol/cm^3 x1/5.81g=9.90umol Fe/g
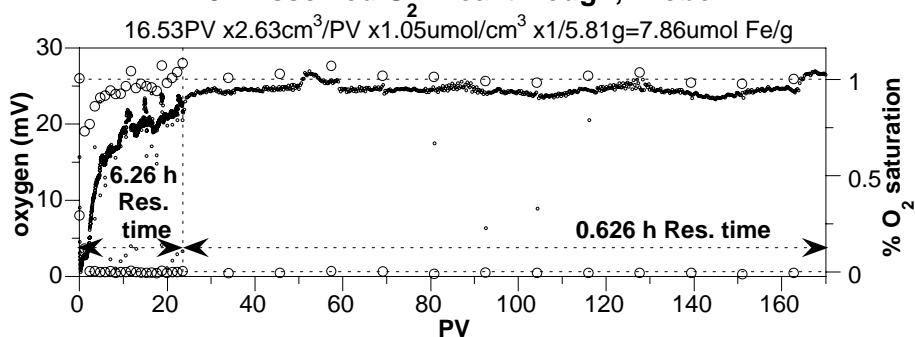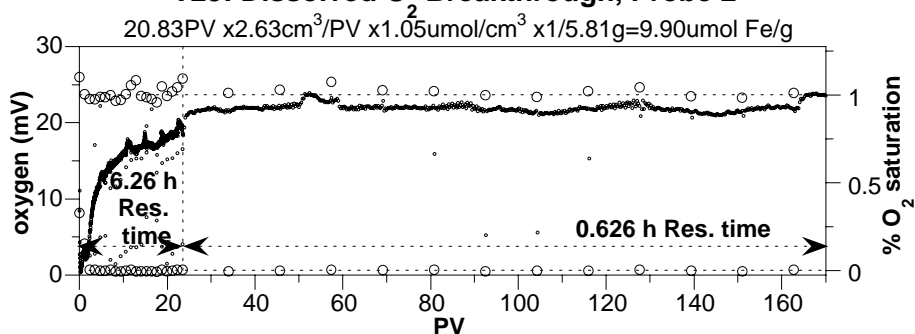
100D Sediment Core (Field Reduced), C4687 D4-91, 84.1' bgs
V26: Dissolved O$_2$ Breakthrough, Probe 1

6.92PV x2.60cm^3/PV x1.05umol/cm^3 x1/5.15g=3.67umol Fe/g

V26: Dissolved O$_2$ Breakthrough, Probe 2

13.43PV x2.60cm^3/PV x1.05umol/cm^3 x1/5.15g=7.12umol Fe/g
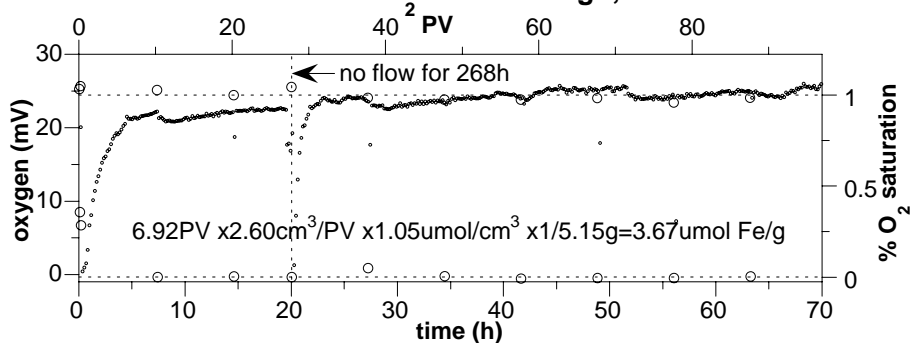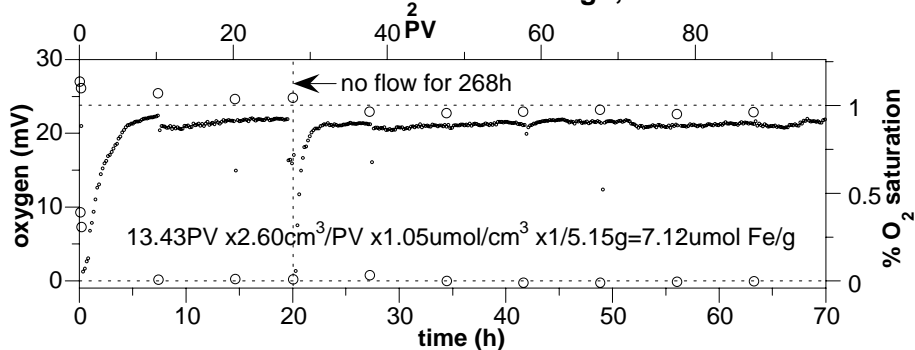
100D Sediment Core (Field Reduced), C4687 D4-91, 85.6' bgs
V27: Dissolved O₂ Breakthrough, Probe 1

no flow for 259h →

18.98PV x2.62cm³/PV x1.05umol/cm³ x1/5.33g=9.80umol Fe/g

V27: Dissolved O₂ Breakthrough, Probe 2

no flow for 259h →

22.37PV x2.62cm³/PV x1.05umol/cm³ x1/5.33g=11.54umol Fe/g
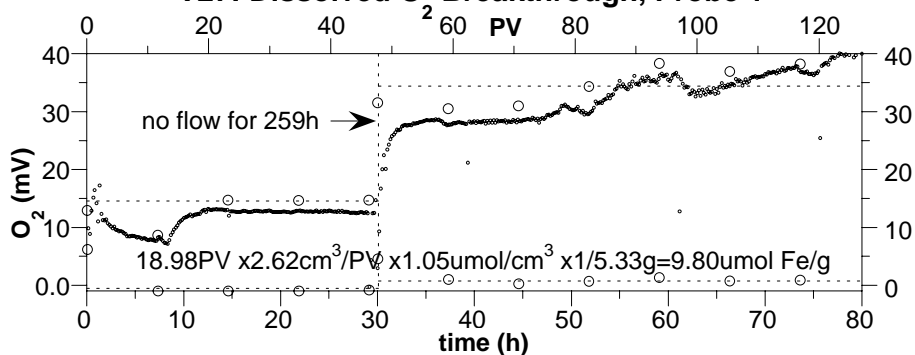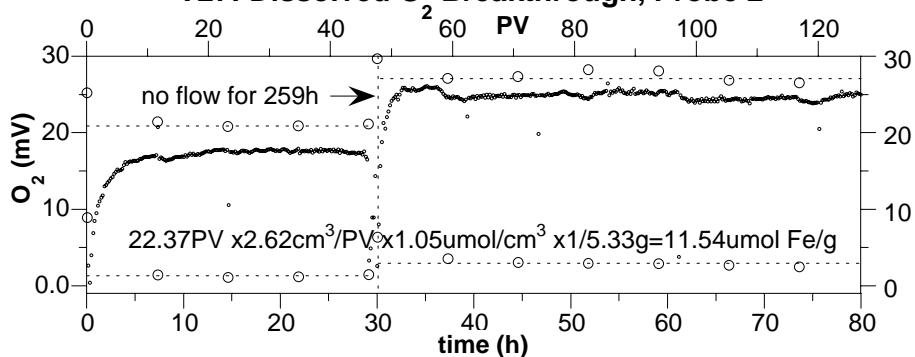
100D Sediment Core (Field Reduced), C 4687 D4-91, 86.6' bgs
V28: Dissolved O₂ Breakthrough, Probe 1
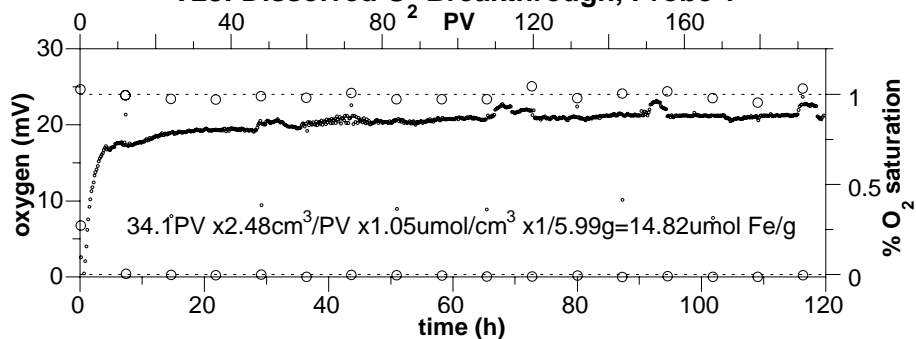
34.1PV x2.48cm³/PV x1.05umol/cm³ x1/5.99g=14.82umol Fe/g

V28: Dissolved O₂ Breakthrough, Probe 2

34.0PV x2.48cm³/PV x1.05umol/cm³ x1/5.99g=14.78umol Fe/g

B.2
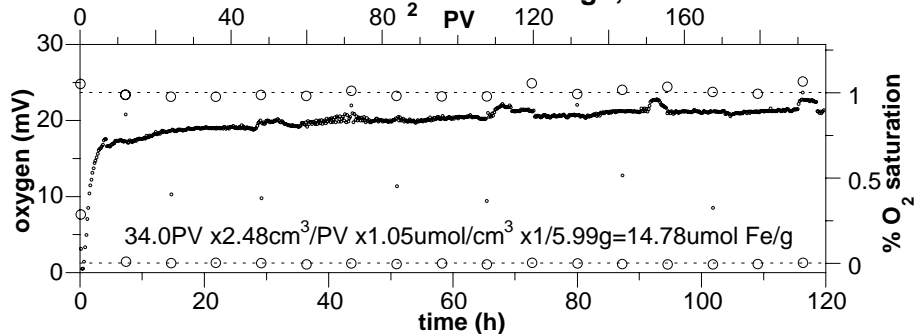
100D Sediment Core (Field Reduced), C4687 D4-91, 88.1' bgs
V29: Dissolved O$_2$ Breakthrough, Probe 1

PV

oxygen (mV)

% O$_2$ saturation

81.26PV x1.97cm^3/PV x1.05umol/cm^3 x1/6.85g=24.54umol Fe/g

time (h)

V29: Dissolved O$_2$ Breakthrough, Probe 2

PV

oxygen (mV)

% O$_2$ saturation

90.94PV x1.97cm^3/PV x1.05umol/cm^3 x1/6.85g=27.46umol Fe/g

time (h)
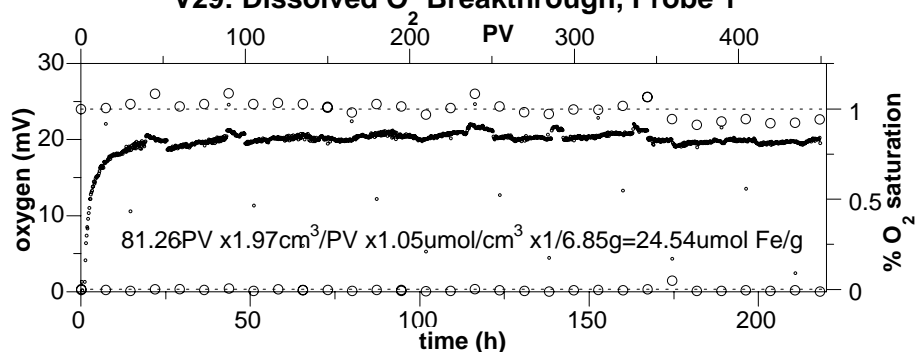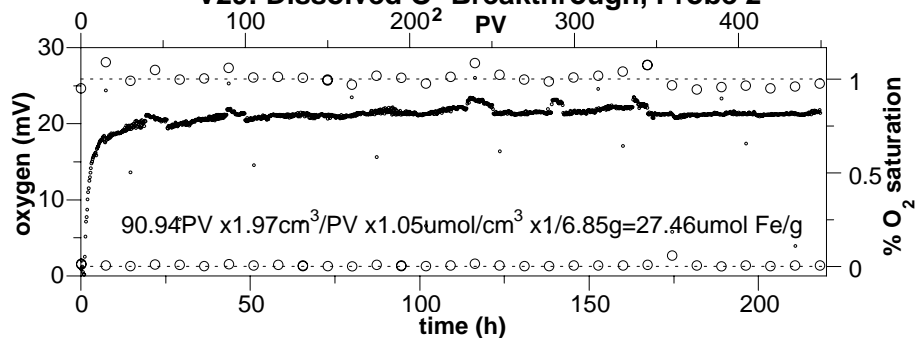
100D Sediment Core (Lab Reduced), C4687 D4-91, 88.1' bgs
V43: Dissolved O$_2$ Breakthrough, Probe 1

PV

oxygen (mV)

% O$_2$ saturation

131.32PV x2.65cm^3/PV x1.05umol/cm^3
x1/4.77g=76.60umol Fe/g

time (h)

V43: Dissolved O$_2$ Breakthrough, Probe 2

PV

oxygen (mV)

% O$_2$ saturation

148.77PV x2.65cm^3/PV x1.05umol/cm^3
x1/4.77g=86.78umol Fe/g

time (h)

B.3
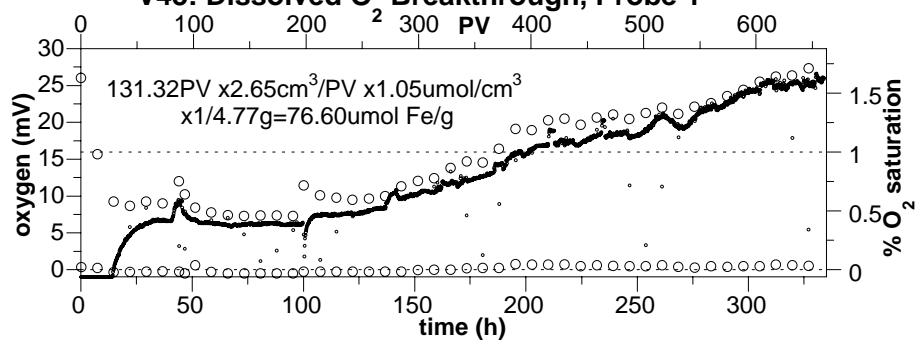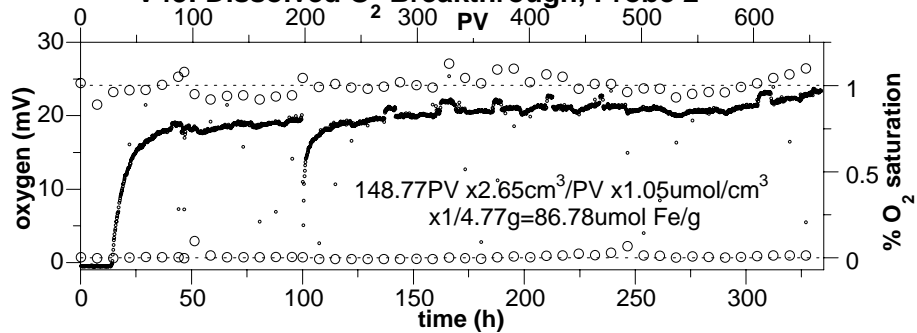
100D Sediment Core (Field Reduced), C4687 D4-91, 89.1' bgs
V30: Dissolved O$_2$ Breakthrough, Probe 1

17.93PV x1.79cm^3/PV x1.05umol/cm^3 x1/7.20g=4.68umol Fe/g

V30: Dissolved O$_2$ Breakthrough, Probe 2

35.85PV x1.79cm^3/PV x1.05umol/cm^3 x1/7.20g=9.36umol Fe/g
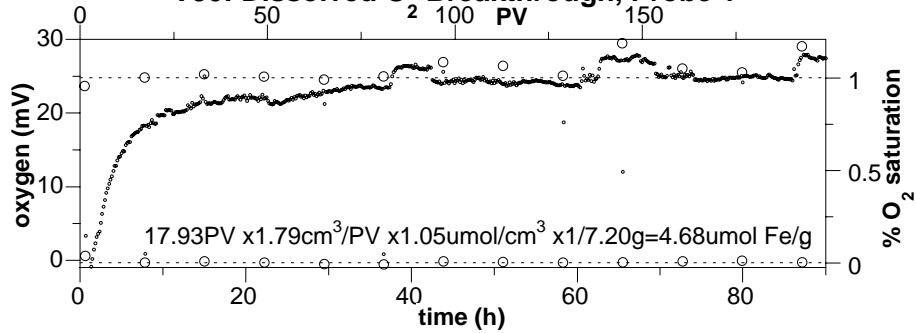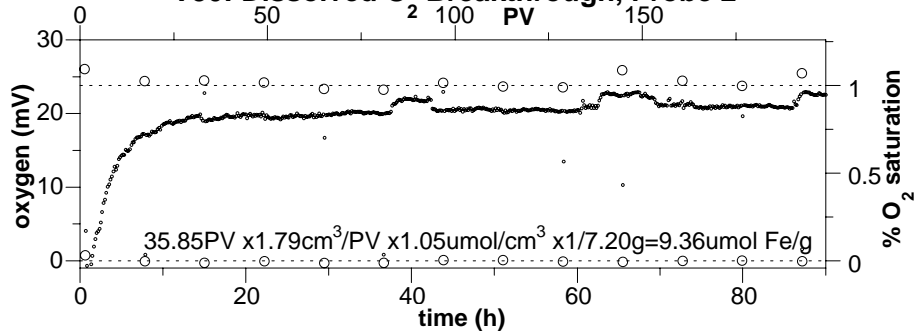
100D Sediment Core (Field Reduced), C4687 D4-91, 90.6' bgs
V31: Dissolved O$_2$ Breakthrough, Probe 1

21.96PV x2.33cm^3/PV x1.05umol/cm^3 x1/5.81g=9.25umol Fe/g

V31: Dissolved O$_2$ Breakthrough, Probe 2

36.12PV x2.33cm^3/PV x1.05umol/cm^3 x1/5.81g=15.21umol Fe/g

B.4
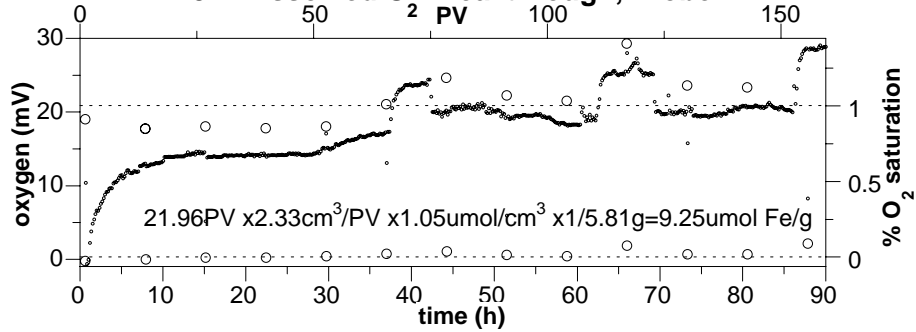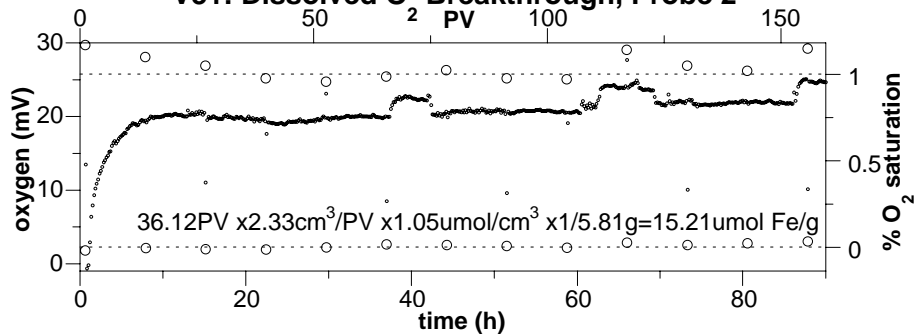
100D Sediment Core (Field Reduced), C4687 D4-91, 91.6' bgs
V32: Dissolved O$_2$ Breakthrough, Probe 1
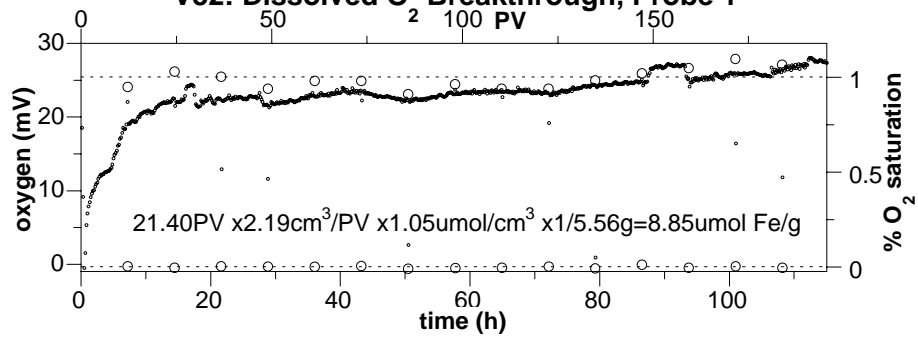
21.40PV x2.19cm^3/PV x1.05umol/cm^3 x1/5.56g=8.85umol Fe/g

V32: Dissolved O$_2$ Breakthrough, Probe 2

26.31PV x2.19cm^3/PV x1.05umol/cm^3 x1/5.56g=10.88umol Fe/g

B.5
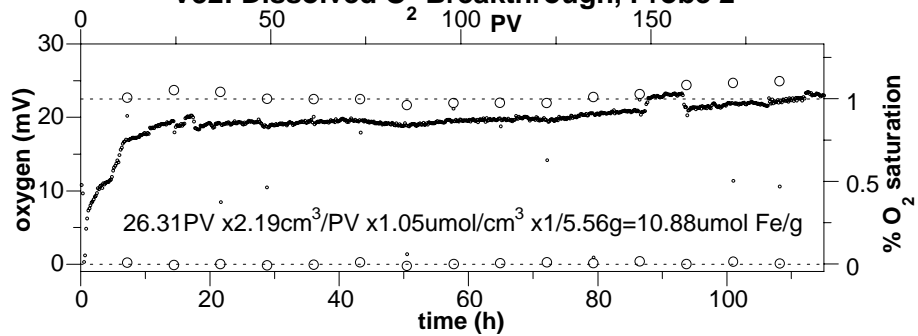
100D Sediment Core (Field Reduced), C4687 D4-91, 93.1' bgs
V33: Dissolved O$_2$ Breakthrough, Probe 1

PV

oxygen (mV)

% O$_2$ saturation

66.28PV x2.11cm^3/PV x1.05umol/cm^3 x1/6.55g=22.42umol Fe/g

time (h)

V33: Dissolved O$_2$ Breakthrough, Probe 2

PV

oxygen (mV)

% O$_2$ saturation

81.48PV x2.11cm^3/PV x1.05umol/cm^3 x1/6.55g=27.56umol Fe/g

time (h)
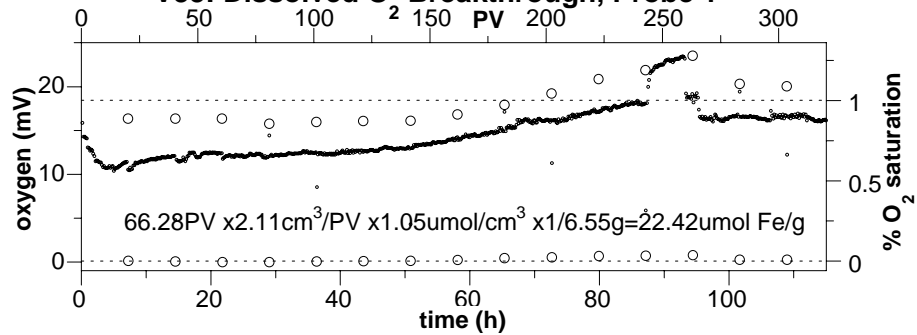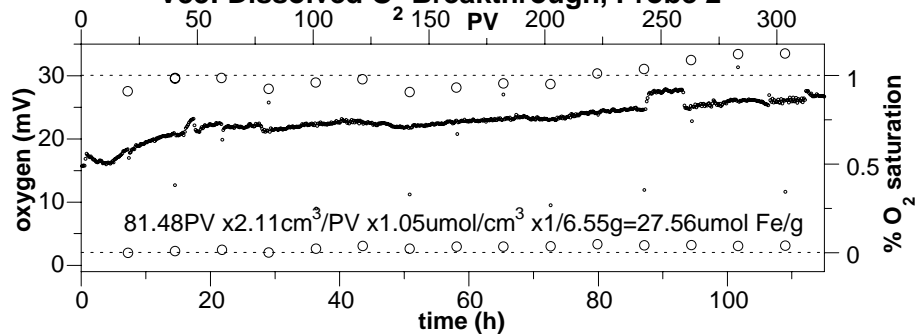
100D Sediment Core (Lab Reduced), C4687 D4-91, 93.1' bgs
V48: Dissolved O$_2$ Breakthrough, Probe 1

oxygen (mV)

% O$_2$ saturation

Q_1=2.735 PV/h

Q_2=1.966 PV/h

127.6PV x2.00cm^3/PV x1.05umol/cm^3 x1/6.28g=42.66umol Fe/g

PV

V48: Dissolved O$_2$ Breakthrough, Probe 2

oxygen (mV)

% O$_2$ saturation

Q_1=2.735 PV/h

Q_2=1.966 PV/h

138.4PV x2.00cm^3/PV x1.05umol/cm^3 x1/6.28g=46.28umol Fe/g

PV

B.6
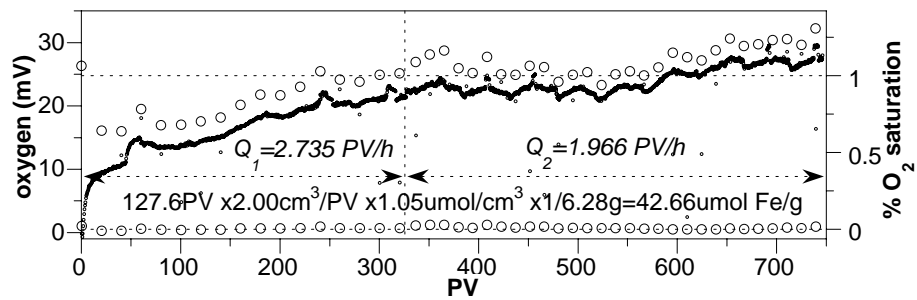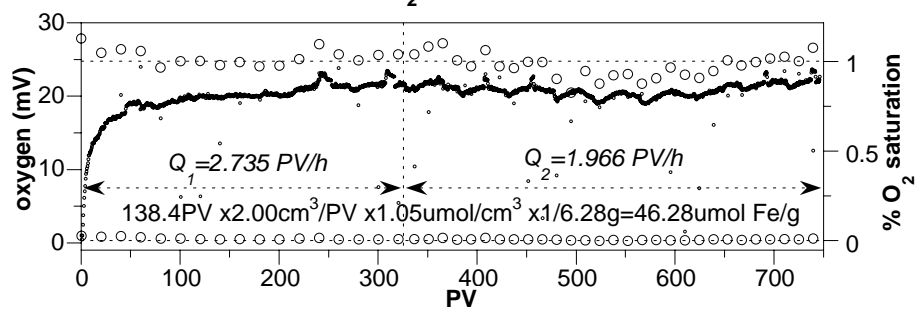
100D Sediment Core (Field Reduced), C4687 D4-91, 94.1' bgs
V34: Dissolved O$_2$ Breakthrough, Probe 1

51.98PV x1.64cm^3/PV x1.05umol/cm^3 x1/7.35g=12.18umol Fe/g

V34: Dissolved O$_2$ Breakthrough, Probe 2

58.03PV x1.64cm^3/PV x1.05umol/cm^3 x1/7.35g=13.60umol Fe/g
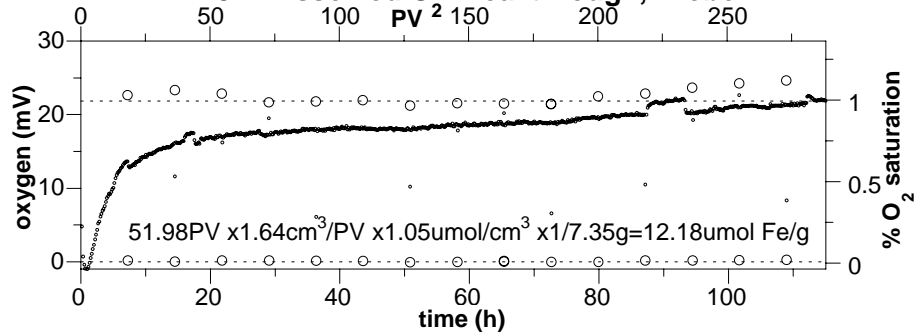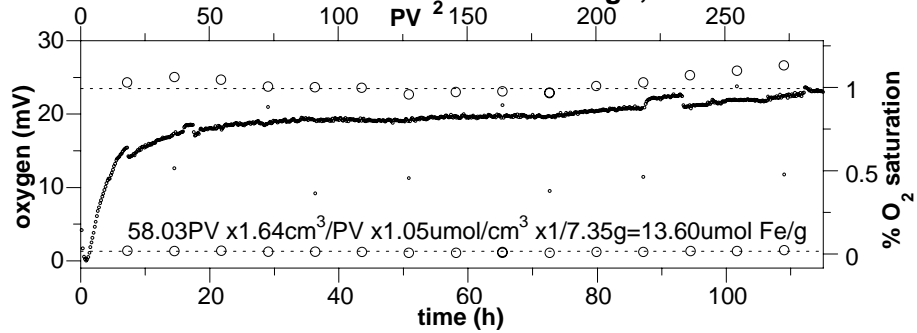
100D Sediment Core (Field Reduced), C4687 D4-91, 95.6' bgs
V35: Dissolved O$_2$ Breakthrough, Probe 1
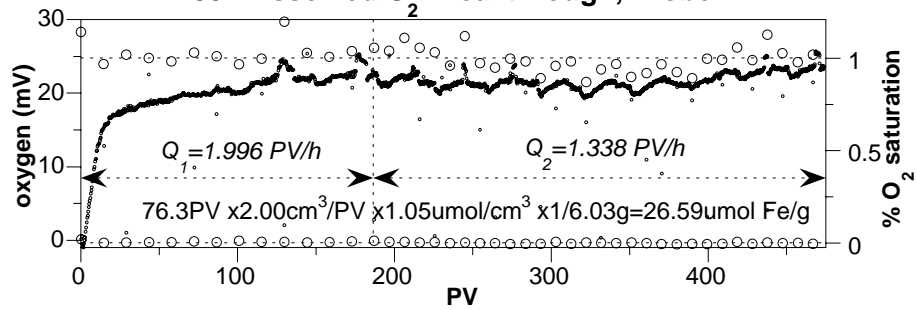
Q_1=1.996 PV/h Q_2=1.338 PV/h

76.3PV x2.00cm^3/PV x1.05umol/cm^3 x1/6.03g=26.59umol Fe/g

V35: Dissolved O$_2$ Breakthrough, Probe 2

Q_1=1.996 PV/h Q_2=1.338 PV/h

103.0PV x2.00cm^3/PV x1.05umol/cm^3 x1/6.03g=35.88umol Fe/g

B.7
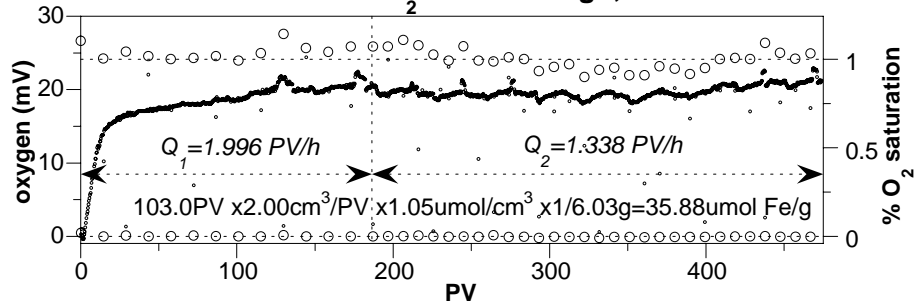
100D Sediment Core (Field Reduced), C4687 D4-91, 96.6' bgs
V36: Dissolved O$_2$ Breakthrough, Probe 1

Q_1=2.198 PV//h Q_2=1.577 PV//h

118.4PV x1.85cm^3/PV x1.05umol/cm^3 x1/6.83g=33.66umol Fe/g

V36: Dissolved O$_2$ Breakthrough, Probe 2

Q_1=2.198 PV//h Q_2=1.577 PV//h

128.5PV x1.85cm^3/PV x1.05umol/cm^3 x1/6.83g=36.54umol Fe/g
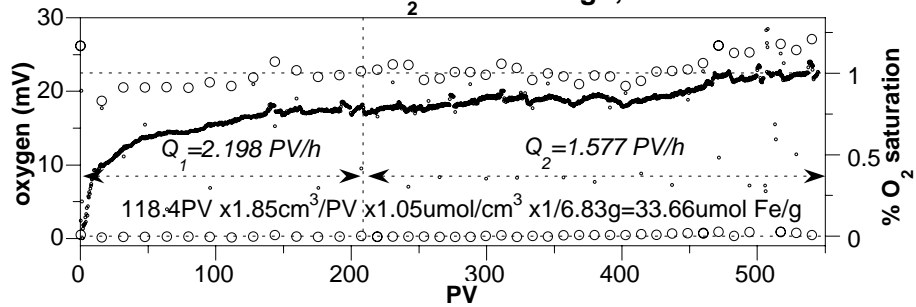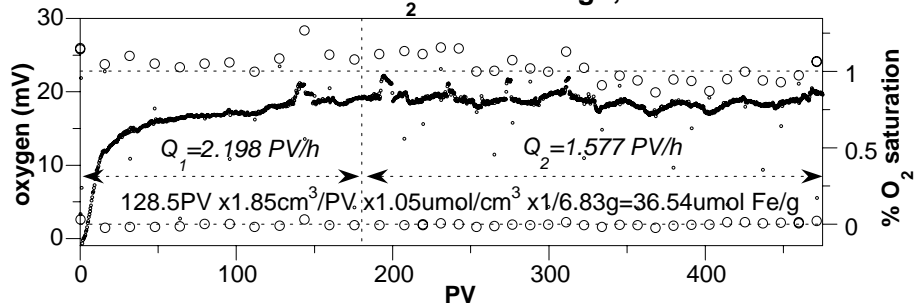
100D Sediment Core (Lab Reduced), C4687 D4-91, 96.6' bgs
V52: Dissolved O$_2$ Breakthrough, Probe 1
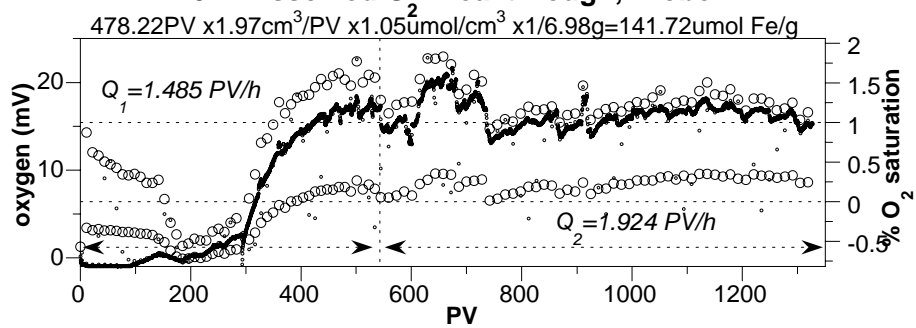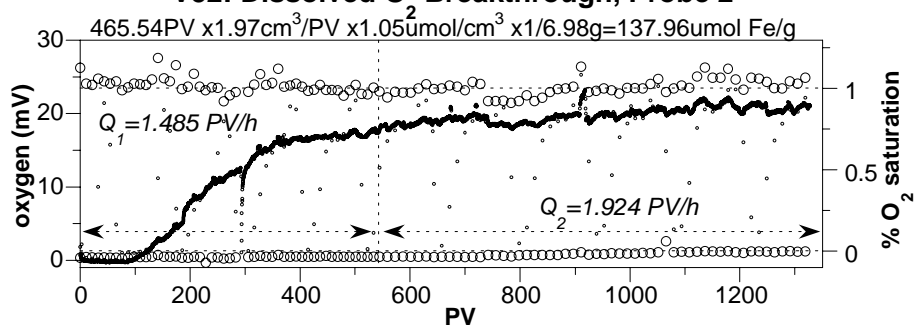
478.22PV x1.97cm^3/PV x1.05umol/cm^3 x1/6.98g=141.72umol Fe/g

Q_1=1.485 PV/h Q_2=1.924 PV//h

V52: Dissolved O$_2$ Breakthrough, Probe 2

465.54PV x1.97cm^3/PV x1.05umol/cm^3 x1/6.98g=137.96umol Fe/g

Q_1=1.485 PV/h Q_2=1.924 PV//h

Appendix C

1-D Oxidation of Field- and Laboratory-Reduced Sediments from 100D Area Borehole C4688 D4-92

Appendix C - 1-D Oxidation of Field- and Laboratory-Reduced Sediments from 100D Area Borehole C4688 D4-92

100D Sediment Core (Field Reduced), C4688 D4-92, 85.1' bgs
V115: Dissolved O$_2$ Breakthrough, Probe 1

$32.46PV \times 1.88cm^3/PV \times 1.05umol/cm^3 \times 1/6.67g = 9.61umol\ Fe/g$

V115: Dissolved O$_2$ Breakthrough, Probe 2

$47.16PV \times 1.88cm^3/PV \times 1.05umol/cm^3 \times 1/6.67g = 13.96umol\ Fe/g$

100D Sediment Core (Field Reduced), C4688 D4-92, 86.1' bgs
V116: Dissolved O$_2$ Breakthrough, Probe 1

$48.37PV \times 2.04cm^3/PV \times 1.05umol/cm^3 \times 1/6.30g = 16.44umol\ Fe/g$

V116: Dissolved O$_2$ Breakthrough, Probe 2

$50.20PV \times 2.04cm^3/PV \times 1.05umol/cm^3 \times 1/6.30g = 17.07umol\ Fe/g$

C.1
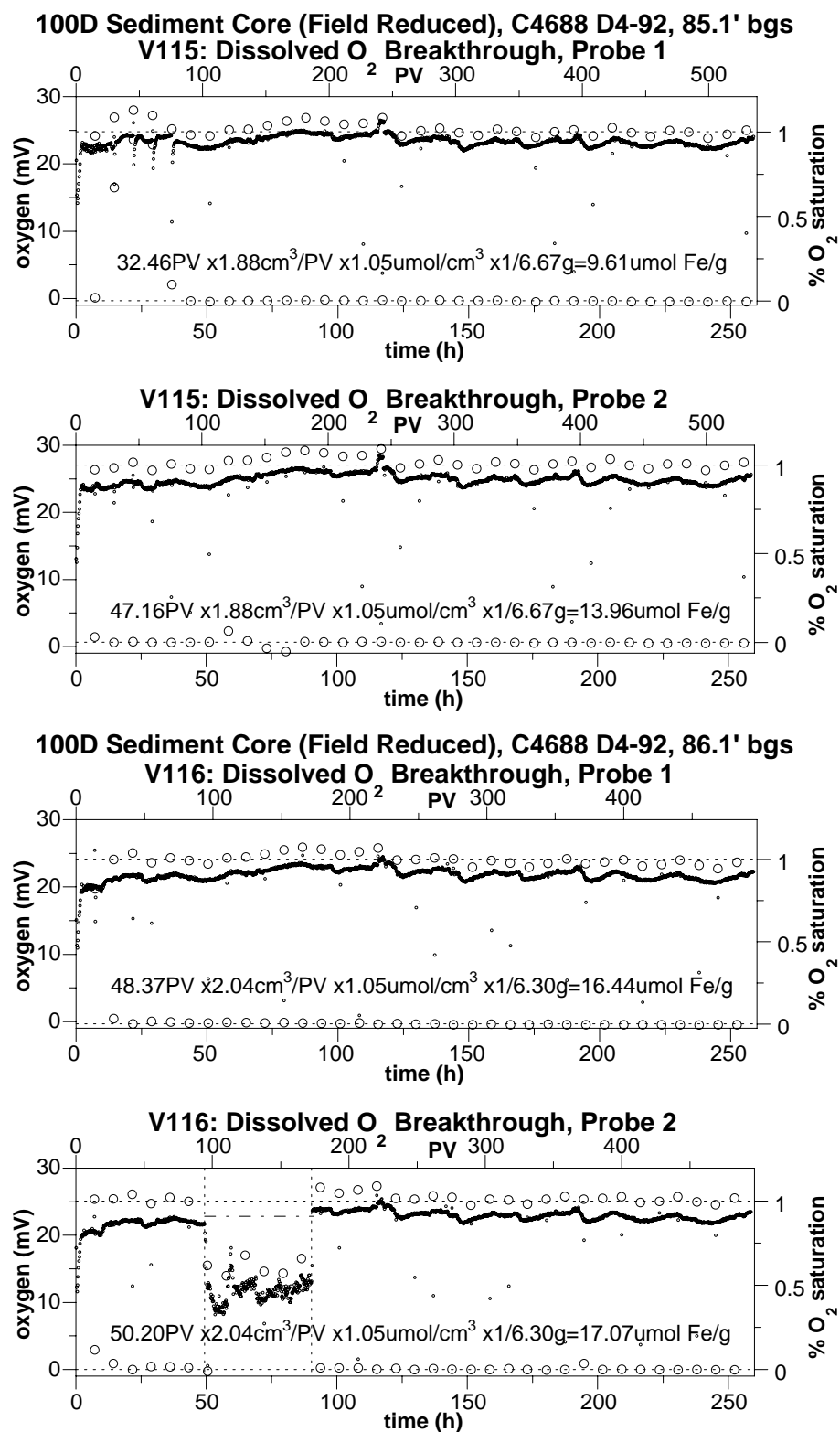
100D Sediment Core (Field Reduced), C4688 D4-92, 87.6' bgs
V117: Dissolved O$_2$ Breakthrough, Probe 1

57.56PV x2.09cm^3/PV x1.05umol/cm^3 x1/6.08g=20.77umol Fe/g

V117: Dissolved O$_2$ Breakthrough, Probe 2

Air Bubble in Probe
Cannot integrate; too much missing

100D Sediment Core (Field Reduced), C4688 D4-92, 88.6' bgs
V118: Dissolved O$_2$ Breakthrough, Probe 1

69.94PV x1.74cm^3/PV x1.05umol/cm^3 x1/7.09g=18.02umol Fe/g

V118: Dissolved O$_2$ Breakthrough, Probe 2

80.87PV x1.74cm^3/PV x1.05umol/cm^3 x1/7.09g=20.84umol Fe/g

C.2
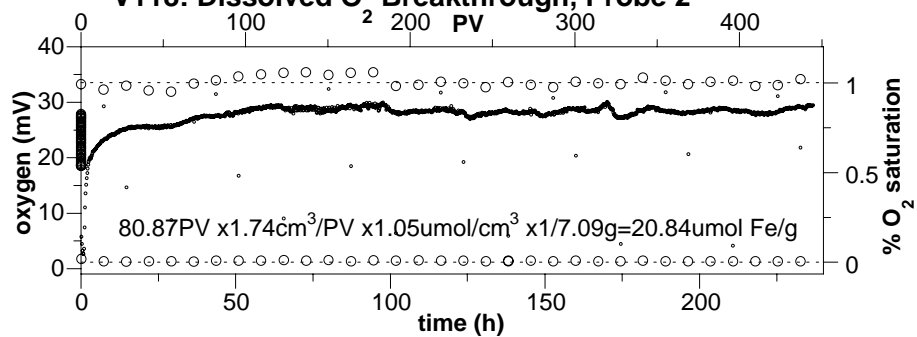
100D Sediment Core (Field Reduced), C4688 D4-92, 90.1' bgs
V73: Dissolved O$_2$ Breakthrough, Probe 1

73.70PV x2.16cm^3/PV x1.05umol/cm^3
x1/6.17g=27.09umol Fe/g

V73: Dissolved O$_2$ Breakthrough, Probe 2

84.29PV x2.16cm^3/PV x1.05umol/cm^3
x1/6.17g=30.98umol Fe/g
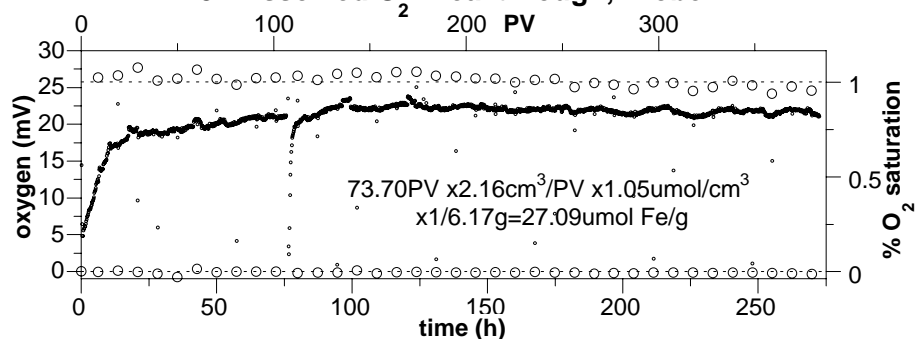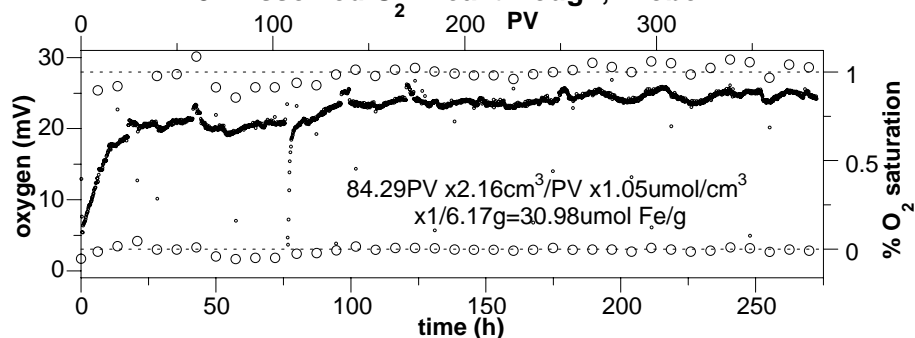
100D Sediment Core (Lab Reduced), C4688 D4-92, 90.1' bgs
V83: Dissolved O$_2$ Breakthrough, Probe 1

127.23PV x1.77cm^3/PV x1.05umol/cm^3 x1/6.91g=34.22umol Fe/g

V83: Dissolved O$_2$ Breakthrough, Probe 2

138.52PV x1.77cm^3/PV x1.05umol/cm^3 x1/6.91g=37.26umol Fe/g

C.3
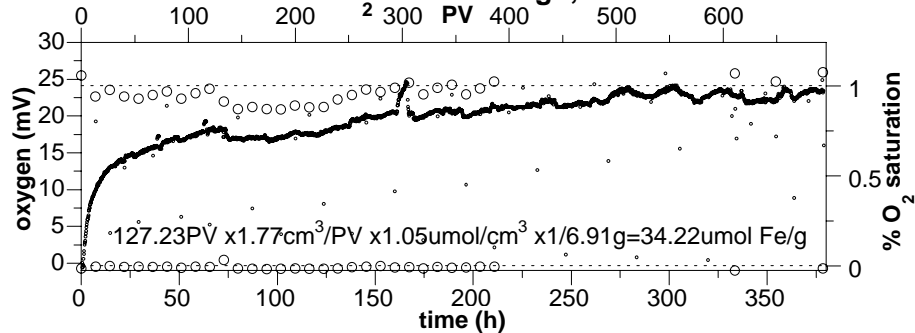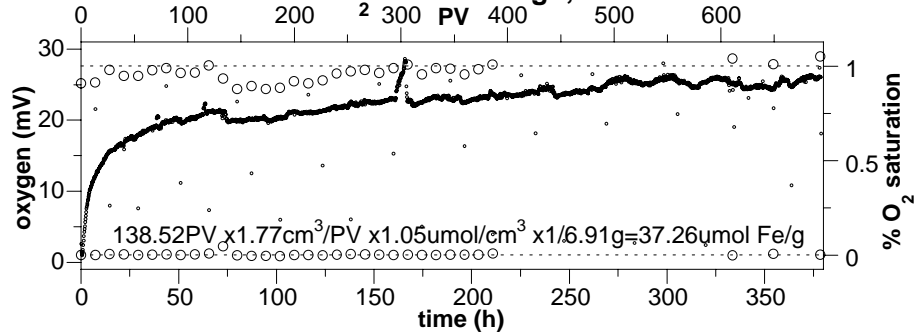
100D Sediment Core (Field Reduced), C4688 D4-92, 91.6' bgs
V119: Dissolved O$_2$ Breakthrough, Probe 1

62.55PV x2.07cm^3/PV x1.05umol/cm^3 x1/6.70g=20.29umol Fe/g

V119: Dissolved O$_2$ Breakthrough, Probe 2

61.89PV x2.07cm^3/PV x1.05umol/cm^3 x1/6.70g=20.08umol Fe/g
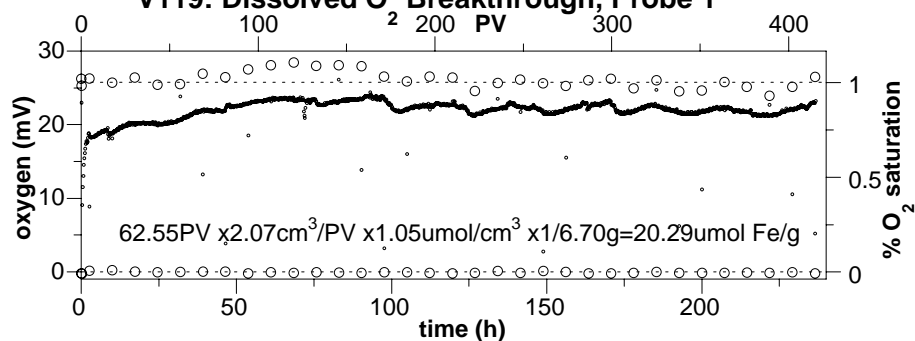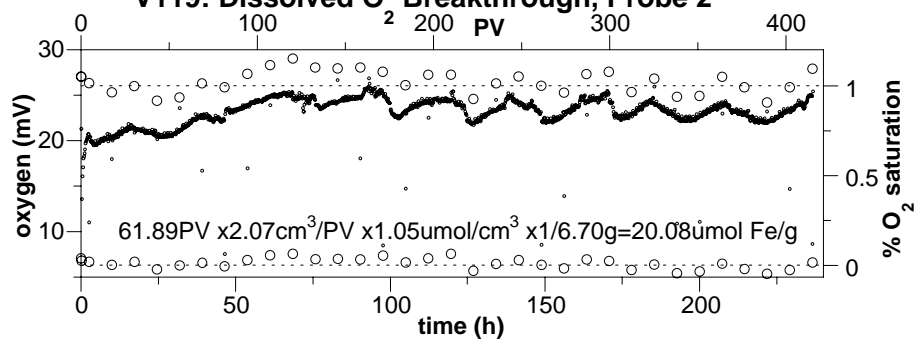
100D Sediment Core (Field Reduced), C4688 D4-92, 92.6' bgs
V120: Dissolved O$_2$ Breakthrough, Probe 1

O$_2$ Norm Avg = 0.890

DAQcard unplugged; 8-68h

40.20PV x2.18cm^3/PV x1.05umol/cm^3 x1/6.63g=13.88umol Fe/g

V120: Dissolved O$_2$ Breakthrough, Probe 2

O$_2$ Norm Avg = 0.885

DAQcard unplugged; 8-68h

40.59PV x2.18cm^3/PV x1.05umol/cm^3 x1/6.63g=14.01umol Fe/g

C.4
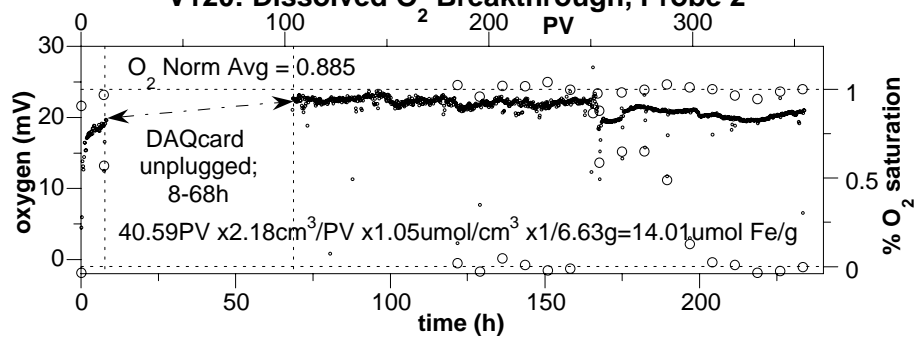
100D Sediment Core (Field Reduced), C4688 D4-92, 95.1' bgs
V74: Dissolved O$_2$ Breakthrough, Probe 1

132.77PV x2.33cm^3/PV x1.05umol/cm^3
x1/6.10g=53.25umol Fe/g
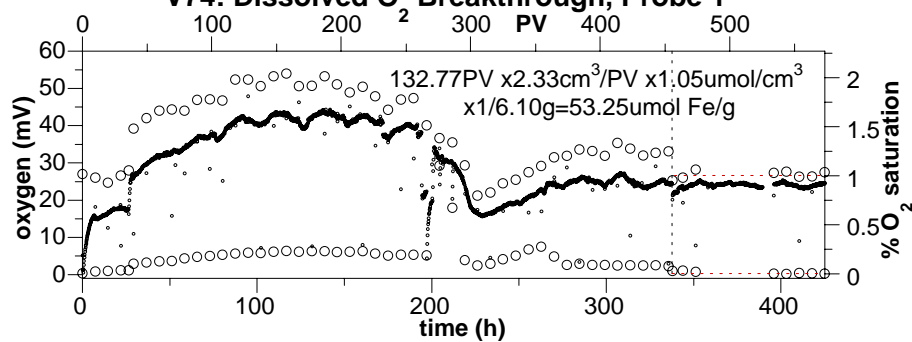
100D Sediment Core (Lab Reduced), C4688 D4-92, 95.1' bgs
V88: Dissolved O$_2$ Breakthrough, Probe 1

145.39PV x2.11cm^3/PV x1.05umol/cm^3
x1/6.16g=52.29umol Fe/g

V88: Dissolved O$_2$ Breakthrough, Probe 2

149.56PV x2.11cm^3/PV x1.05umol/cm^3
x1/6.16g=53.79umol Fe/g

C.5
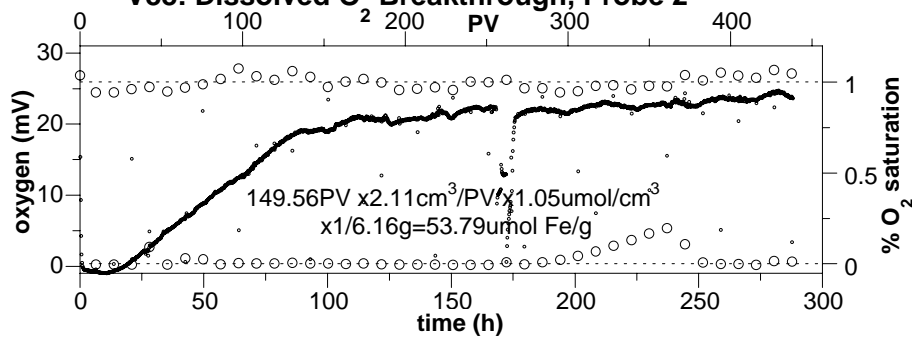
100D Sediment Core (Field Reduced), C4688 D4-92, 97.6' bgs
V121: Dissolved O$_2$ Breakthrough, Probe 1

51.19PV x2.57cm^3/PV x1.05umol/cm^3 x1/5.28g=26.16umol Fe/g

V121: Dissolved O$_2$ Breakthrough, Probe 2

Integrated from 0-50h,
90% assumed for 50-265.8h

40.15PV x2.57cm^3/PV x1.05umol/cm^3 x1/5.28g=20.52umol Fe/g
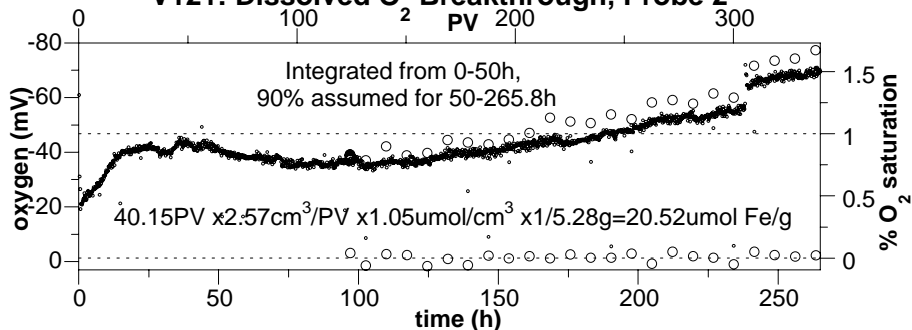
100D Sediment Core (Field Reduced), C4688 D4-92, 100.6' bgs
V75: Dissolved O$_2$ Breakthrough, Probe 1
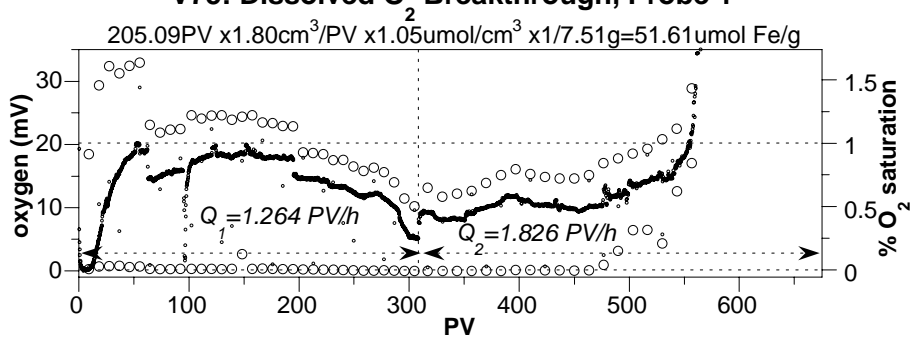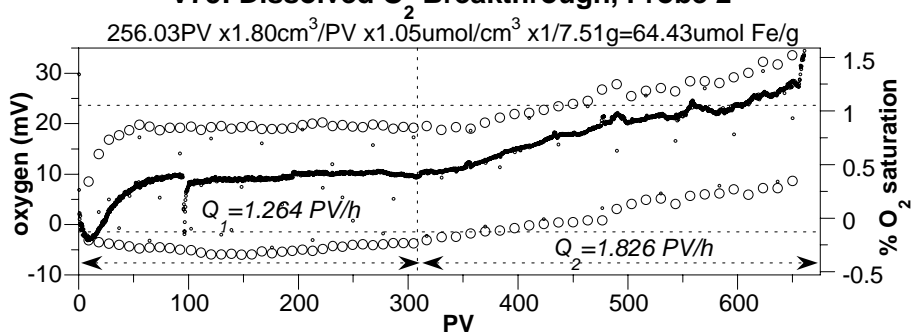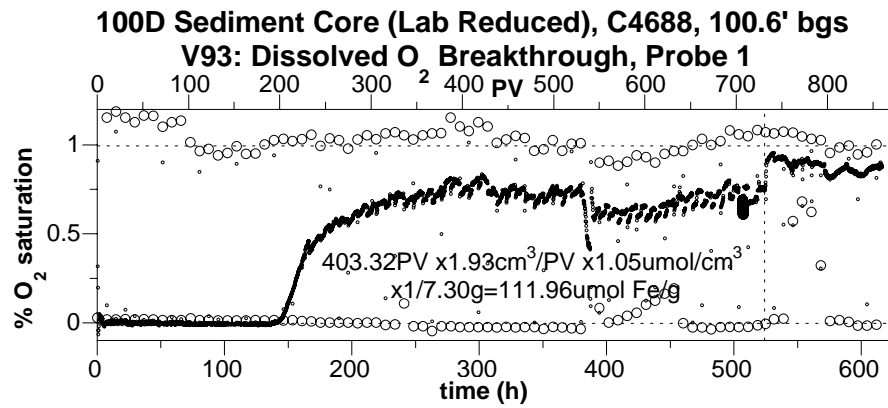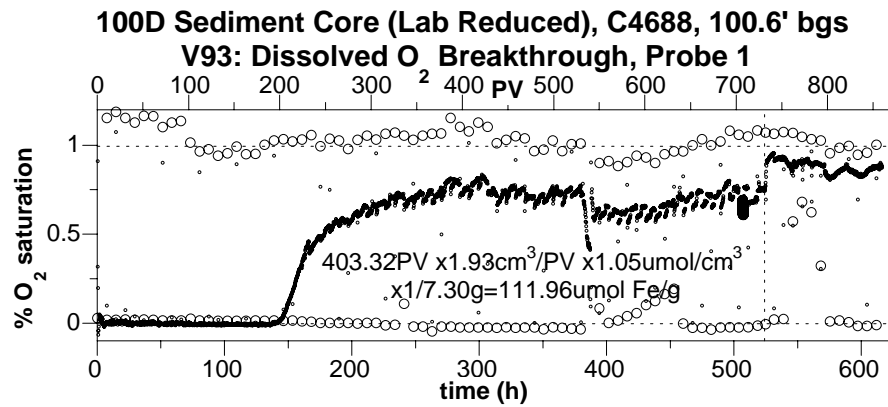
205.09PV x1.80cm^3/PV x1.05umol/cm^3 x1/7.51g=51.61umol Fe/g

Q$_1$=1.264 PV/h

Q$_2$=1.826 PV/h

V75: Dissolved O$_2$ Breakthrough, Probe 2

256.03PV x1.80cm^3/PV x1.05umol/cm^3 x1/7.51g=64.43umol Fe/g

Q$_1$=1.264 PV/h

Q$_2$=1.826 PV/h

C.6

100D Sediment Core (Lab Reduced), C4688, 100.6' bgs

V93: Dissolved O$_2$ Breakthrough, Probe 1

403.32PV x1.93cm^3/PV x1.05umol/cm^3 x1/7.30g=111.96umol Fe/g

100D Sediment Core (Lab Reduced), C4688, 100.6' bgs

V93: Dissolved O$_2$ Breakthrough, Probe 1

403.32PV x1.93cm^3/PV x1.05umol/cm^3 x1/7.30g=111.96umol Fe/g

C.7

Appendix D

1-D Oxidation of Field- and Laboratory-Reduced Sediments from 100D Area Borehole C4689 D4-93

Appendix D - 1-D Oxidation of Field- and Laboratory-Reduced Sediments from 100D Area Borehole C4689 D4-93

100D Sediment Core (Field Reduced), C4689 D4-93, 88.1' bgs
V95: Dissolved O$_2$ Breakthrough, Probe 1

61.19PV x2.28cm^3/PV x1.05umol/cm^3 x1/6.07g=24.13umol Fe/g
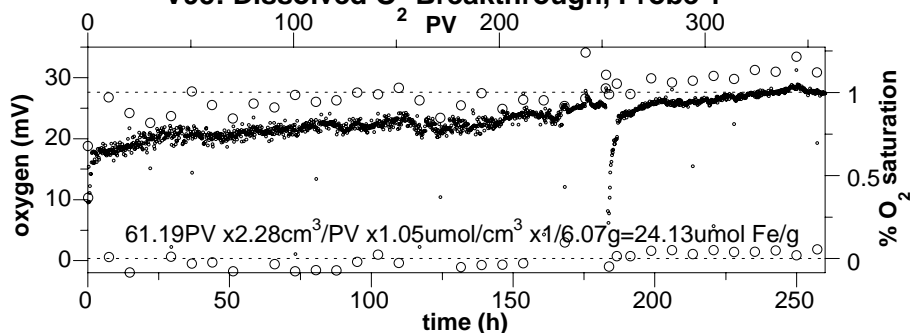
V95: Dissolved O$_2$ Breakthrough, Probe 2
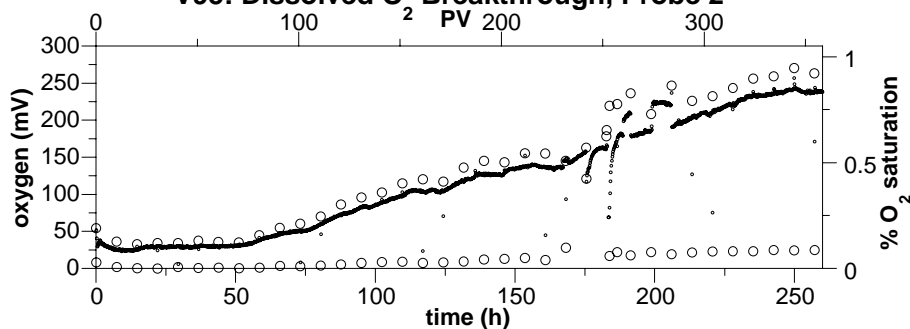
100D Sediment Core (Lab Reduced), C4689 D4-93, 88.1' bgs
V103: Dissolved O$_2$ Breakthrough, Probe 1

279.48PV x1.86cm^3/PV

x1.05umol/cm^3 x1/7.28g=74.98umol Fe/g

V103: Dissolved O$_2$ Breakthrough, Probe 2

264.39PV x1.86cm^3/PV

x1:05umol/cm^3 x1/7.28g=70.93umol Fe/g

100D Sediment Core (Field Reduced), C4689 D4-93, 91.1' bgs
V96: Dissolved O₂ Breakthrough, Probe 1

161.1PV x2.00cm³/PV x1.05umol/cm³ x1/6.37g=53.11umol Fe/g

V96: Dissolved O₂ Breakthrough, Probe 2

163.9PV x2.00cm³/PV x1.05umol/cm³ x1/6.37g=54.04umol Fe/g
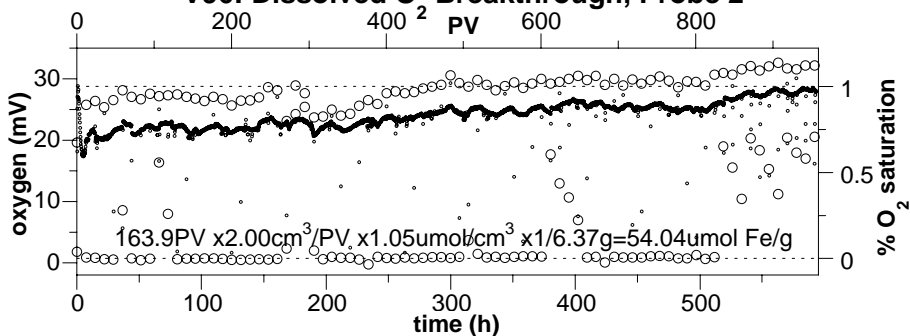
100D Sediment Core (Lab Reduced), C4689 D4-93, 91.1' bgs
V107: Dissolved O₂ Breakthrough, Probe 1

241.65PV x2.05cm³/PV x1.05umol/cm³ x1/6.16g=84.44umol Fe/g

$Q_1=1.910 \ PV/h$

$Q_2 = 0.633 \ PV/h$

$Q_3=1.771 \ PV/h$

V107: Dissolved O₂ Breakthrough, Probe 2

254.07PV x2.05cm³/PV x1.05umol/cm³ x1/6.16g=88.78umol Fe/g

$Q_1=1.910 \ PV/h$

$Q_2 = 0.633 \ PV/h$

$Q_3=1.771 \ PV/h$

D.2
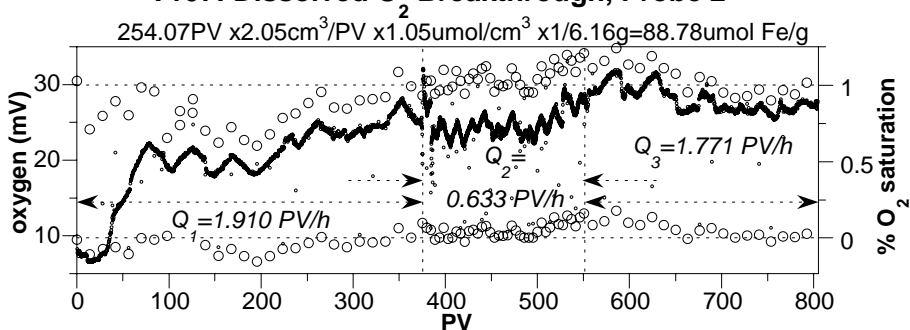
100D Sediment Core (Field Reduced), C4689 D4-93, 93.1' bgs
V97: Dissolved O$_2$ Breakthrough, Probe 1

101.5PV x1.96cm^3/PV x1.05umol/cm^3 x1/6.62g=31.56umol Fe/g

V97: Dissolved O$_2$ Breakthrough, Probe 2

126.6PV x1.96cm^3/PV x1.05umol/cm^3 x1/6.62g=39.36umol Fe/g
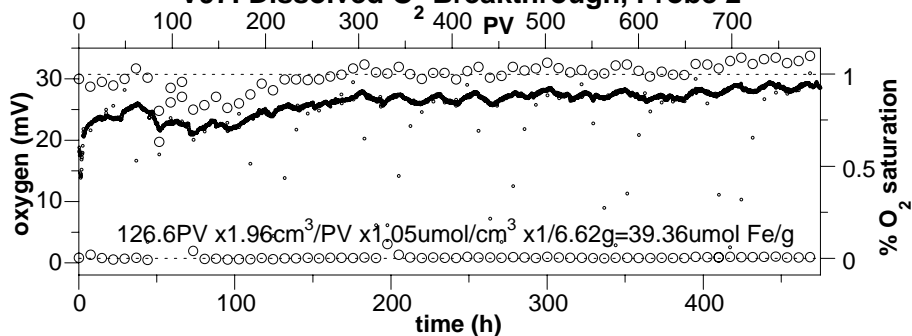
100D Sediment Core (Field Reduced), C4689 D4-93, 95.6' bgs
V130: Dissolved O$_2$ Breakthrough, Probe 1

113.19PV x2.23cm^3/PV x1.05umol/cm^3 x1/5.33g=49.73umol Fe/g

V130: Dissolved O$_2$ Breakthrough, Probe 2

126.51PV x2.23cm^3/PV x1.05umol/cm^3 x1/5.33g=55.57umol Fe/g

D.3
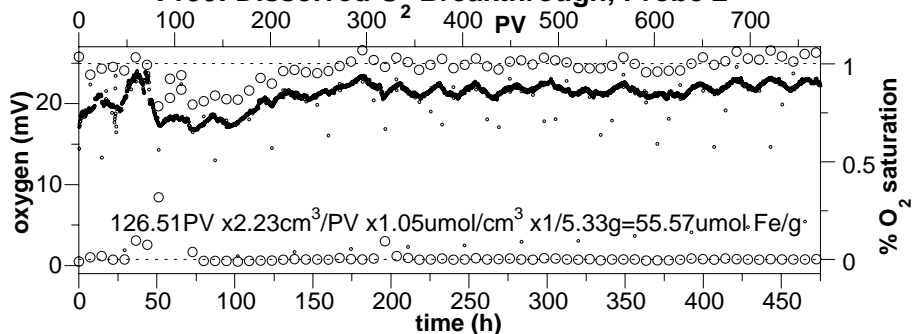
100D Sediment Core (Field Reduced), C4689 D4-93, 96.6' bgs
V131: Dissolved O$_2$ Breakthrough, Probe 1

143.32PV x1.77cm^3/PV x1.05umol/cm^3 x1/7.14g=37.30umol Fe/g

V131: Dissolved O$_2$ Breakthrough, Probe 2

181.80PV x1.77cm^3/PV x1.05umol/cm^3 x1/7.14g=47.32umol Fe/g
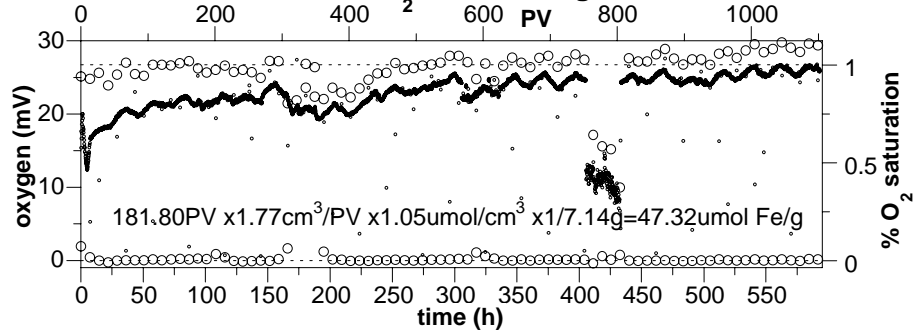
100D Sediment Core (Lab Reduced), C4689 D4-93, 96.6' bgs
V113: Dissolved O$_2$ Breakthrough, Probe 1
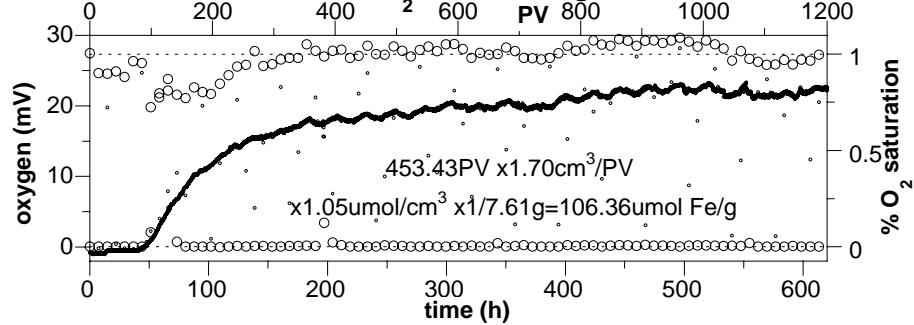
453.43PV x1.70cm^3/PV

x1.05umol/cm^3 x1/7.61g=106.36umol Fe/g

V113: Dissolved O$_2$ Breakthrough, Probe 2

509.32PV x1.70cm^3/PV

x1.05umol/cm^3 x1/7.61g=119.47umol Fe/g
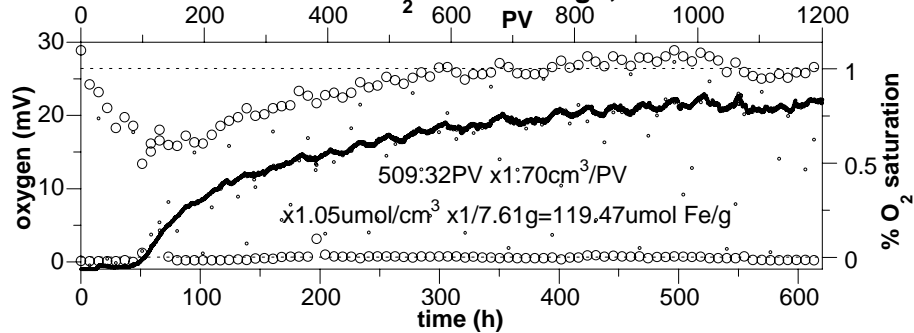
Appendix E

1997 to 2005 Redox Conditions from Core Analysis

Appendix E – 1997 to 2005 Redox Conditions from Core Analysis

Table E.1. Laboratory (maximum) Reductive Capacity of 100 D Area Sediments in April 1997
(maximum reductive capacity 24.34 ± 5.29 μmol/g)

#	exp. type	soil	< 4 mm	res. time (h/pv)	duration (pv)	dith. (mol /L)	buffer (mol /L)	btc loss[1] (μmol)	disp. loss[1] (μmol)	reduced[3] (μmol)	half-life[4] (h)	btc loss[1] (μmol)	fraction[5] oxidized	half-life[4] (h)	maximum red. capacity whole sediment (μmol /g)
			experimental parameters					< 4 mm fraction of sediment reduction by dithionite				< 4 mm fraction of sediment oxidation by dissolved O$_2$			
11	ox.	D4-4, 94'	0.923	4.71	3.5	anoxic	--	--	--	--	--	1.04	1.76*	--	
12	red.	D4-2, 92.3'	0.453	1.58	11	0.017	0.16	196.	92.	104.	3.48	--	--	--	47.11
13	red.	D4-5, 93.6'	0.412	1.83	11	0.052	0.24	0.	0.	--	4.71	--	--	--	
14	red.	D4-4, 93.5'	0.923	2.31	19	0.115	0.36	740.	705.	35.	6.54	--	--	--	32.31
15	ox.	D4-4, 93.5'	0.923	0.77	95	--	--	--	--		--	66.	0.47	0.75	16.5
16	red.	D4-4, 93.5'	0.923	2.12	22	0.071	0.36	360.	329.	31.	5.12	--	--	--	28.61
17	ox.	D4-4, 93.5'	0.923	0.71	170	--	--	--	--	--	--	82.	0.66	--	20.5
18	red.	D4-4, 93.5'	0.923	2.15	41	0.012	0.04	148.	121.	27.	4.00	--	--	--	24.92
19	ox.	D4-4, 93.5'	0.923	0.72	140	--	--	--	--	--	--	69.	0.64	--	17.25
20	ox.	D4-4, 93.5'	0.923	0.74	200	0.0064	0.02	--	--	--	--	64.	--	--	16.00
21	red.	D4-4, 93.5'	0.923	2.21	20	0.127	0.18	430.	401.	29.	3.94	--	--	--	26.77
22	ox.	D4-4, 93.5'	0.923	0.74	190	--	--	--	--	--	--	94.	0.81	--	23.5
23	red.	D4-3, 84.3'	0.534	2.12	24	0.102	0.09	715.	676.	39.	6.66	--	--	--	20.83
24	ox.	D4-3, 84.3'	0.534	0.69	240	--	--	--	--	--	--	109.	0.70	--	27.25
25	red.	D4-3, 84.3'	0.534	2.71	30	0.111	0.36	640.	610.	30.	5.96	--	--	--	16.02
26	ox.	D4-3, 84.3'	0.534	0.91	220	--	--	--	--	--	--	93.	0.77	1.34	23.25

[1] mass injected - breakthrough mass

[2] loss of injection mass by disproportionation assumes a 27 h half-life (rxn 2)

[3] breakthrough mass loss - disportionation

[4] based on slope change for dithionite or constant concentration for dissolved oxygen

[5] 0.25*mass loss of dissolved oxygen/mass reduced, based on stoichiometry of rxn 13.

*column capacity 0.59 μmol oxygen-free water, remaining 0.45 μmol assumed trapped air (0.5% of pore volume)

mean ± standard deviation: 24.34 ± 5.29

Table E.2. Field and Maximum Reductive Capacity of 100D Area Sediments in August 1999
(average field reduced 11.2 ± 7.4 μmol/g, lab reduced (maximum) 17.4 ± 5.3 μmol/g)

	experimental parameters				dithionite btc		oxygen breakthrough			Fe(II) for whole sediment		
				res.	Fe	red.rate	injection	btc mass	Fe(II)	Fe(II)	Fe(II)	fraction
sediment	experiment	name	fraction	time	reduced	half-life	mass[4]	loss	oxidized	lab reduced	field reduced	field
			< 4 mm	(h/pv)	(μmol/g)	(h)	(mol)	(mol)	(μmol/g)	(μmol/g)	(μmol/g)	reduced*
					<4 mm				<4 mm	whole sediment	whole sediment	
B8776, 84.5'	oxidation of field red.	MM	0.363	0.89			6.48E-05	2.24E-05	6.82		**	**
B8776, 90'	oxidation of field red.	MN	0.437	0.50			8.42E-05	3.42E-05	14.7		6.42	0.369
B8776, 84.5'	reduction after MM	MT	0.363	5.63	41.5	6.35				15.1		
B8776, 84.5'	oxidation, after MT	MU	0.363	0.56			4.55E-04	2.21E-04	38.4	14.0		
B8775, 88'	oxidation of field red.	MW	0.442	0.86			5.75E-04	2.47E-04	45.9		20.3	1.163
B8777, 95'	oxidation of field red.	MX	0.435	1.30			1.85E-04	1.08E-04	40.2		17.5	1.005
B8776, 94.8'	oxidation of field red.	MY	0.382	1.30					46.0		17.6	1.010
B8775, 82.8'	oxidation of field red.	MZ	0.462	1.20			2.18E-04	7.41E-05	35.7		16.5	0.752
B8775, 82.8'	reduction after MZ	MZC	0.462	4.25	40.8	7.26				18.8		
B8775, 82.8'	oxidation after MZC	MZD	0.462	0.48			1.59E-04	9.88E-05	47.5	22.0		
B8775, 93'	oxidation of field red.	MZR	0.435	0.61					5.13		2.23	0.128
B8777, 85'	oxidation of field red.	MZS	0.374	0.43					9.95		3.72	0.213
B8777, 90'	oxidation of field red.	MZT	0.357	0.45					16.3		5.81	0.333

*relative to the average maximum reducible iron (17.4 μmol Fe^{II}/g)
 or the lab reduced value for that sediment sample

** core was oxidized during transport to the laboratory

average maximum reducible iron = 17.4±5.3 μmol Fe^{II}/g

average field reduced iron = 11.2±7.4 μmol Fe^{II}/g

Table E.3. Field and Maximum Reductive Capacity of 100 D Area Sediments in March 2002
(average field reduced 10.6 ± 6.6 µmol/g, lab reduced [maximum] 40 ± 15 µmol/g)

					Fe(II) for < 4 mm			Fe(II) for whole sediment		
					field	laboratory		Fe(II)	Fe(II)	fraction
	depth		bulk density	porosity	reduced	dith.	reduced	field reduced	lab reduced	field
borehole	(ft)	<4mm	(g/cm³)	(cm³/cm³)	(µmol/g)	inj.	(µmol/g)	(µmol/g)	(µmol/g)	reduced*
199-D4-87	80.5-81	0.322	1.65	0.365	17.5	N		5.65		0.141
	86-86.5'	0.316	1.73	0.326	24.1	Y	139	7.63	43.9	0.174
	88.5-89'	0.306	1.47	0.437	28.7	N		8.78	--	0.219
	90.5-91'	0.280	1.67	0.324	7.53	N		2.11	--	0.053
	92-92.5'	0.280	1.35	0.450	47.1	N		13.2	--	0.330
	96.5-97'	0.177	1.40	0.515	28.1	Y	190	4.98	33.7	0.148
199-D4-88	84-84.5'	0.316	1.71	0.352	4.40	Y	156	1.39	49.3	0.028
	87.5-88'	0.319	1.60	0.396	41.1	N		13.0	--	0.325
	88.5-89'	0.322	1.66	0.376	66.7	N		21.3	--	0.532
	89.5-90'	0.329	1.51	0.368	66.3	Y	62.6	21.8	20.6	1.059
	94.5-95'	0.196	1.52	0.343	24.0	Y	155	4.69	30.4	0.154
199-D4-89	87-87.5'	0.410	1.62	0.339	22.9	Y	163	9.38	66.9	0.140
	89-89.5	0.362	1.73	0.304	49.8	N		18.0	--	0.451
	90-90.5	0.341	1.72	0.335	18.4	N		6.28	--	0.157
	91.5-92'	0.287	1.65	0.363	50.9	Y	123	18.4	35.2	0.523
	96-96.5'	0.373	1.41	0.365	36.6	N		13.7	--	0.341

* relative to maximum reducible iron for each sample or average   ave: 10.6 ± 6.6   40.0 ± 15.0   0.298

Table E.4. Reductive Capacity and Iron Extraction Data for D4-90, C4686 (upgradient of D4-37) in April 2005

depth (ft)	mass fraction < 4 mm	field reductive capacity* 1h 0.5M HCl (µmol/g)	field reductive capacity* column O_2 ox. (µmol/g)	maximum reductive capacity* 1h 0.5M HCl (µmol/g)	maximum reductive capacity* column O_2 ox. (µmol/g)	ratio capacity O_2/HCl	reduced fraction field/average 1h 0.5M HCl	reduced fraction field/average column O_2 ox.	total iron oxides* Fe^{II} 2 wk 5M HCl (µmol/g)	total iron oxides* Fe^{II+III} 2 wk 5M HCl (µmol/g)
79.1	0.549	0.066					0.005		78.1	231
81.6	0.583	0.01		14.2			0.001		54.1	140
82.6	0.352	0.36	water 83.5'	8.80			0.029		38.2	97.4
83.6	0.482	0.48		10.2			0.039		37.9	92.6
85.1	0.357	1.53	8.20	8.63		5.37	0.123	0.235	36.7	85.4
86.1	0.406	1.82	8.72	10.7		4.80	0.147	0.250	31.7	77.3
87.6	0.490	3.55	10.42	14.1		2.93	0.287	0.299	57.0	120.3
87.9	0.490	3.57					0.289			
88.6	0.509	3.31	11.4	7.33	47.9	3.45	0.267	0.327	72.0	136.3
88.9	0.634	4.77	14.26	26.7		6.53	0.386	0.409		
90.6	0.634	0.57	8.96	11.4		15.81	0.046	0.257	34.0	88.2
90.6	0.634	0.56					0.046		31.9	83.9
90.9	0.503	0.77					0.063			
92.1	0.503	0.93	11.0		30.6	11.85	0.075	0.235	23.4	56.6
92.4	0.503	1.70					0.137			
93.1	0.503	1.95	8.52	12.2		4.38	0.157	0.244	40.8	99.2
93.4	0.414	1.02					0.082			
94.6	0.414	0.51	8.08			15.79	0.041	0.232		
94.9	0.414	0.51		8.34			0.041		43.4	101
95.6	0.414	2.83	2.01	12.4	26.2	0.71	0.229	0.043	48.6	137
95.9	0.784	5.19				2.11	0.420			
95.9	0.784	4.99				2.11	0.403		88.8	243
96.6	0.784	6.51		23.1			0.526		70.6	164
mean ± std dev:		2.35 ± 1.87	9.16 ± 3.16	13.2 ± 6.17	34.9 ± 11.5	6.32 ± 5.26	0.190 ± 0.151	0.249 ± 0.112	49.2 ± 19.1	122 ± 52.6
	for the full grain size distribution									
	** ratio of maximum reductive capacity (0_2 / 0.5M HCl)									

Table E.5. Reductive Capacity and Iron Extraction Data for D4-91, C4687 (downgradient of D4-37) in April 2005

depth (ft)	mass fraction < 4 mm	field reductive capacity* 1h 0.5M HCl (µmol/g)	field reductive capacity* column O_2 ox. (µmol/g)	maximum reductive capacity* 1h 0.5M HCl (µmol/g)	maximum reductive capacity* column O_2 ox. (µmol/g)	ratio capacity (O_2 / HCl)	reduced fraction field/average 1h 0.5M HCl	reduced fraction field/average column O_2 ox.	total iron oxides* Fe^{II} 2 wk 5M HCl (µmol/g)	total iron oxides* Fe^{II+III} 2 wk 5M HCl (µmol/g)
79.1	0.549	0.038							71.4	150
80.6	0.549	0.005				4.09**			32.5	101
81.6	0.583	0.01				2.01**			30.7	76
83.1	0.352	0.66	3.12	12.9	water 83.5'	3.95**	0.053	0.080	39.4	98.7
84.1	0.482	0.04	2.60	15.4		0.97	0.003	0.067	54.7	155
85.1	0.357	1.08	3.81	10.3		3.53	0.086	0.098	75.3	147
85.6	0.406	2.91	6.00	13.6		2.07	0.233	0.154	58.6	156
88.1	0.490	2.58	12.8	9.80	42.6	4.95	0.206	0.328	63.7	114
89.1	0.490	4.17	5.51			1.32	0.334	0.142		
90.6	0.509	3.21	9.29	11.2		2.89	0.258	0.239	29.5	69.1
91.6	0.634	5.29	6.90	12.8		1.30	0.424	0.177		
93.1	0.634	5.27	22.7	13.4	29.3	4.31	0.422	0.585	60.0	144
94.1	0.634	6.41	9.81			1.53	0.513	0.252	128.5	326
95.6	0.503	3.89	18.8			4.84	0.312	0.485	46.6	123
96.6	0.503	4.86	21.2	17.6	69.3	4.36	0.389	0.545	68.5	155
97.9	0.414	0.01	> 2000 psi	6.67					9.2	315
mean ± std dev:		3.97 ± 1.57	10.8 ± 7.10	12.4 ± 3.06	47.1 ± 20.4	2.92 ± 1.54	0.318 ± 0.126	0.300 ± 0.178	54.9 ± 28.5	152 ± 77.1
	for the full grain size distribution									
	** ratio of maximum reductive capacity (0_2 / 0.5M HCl)									

Table E.6. Reductive Capacity and Iron Extraction Data for D4-92, C4688 (upgradient of D4-26) in April 2005

depth (ft)	mass fraction < 4 mm	field reductive capacity* 1h 0.5M HCl (μmol/g)	field reductive capacity* column O$_2$ ox. (μmol/g)	maximum reductive capacity* 1h 0.5M HCl (μmol/g)	maximum reductive capacity* column O$_2$ ox. (μmol/g)	ratio capacity (O$_2$ / HCl)	reduced fraction field/average 1h 0.5M HCl	reduced fraction field/average column O$_2$ ox.	total iron oxides* Fe^{II} 2 wk 5M HCl (μmol/g)	total iron oxides* Fe^{II+III} 2 wk 5M HCl (μmol/g)
78.1	0.496	4.30					0.345		79.6	150
80.6	0.471	2.21					0.177		54.7	110
82.6	0.379	0.32	water 83.5'	8.14			0.025		42.3	89.5
83.6	0.402	0.44		9.90			0.036		53.5	113
85.1	0.361	0.41	4.25	7.40		10.4	0.033	0.109	55.5	91.3
85.4	0.390	2.84					0.227			
86.1	0.390	2.30	6.54	8.93		2.85	0.184	0.168	41.0	85.2
87.4	0.608	3.69	12.63	13.7		3.42	0.296	0.325	76.0	143
87.6	0.608	6.02					0.482			
87.9	0.545	5.46					0.437			
88.6	0.545	5.78	10.59	13.7		1.83	0.463	0.272	71.0	146
88.9	0.545	4.33					0.347			
90.1	0.997	10.6	28.95		35.6	2.73	0.849	0.745	165	287
90.4	0.437	4.28				2.92	0.343			
91.6	0.444	3.80	8.96	11.3		2.36	0.305	0.231	60.6	123
91.6	0.444	3.71					0.298		60.1	124
91.9	0.459	5.31					0.426			
92.6	0.459	4.53	6.40	13.2		1.41	0.363	0.165	50.3	113
94.1	0.431	4.89		11.6			0.391		49.6	102
95.1	0.503	6.78	26.78	14.7	26.7	3.95	0.543	0.689	95.9	193
96.6	0.572	5.19		19.9		1.82	0.416		60.3	129
97.6	0.584	5.20	15.28	21.3		2.94	0.416	0.393	84.4	222
99.6	0.421	1.28		3.75			0.103		62.7	167
100.6	0.379	6.95	21.99	6.56	41.6	3.16	0.557	0.566	58.7	132
102.1	0.379	0.01				6.34	0.000		5.65	142
mean ± std dev:		4.26 ± 2.46	14.2 ± 8.81	12.0 ± 4.97	34.6 ± 7.50	2.98 ± 1.28	0.358 ± 0.186	0.366 ± 0.227	65.6 ± 33.0	144 ± 52.0

* for the full grain size distribution

** ratio of maximum reductive capacity (0$_2$ / 0.5M HCl)

Table E.7. Reductive Capacity and Iron Extraction Data for D4-93, C4689 (downgradient of D4-26)

depth (ft)	mass fraction < 4 mm	field reductive capacity* 1h 0.5M HCl (µmol/g)	field reductive capacity* column O$_2$ ox. (µmol/g)	maximum reductive capacity* 1h 0.5M HCl (µmol/g)	maximum reductive capacity* column O$_2$ ox. (µmol/g)	ratio capacity (O$_2$ / HCl)	reduced fraction field/average 1h 0.5M HCl	reduced fraction field/average column O$_2$ ox.	total iron oxides* Fe^{II} 2 wk 5M HCl (µmol/g)	total iron oxides* Fe^{II+III} 2 wk 5M HCl (µmol/g)
79.1	0.507	1.62					0.130		74.5	149
80.6	0.450	1.42					0.113		64.5	126
81.6	0.418	0.19					0.015		40.3	95.2
81.6	0.418	0.17	water 82.5'				0.014		41.9	125
82.9	0.521	2.19		12.45			0.186		86.5	169
84.1	0.409	0.72		9.04			0.061		50.2	97.4
85.6	0.958	4.63		18.82			0.392		132	260
86.6	0.401	0.85		5.49			0.072		47.9	96.0
88.1	0.737	5.28	17.78		53.8	3.37	0.448	0.354	98.9	163
89.1	0.491	4.38		12.18		6.72	0.371		58.2	113
91.1	0.671	5.59	35.95	16.85	58.1	6.43	0.474	0.716	111	203
93.1	0.476	3.68				3.45	0.312		62.8	145
93.1	0.476	3.63	16.88			4.65	0.307	0.336	66.9	153
94.1	0.404	2.64	failed	5.09			0.224		114	170
95.6	0.660	0.83	34.75	12.59		6.59	0.070	0.692	88.9	267
96.6	0.342	5.27	14.47	13.62	38.6	2.75	0.447	0.288	73.0	175
98.6	0.417	1.42				4.83	0.120		62.8	165
100.1	0.344	0.19					0.016		37.4	87.5
100.9	0.360	0.00					0.000		5.30	150
mean ± std dev:		2.75 ± 2.00	24.0 ± 10.5	11.8 ± 4.63	50.2 ± 10.2	4.80 ± 1.34	0.233 ± 0.170	0.477 ± 0.209	73.0 ± 32.9	161 ± 53.0
	for the full grain size distribution									
	** ratio of maximum reductive capacity (0$_2$ / 0.5M HCl)									

Appendix F

August 7, 2002 Multilevel Sampler Data

Wells D4-7, D4-9, and D4-16 (Westbay Well)

Appendix F

August 7, 2002 Multilevel Sampler Data
Wells D4-7, D4-9, and D4-16 (Westbay Well)

Well ID	depth* (ft)	Sample Date	Time	Conductivity (mS)	Temp (C)	pH	CrVI #1 mg/L
7L (top)	85.9	8/7/02	12:30	1423	21.8	8.14	0.01
7K	87.1	8/7/02	12:25	1401	21.6	8.15	0.01
7J	88.3	8/7/02	12:20	1304	21.4	8.17	0.01
7I	89.4	8/7/02	12:15	1244	21.2	8.17	0.01
7H	90.8	8/7/02	12:07	1191	21.4	8.17	0.01
7G	92.0	8/7/02	12:00	1190	21.2	8.17	0.01
7F	92.9	8/7/02	11:52	1184	21.0	8.18	0.01
7E	94.0	8/7/02	11:45	1192	21.2	8.17	0.01
7D	95.7	8/7/02	11:35	1186	21.1	8.17	0.01
7C	97.0	8/7/02	11:28	1185	21.0	8.19	0.01
7B	98.1	8/7/02	11:20	1190	20.1	8.17	0.01
7A	99.3	8/7/02	11:15	1407	20.0	8.21	0.01
9L (top)	85.9	8/7/02	14:15	1193	21.9	7.93	0.02
9K	87.1	8/7/02	14:13	1313	21.7	7.93	0.04
9J	88.3	8/7/02	14:07	1235	21.8	7.97	0.05
9I	89.4	8/7/02	13:57	1123	21.6	7.96	0.06
9H	90.8	8/7/02	13:53	1064	21.7	7.96	0.06
9G	92.0	8/7/02	13:48	1023	21.5	7.93	0.06
9F	92.9	8/7/02	13:43	1039	21.4	7.93	0.06
9E	94.0	8/7/02	13:27	1033	21.3	7.94	0.06
9D	95.7	8/7/02	13:24	1035	21.1	7.92	0.06
9C	97.0	8/7/02	13:17	1028	20.7	7.92	0.06
9B	98.1	8/7/02	13:07	1048	20.6	7.93	0.06
9A	99.3	8/7/02	13:02	933	19.9	8.00	0.00
D4-16 upper		8/7/02	14:34	1074	22.3	8.11	0.03
D4-16 middle		8/7/02	14:40	908	21.5	8.33	0.00
D4-16 lower		8/7/02	14:50	1057	21.1	8.47	0.00

* mutli level sampler interval 1.1 ft

Calibration Notes
EC: 103.2 ms/cm, 1001 ms/cm standards @ 22.5 C, 10:00
Ph: 4, 7, 10 9:45

Appendix G

April 16, 2004 Multilevel Sampler Data

Appendix G - April 16, 2004 Multilevel Sampler Data
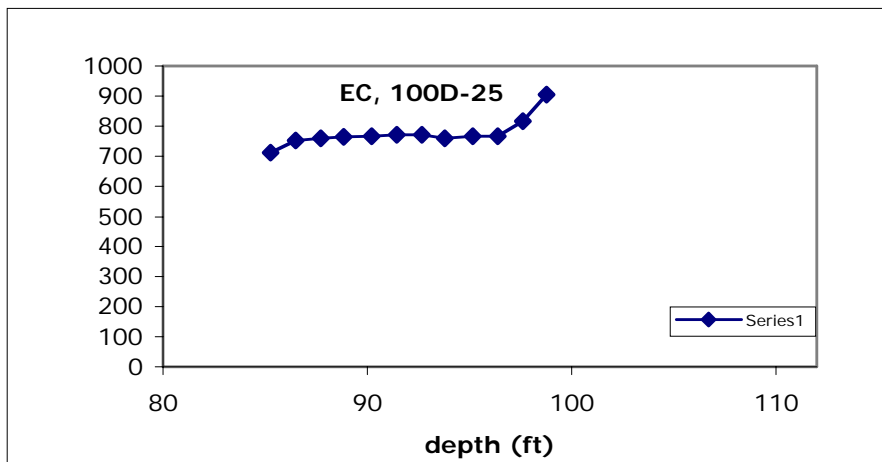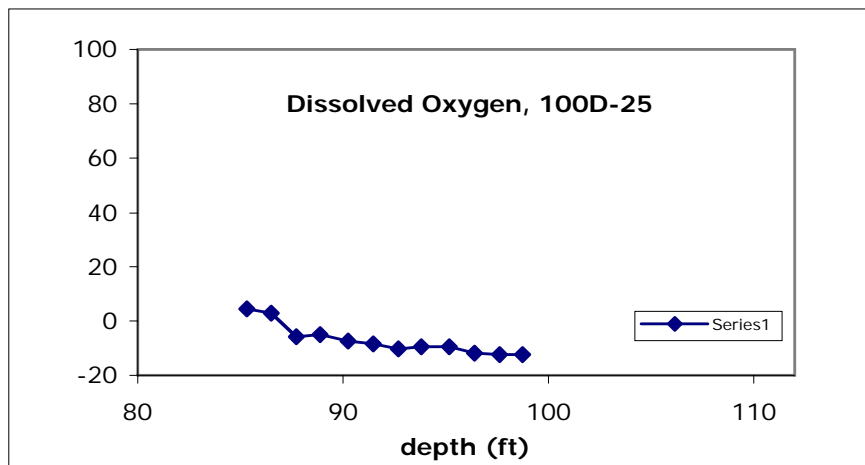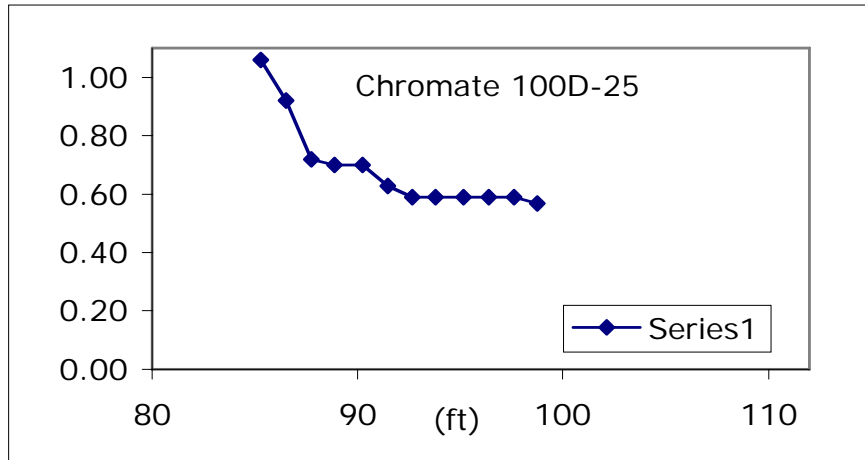
Chromate 100D-25

Dissolved Oxygen, 100D-25

EC, 100D-25

Oxygen decrease with depth (anoxic, then reducing >96 ft).
EC increase with depth.
Chromate decreasing in reduced environment.

Chromate, 100D-26

Dissolved Oxygen, 100D-26

Electrical Conductivity, 100D-26
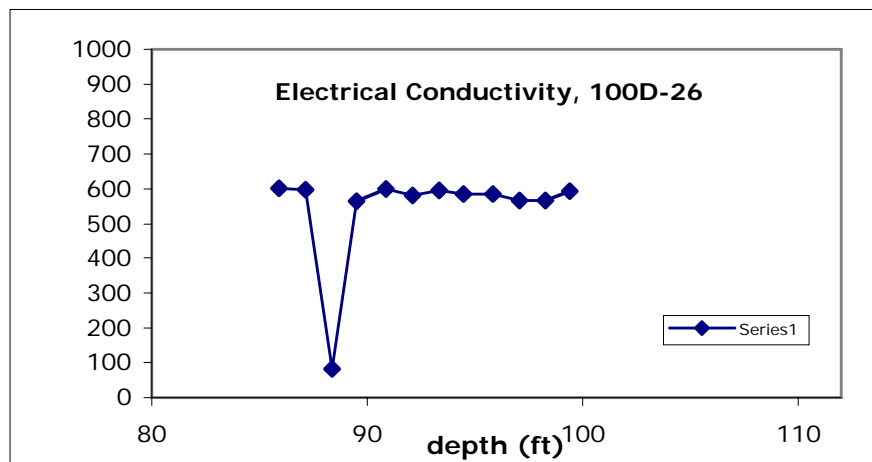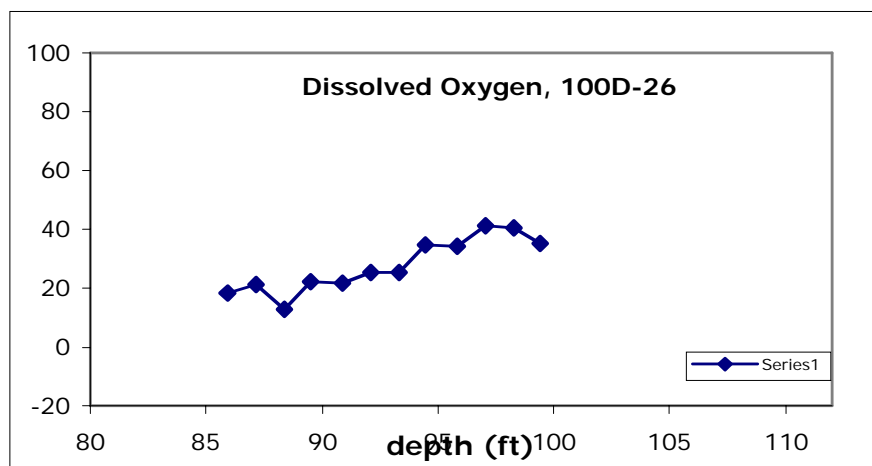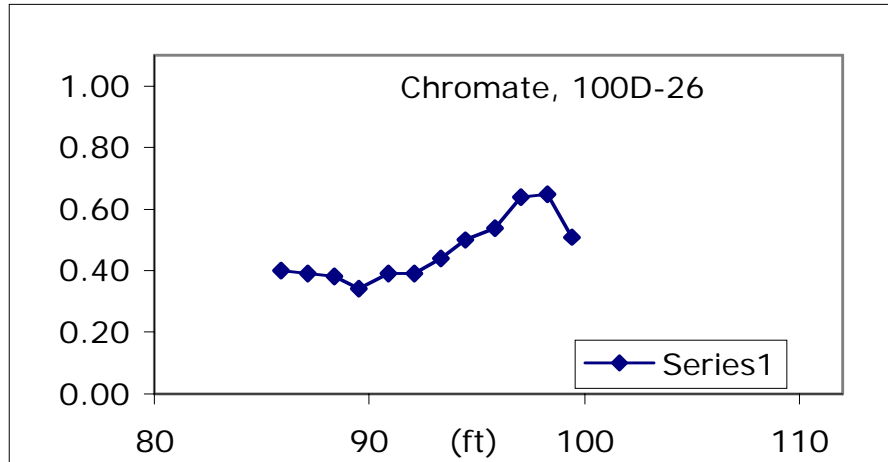
Oxygen increase with depth.

EC constant.

Chromate large, increasing with depth.

EBF data: high K at 95, 99 ft (bottom) (EBF data correlate with chromate).
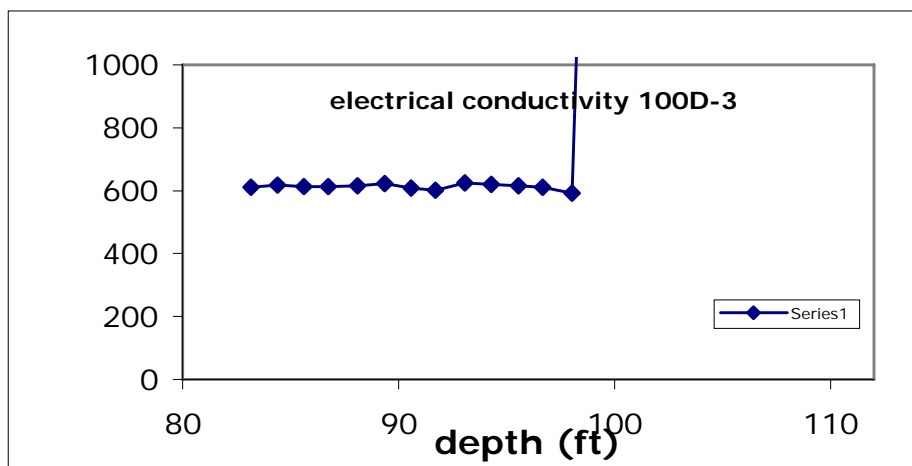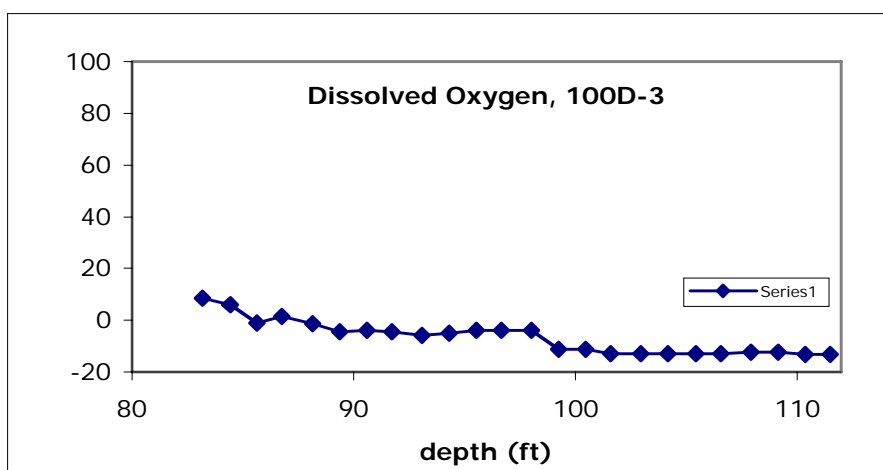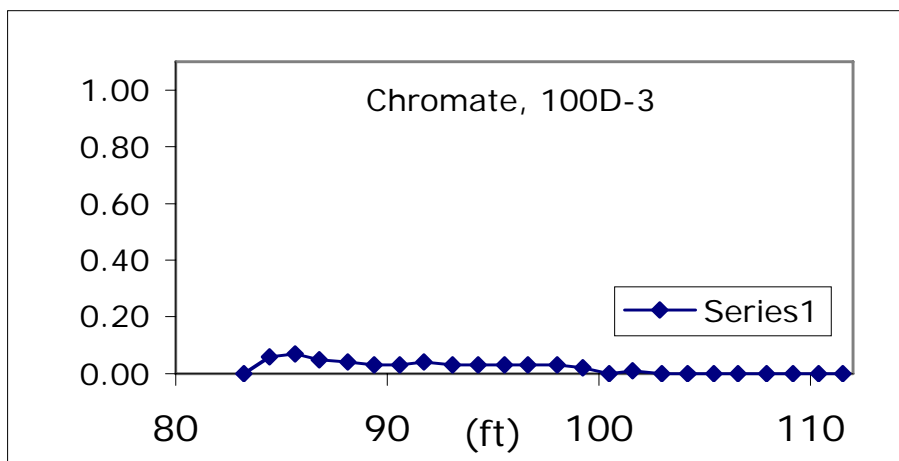
Chromate, 100D-3

Dissolved Oxygen, 100D-3

electrical conductivity 100D-3

Oxygen decrease with depth (anoxic, then reducing >96 ft).
EC increase with depth.
Chromate decreasing in reduced environment.

Chromate, 100D-31

Dissolved Oxygen, 100D-31

Electrical Conductivity, 100D-31
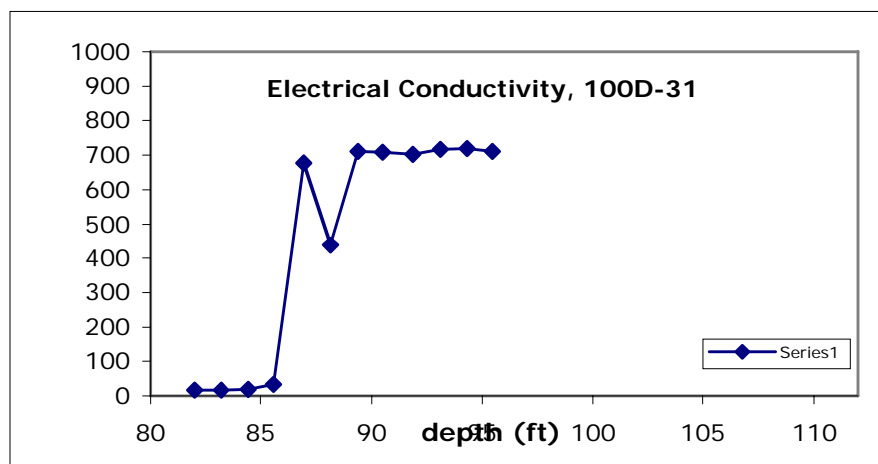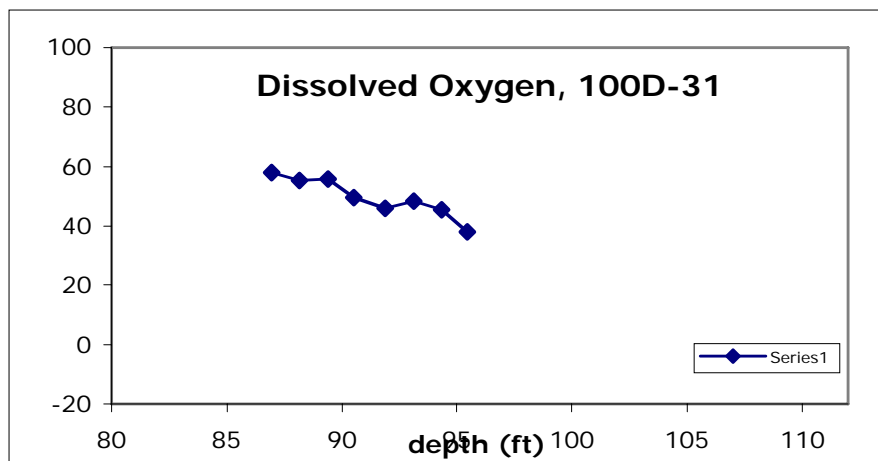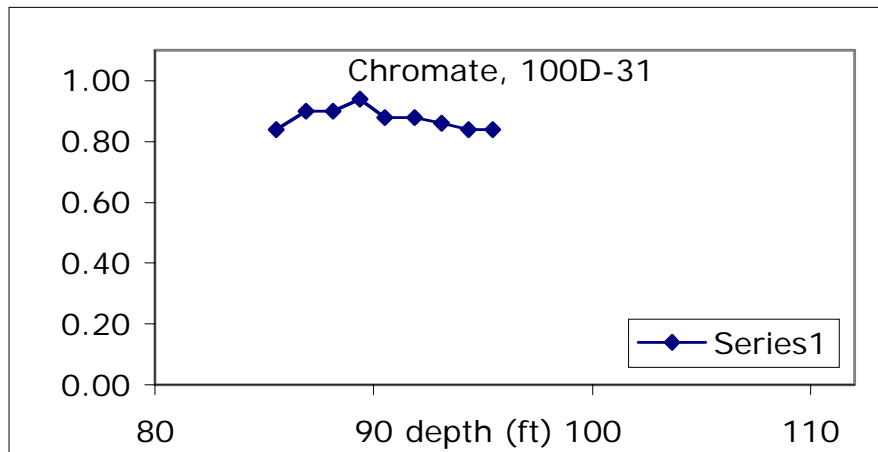
Oxygen constant (half saturation).
EC constant.
Chromate large, constant.
EBF data: mainly high flow.
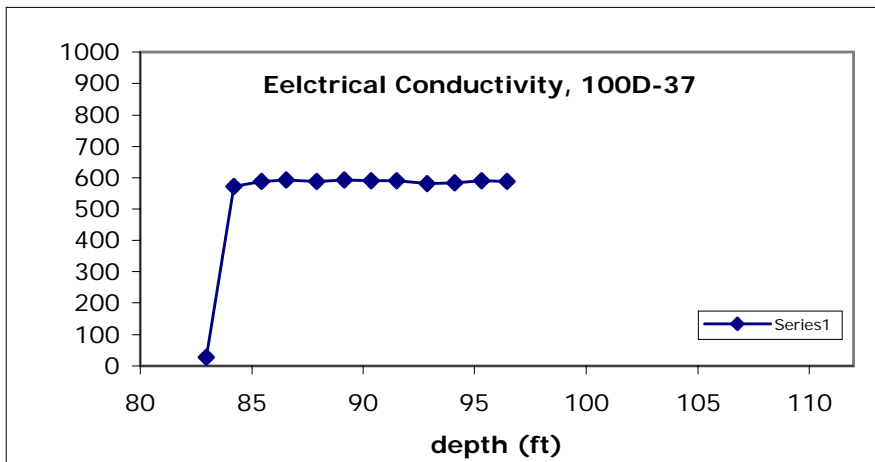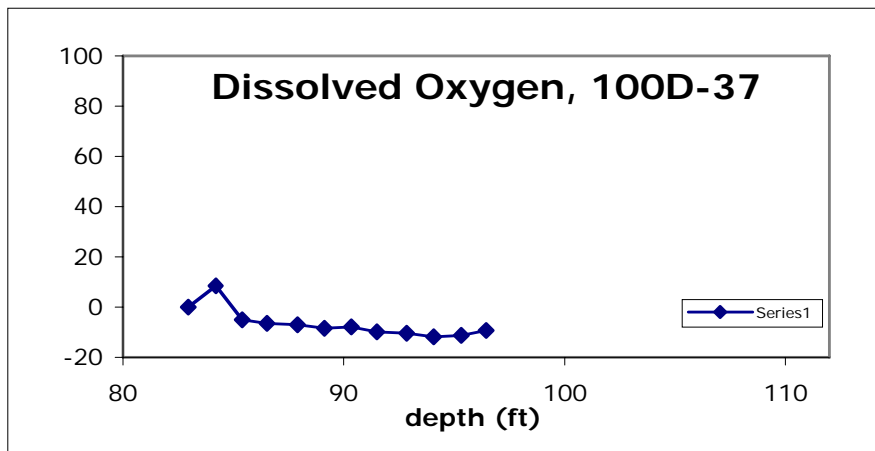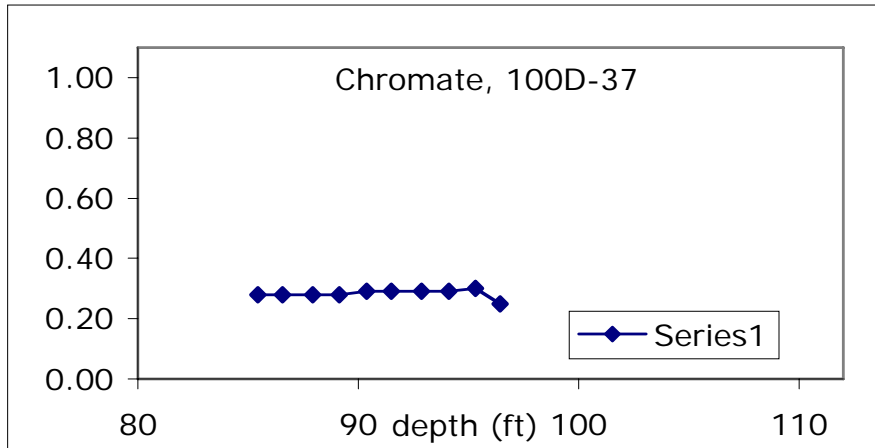
Chromate, 100D-37

Dissolved Oxygen, 100D-37

Eelctrical Conductivity, 100D-37

Oxygen constant (reducing env.).
EC constant.
Chromate large, constant.

Chromate, 100D-40

Dissolved Oxygen, 100D-40

Electrical Conductivity, 100D-40
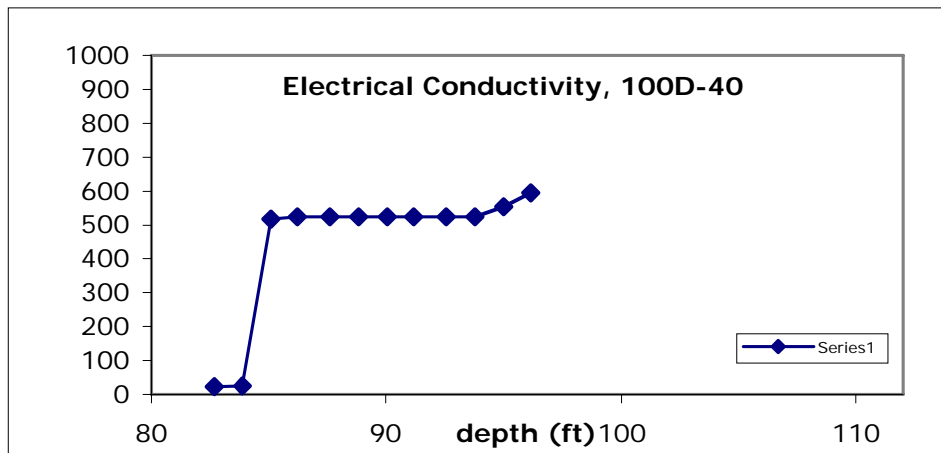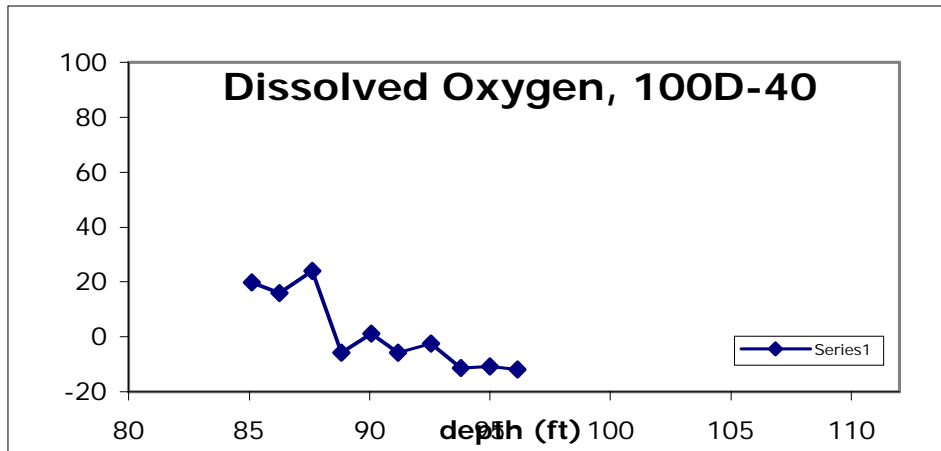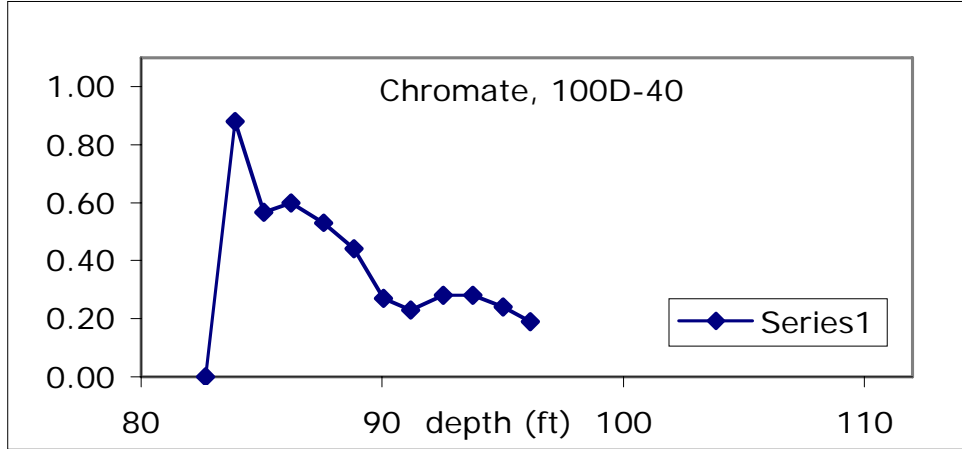
Oxygen oxic,then decreasing with depth (reducing env.).
EC constant, slight increase with depth.
Chromate decreasing with depth, but nonzero.
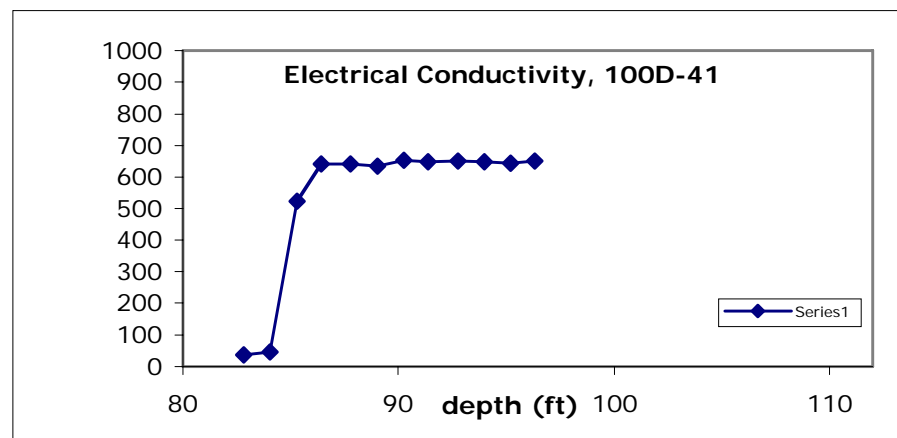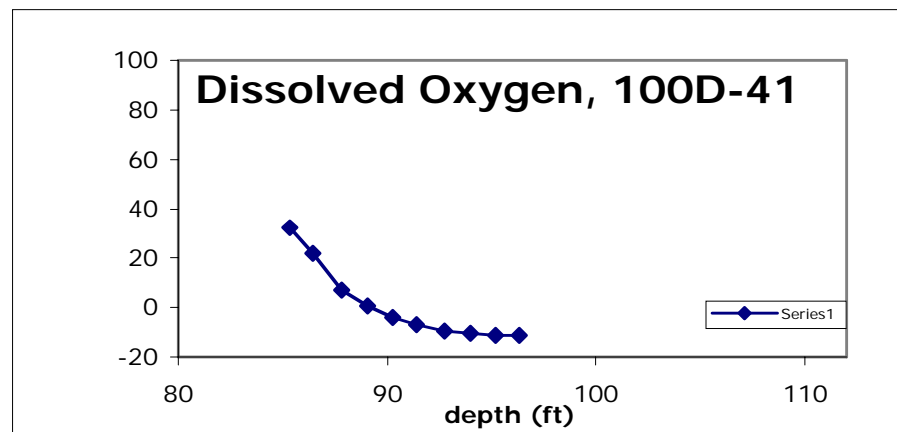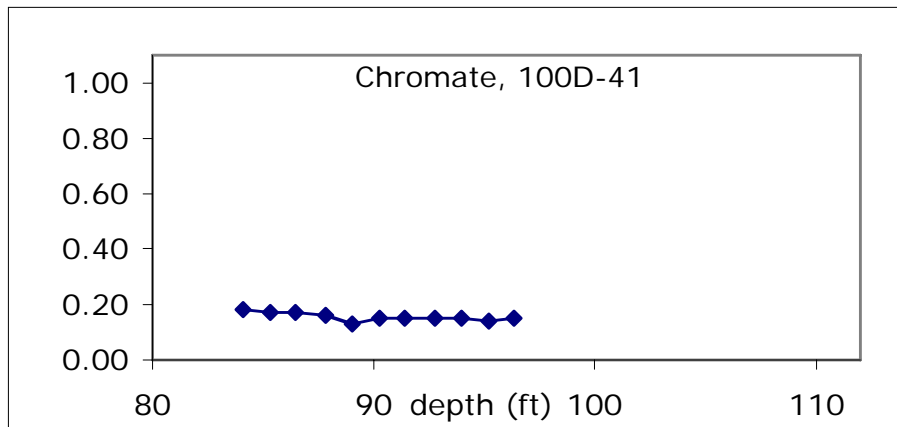
Chromate, 100D-41

Dissolved Oxygen, 100D-41

Electrical Conductivity, 100D-41

Oxygen oxic, then decreasing with depth (reducing env.).
EC constant.
Chromate constant, nonzero.

Chromate, 100D-45

Dissolved Oxygen, 100D-45

Electrical Conductivity, 100D-45
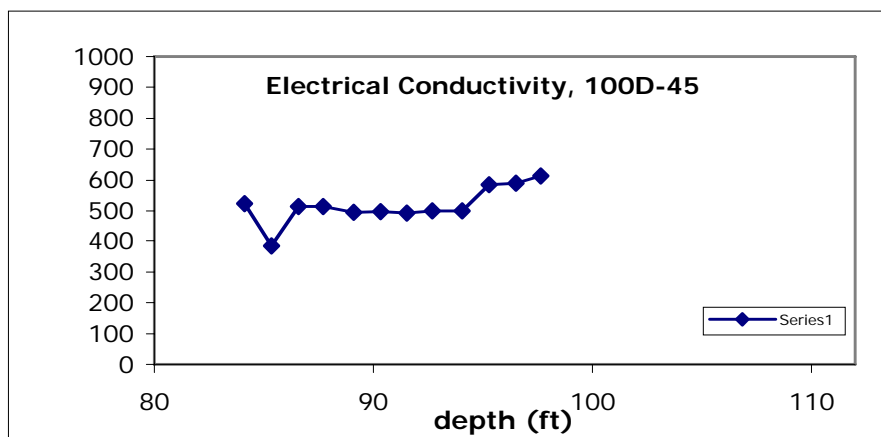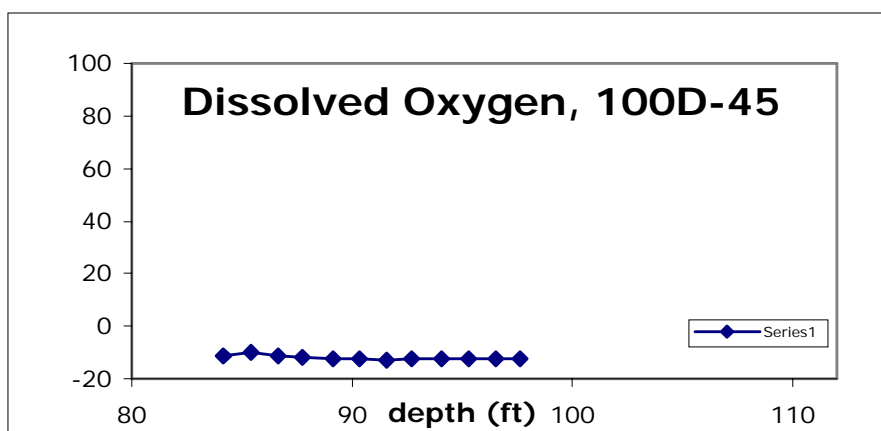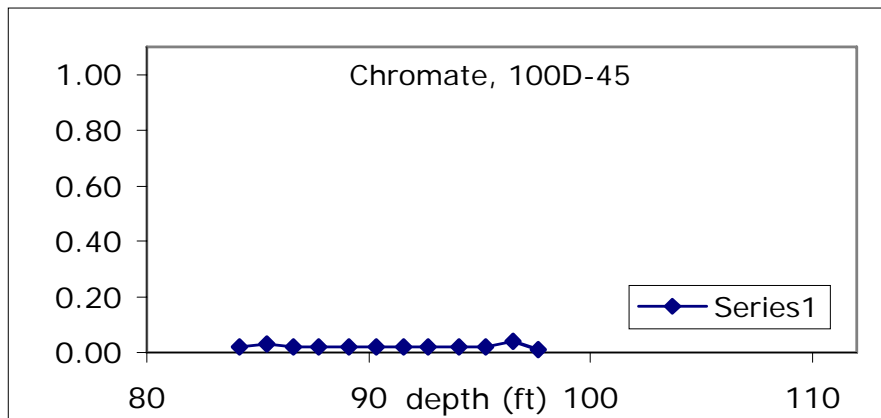
Oxygen constant (reducing env.).
EC constant.
Chromate constant, nonzero.

Appendix H

2005 Core Pictures of Boreholes C4686, C4687, C4688, C4689

Appendix H - 2005 Core Pictures of Boreholes C4686, C4687, C4688, and C4689

depth (ft)	C4686	C4687	C4688	C4689
79				
79.5				
80.5				
81				
81.5				
82				

scale 4"

depth (ft)	C4686	C4687	C4688	C4689

82.5

83

83.5

84

84.5

85

4"

scale

H.3

depth (ft)	C4686	C4687	C4688	C4689

85.5

86

86.5

87

87.5

88

4"

scale

H.4

depth (ft)	C4686	C4687	C4688	C4689

4"
scale

H.5

depth (ft)	C4686	C4687	C4688	C4689
91.5				
92				
92.5				
93				
93.5				
94				

scale 4"

depth (ft)	C4686	C4687	C4688	C4689
94.5				
95				
95.5				
96				
96.5				
97				

4"

scale

H.7

depth (ft)	C4686	C4687	C4688	C4689

scale 4"

depth (ft)	C4686	C4687	C4688	C4689
100.5				
101				
101.5				
102				
102.5				
103				

4"

scale

H.9

Appendix I

2002 Core Pictures of Boreholes D4-87, D4-88, and D4-89

Appendix I - 2002 Core Pictures of Boreholes D4-87, D4-88, D4-89

Well #83, 79'

Well #88, 79.5'

Well #89, 79.5'

Well #89, 80'

Well #87, 80.5'

Well #88, 80.5'

Well #89, 80.5'

Well #87, 81'

Well #88, 81'

Well #89, 81'

Well #88, 81.5'

Well #88, 82'

Well #89, 82'

Well #89, 82.5'

Well #87, 82.5'

Well #87, 83'

Well #89, 83.5'

Well #87, 84'

Well #87, 84.5'

Well #88, 84'

Well #88, 84.5'

Well #88, 85'

Well #88, 85.5'

Well #89, 84'

Well #89, 85.5'

Well #89, 86'

Well #87, 86.5'

Well #87, 87'

Well #88, 87'

Well #89, 87'

Well #87, 87.5'

Well #88, 87.5'

Well #89, 87.5'

Well #87, 88'

Well #87, 88.5'

Well #88, 88.5'

Well# -88, 89'

Well# 89, 89'

Well# 88, 89.5'

Well# 89, 89.5'

Well# 88, 90'

Well# 89, 90'

Well# 87, 90.5'

Well# 89, 90.5'

Well# 87, 91'

Well# 88, 91'

I.5

Well# 88, 91.5'

Well# 89, 91.5'

Well# 87, 92'

Well# 89, 92'

Well# 87, 92.5'

Well# 87, 93.5'

Well# 88, 93.5'

Well# 89, 93.5'

Well# 87, 94'

Well# 88, 94'

Well# 89, 94'

Well# 88, 94.5'

Well# 89, 94.5'

Well# 87, 95'

Well# 88, 95'

Well# 89, 95'

Well# 87, 95.5'

Well# 89, 96'

Well #87, 96.5'

Well #87, 97'

Well #87, 97.5'

Well #87, 98'

Well #89, 96.5'

Appendix J

Sieve Analysis and Log Grain Size Fit

for Borehole C4686 D4-90

Appendix J - Sieve Analysis and Log Grain Size Fit
for Borehole C4686 D4-90

Sieve Analysis Data for Sample 75.0-75.5'

C4686, 75.0-75.5

Sieve Analysis Data for Sample 76.0-76.5

C4686, 76.0-76.5

J.2

Sieve Analysis Data for Sample 77.5-78.0'

C4686, 77.5-80.0

Sieve Analysis Data for Sample 78.5-79.0'

C4686, 78.5-79.0

Sieve Analysis Data for Sample 80.0-80.5'

C4686, 80.0-80.5
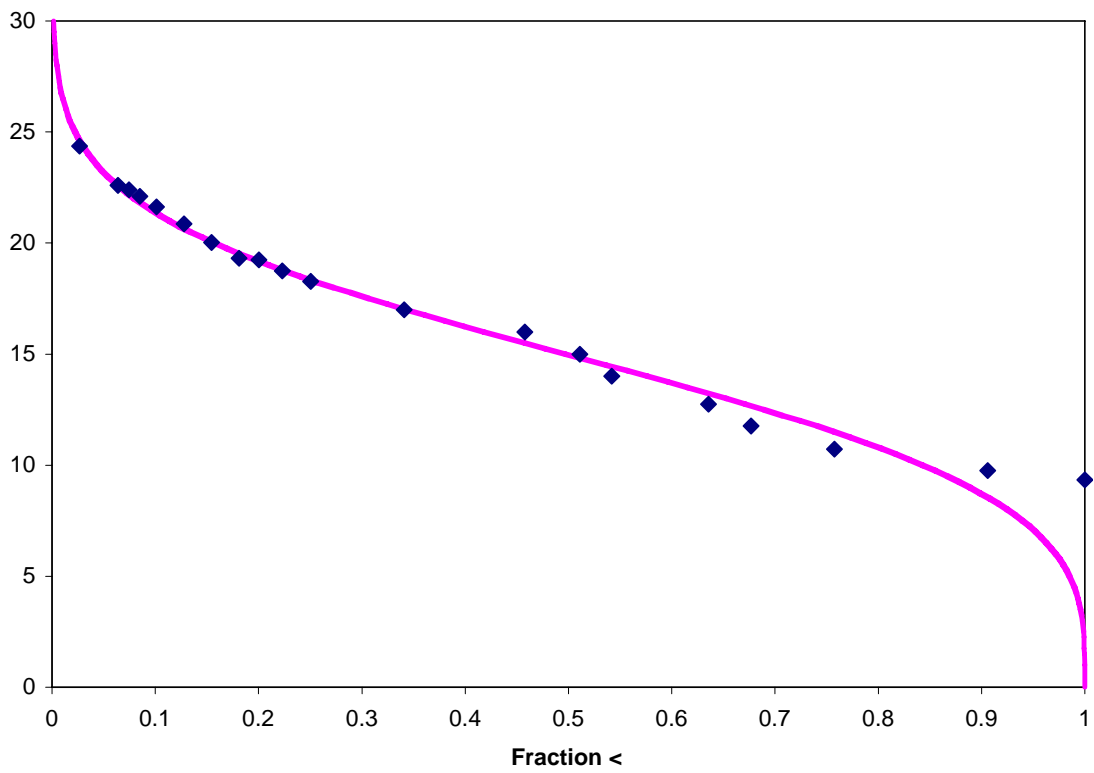
J.5

Sieve Analysis Data for Sample 81.0-81.5'

C4686, 81.0-81.5

Sieve Analysis Data for Sample 82.0-82.5'

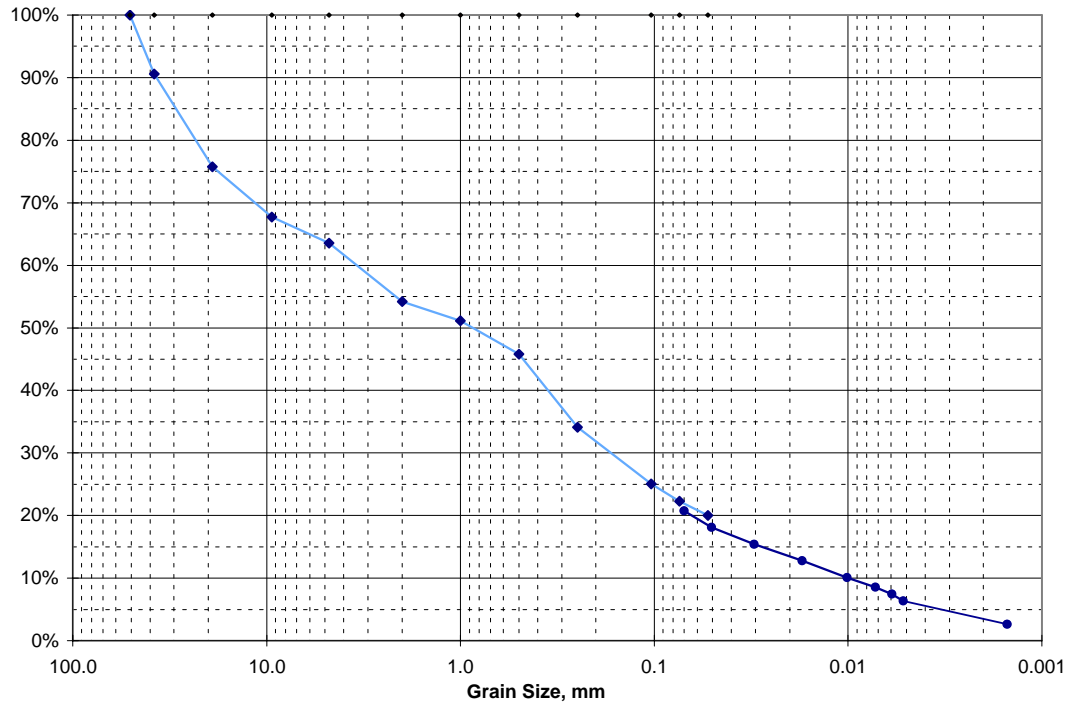**U.S. Std. Sieve Opening in Inches**

Hydrometer

Grain Size, mm

Fraction <

C4686, 82.0-82.5

Sieve Analysis Data for Sample 83.0-83.5'

U.S. Std. Sieve Opening in Inches

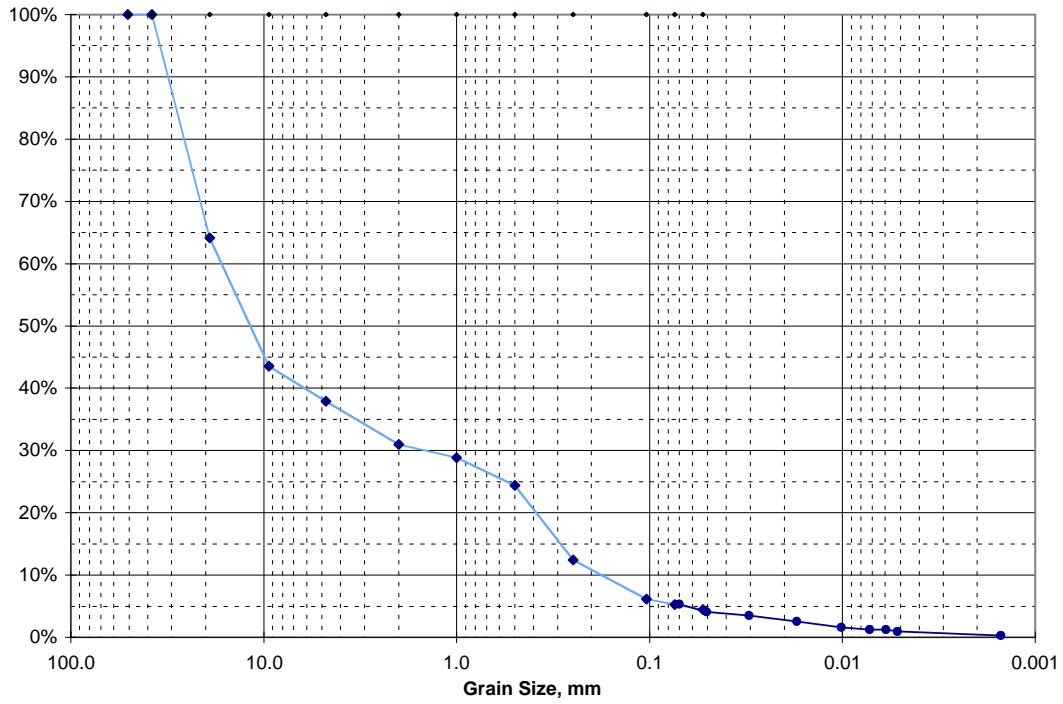**Hydrometer**

Grain Size, mm

Fraction <

C4686, 83.0-83.5

Sieve Analysis Data for Sample 84.5-85.0'

U.S. Std. Sieve Opening in Inches

Hydrometer

Grain Size, mm

Fraction <

C4686, 84.5-85.0

Sieve Analysis Data for Sample 85.5-86.0'

C4686, 85.5-86

J.10

Sieve Analysis Data for Sample 87.0-87.5'

C4686, 87.0-87.5

Sieve Analysis Data for Sample 88.0-88.5'

U.S. Std. Sieve Opening in Inches
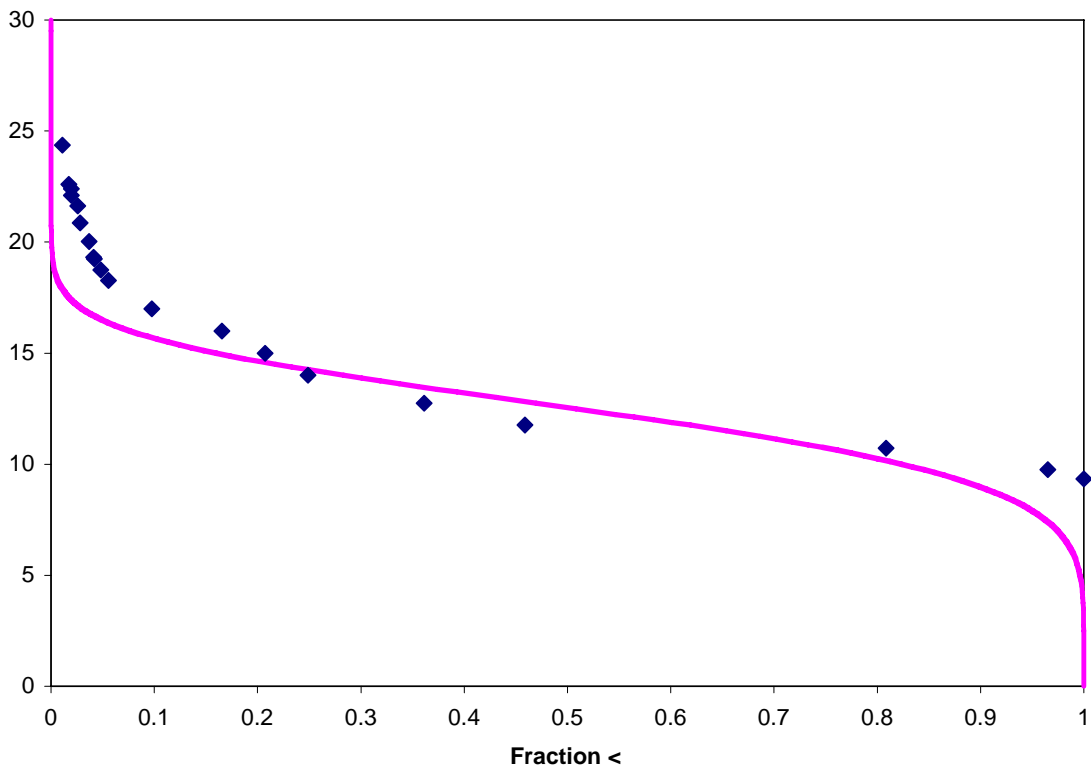
Hydrometer

C4686, 88.0-88.5

Sieve Analysis Data for Sample 90.0-90.5'

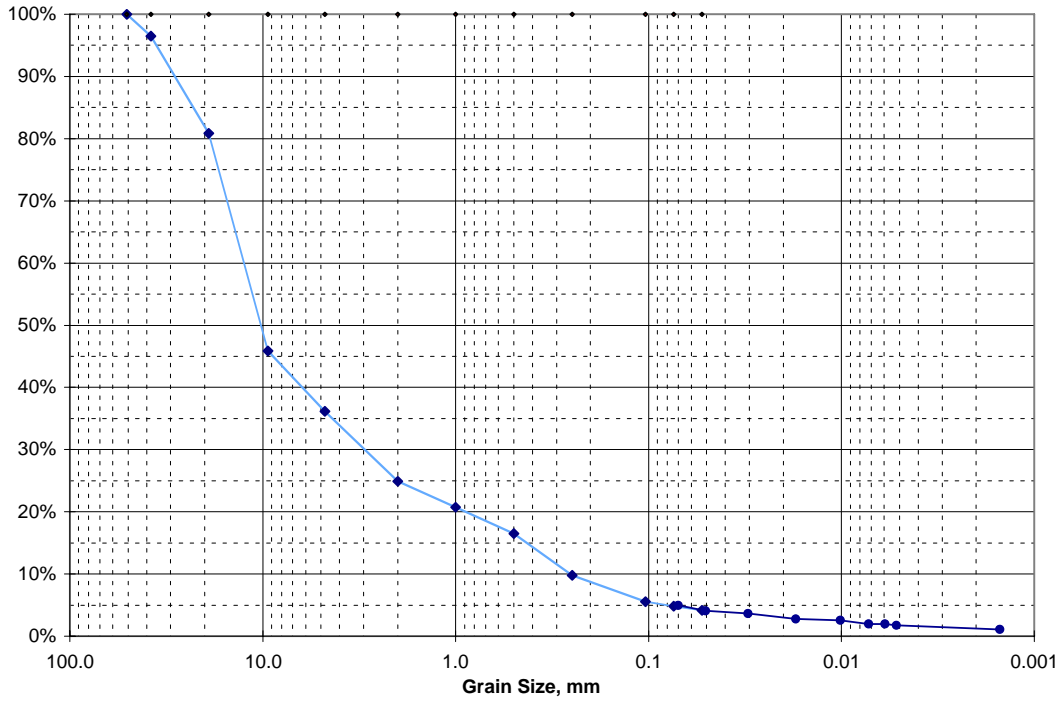U.S. Std. Sieve Opening in Inches

Hydrometer

Grain Size, mm

Fraction <

C4686, 90.0-90.5

Sieve Analysis Data for Sample 91.0-91.5'
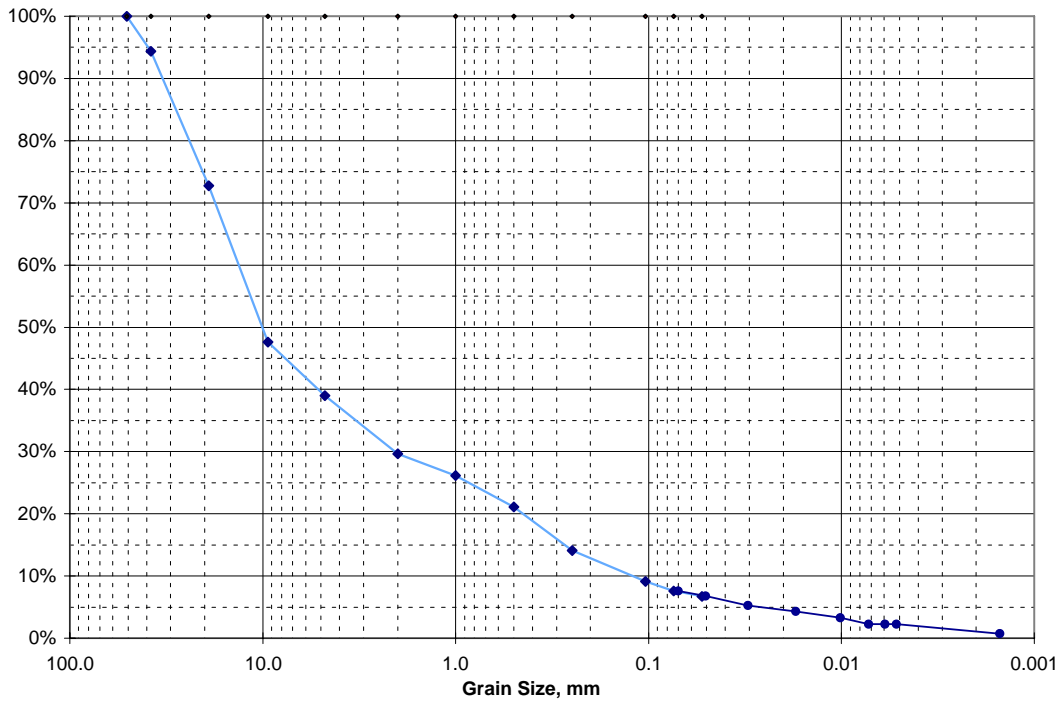
U.S. Std. Sieve Opening in Inches

Hydrometer

Grain Size, mm

Fraction <

C4686, 91.0-91.5

J.14

Sieve Analysis Data for Sample 92.5-93.0'

C4686, 92.5-93.0

Sieve Analysis Data for Sample 93.5-94.0'

C4686, 93.5-94.0

Sieve Analysis Data for Sample 94.0-94.5'

C4686, 94.0-94.5

Sieve Analysis Data for Sample 95.0-95.5'

U.S. Std. Sieve Opening in Inches

Hydrometer

Grain Size, mm

Fraction <

C4686, 95.0-95.5

Sieve Analysis Data for Sample 99.0-99.5'

C4686, 99.0-99.5

Sieve Analysis Data for Sample 100.0-100.5'

U.S. Std. Sieve Opening in Inches

Hydrometer
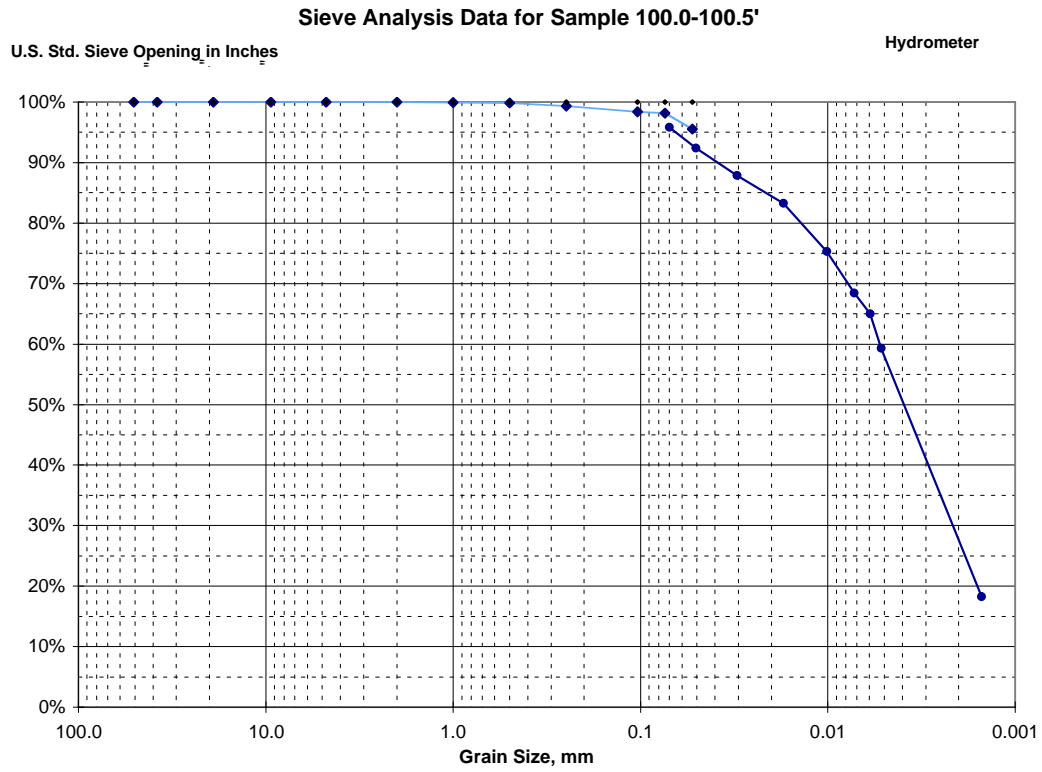
Grain Size, mm

C4686, 100.0-100.5

Appendix K

Sieve Analysis and Log Grain Size Fit

for Borehole C4687 D4-91

Appendix K - Sieve Analysis and Log Grain Size Fit for Borehole C4687 D4-91

Sieve Analysis Data for Sample 75.3-75.8'
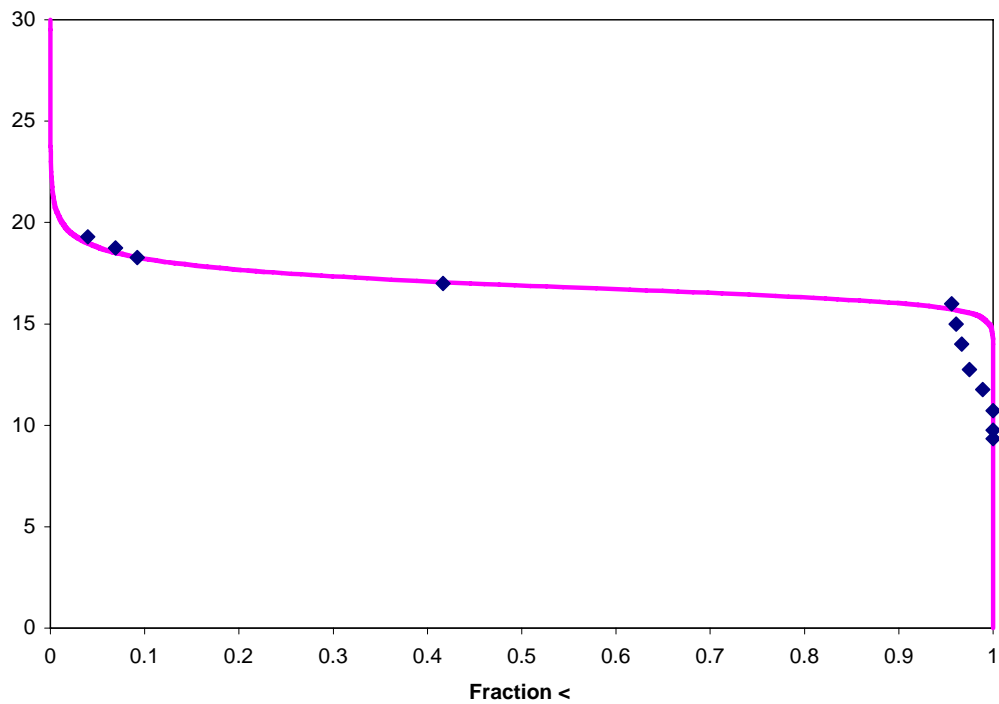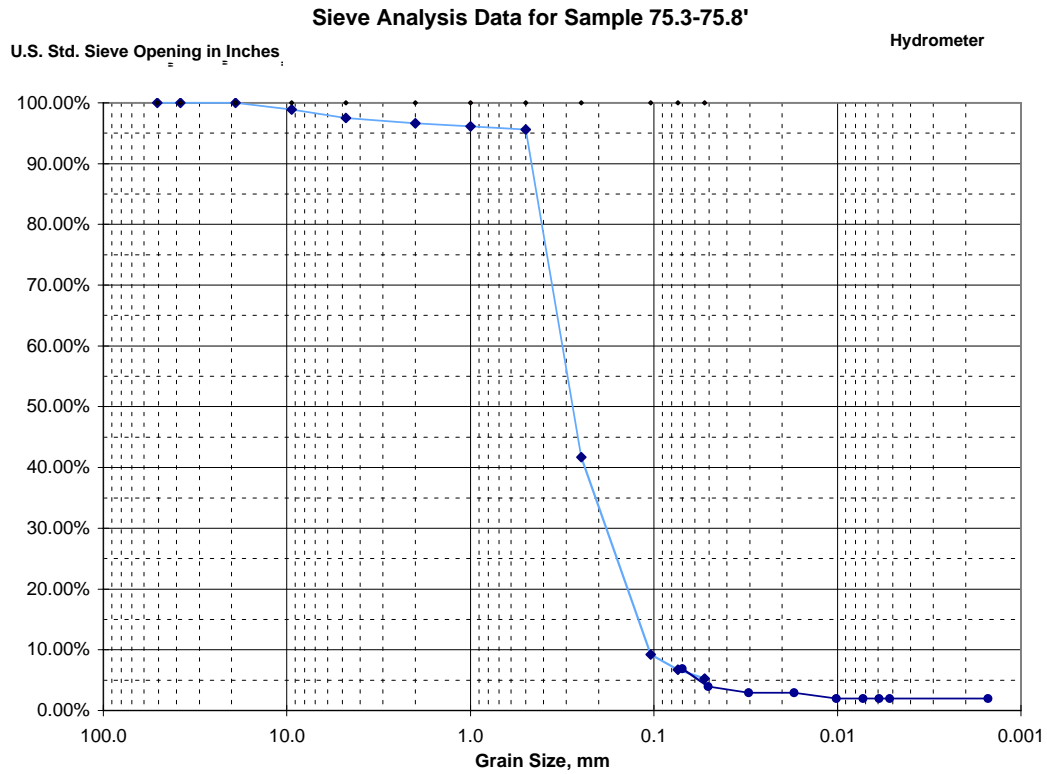
C4687, 75.3-75.8

Sieve Analysis Data for Sample 76.3-76.8
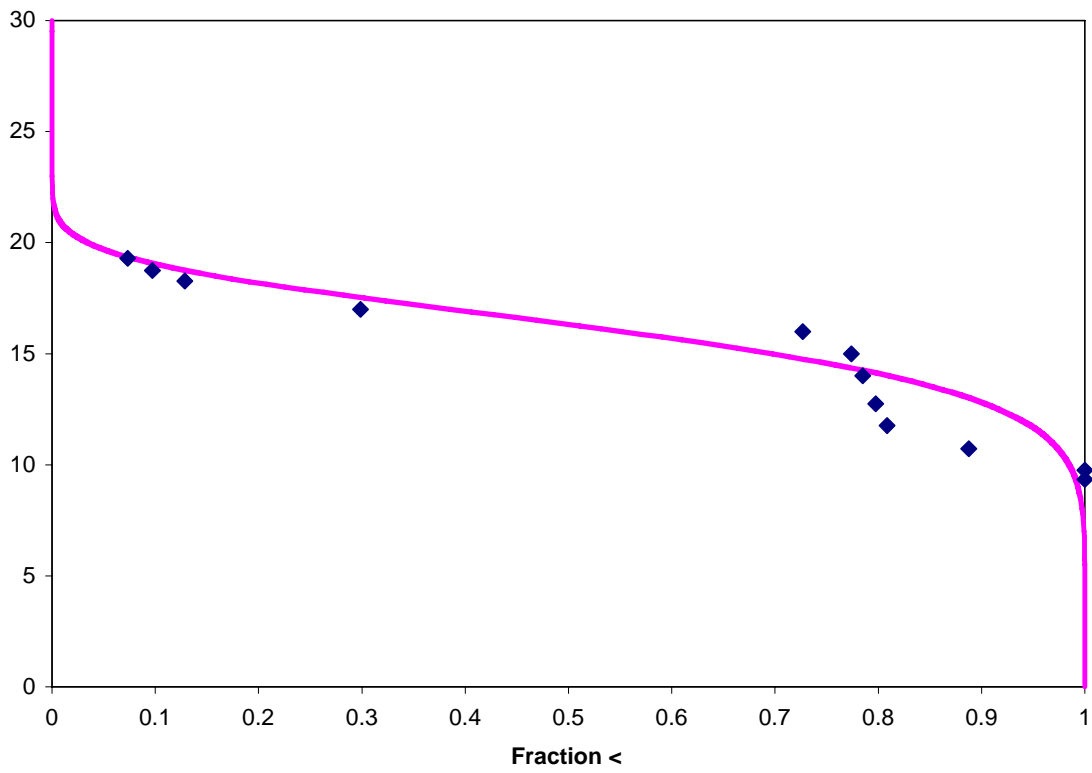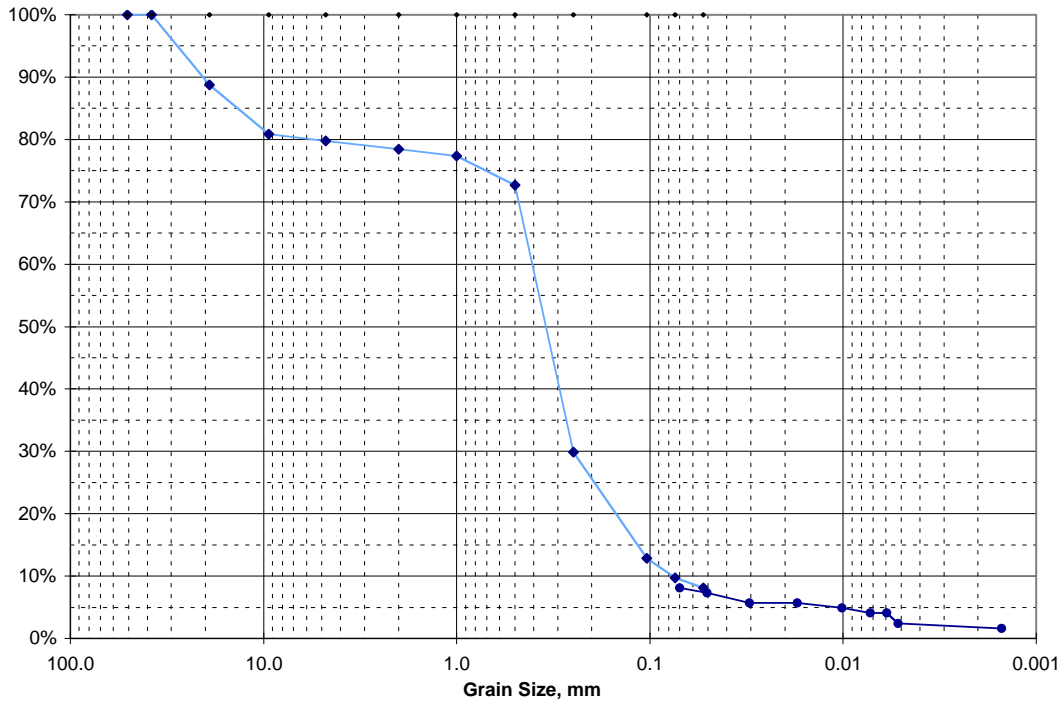
C4687, 76.3-76.8

K.2

Sieve Analysis Data for Sample 77.5-78'
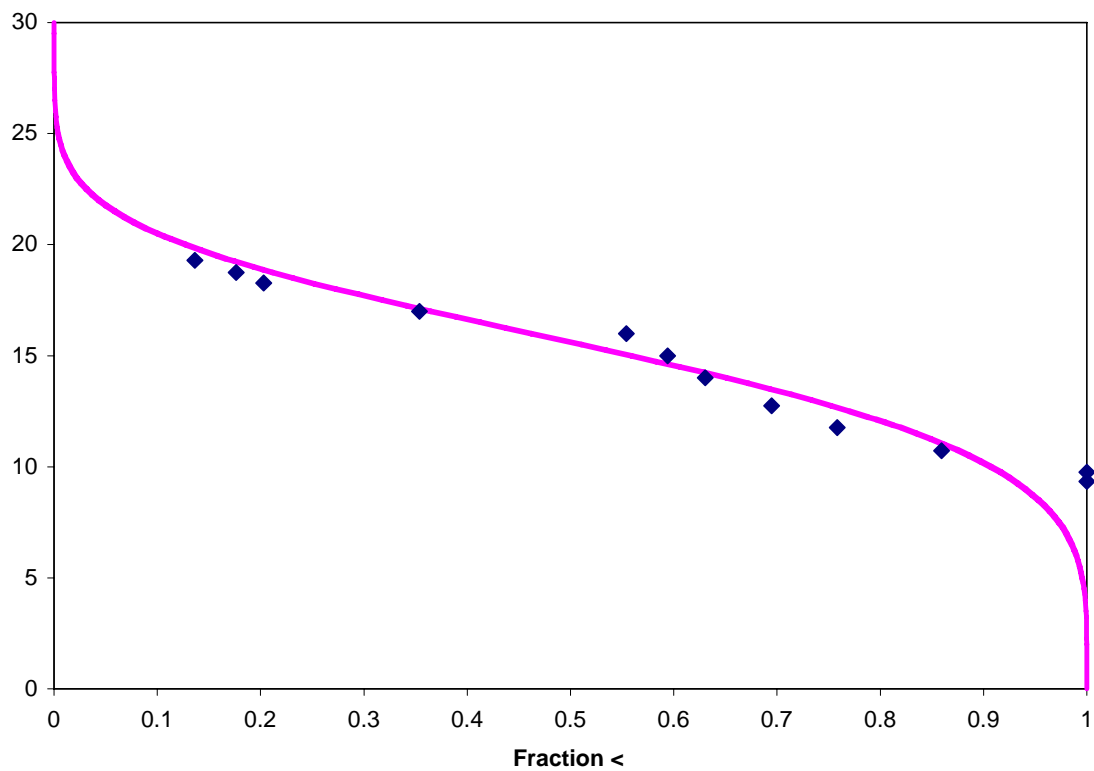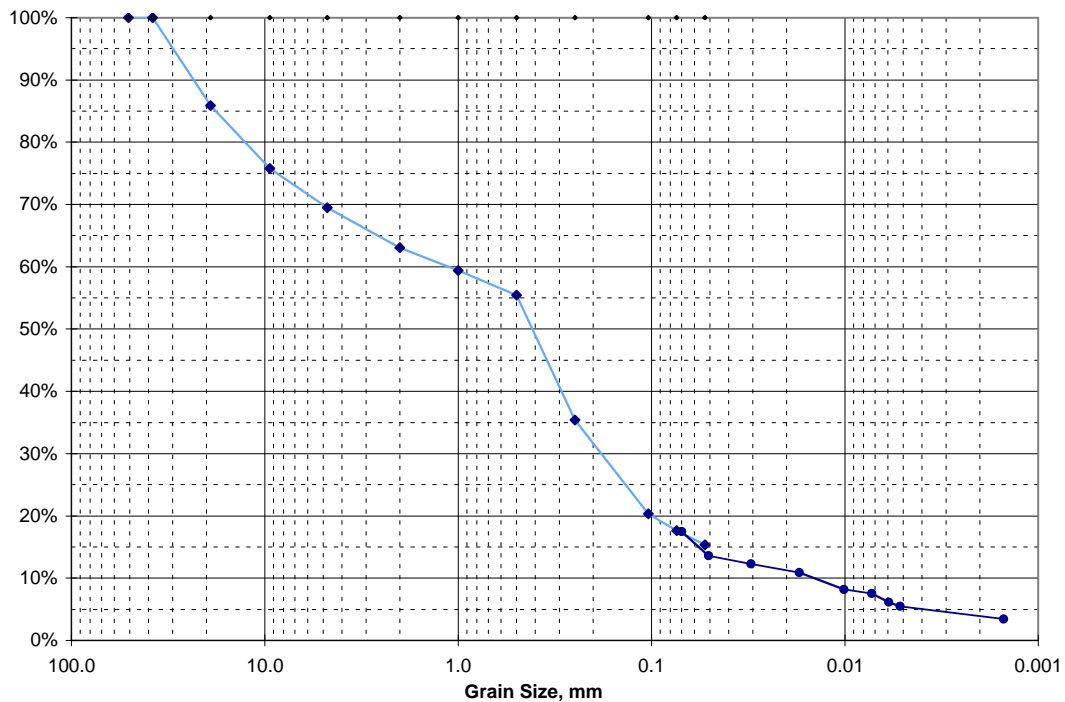
C4687, 77.5-78.0

Sieve Analysis Data for Sample 78.5-79'

U.S. Std. Sieve Opening in Inches

Grain Size, mm

Fraction <

C4687, 78.5-79.0

Sieve Analysis Data for Sample 80-80.5'
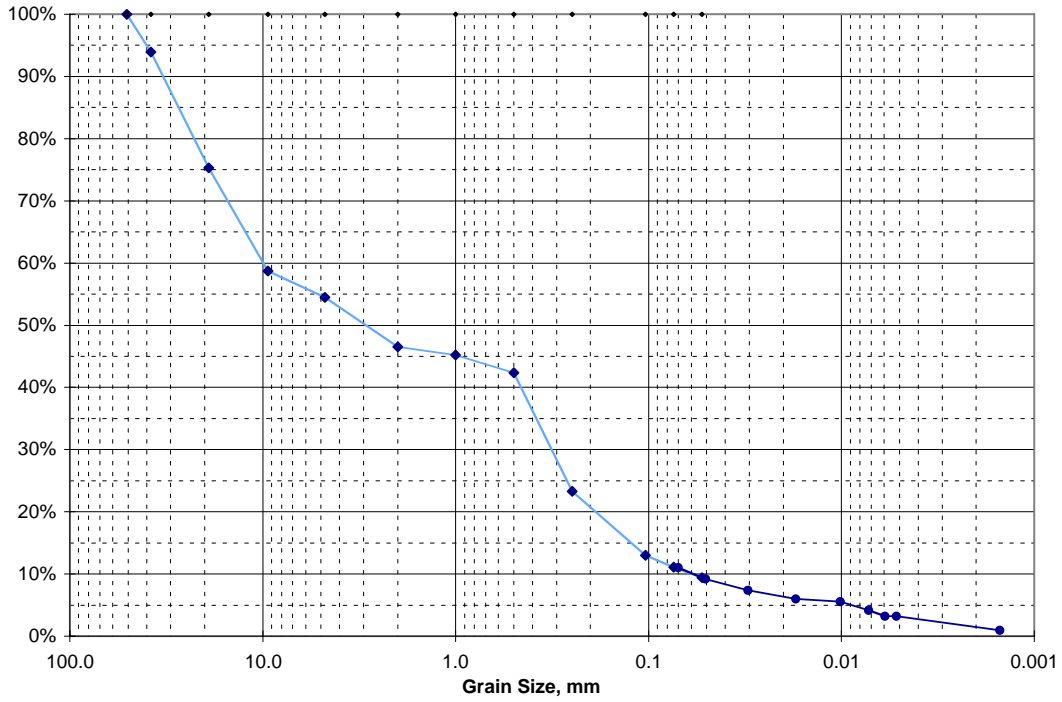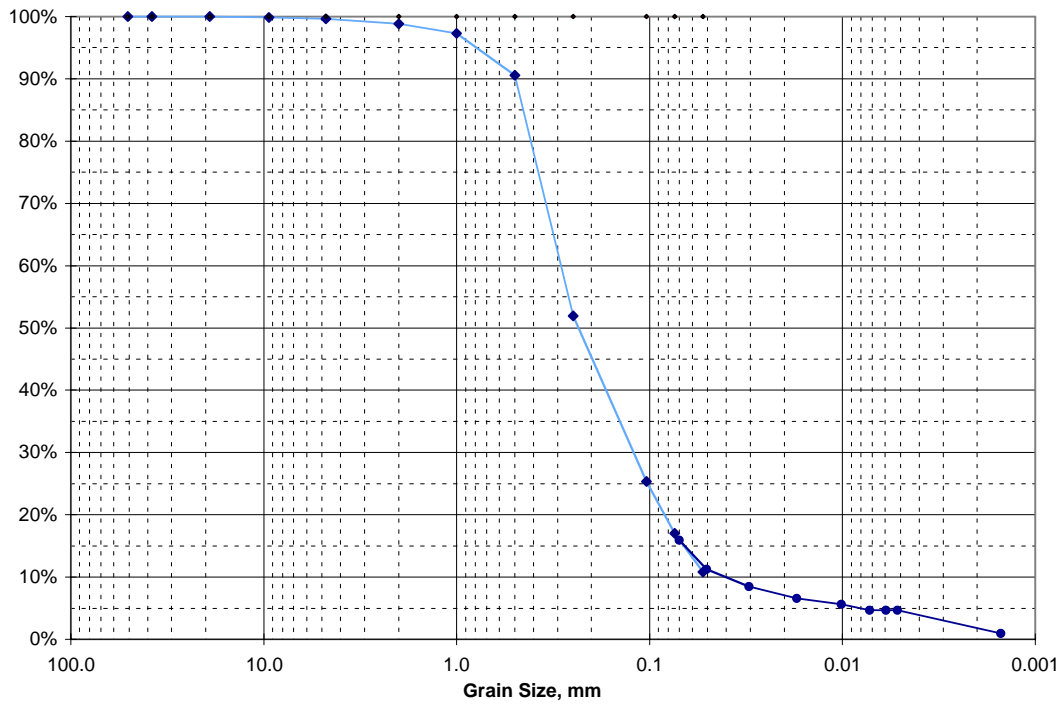
U.S. Std. Sieve Opening in Inches

Hydrometer

Grain Size, mm

Fraction <
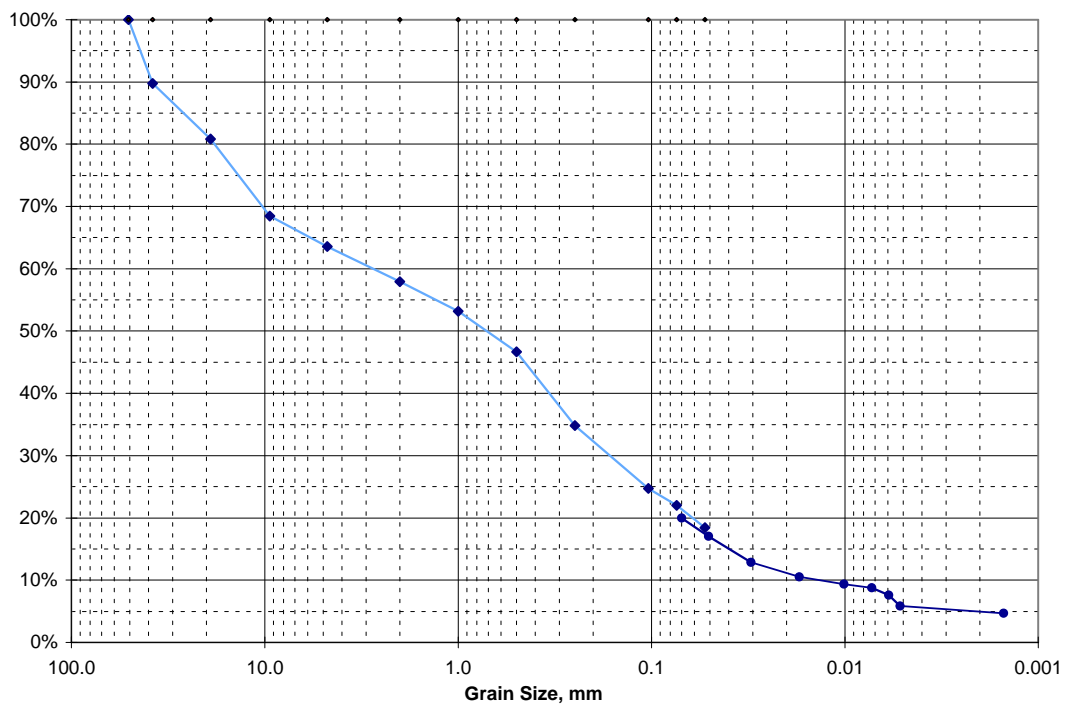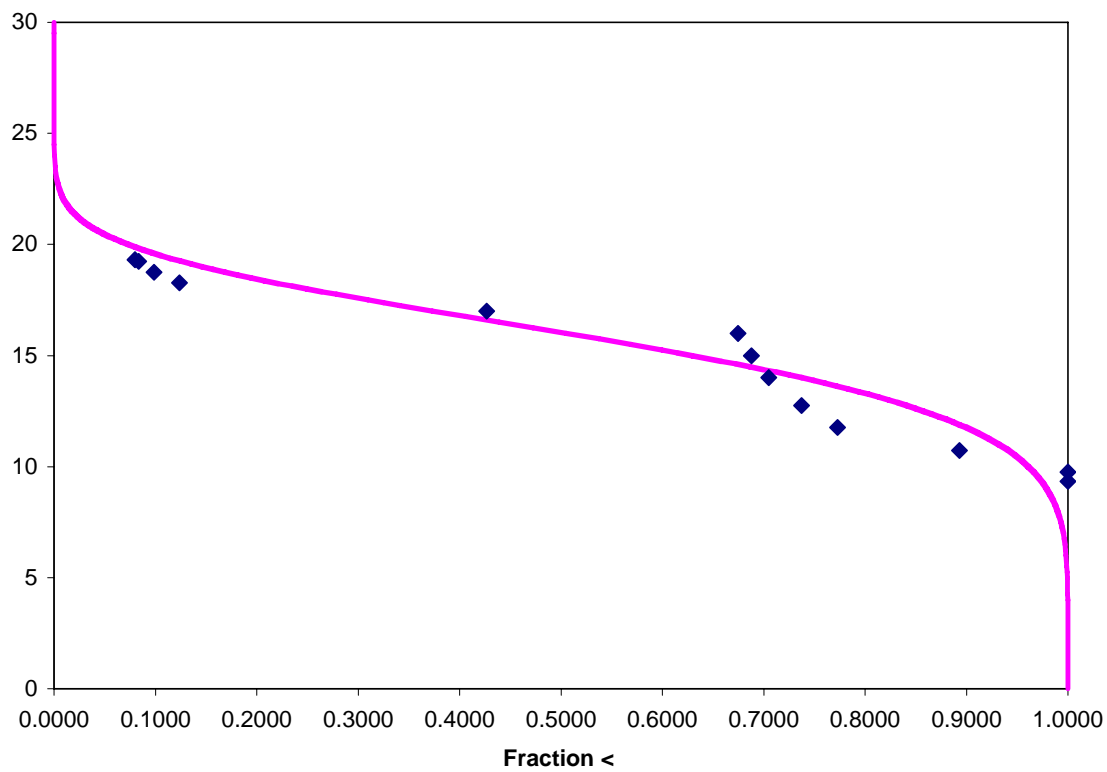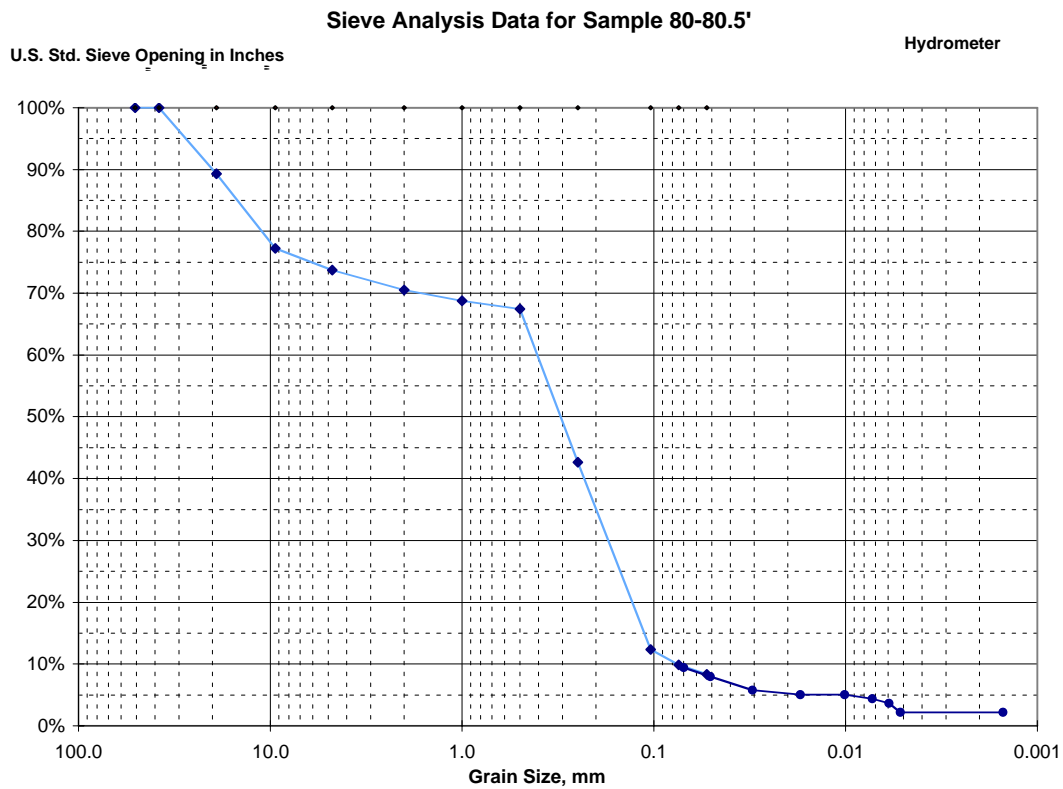
C4687, 80.0-80.5

Sieve Analysis Data for Sample 81-81.5'
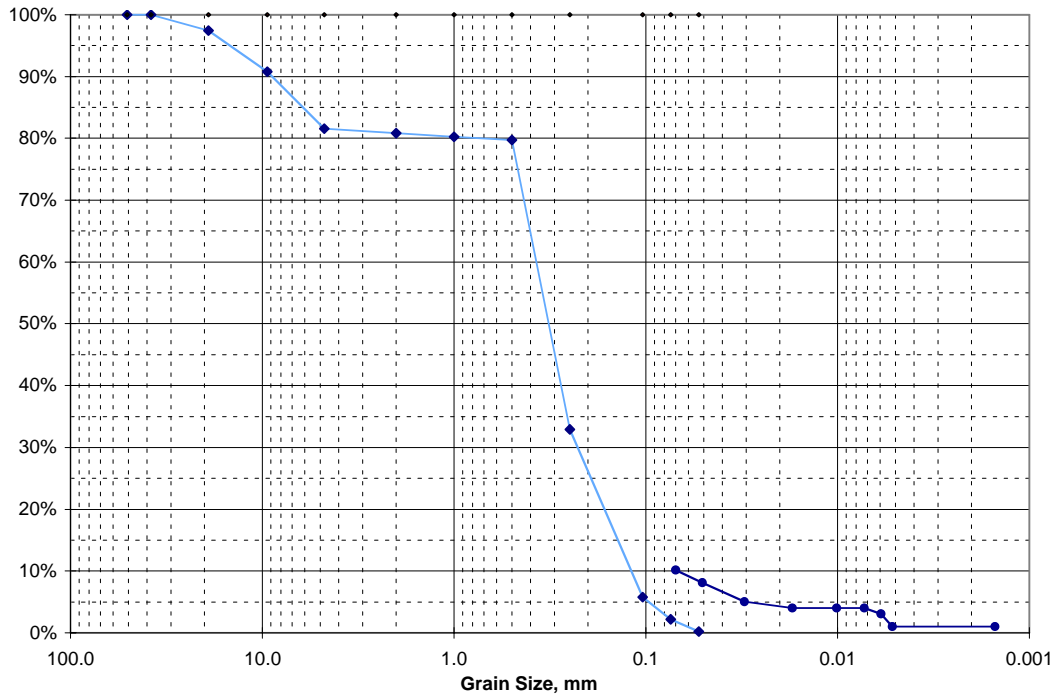
C4687, 81.0-81.5

Sieve Analysis Data for Sample 82.5-83.0'

C4687, 82.5-83.0
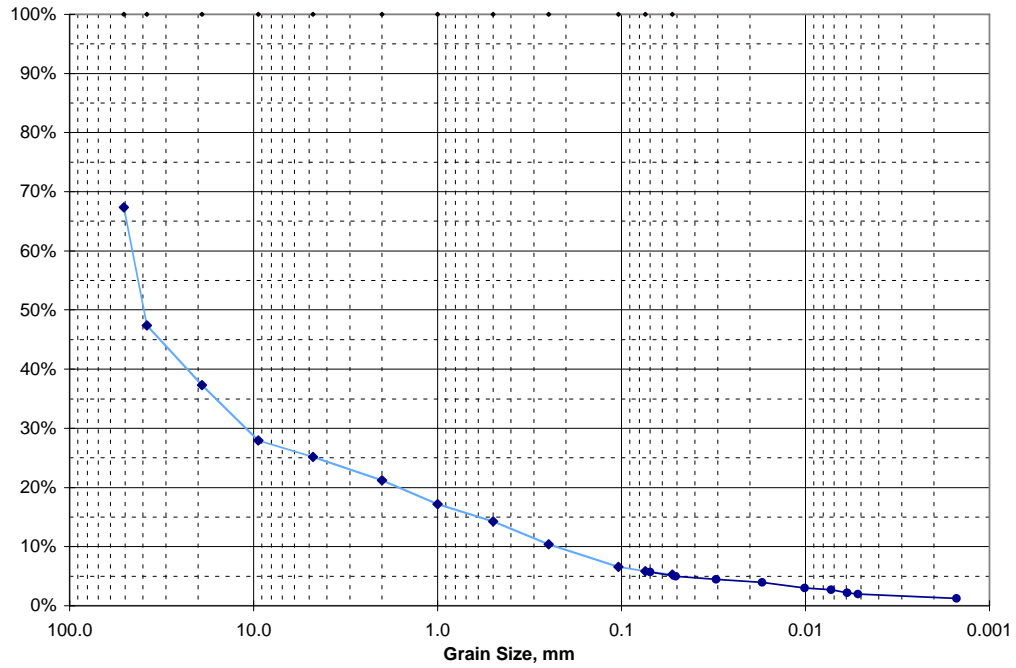
Sieve Analysis Data for Sample 83.5-84'
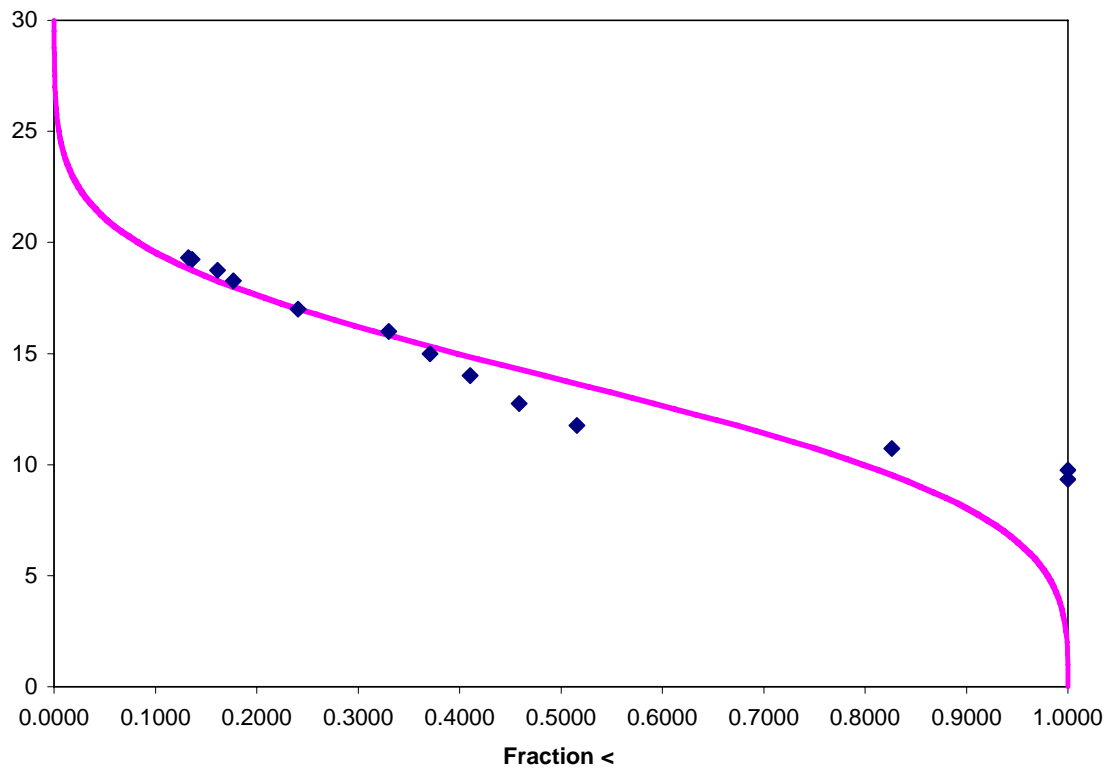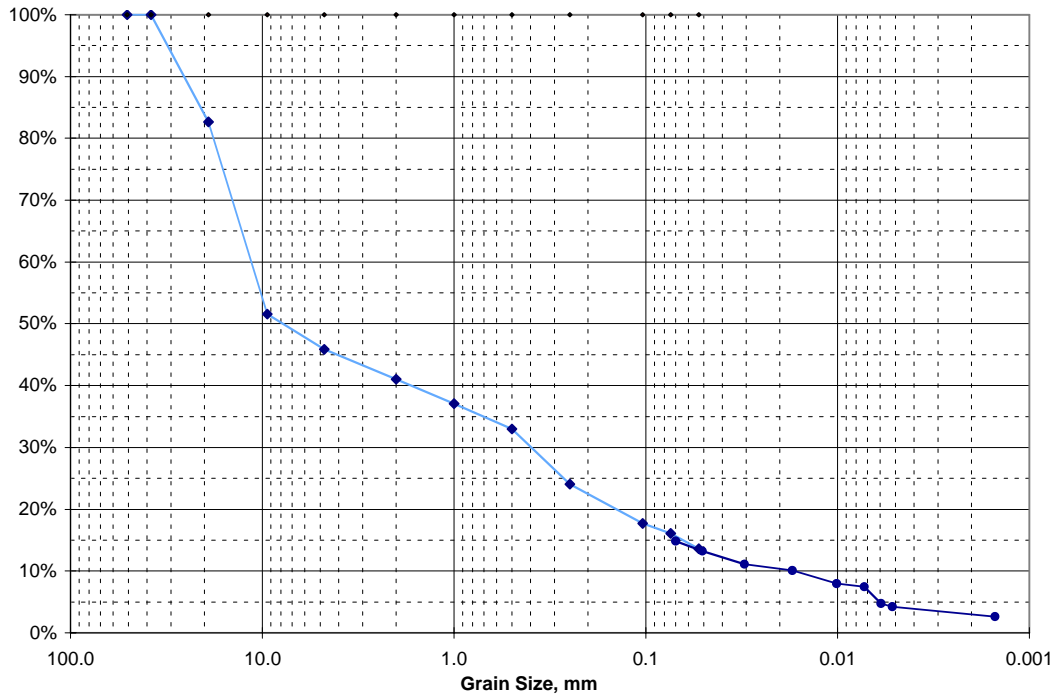
C4687, 83.5-84.0

Sieve Analysis Data for Sample 85-85.5'

C4687, 85.0-85.5

K.9
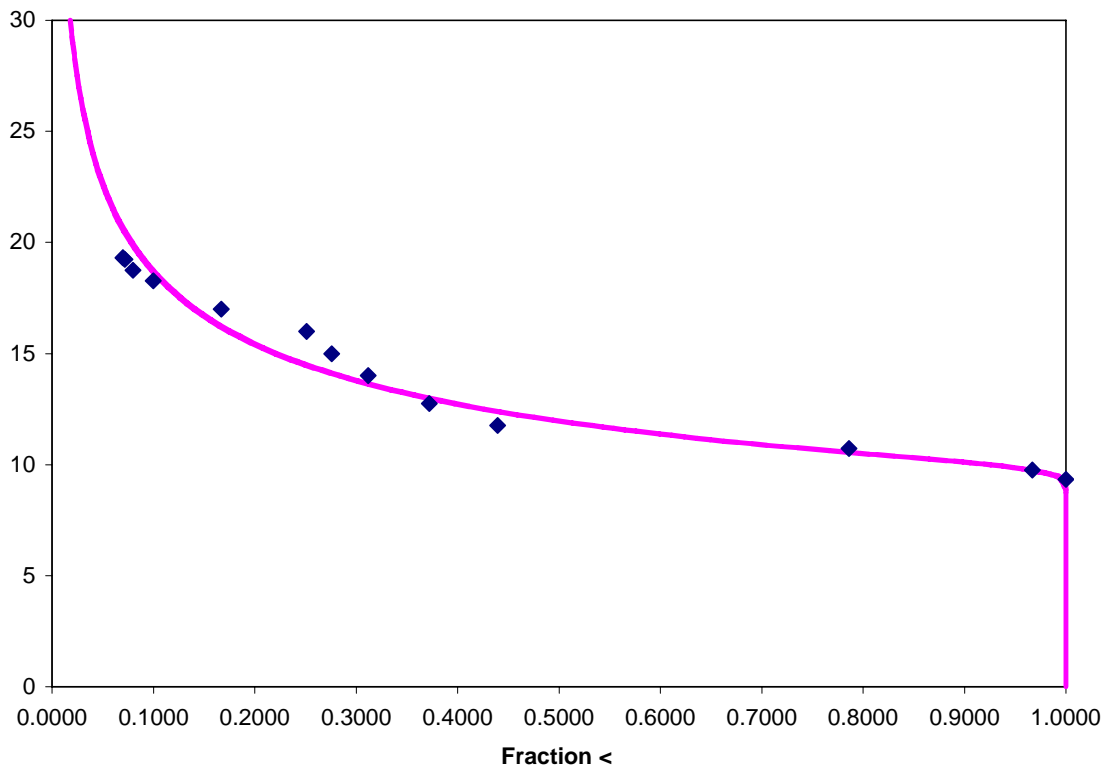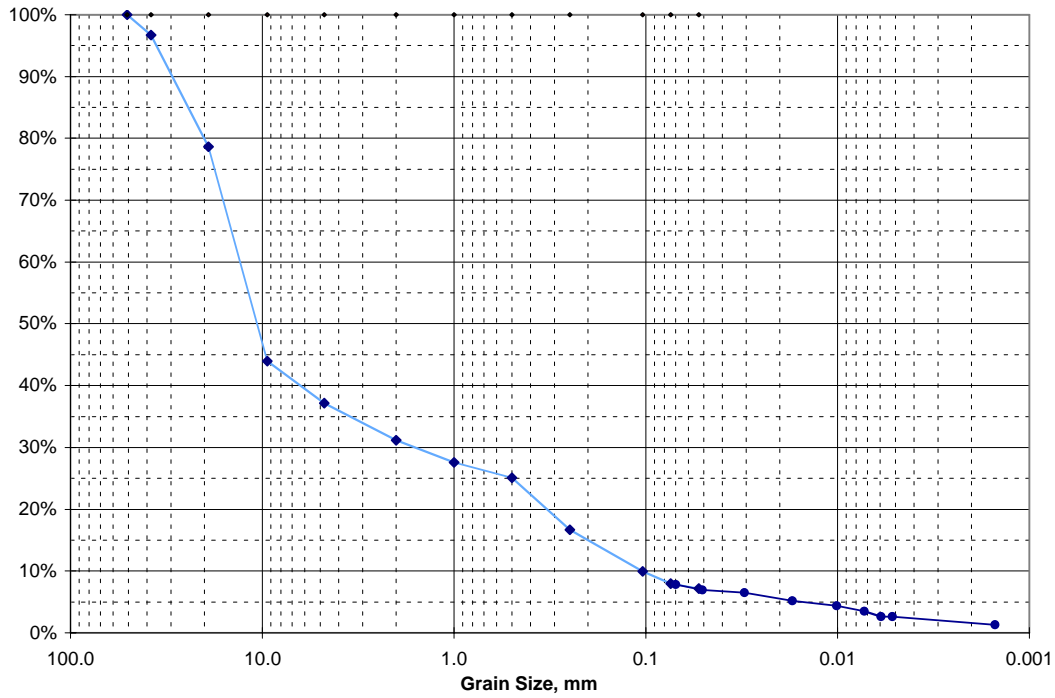
Sieve Analysis Data for Sample 86-86.5'

U.S. Std. Sieve Opening in Inches

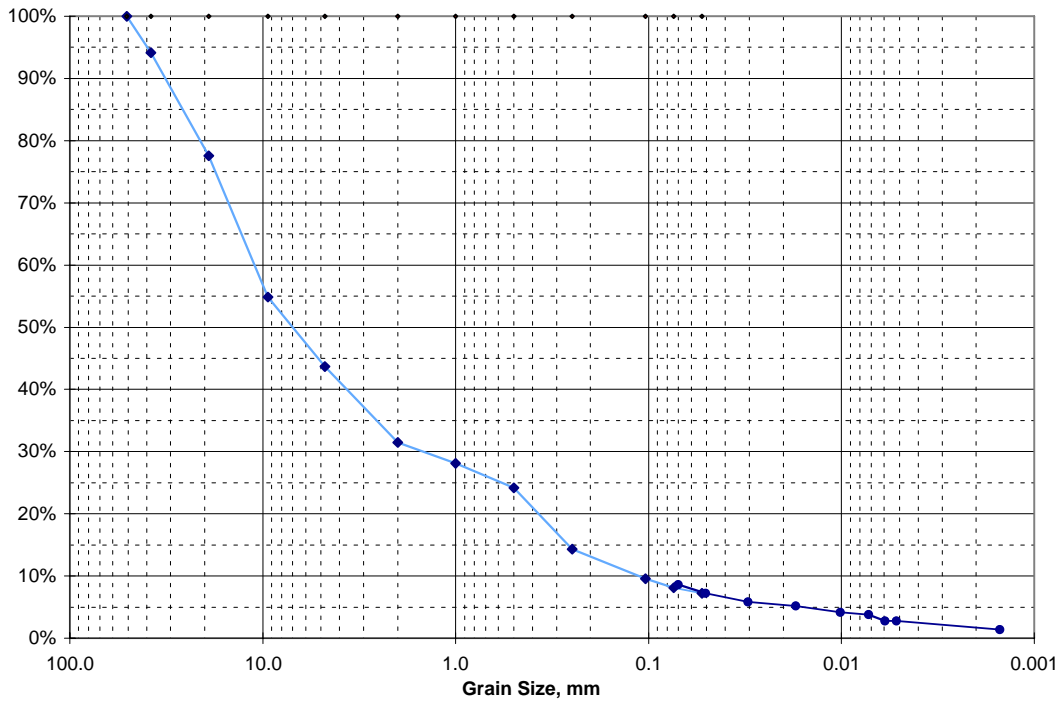Hydrometer

Grain Size, mm

Fraction <

C4687, 86.0-86.5
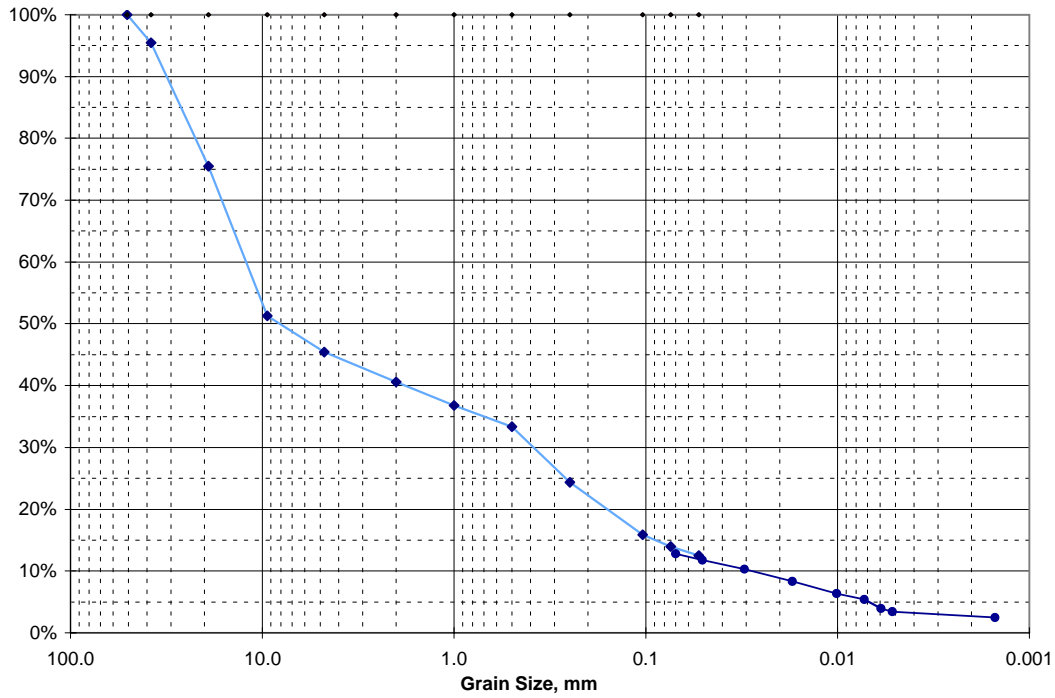
Sieve Analysis Data for Sample 87.5-88'

U.S. Std. Sieve Opening in Inches

Hydrometer

Grain Size, mm

Fraction <
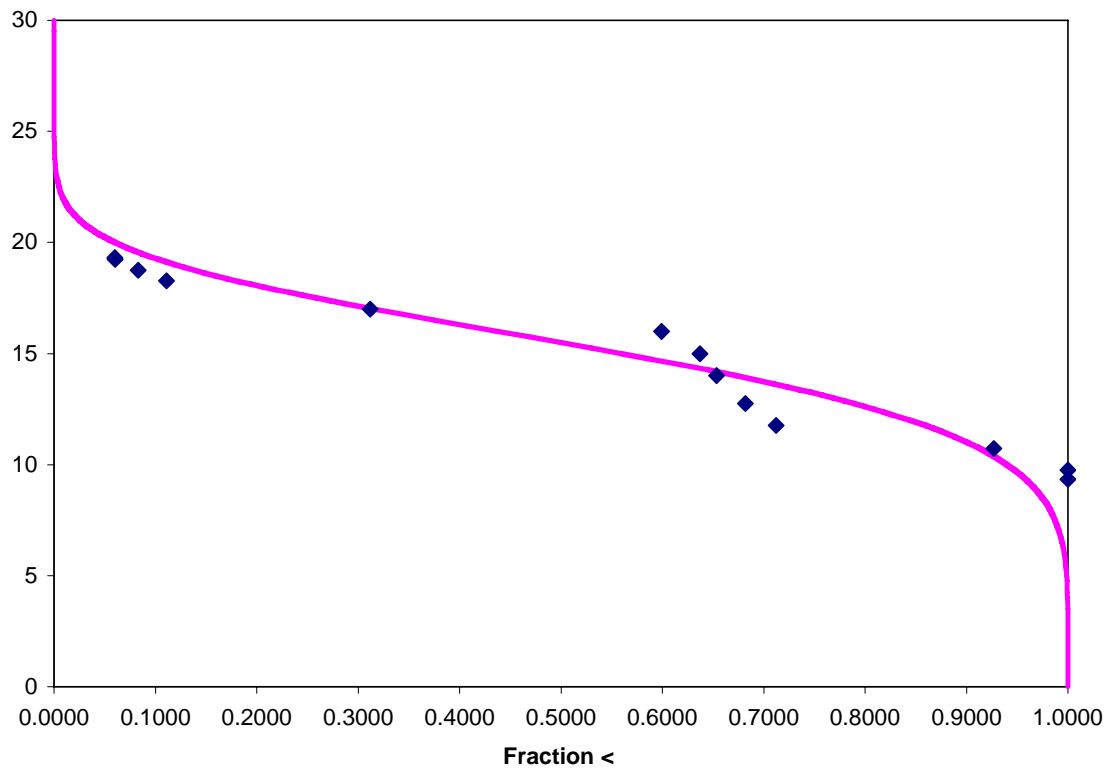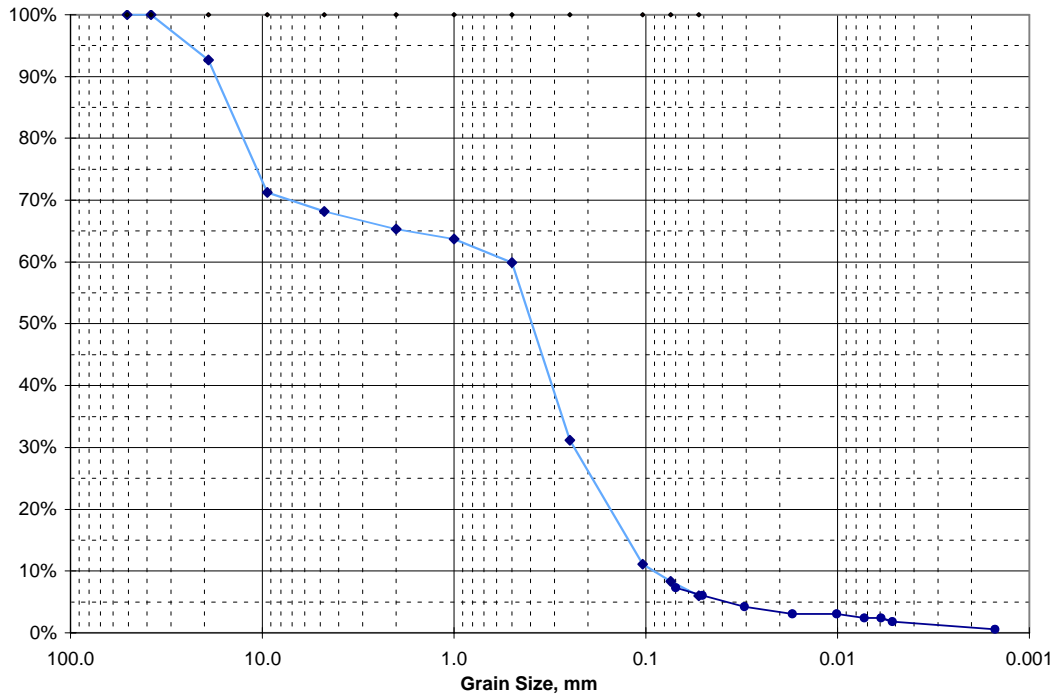
C4687, 87.5-88.0
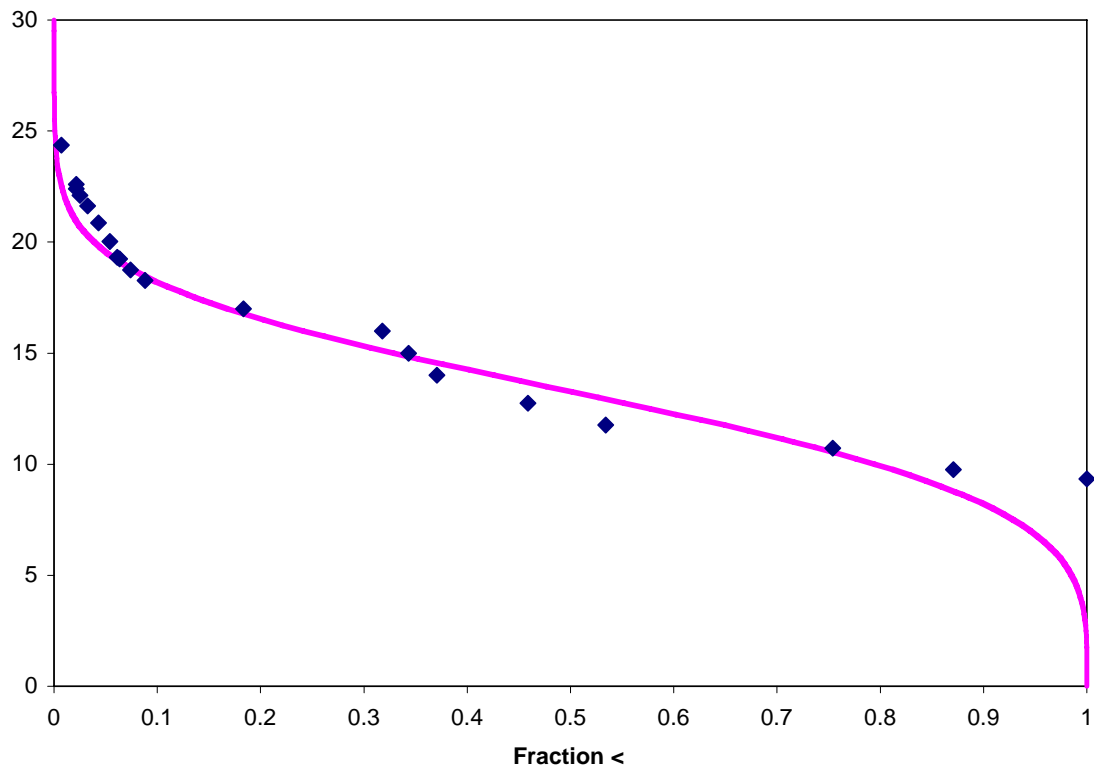
Sieve Analysis Data for Sample 88.5-89'

C4687, 88.5-89.0

K.12

Sieve Analysis Data for Sample 91.0-91.5'
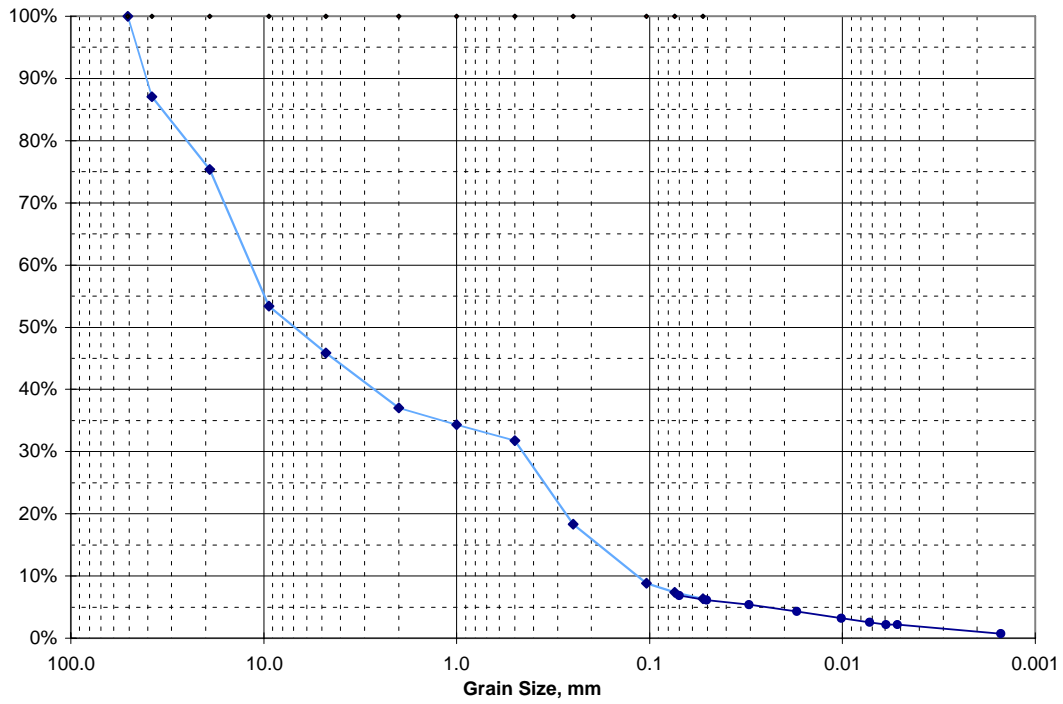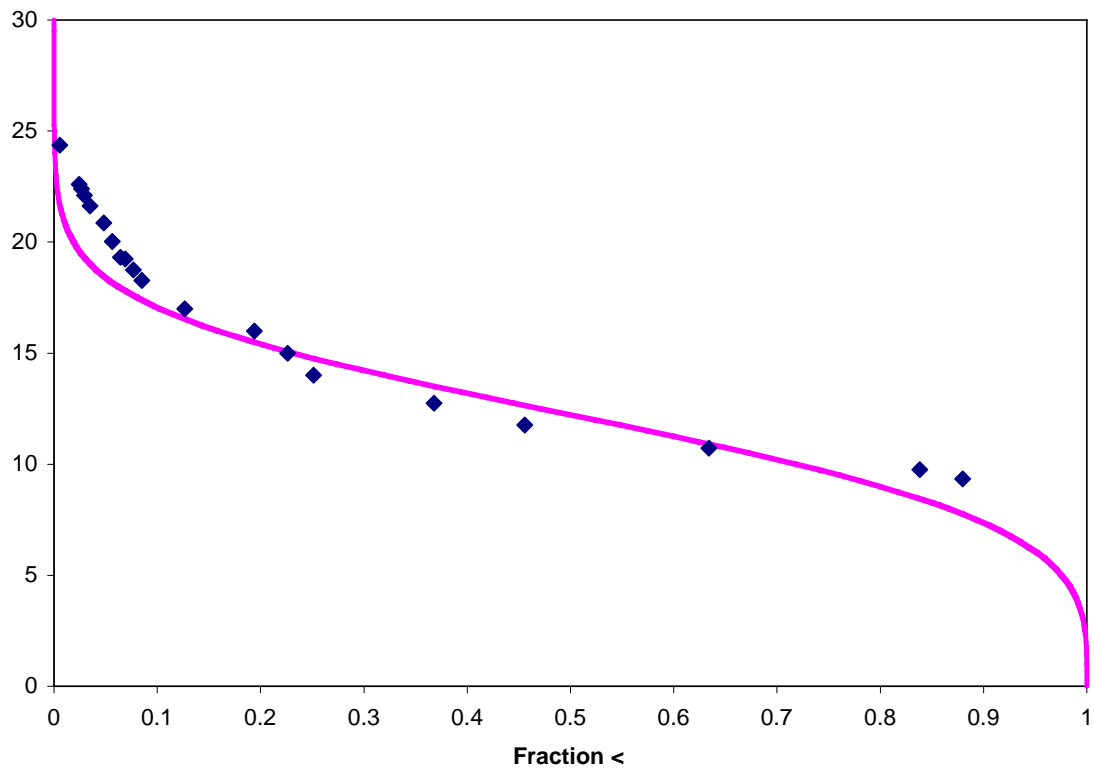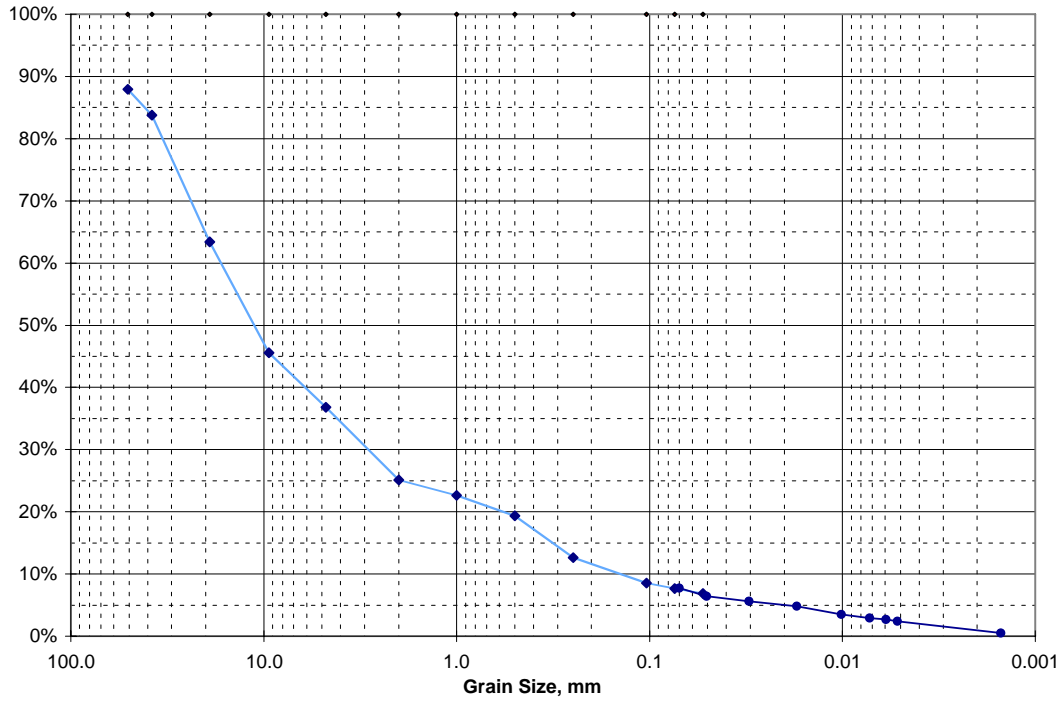
U.S. Std. Sieve Opening in Inches

Hydrometer

Grain Size, mm

Fraction <

C4687, 91.0-91.5

K.13

Sieve Analysis Data for Sample 92.5-93.0'

C4687, 92.5-93.0

Sieve Analysis Data for Sample 93.5-94.0'

C4687, 93.5-94.0

Sieve Analysis Data for Sample 95.0-95.5'

C4687, 95.0-95.5

Sieve Analysis Data for Sample 96.0-96.5'

C4687, 96.0-96.5

K.17

Sieve Analysis Data for Sample 97.3-97.8'

C4687, 97.3-98.8

K.18

Sieve Analysis Data for Sample 98.3-98.8'
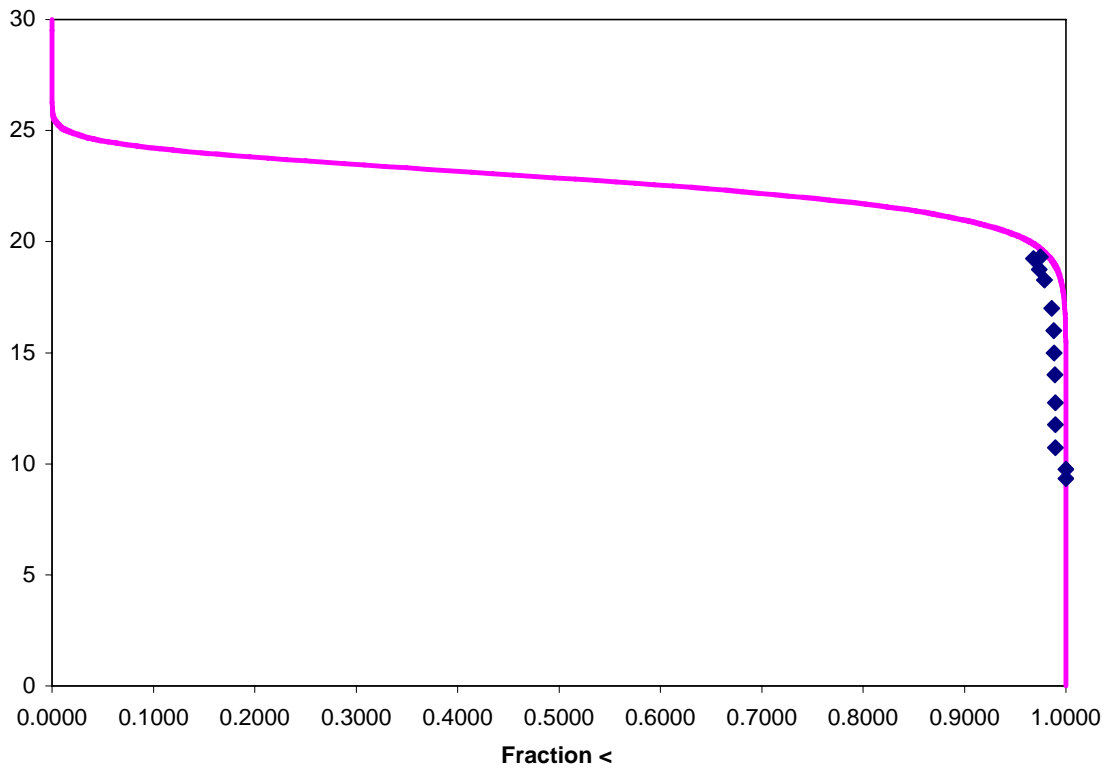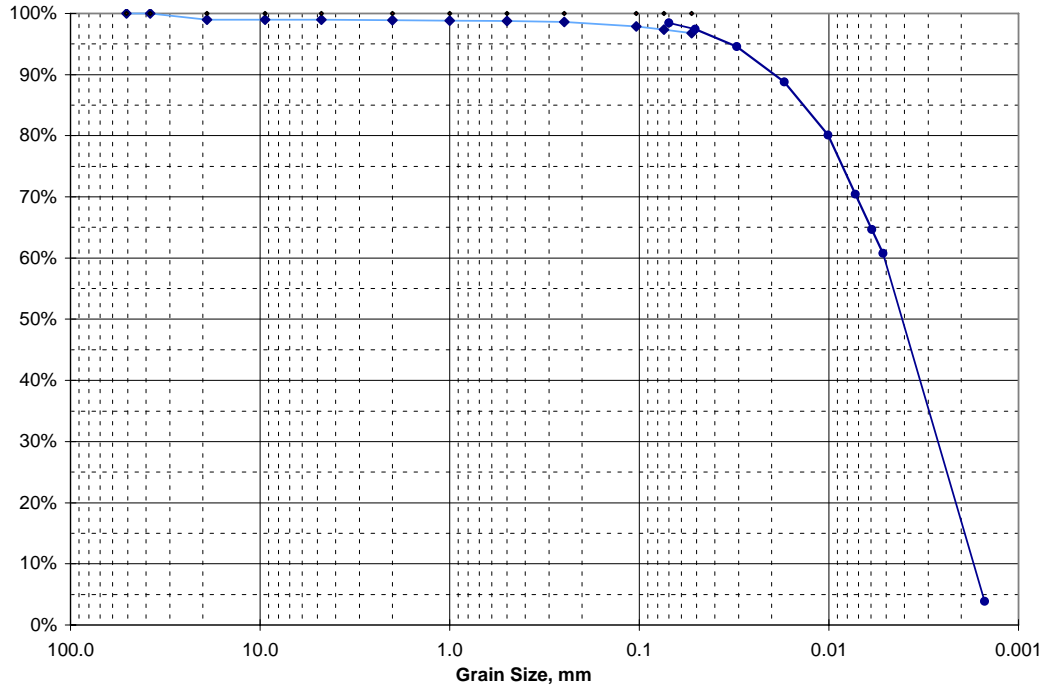
C4687, 98.3-98.8

K.19

Appendix L

Sieve Analysis and Log Grain Size Fit

for Borehole C4688 D4-92

Appendix L - Sieve Analysis and Log Grain Size Fit for Borehole C4688 D4-92

Sieve Analysis Data for Sample 75.0-75.5'
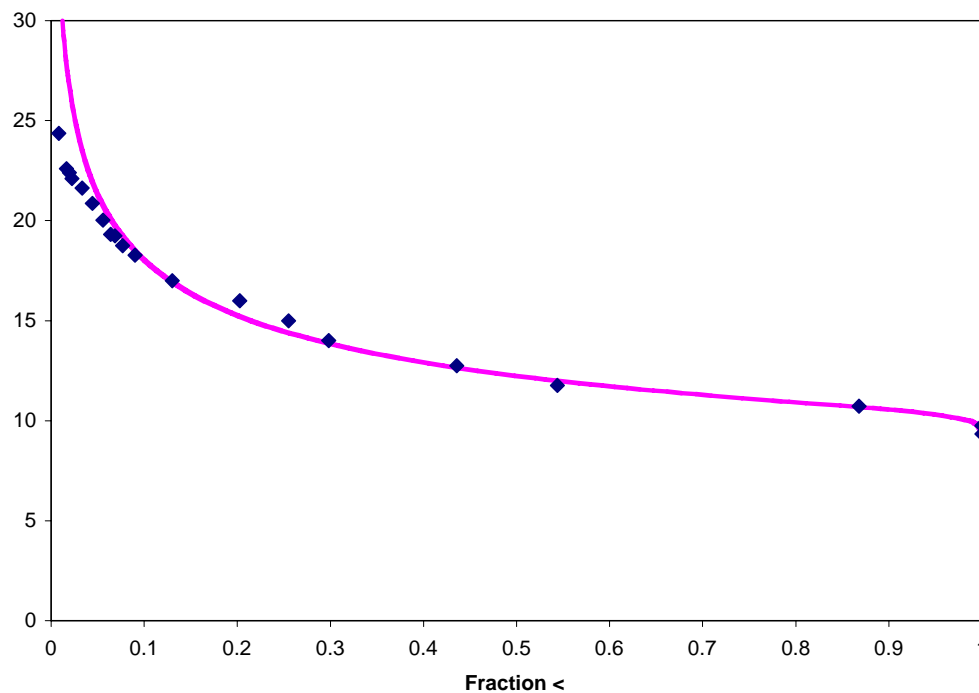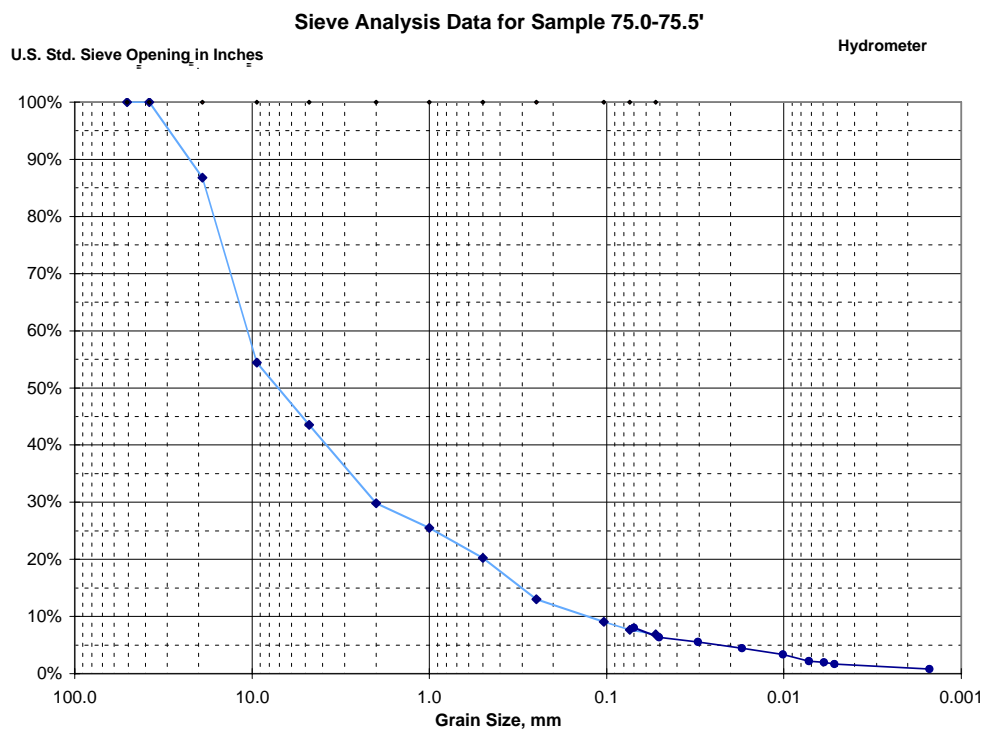
C4688, 75.0-75.5
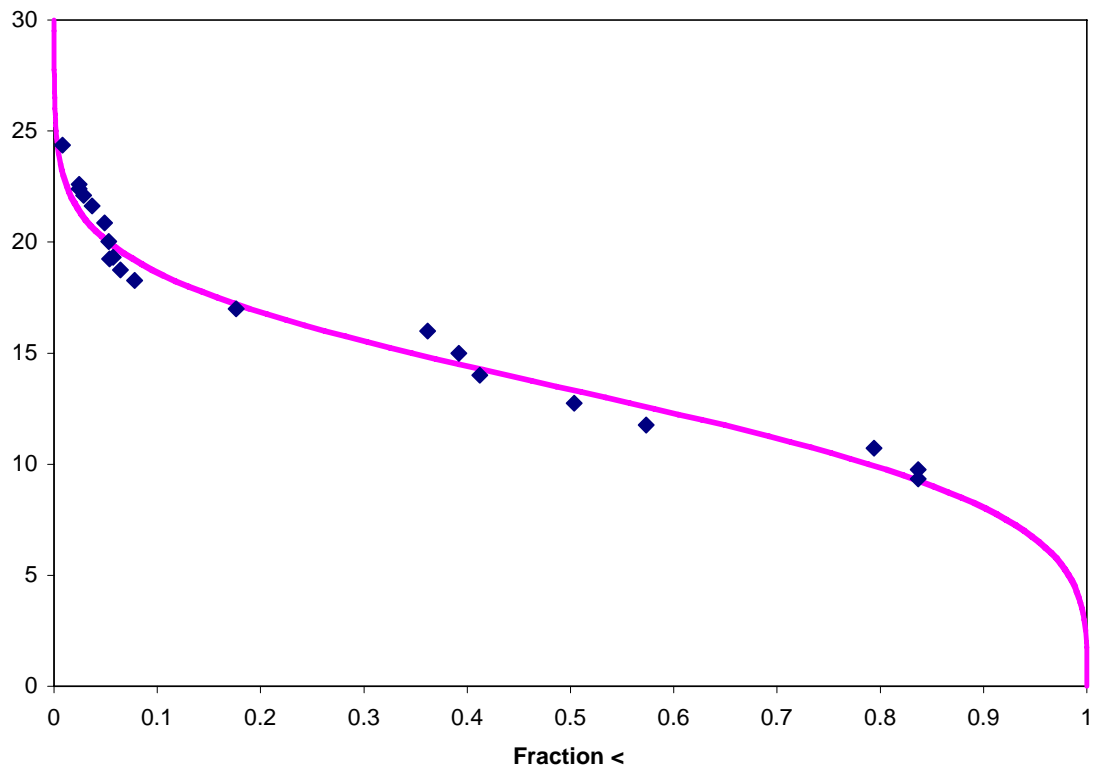
Sieve Analysis Data for Sample 76.0-76.5'
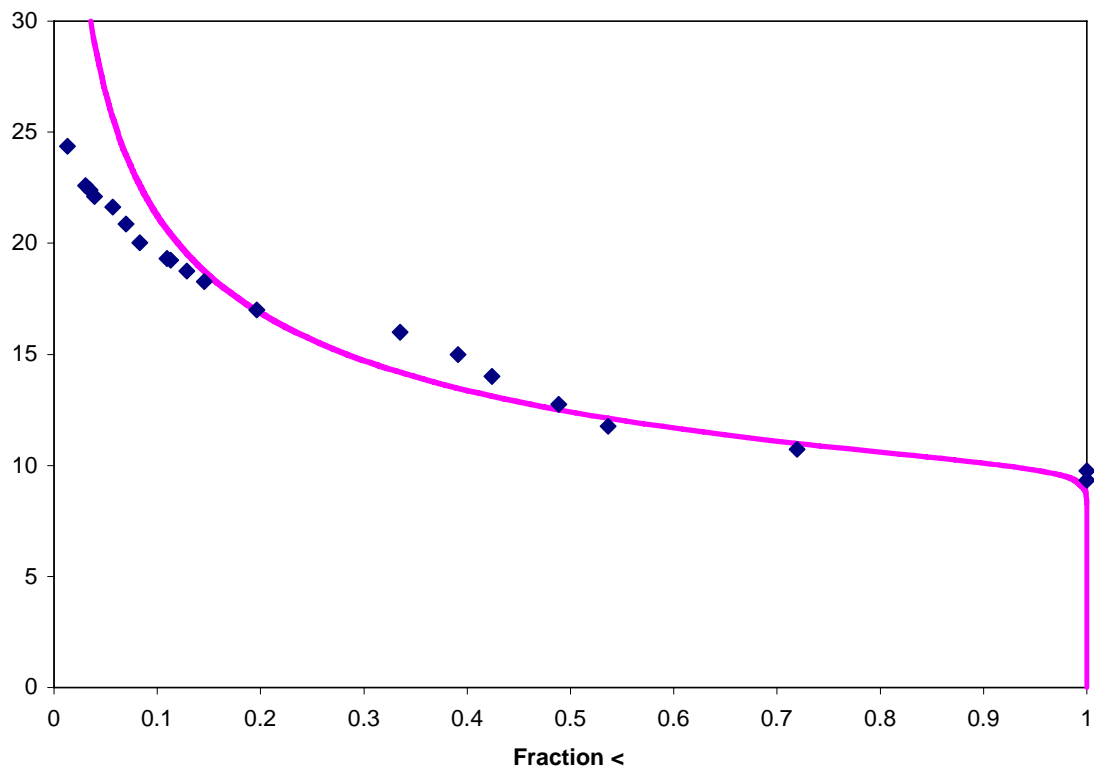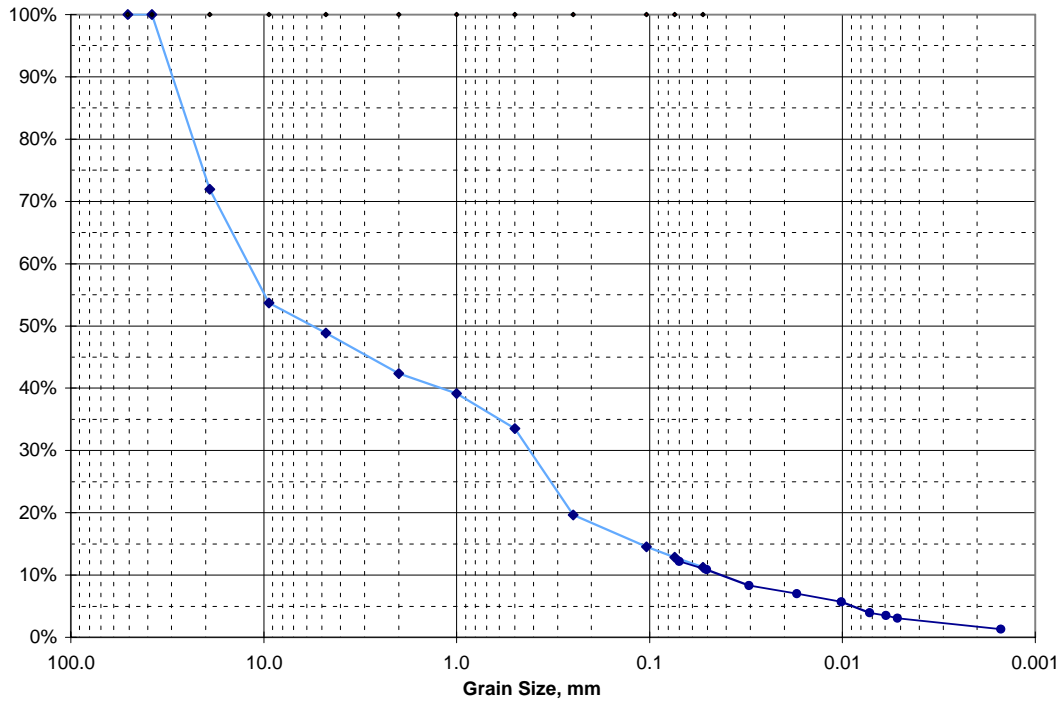
C4688, 76.0-76.5

Sieve Analysis Data for Sample 77.5-78.0'
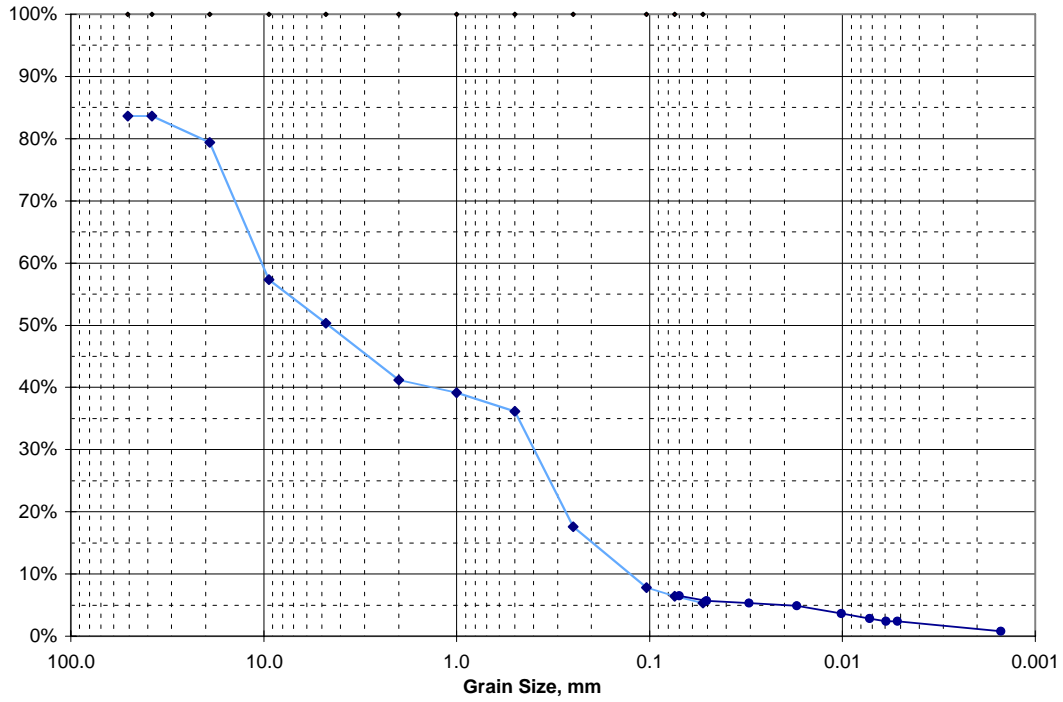
U.S. Std. Sieve Opening in Inches
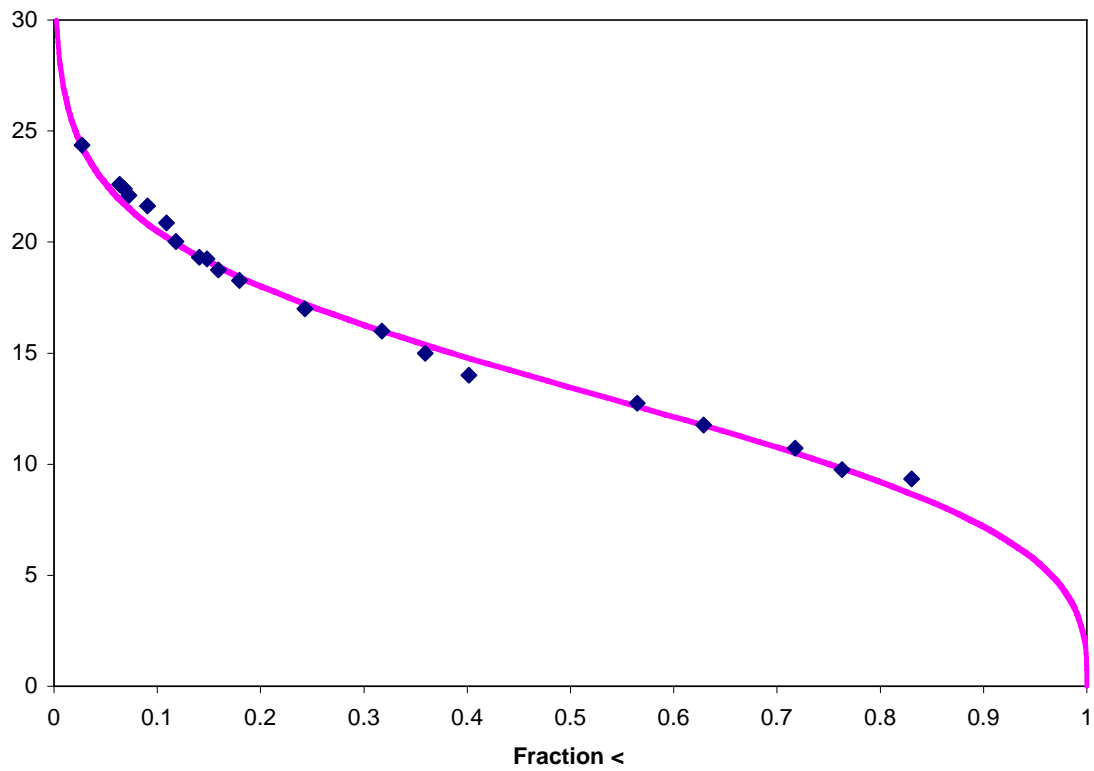
Hydrometer

Grain Size, mm

Fraction <
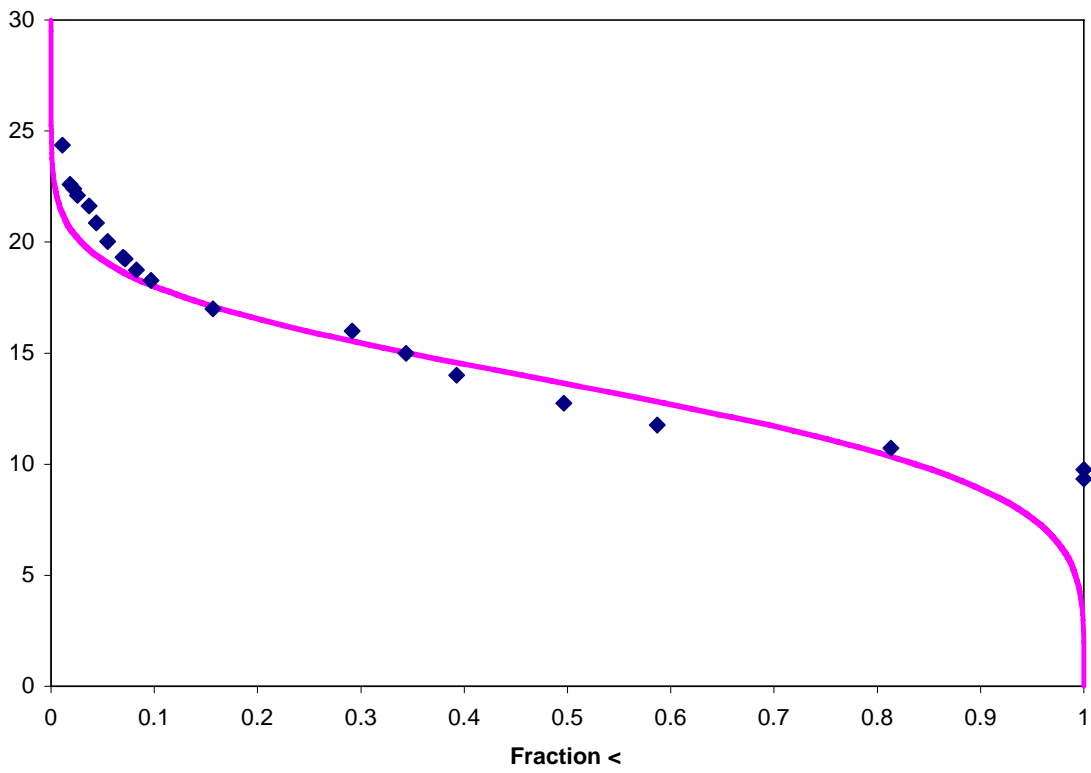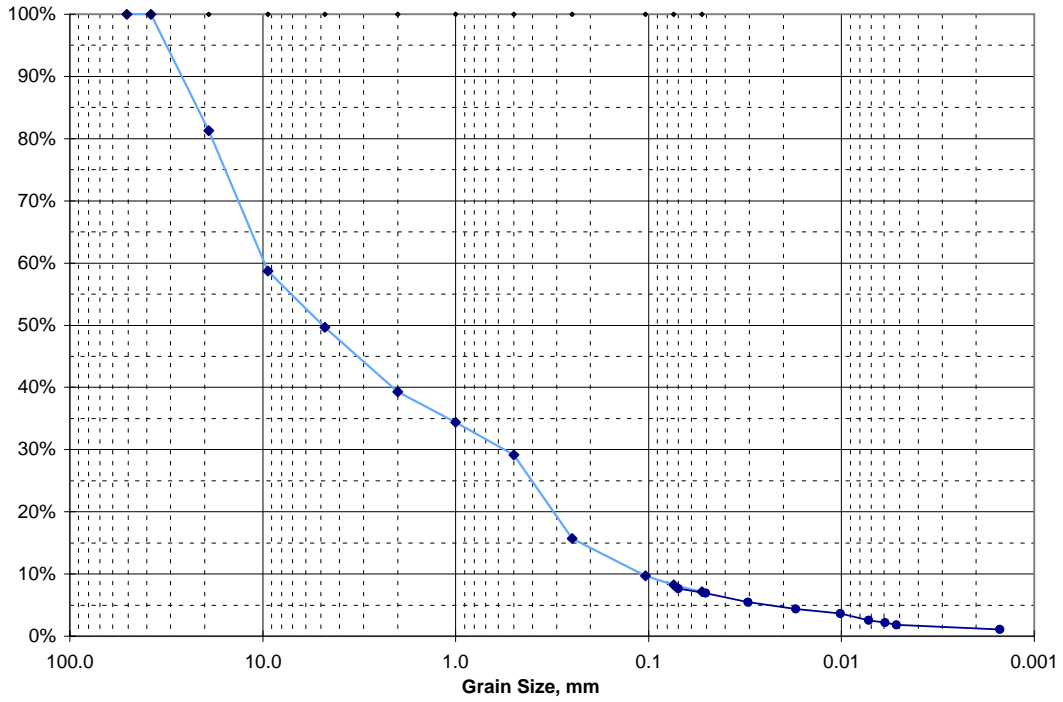
C4688, 77.5-78.0

Sieve Analysis Data for Sample 78.5-79.0'

U.S. Std. Sieve Opening in Inches
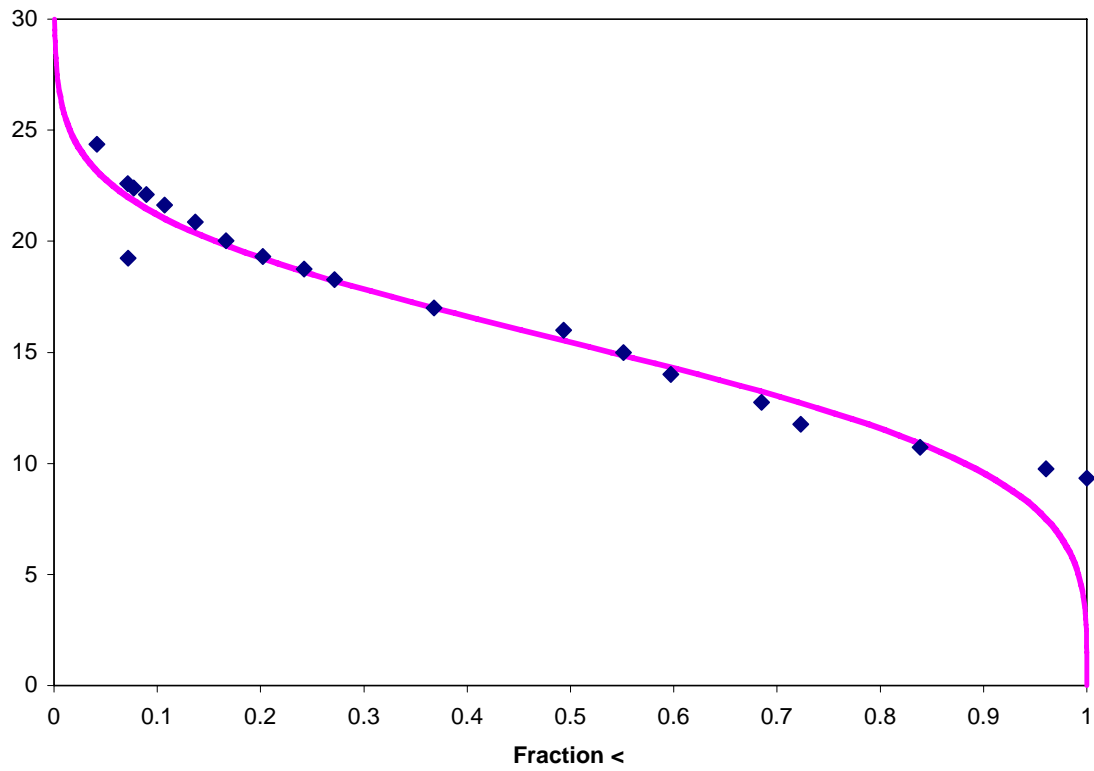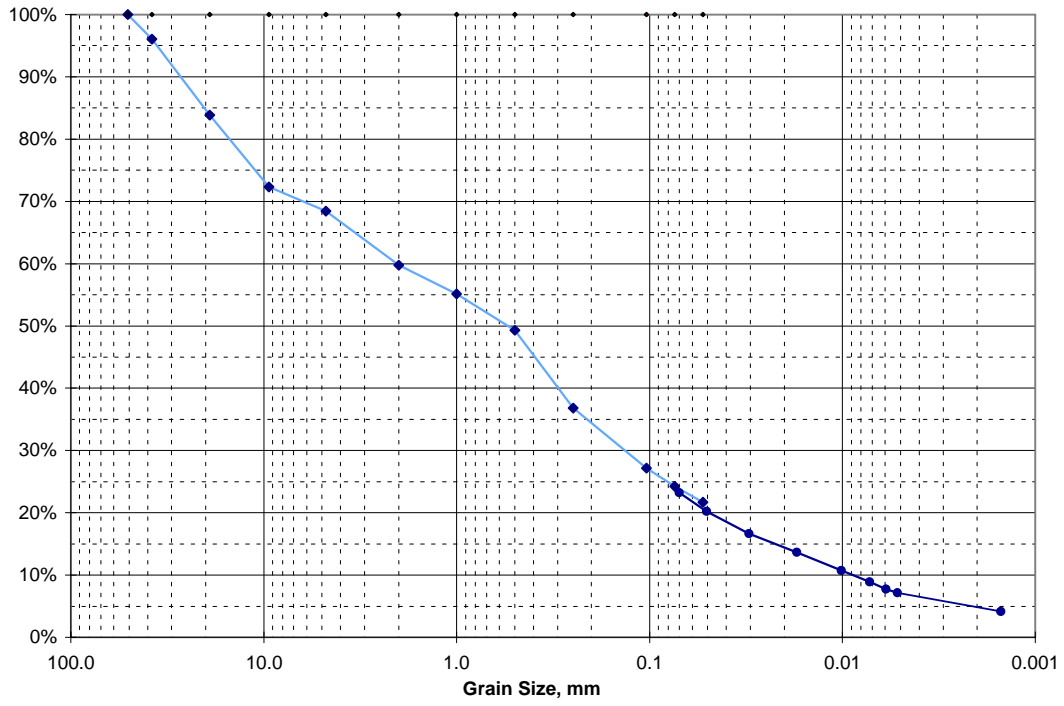
Hydrometer


Grain Size, mm

Fraction <

C4688, 78.5-79.0

Sieve Analysis Data for Sample 80.0-80.5'
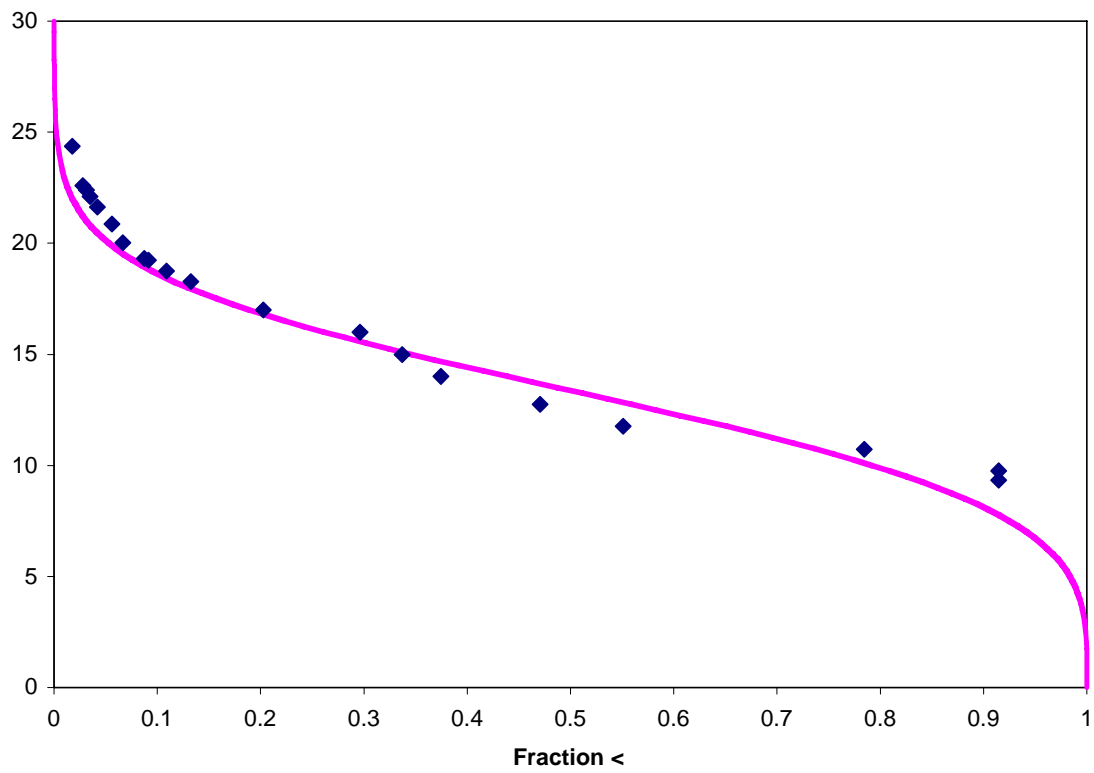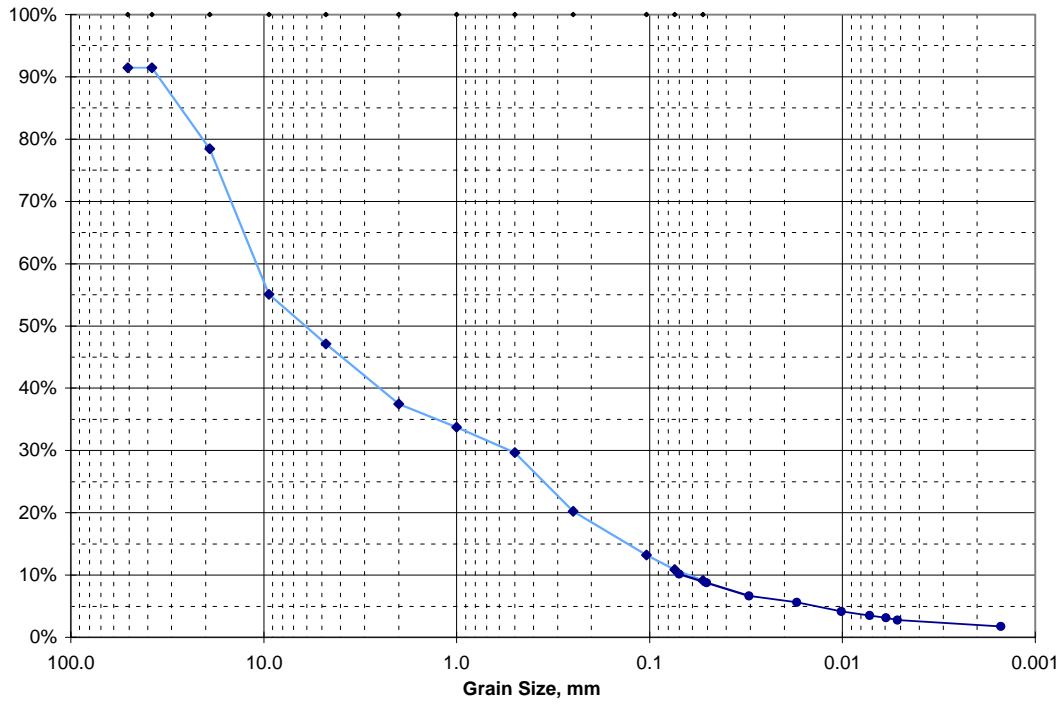
C4688, 80.0-80.5

L.5

Sieve Analysis Data for Sample 81.0-81.5'

C4688, 81.0-81.5

L.6

Sieve Analysis Data for Sample 82.0-82.5'

U.S. Std. Sieve Opening in Inches

Grain Size, mm

Fraction <
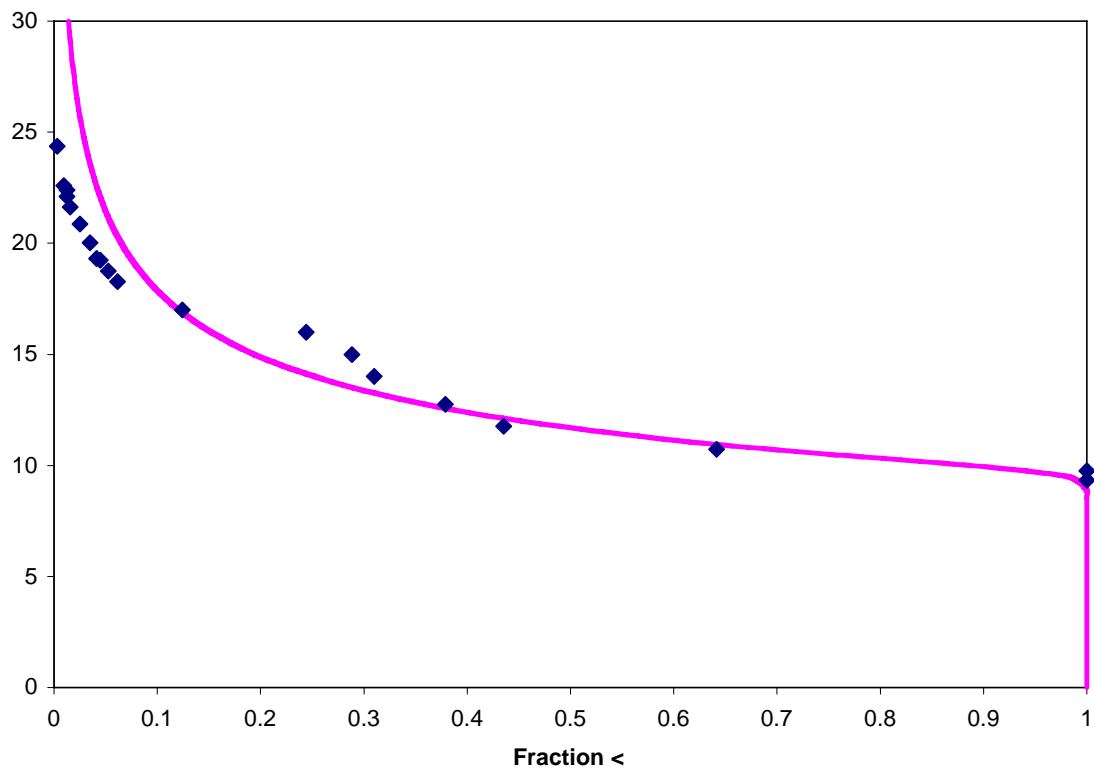
C4688, 82.0-82.5

Sieve Analysis Data for Sample 83.0-83.5'
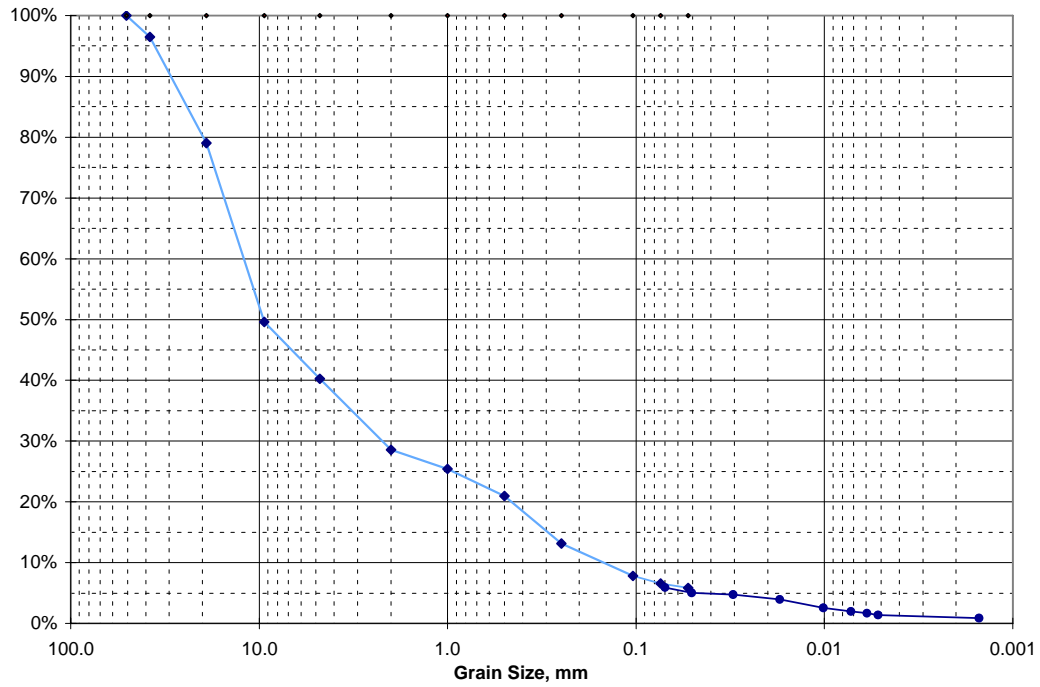
C4688, 83.0-83.5

Sieve Analysis Data for Sample 84.5-85.0'

C4688, 84.5-85.0

L.9

Sieve Analysis Data for Sample 84.5-85.0'

C4688, 84.5-85.0

Sieve Analysis Data for Sample 85.5-86.0'
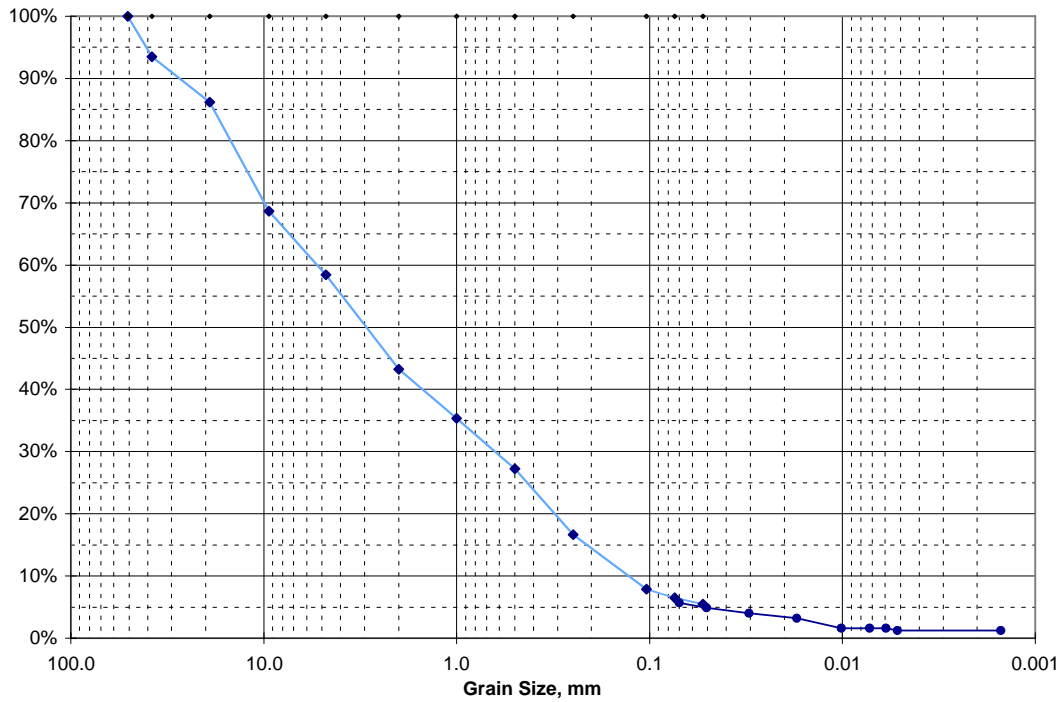
U.S. Std. Sieve Opening in Inches

Grain Size, mm

Fraction <
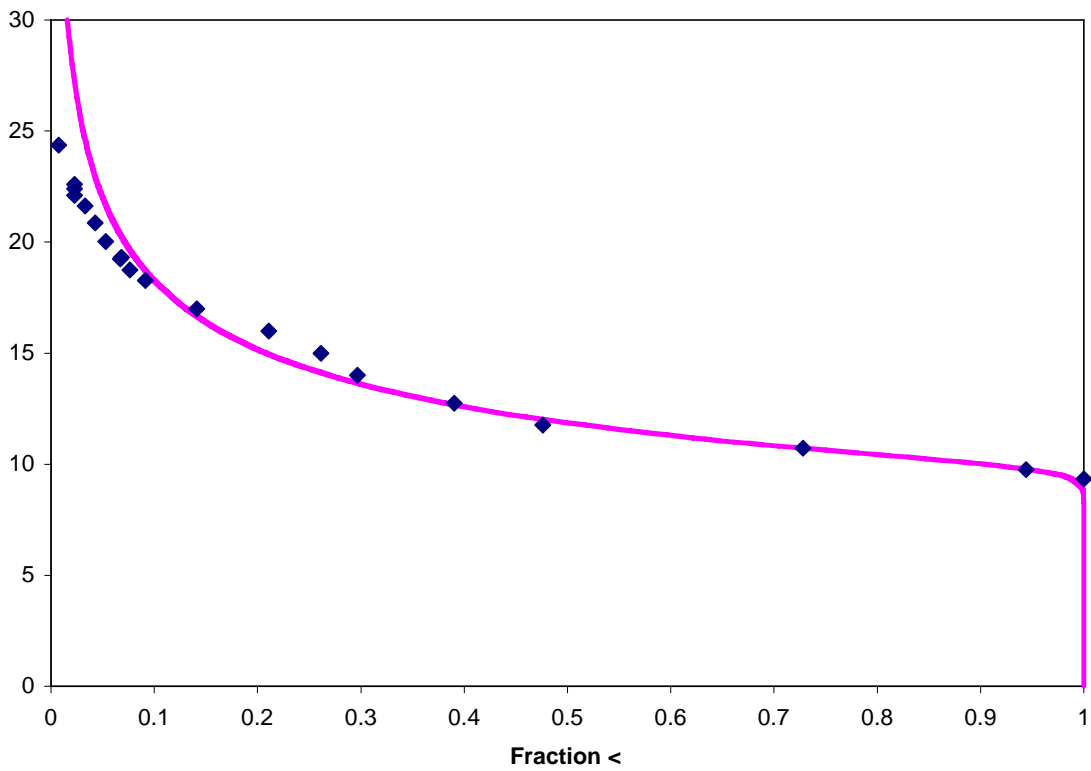
C4688, 85.5-86.0

Sieve Analysis Data for Sample 87.0-87.5'

U.S. Std. Sieve Opening in Inches
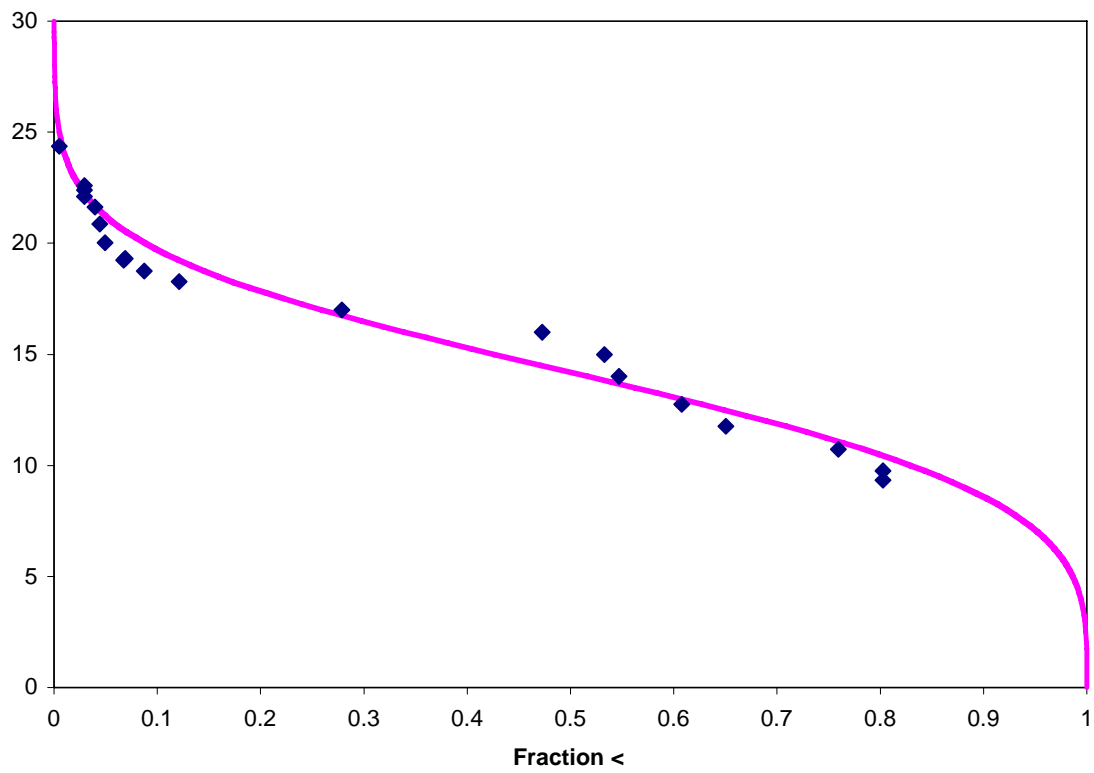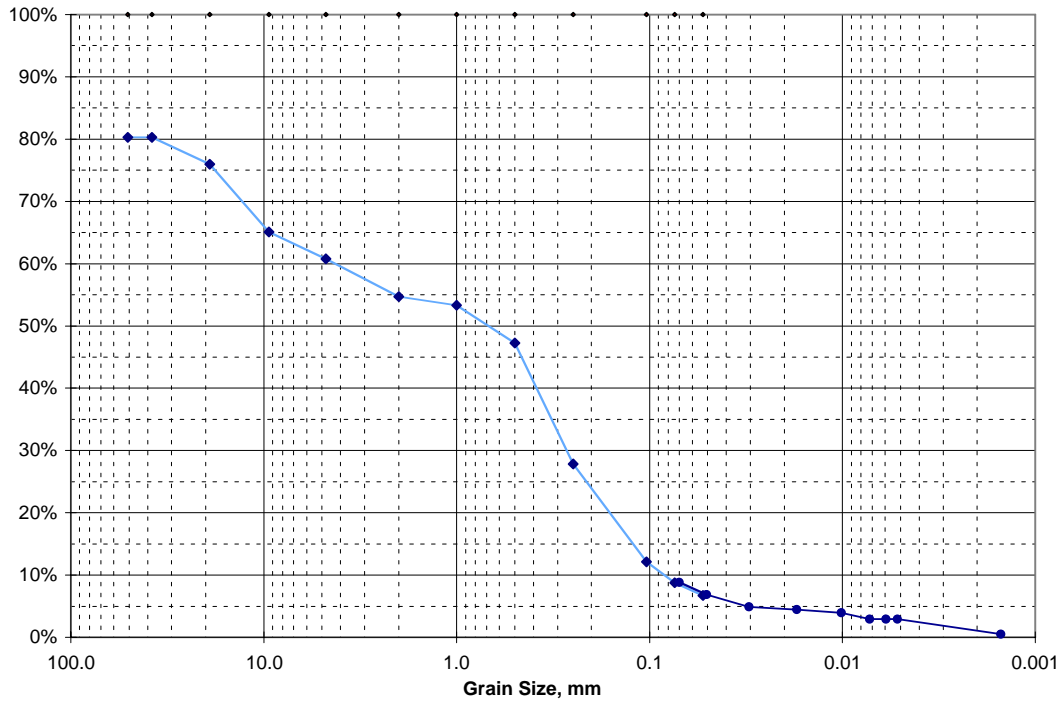
Grain Size, mm
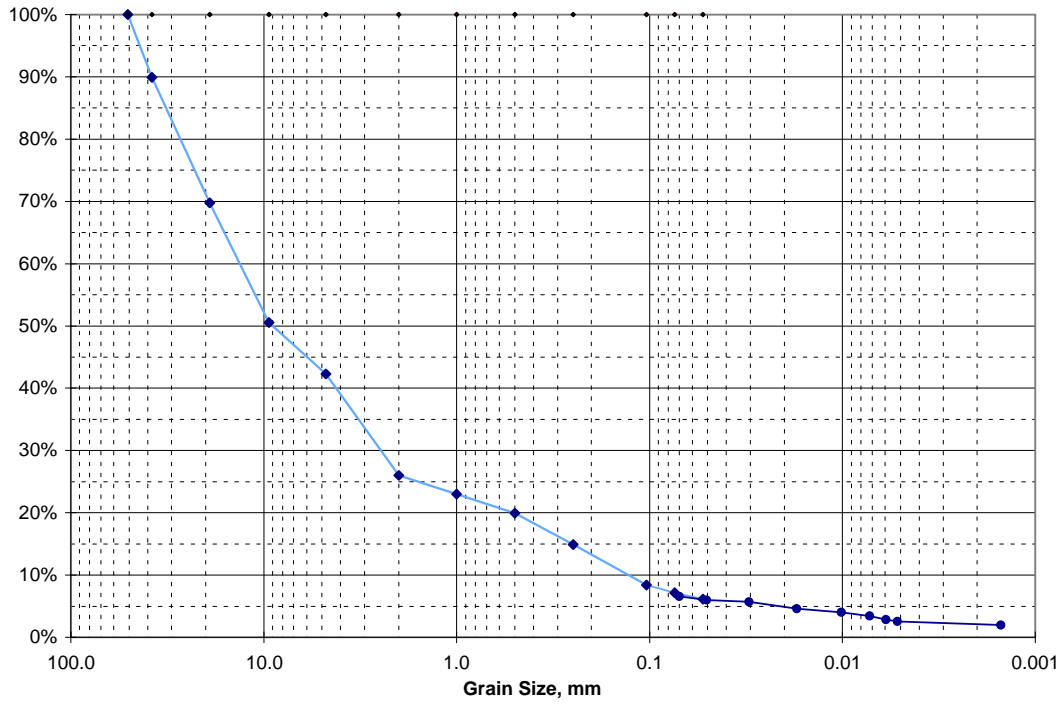

Fraction <

C4688, 87.0-87.5

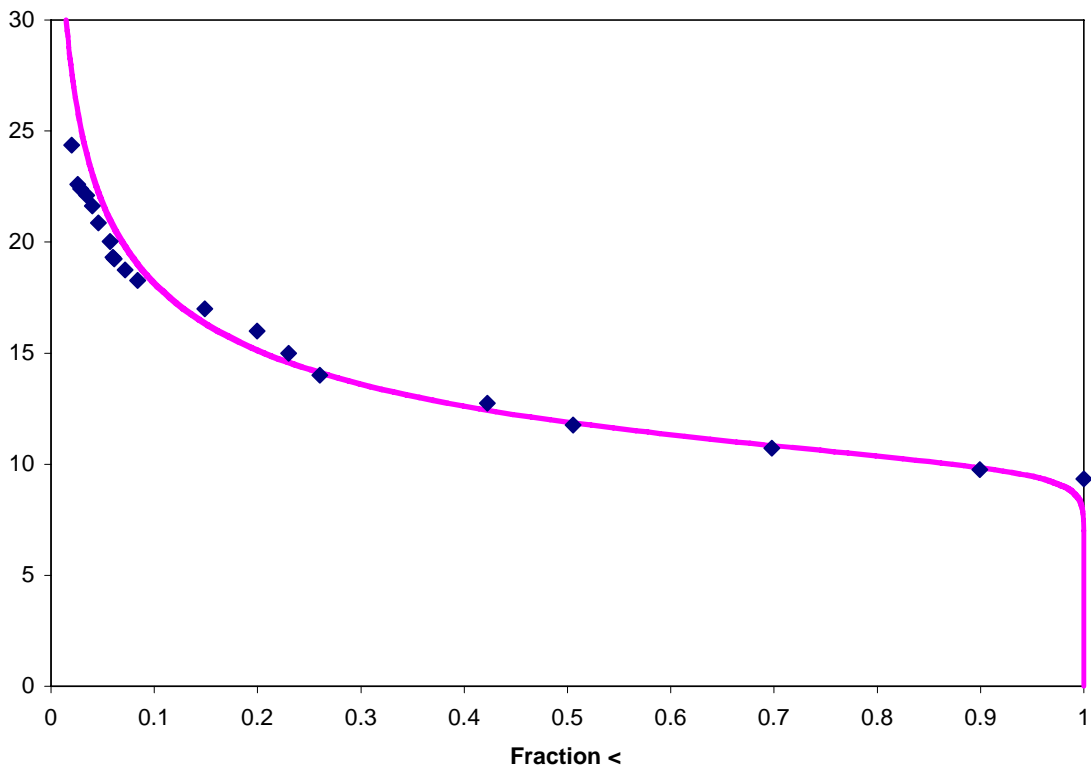## Sieve Analysis Data for Sample 88.0-88.5'
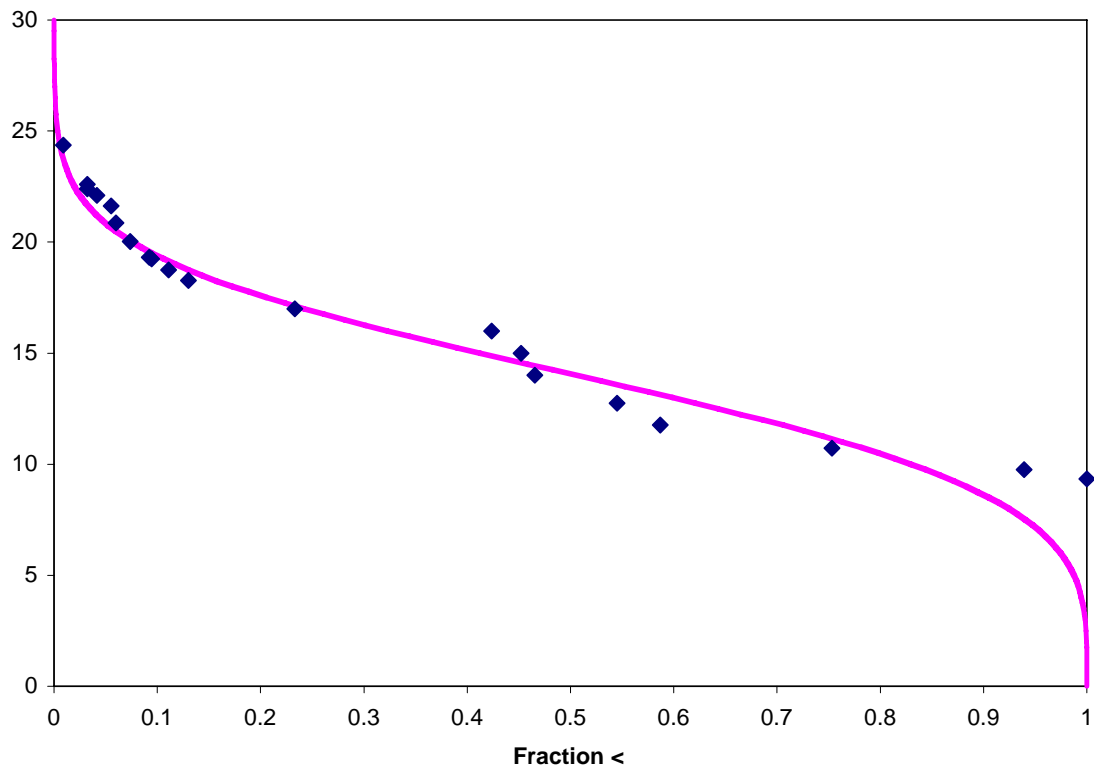
C4688, 88.0-88.5

Sieve Analysis Data for Sample 89.5-90.0'

U.S. Std. Sieve Opening in Inches
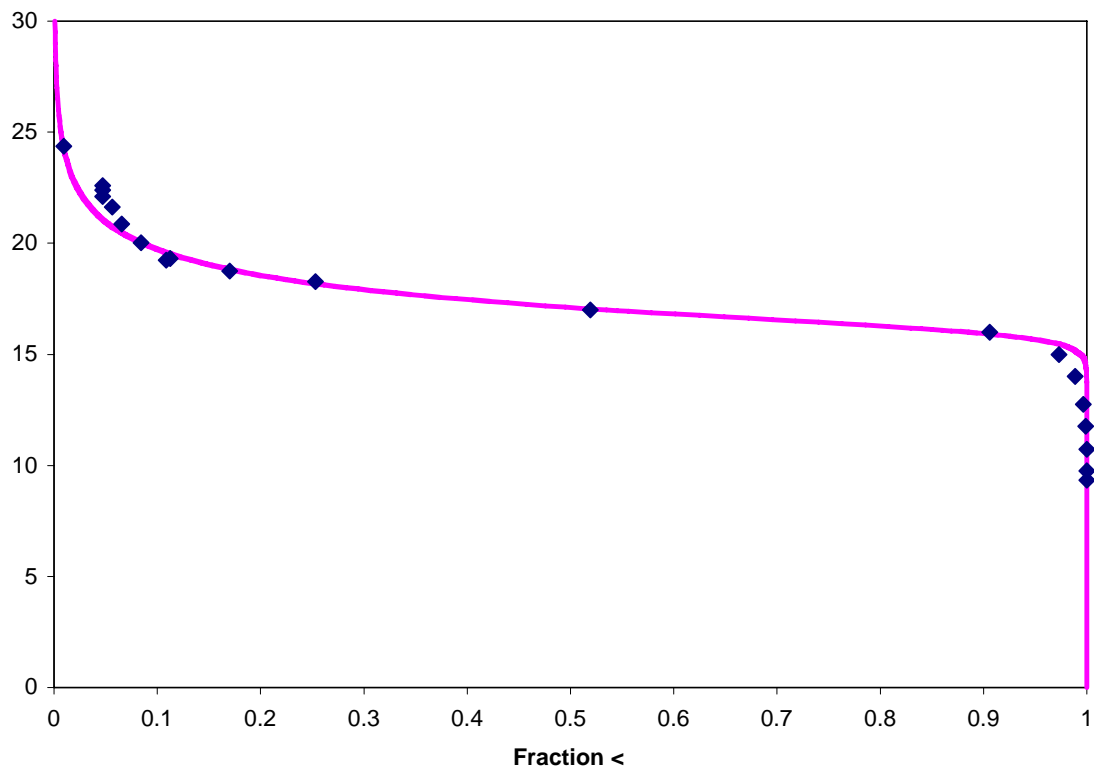
Hydrometer

Grain Size, mm

Fraction <

C4688, 89.5-90.0

L.14

Sieve Analysis Data for Sample 90.5-91.0'

C4688, 90.5-91.0

L.15
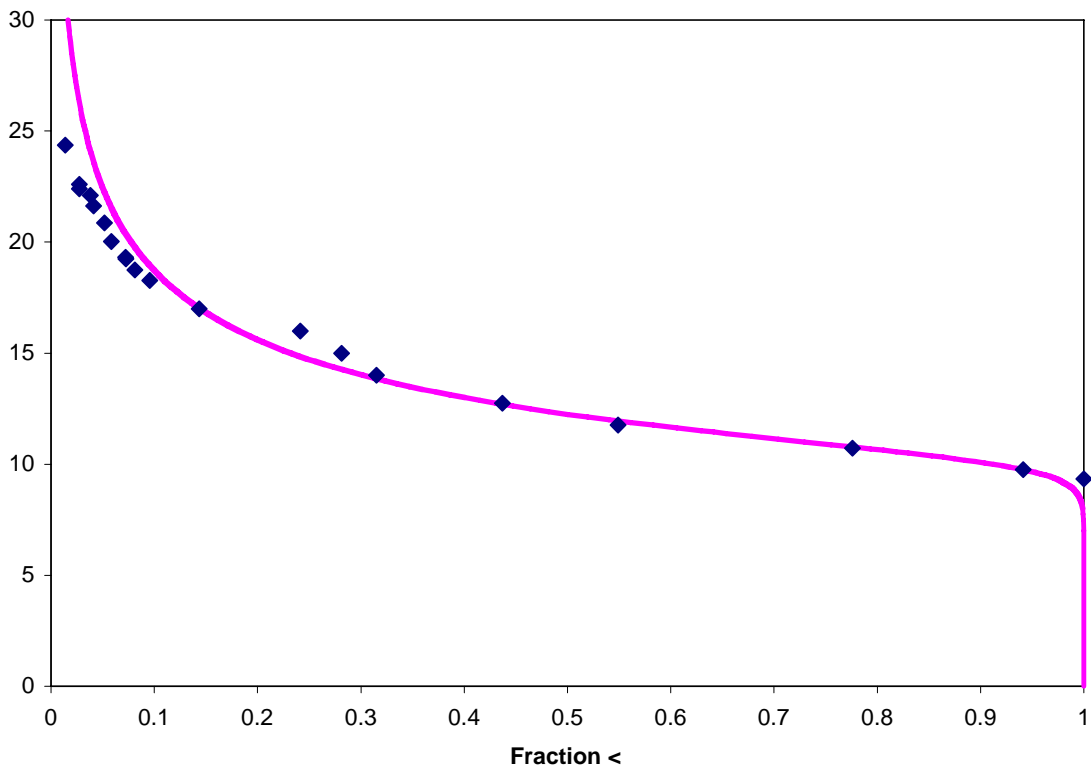
Sieve Analysis Data for Sample 92.0-92.5'

C4688, 92.0-92.5

Sieve Analysis Data for Sample 93.0-93.5'

U.S. Std. Sieve Opening in Inches

C4688, 93.0-93.5

Sieve Analysis Data for Sample 94.5-95.0'
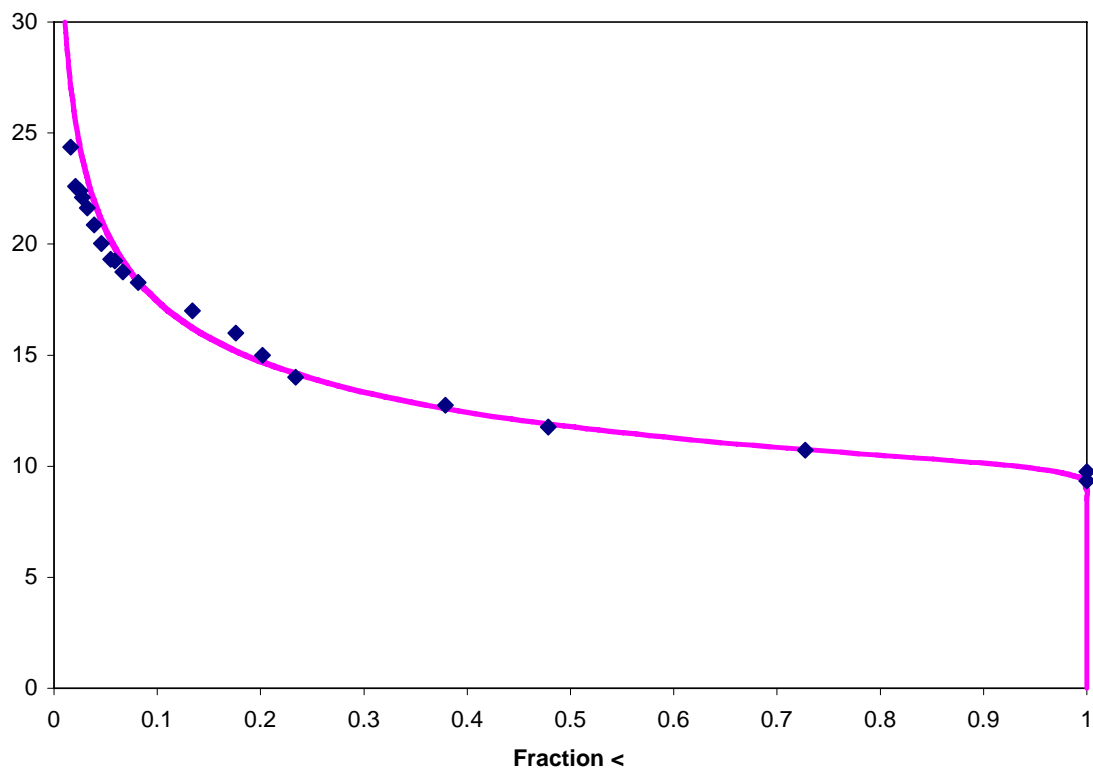
U.S. Std. Sieve Opening in Inches

C4688, 94.5-95.0

Sieve Analysis Data for Sample 95.5-96.0'
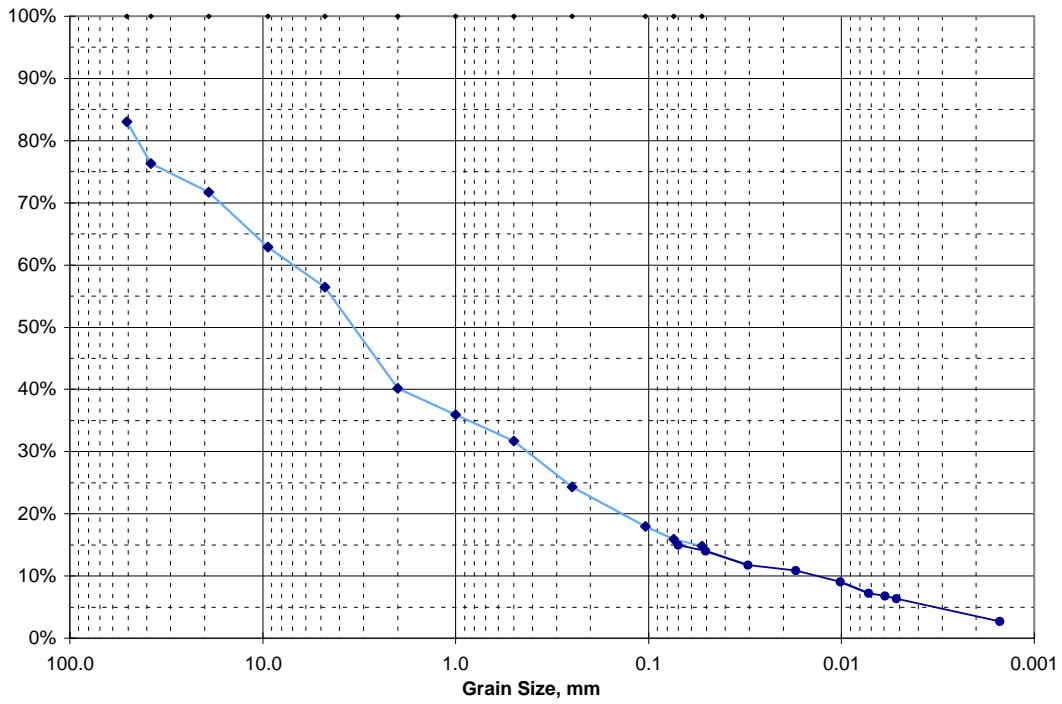
C4688, 95.5-96.0

Sieve Analysis Data for Sample 97.0-97.5'
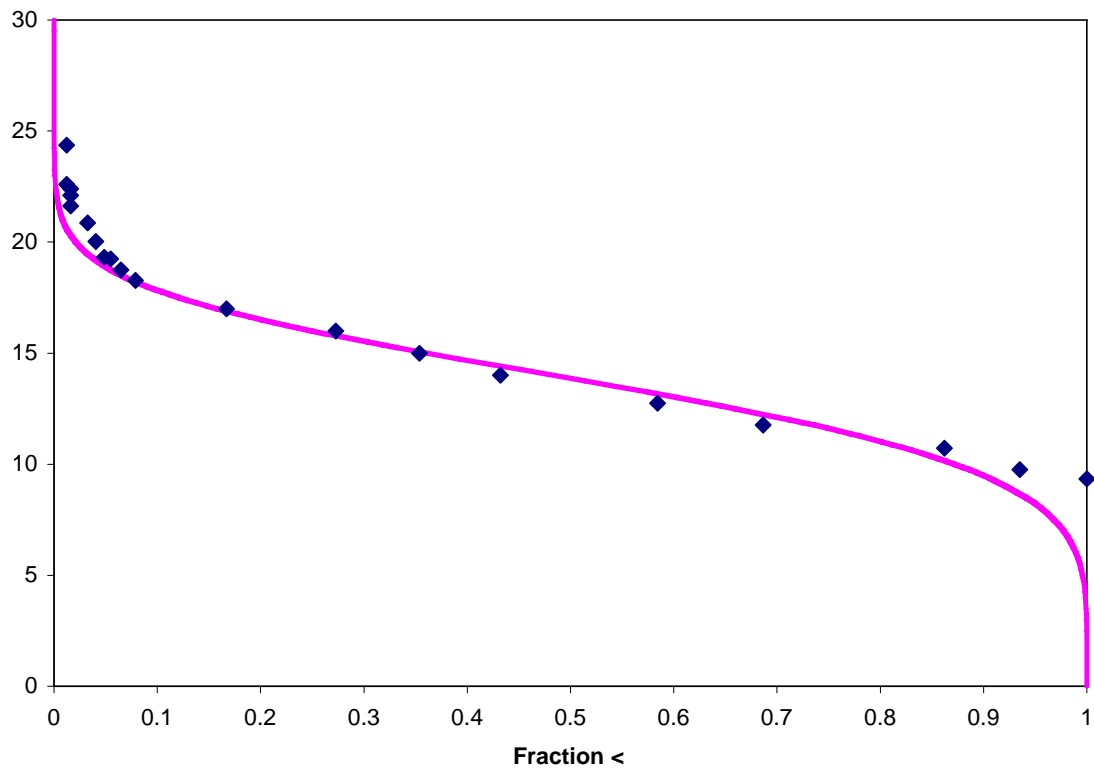
C4688, 97.0-97.5

L.20

Sieve Analysis Data for Sample 98.0-98.5'
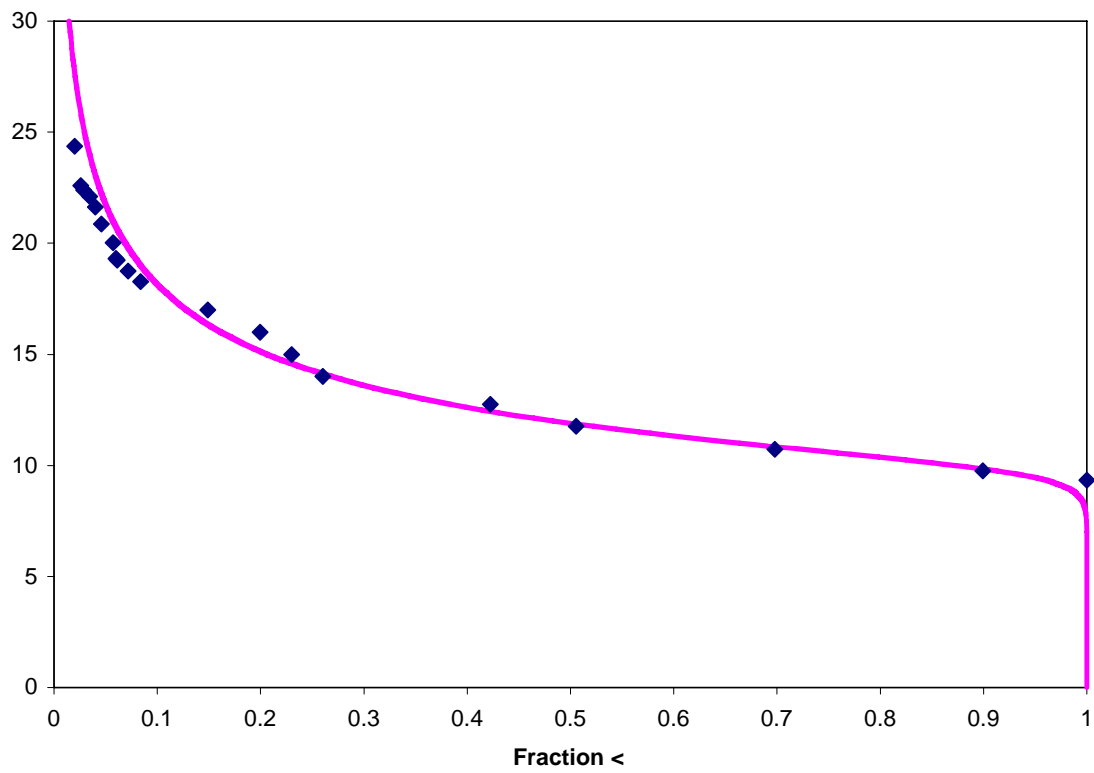
C4688, 98.0-98.5

Sieve Analysis Data for Sample 100.0-100.5'

U.S. Std. Sieve Opening in Inches

C4688, 100.0-100.5
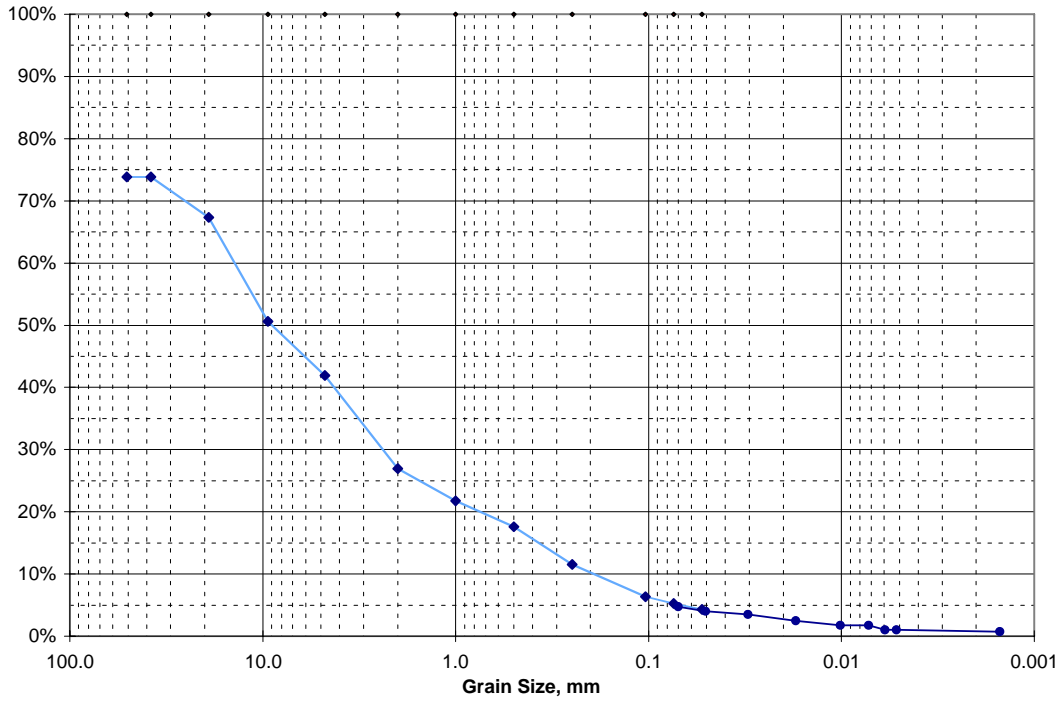
Sieve Analysis Data for Sample 101.5-102.0'
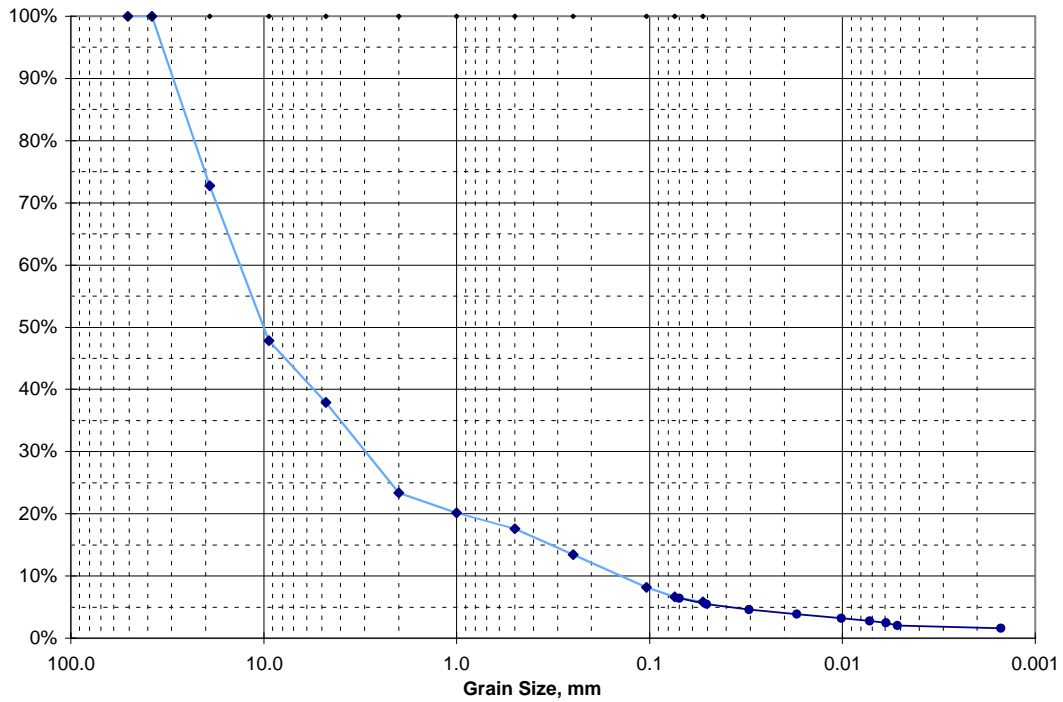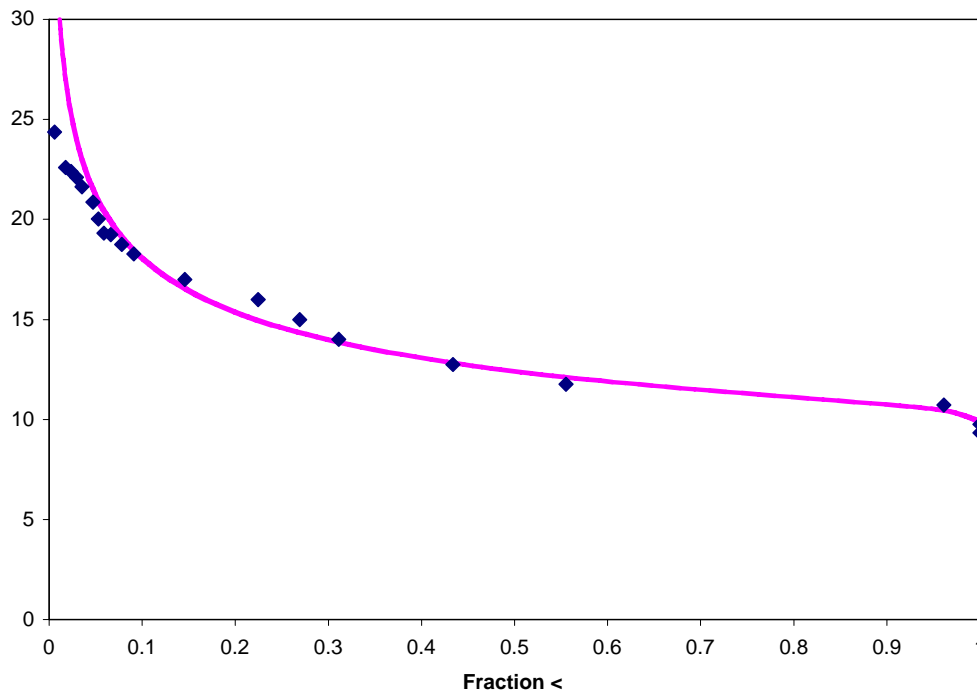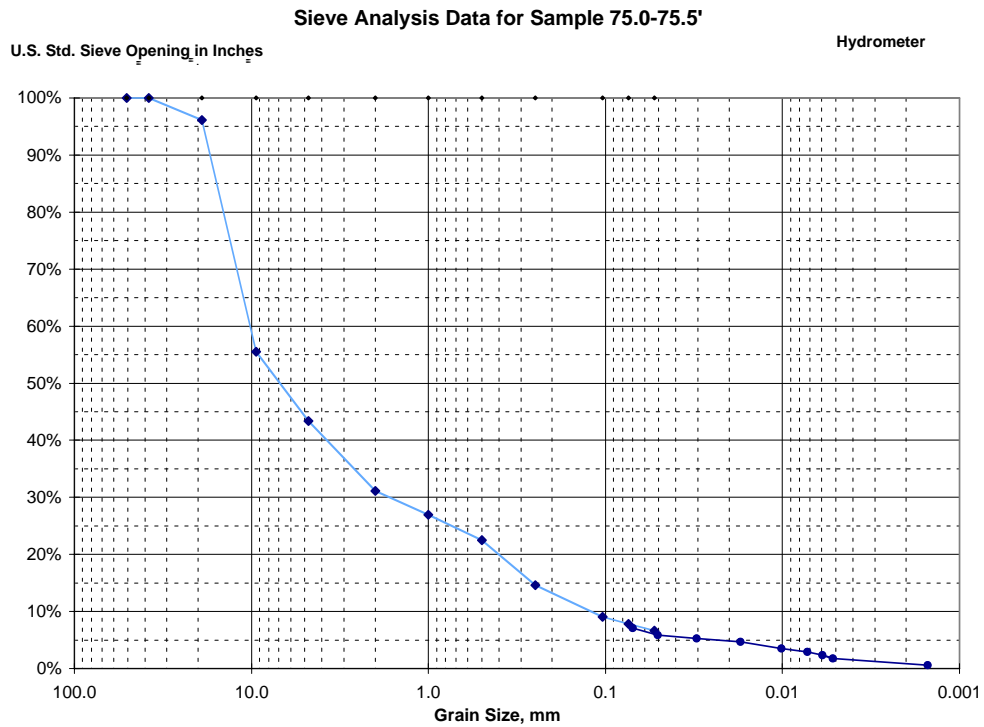
C4688, 101.5-102.0

Appendix M

Sieve Analysis and Log Grain Size Fit for Borehole C4689 D4-93

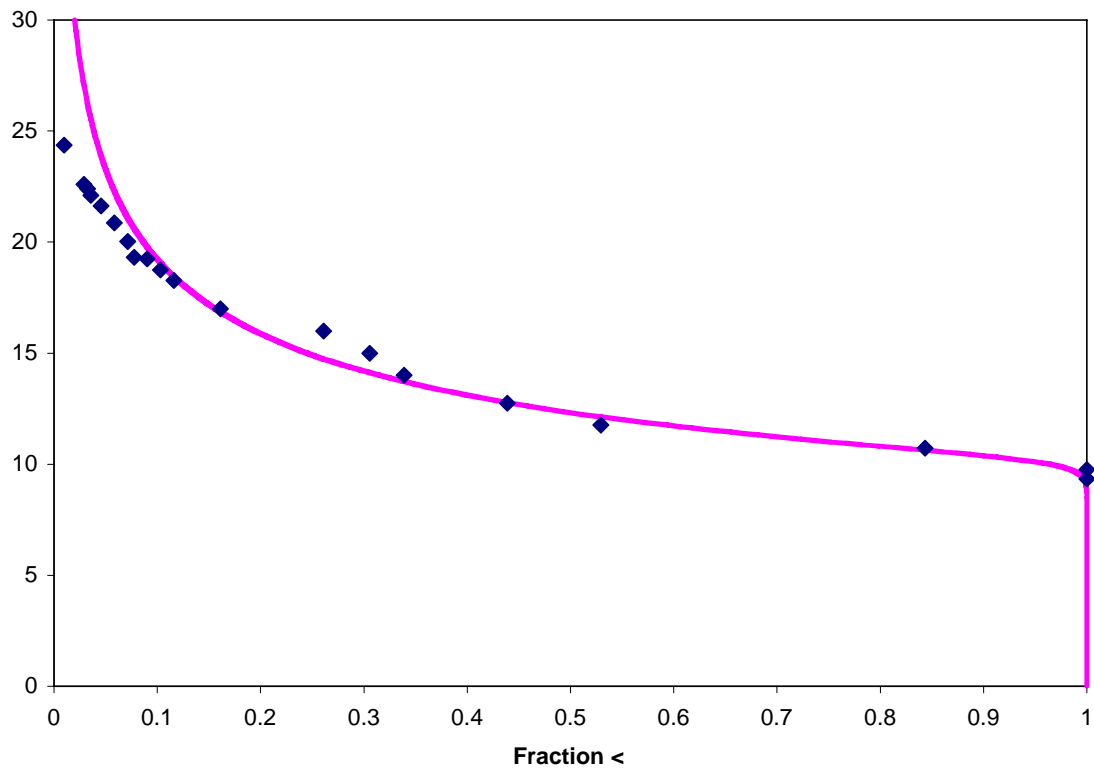# Appendix M - Sieve Analysis and Log Grain Size Fit
for Borehole C4689 D4-93
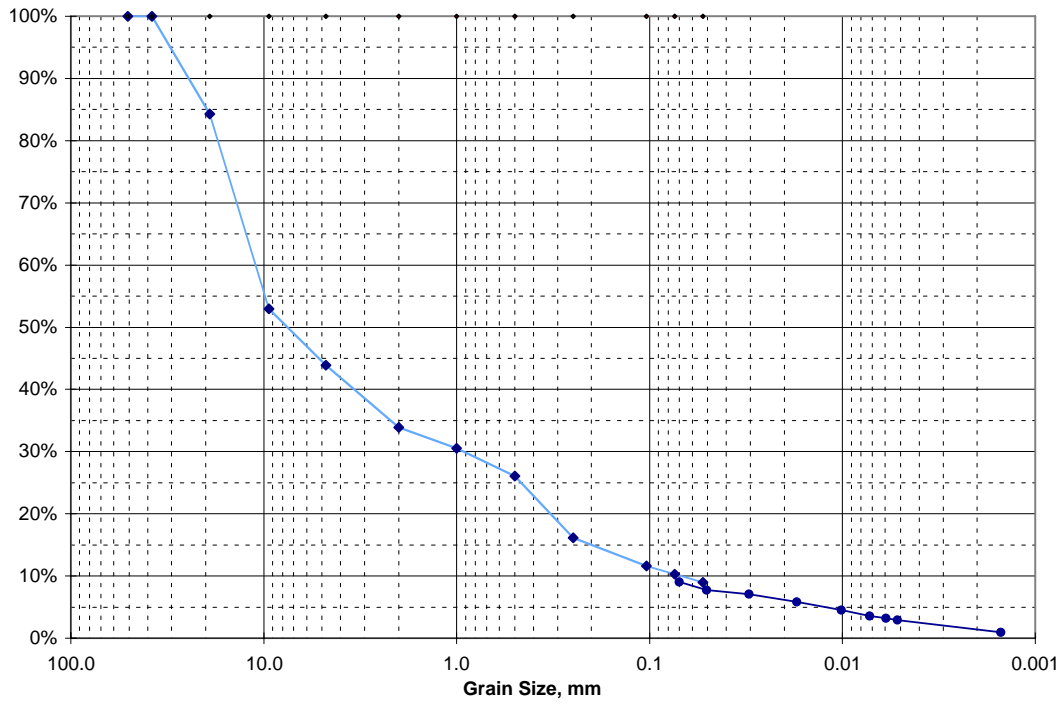
Sieve Analysis Data for Sample 75.0-75.5'

C4689, 75.0-75.5

Sieve Analysis Data for Sample 76.0-76.5'

U.S. Std. Sieve Opening in Inches

Hydrometer

Grain Size, mm

Fraction <

C4689, 76.0-76.5

Sieve Analysis Data for Sample 77.5-78.0'

Hydrometer

U.S. Std. Sieve Opening in Inches

Grain Size, mm

Fraction <

C4689, 77.5-78.0
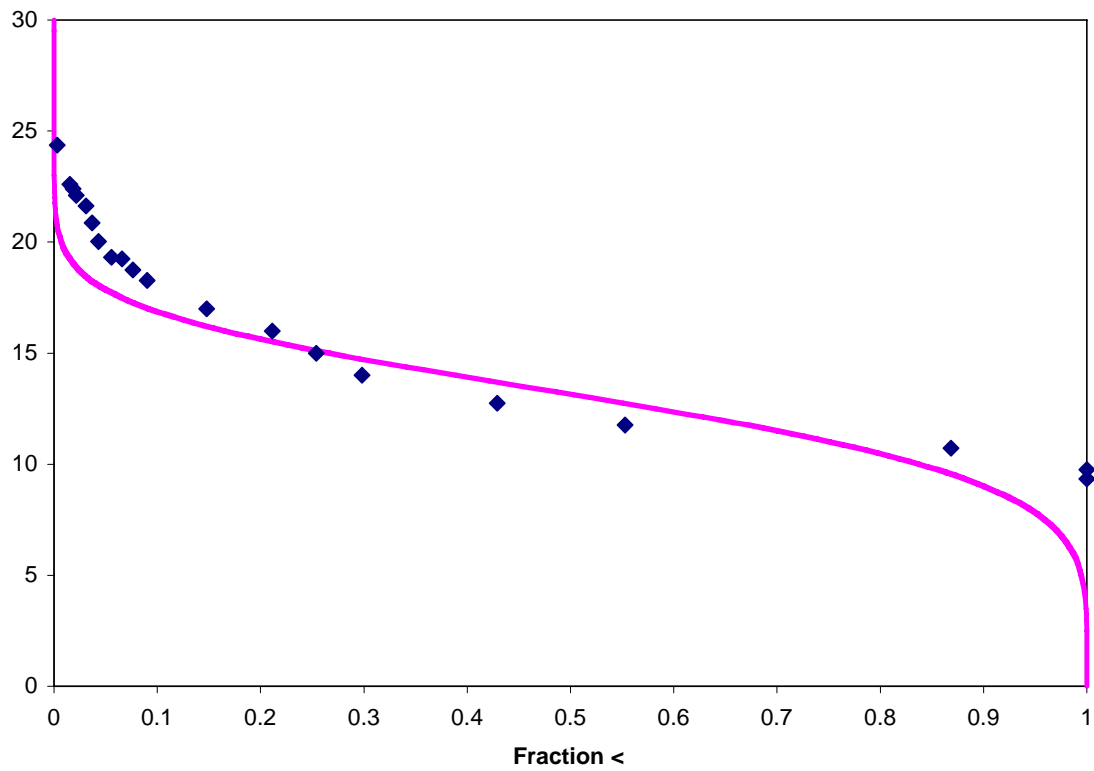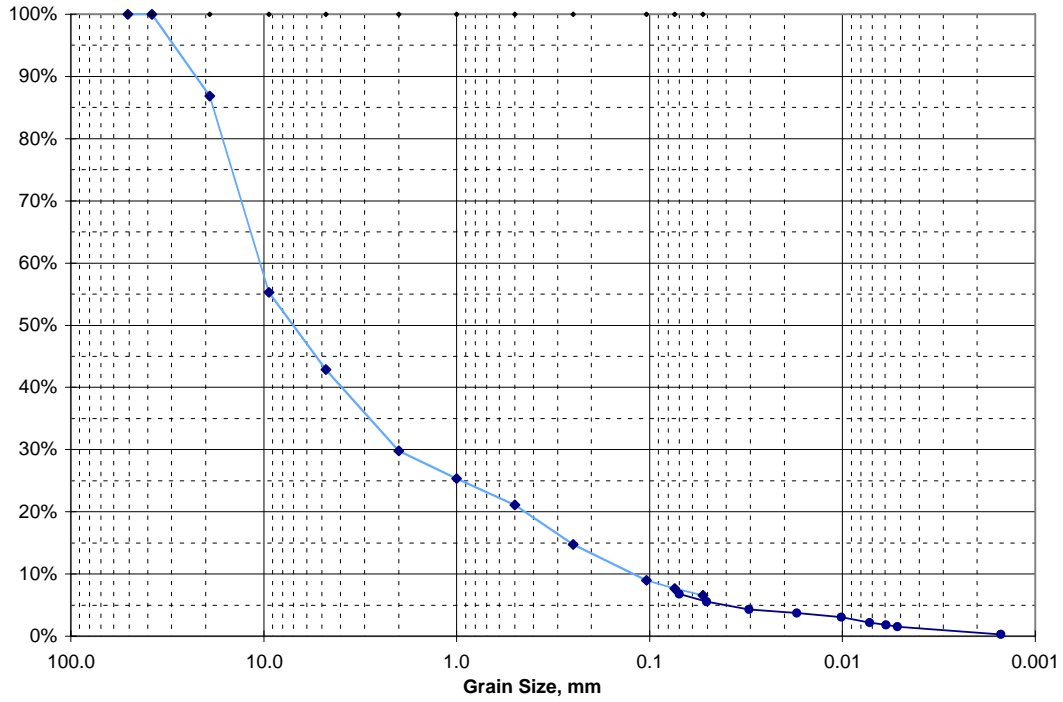
Sieve Analysis Data for Sample 78.5-79.0'

C4689, 78.5-79.0

M.4

Sieve Analysis Data for Sample 80.0-80.5'

U.S. Std. Sieve Opening in Inches
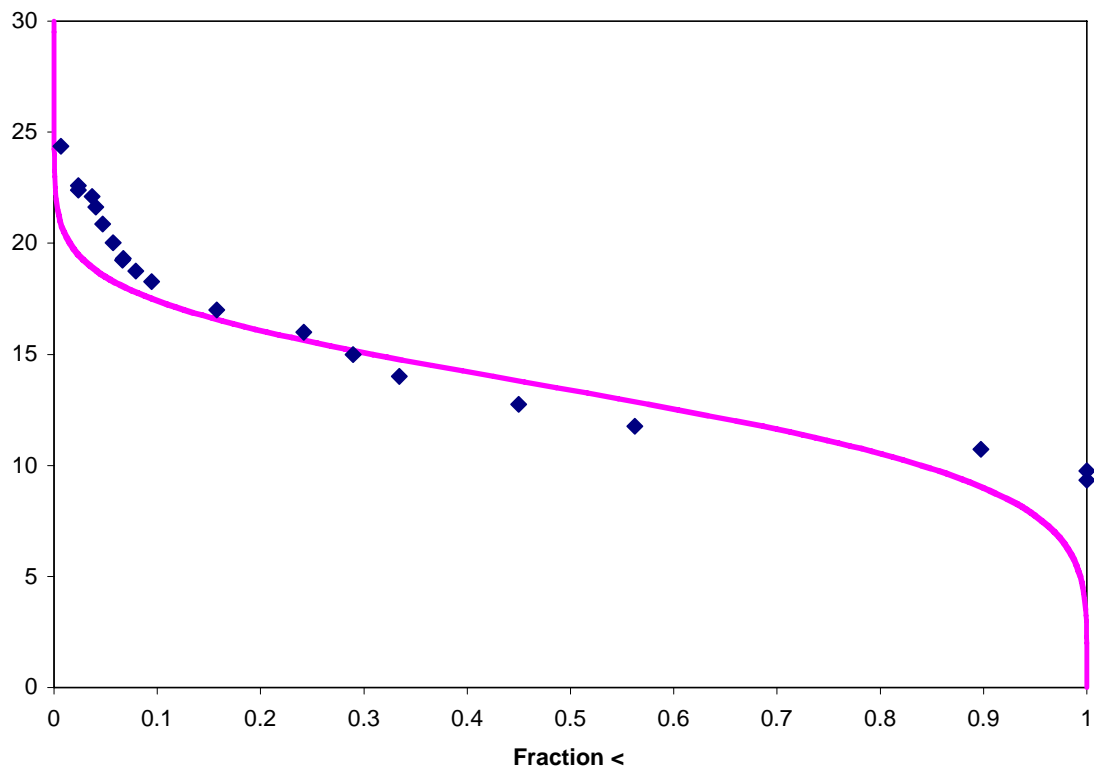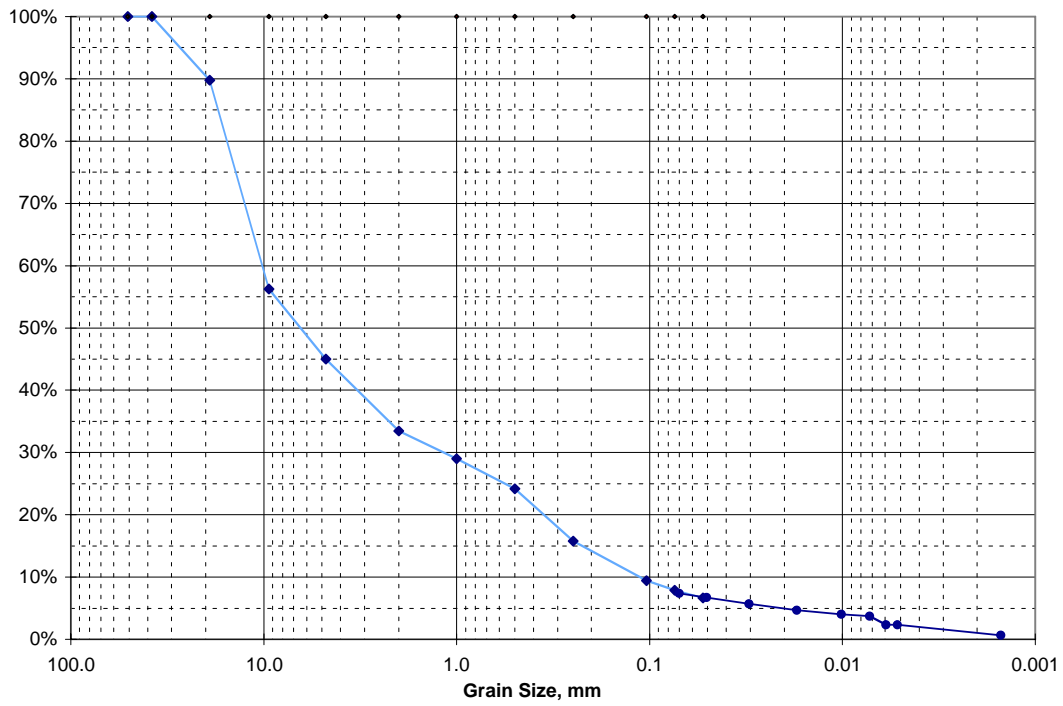
Hydrometer

Grain Size, mm

Fraction <

C4689, 80.0-80.5

M.5

Sieve Analysis Data for Sample 81.0-81.5'

C4689, 81.0-81.5

M.6
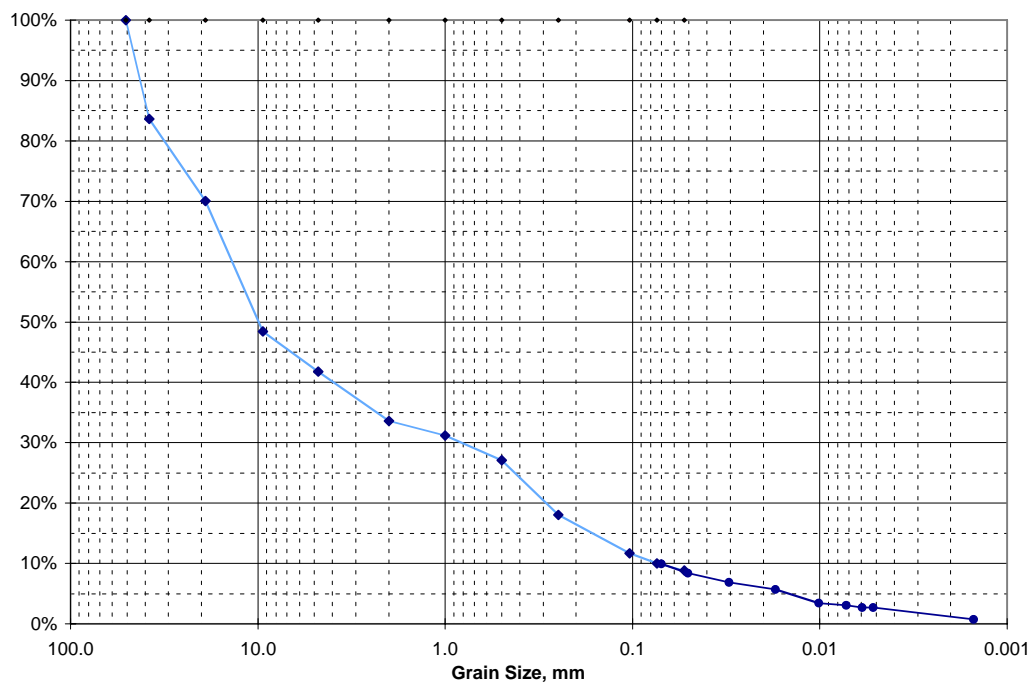
Sieve Analysis Data for Sample 82.5-83.0'

U.S. Std. Sieve Opening in Inches
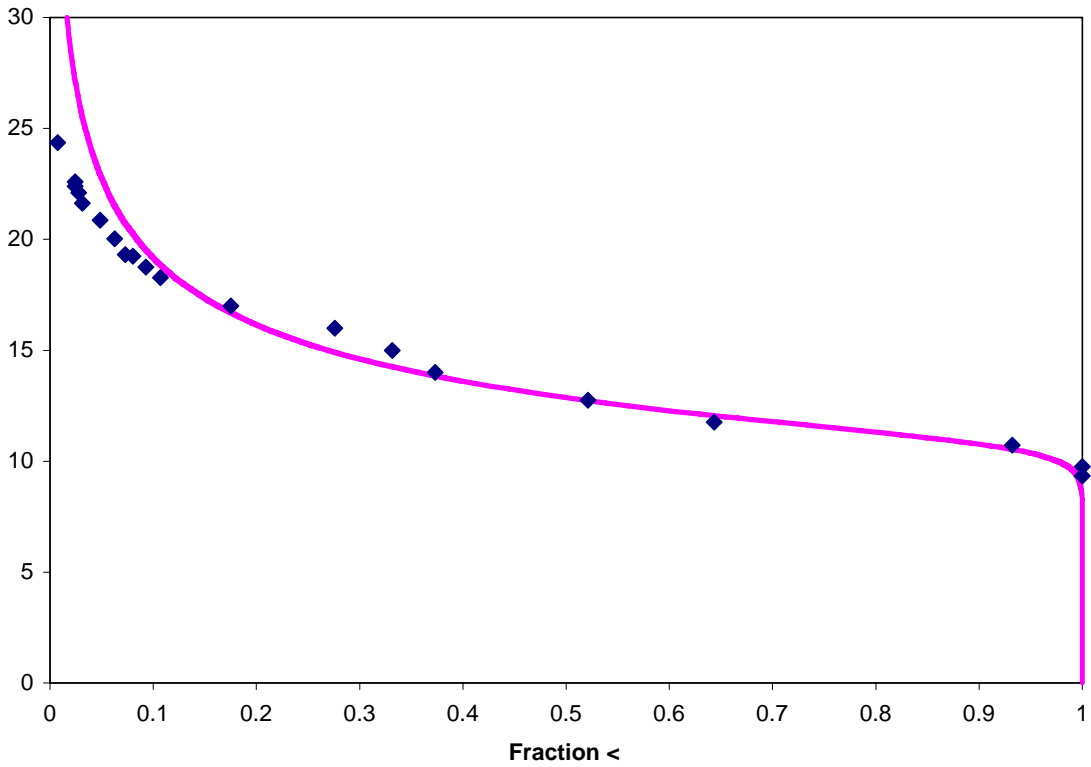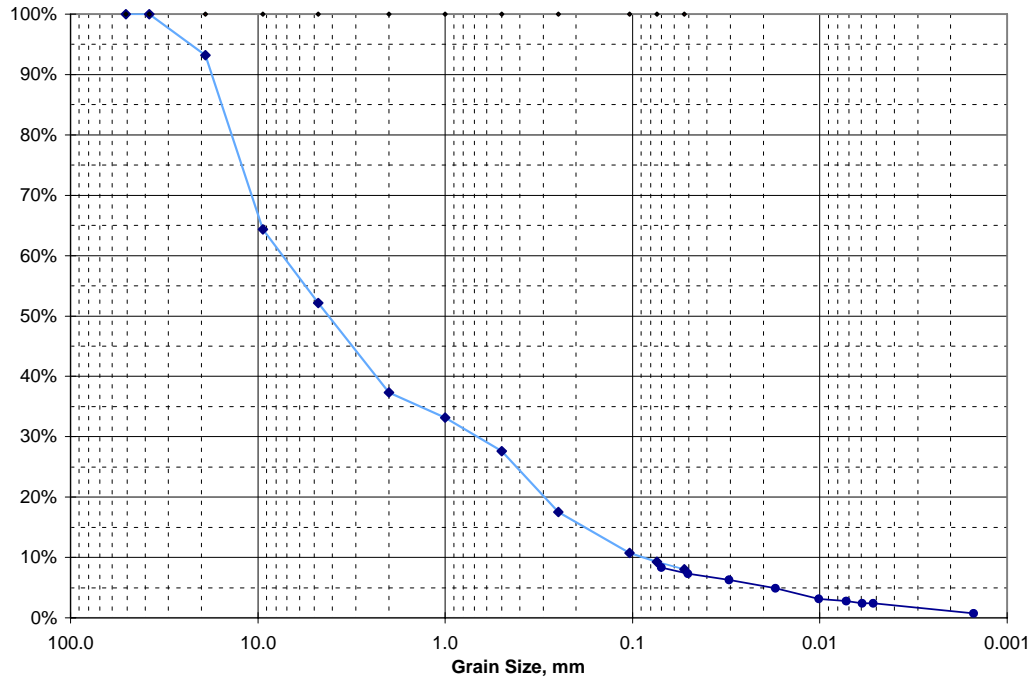
Hydrometer

C4689, 82.5-83.0

M.7

Sieve Analysis Data for Sample 83.5-84.0'

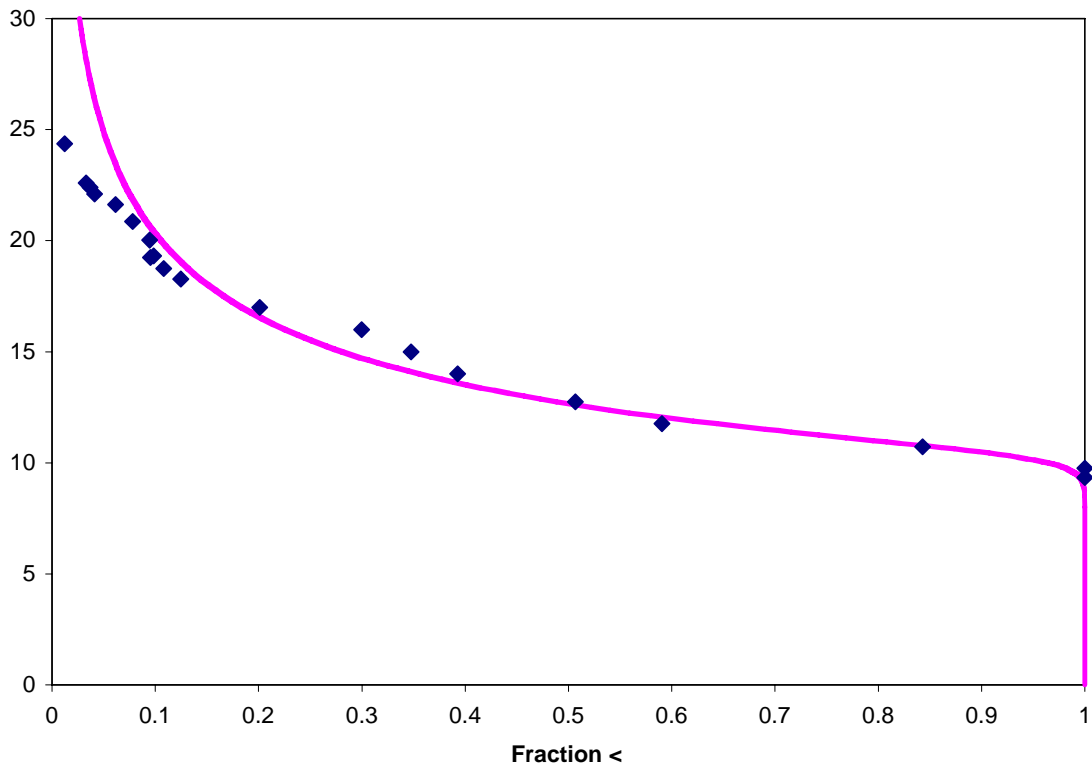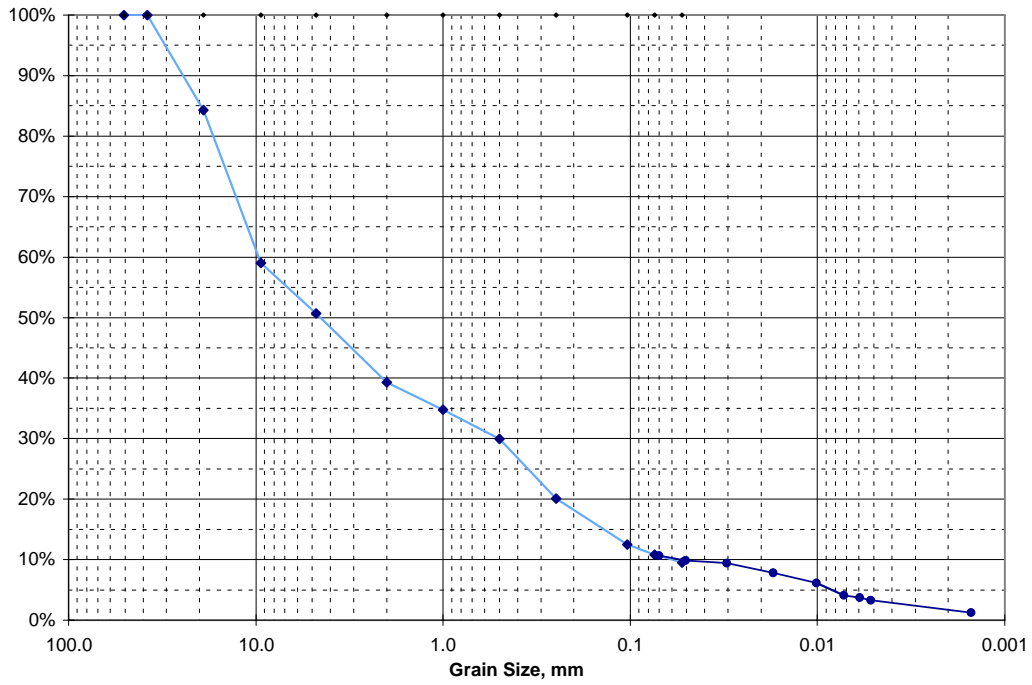U.S. Std. Sieve Opening in Inches

Hydrometer

Grain Size, mm

Fraction <

C4689, 83.5-84.0

M.8
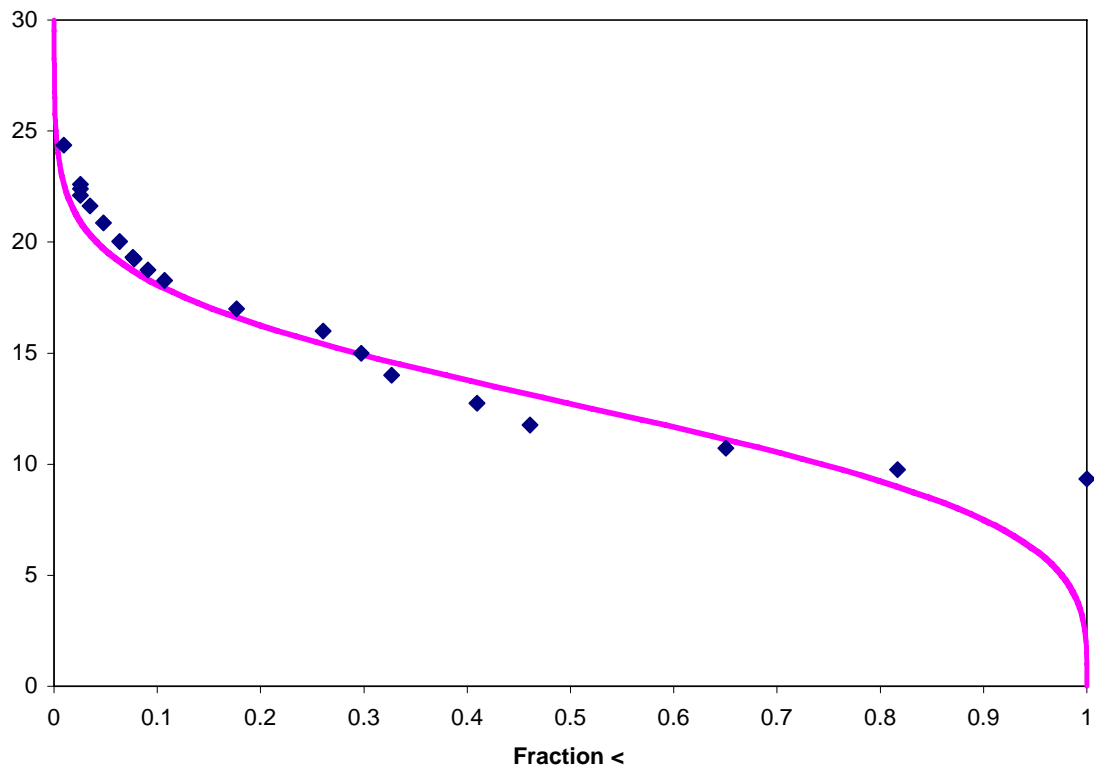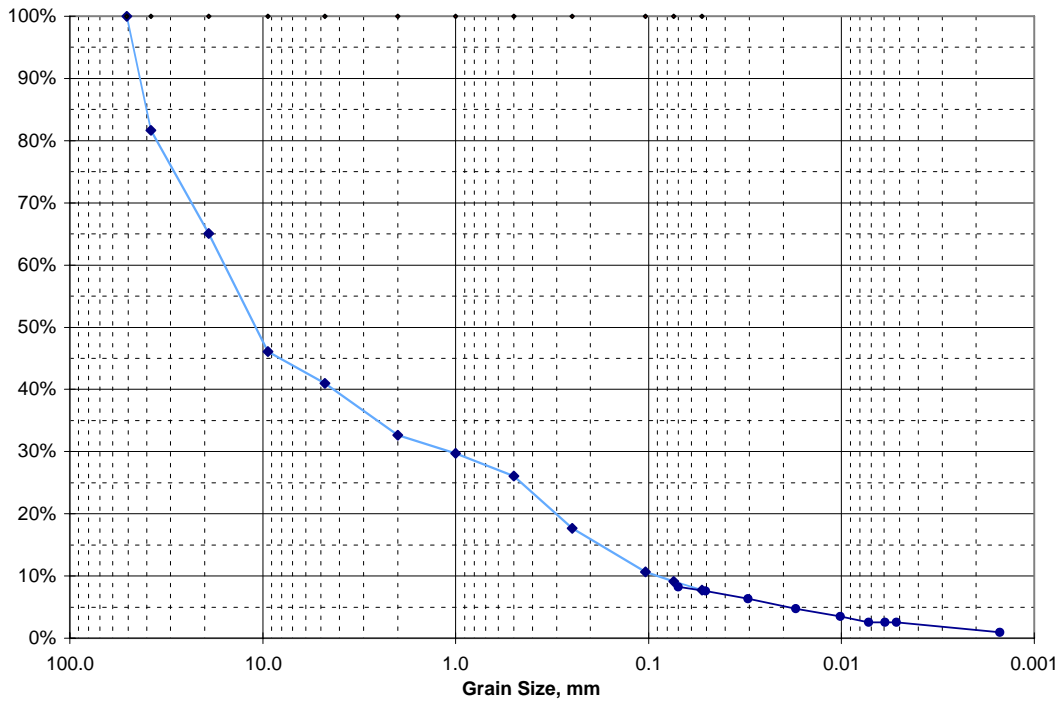
Sieve Analysis Data for Sample 85.0-85.5'
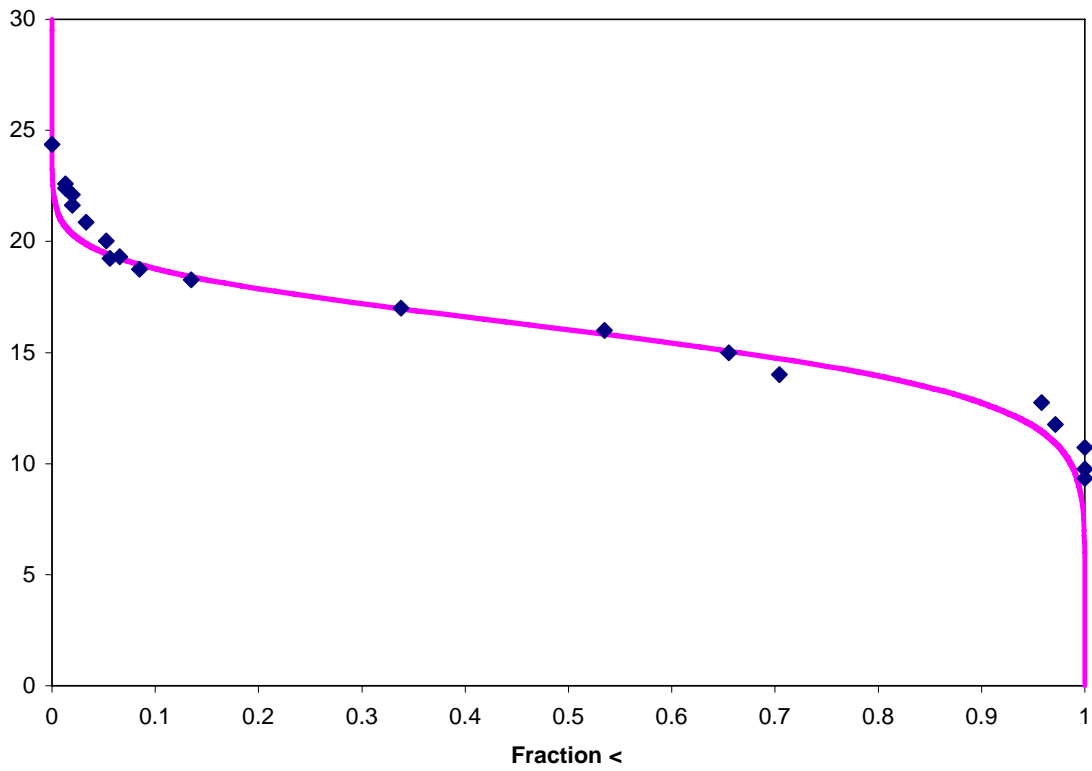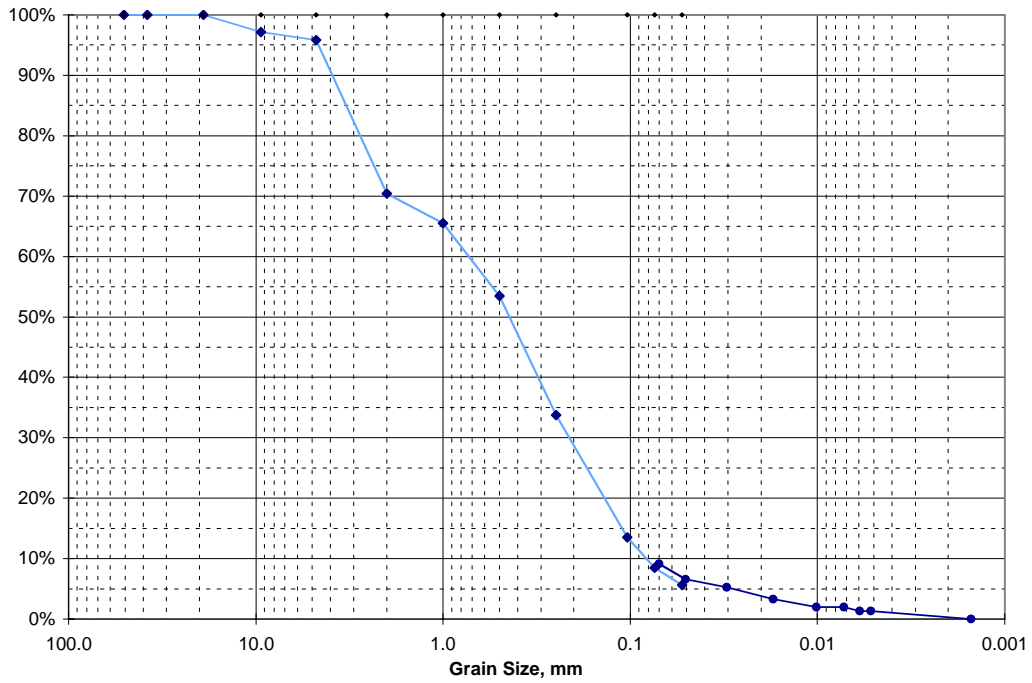
C4689, 85.0-85.5

M.9

Sieve Analysis Data for Sample 86.0-86.5'

C4689, 86.0-86.5

Sieve Analysis Data for Sample 87.5-88.0'

C4689, 87.5-88.0

M.11
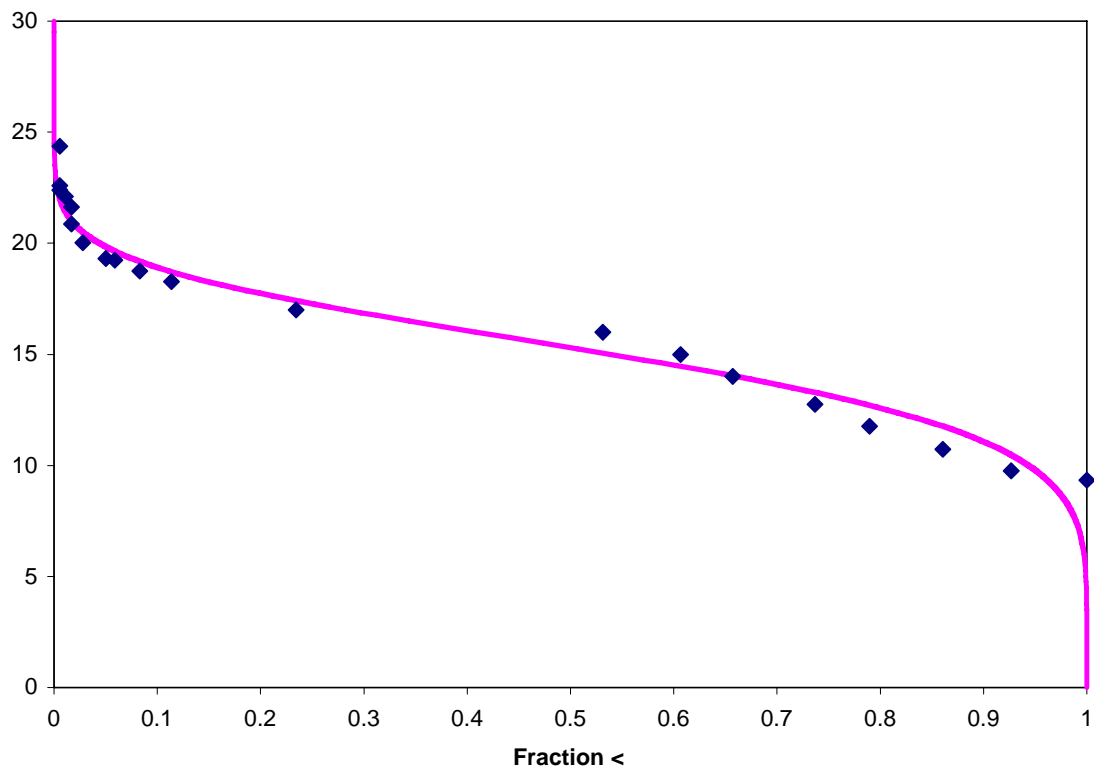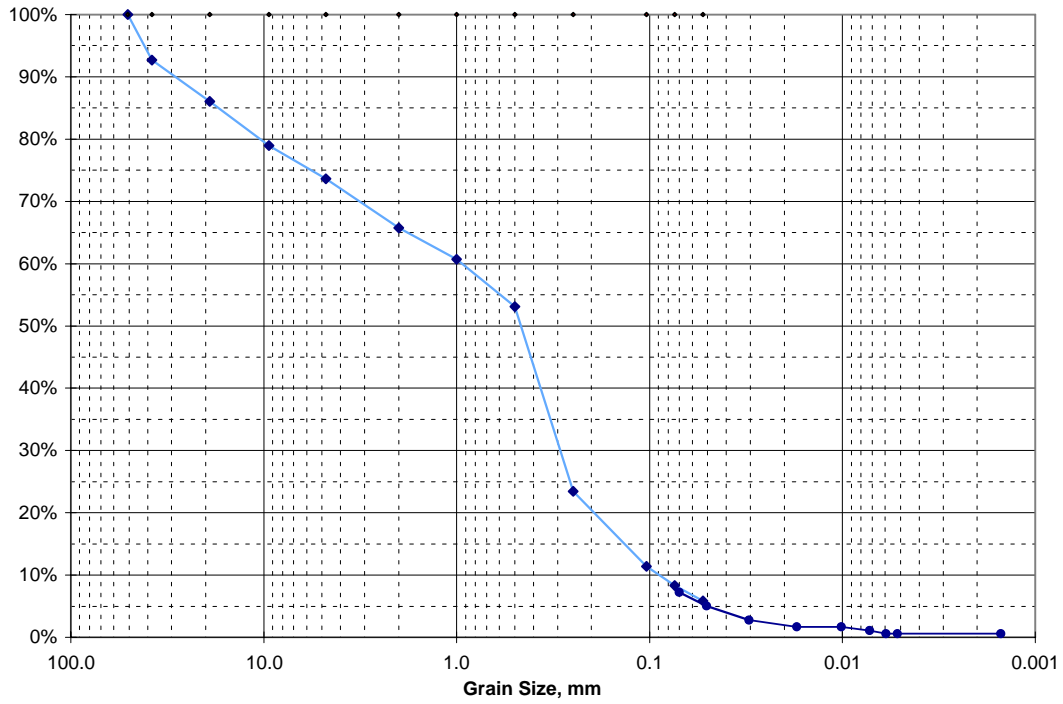
Sieve Analysis Data for Sample 88.5-89.0'

C4689, 88.5-89.0

M.12

Sieve Analysis Data for Sample 90.5-91.0'

C4689, 90.5-91.0

M.13
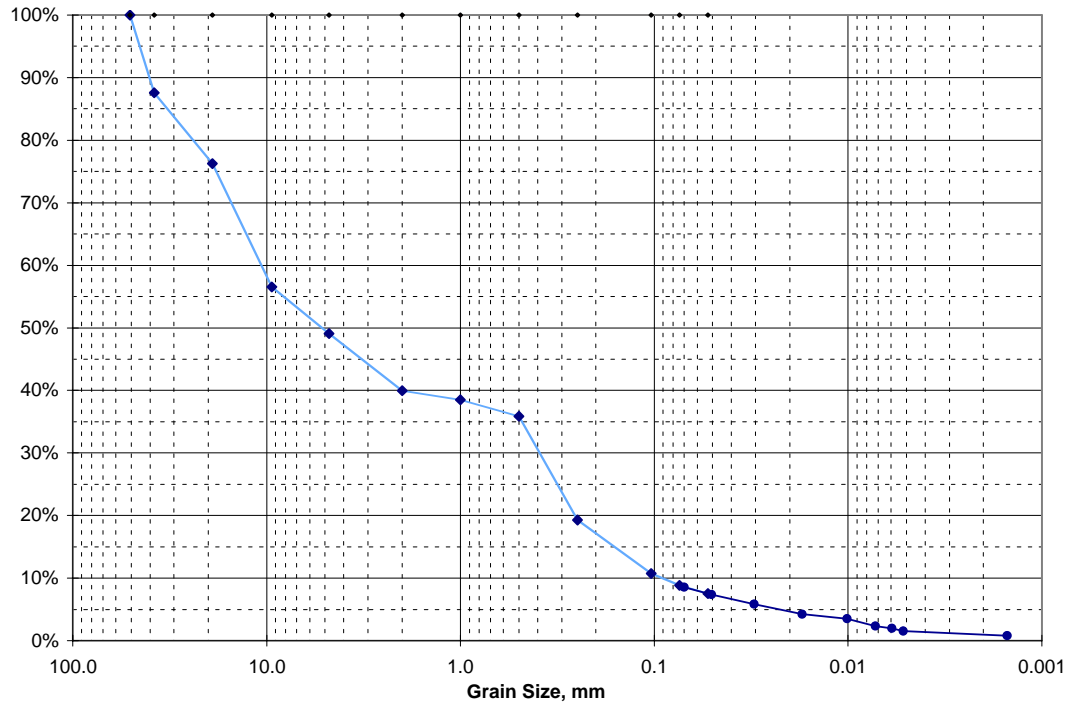
Sieve Analysis Data for Sample 91.5-92.0'

C4689, 91.5-92.0

M.14

Sieve Analysis Data for Sample 93.5-94.0'

C4689, 93.5-94.0

M.15
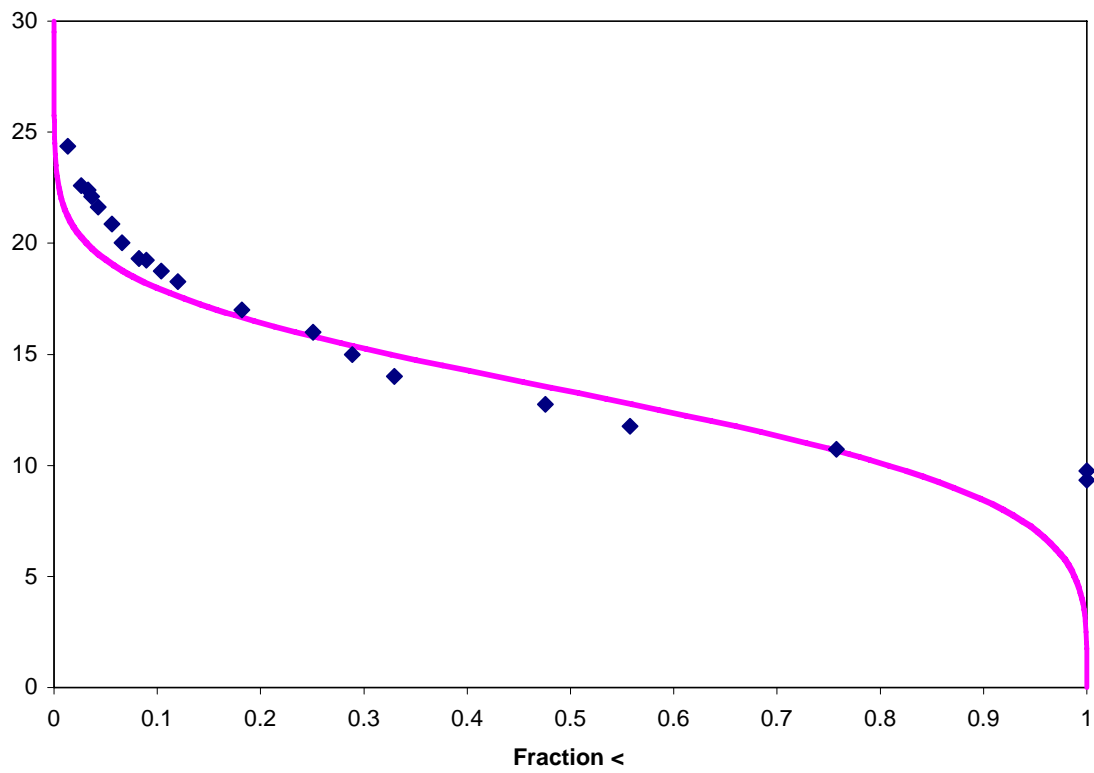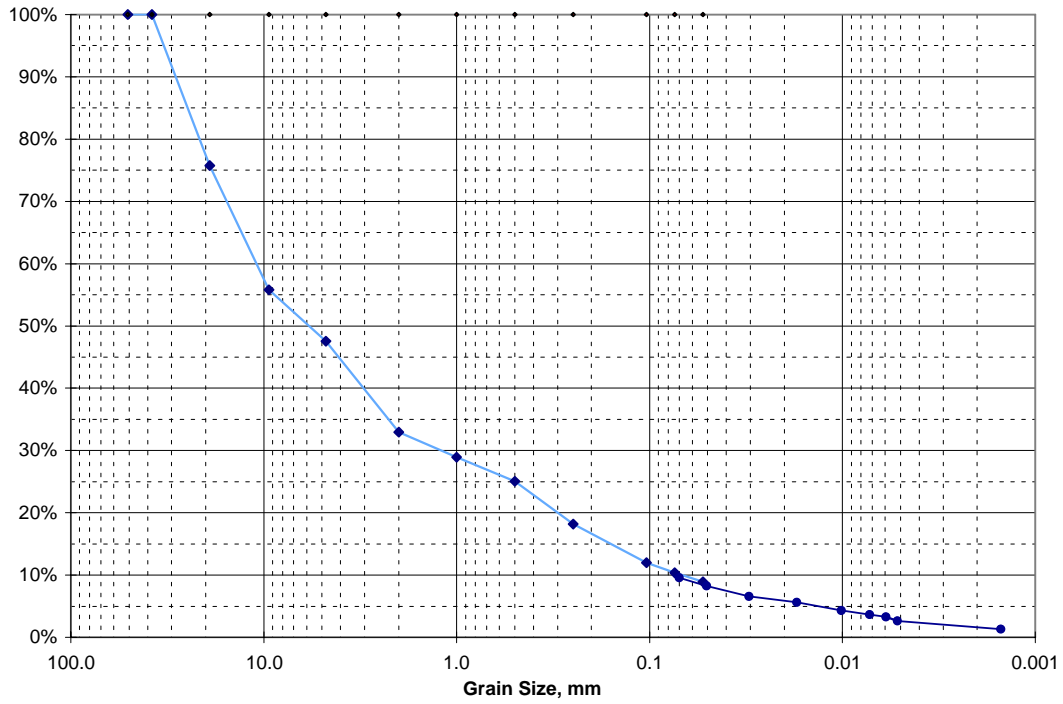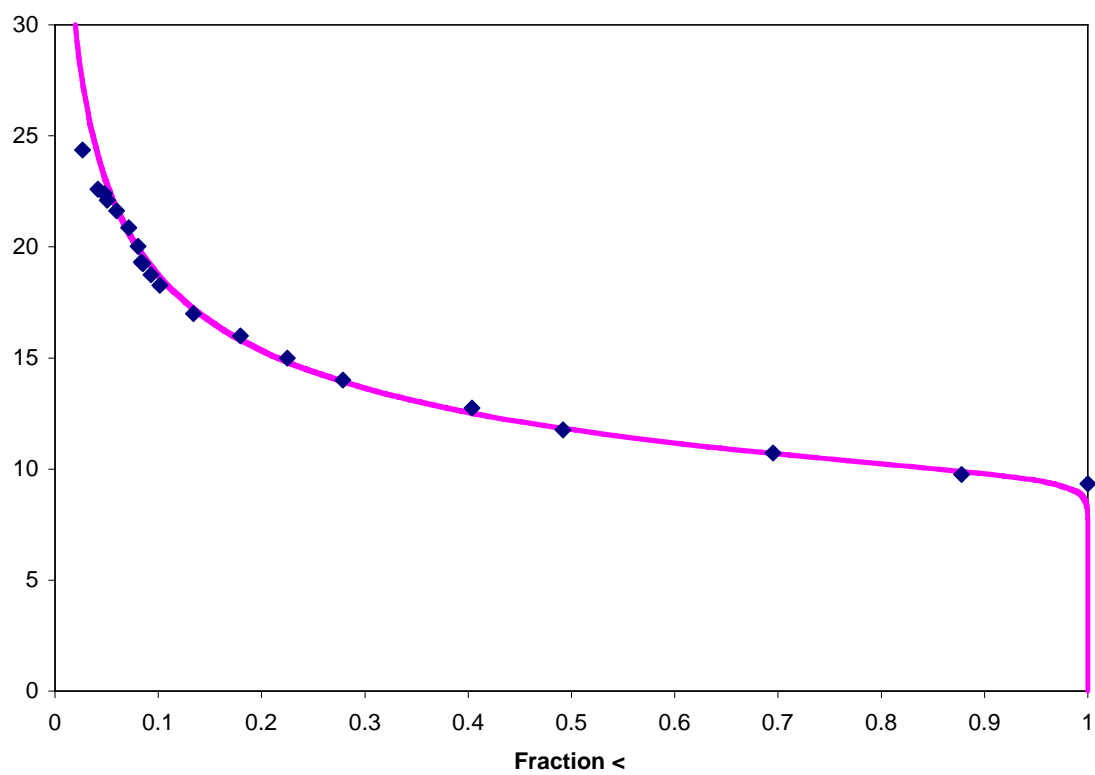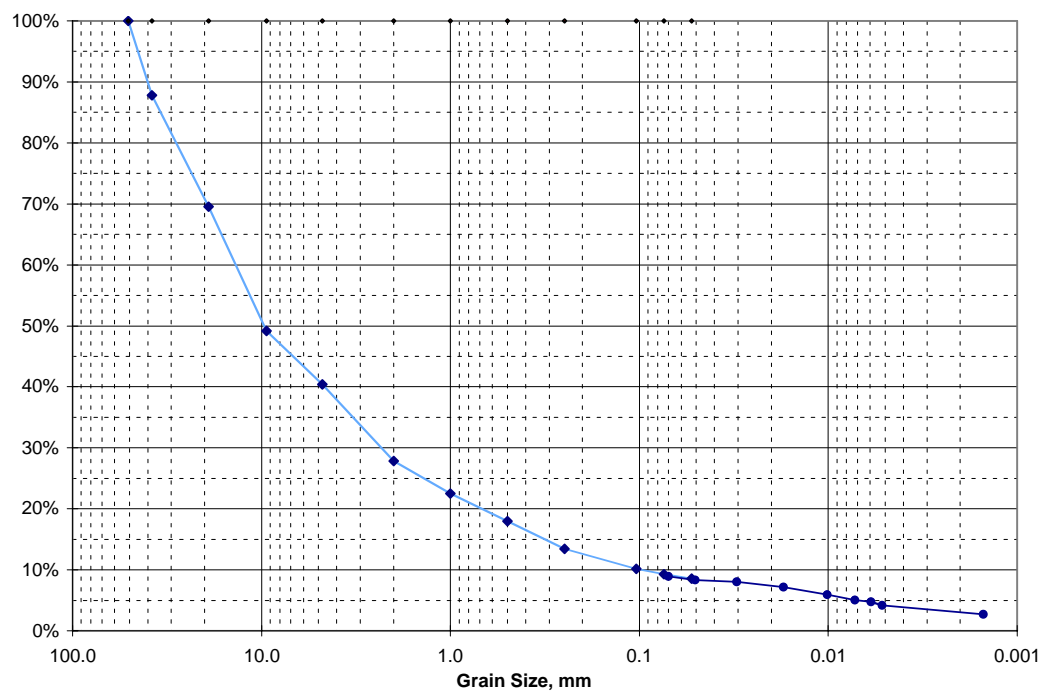
Sieve Analysis Data for Sample 95.0-95.5'
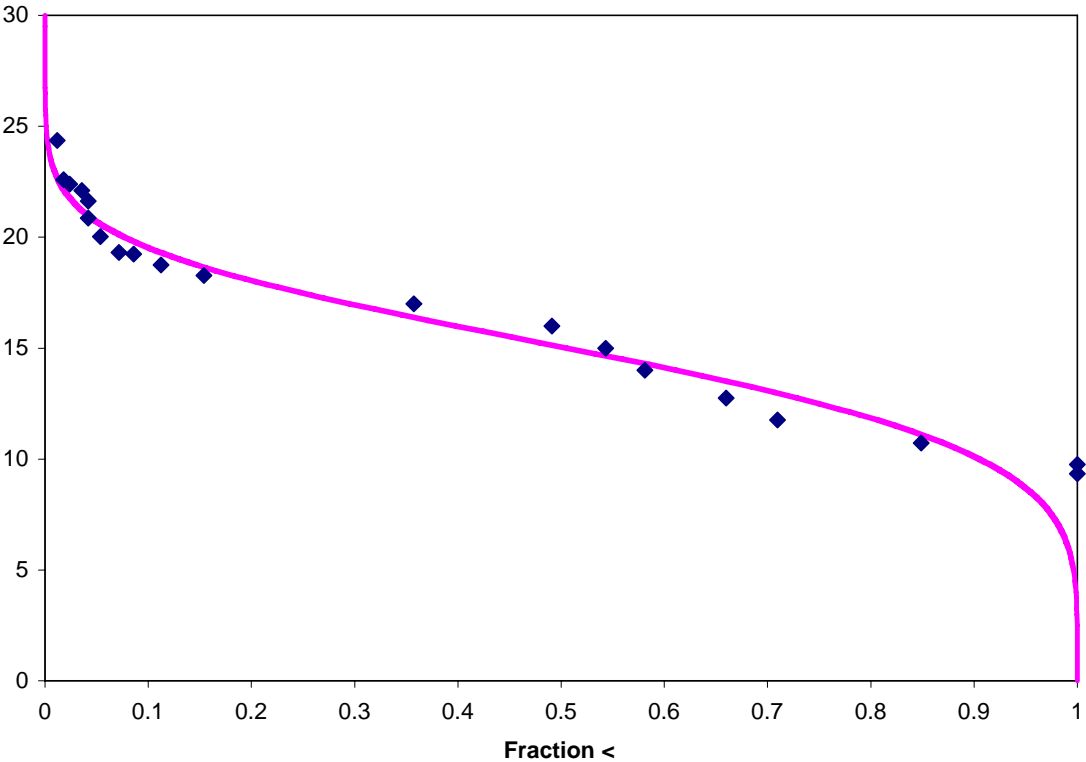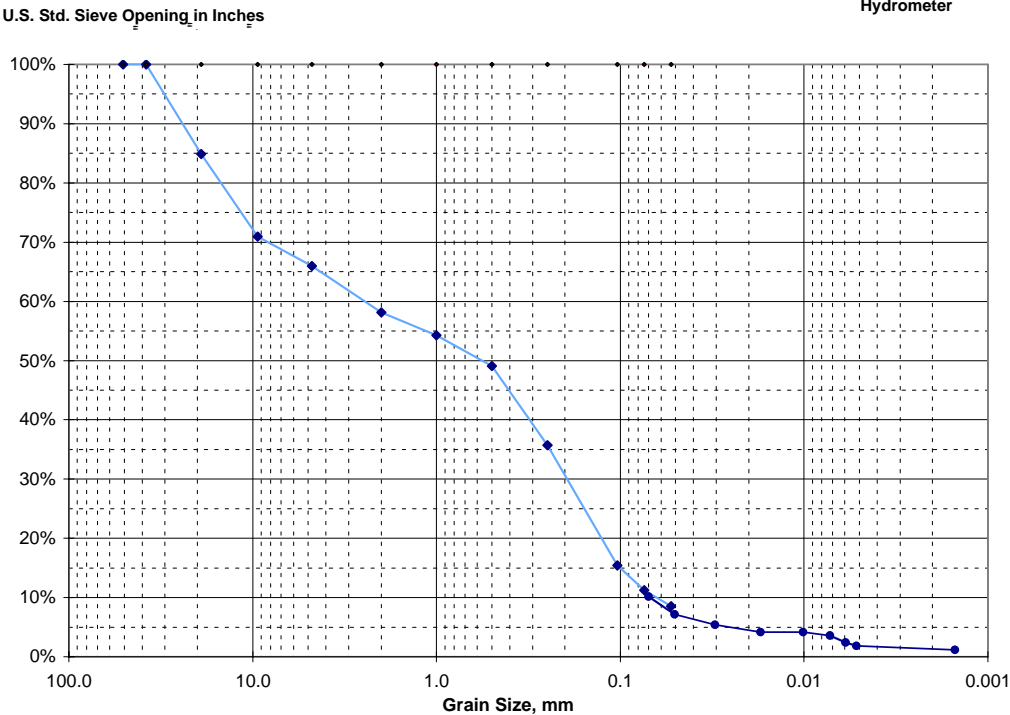
C4689, 95.0-95.5

Sieve Analysis Data for Sample 96.0-96.5'
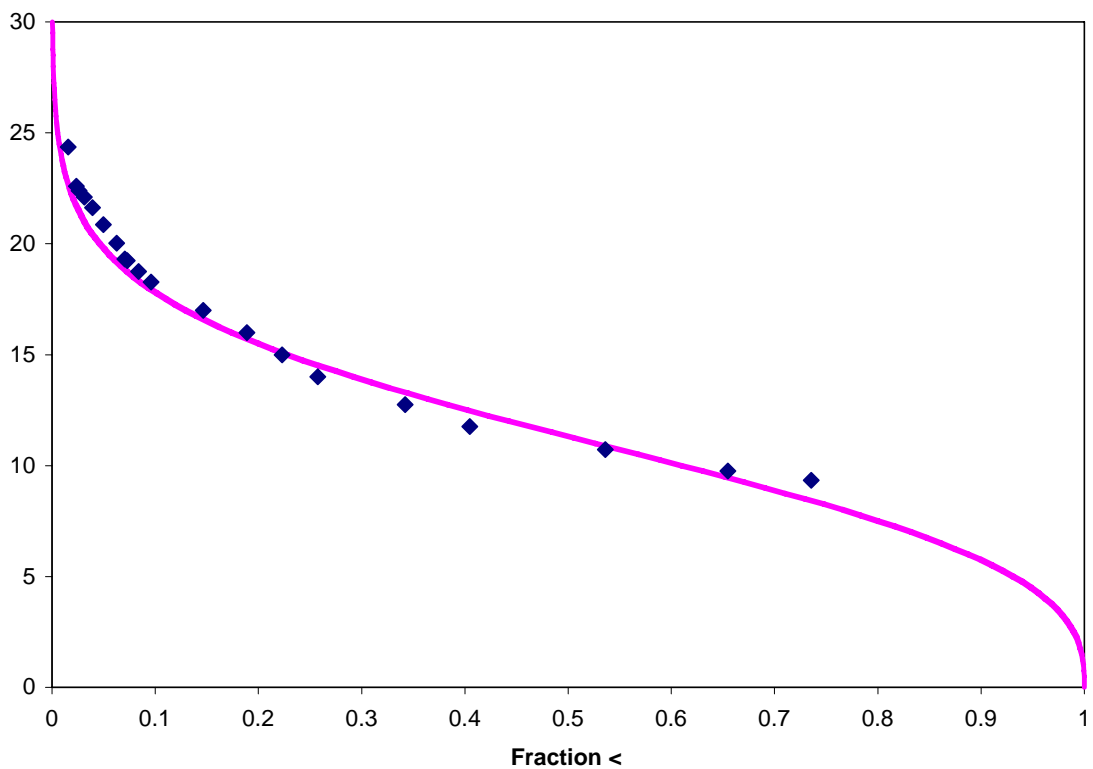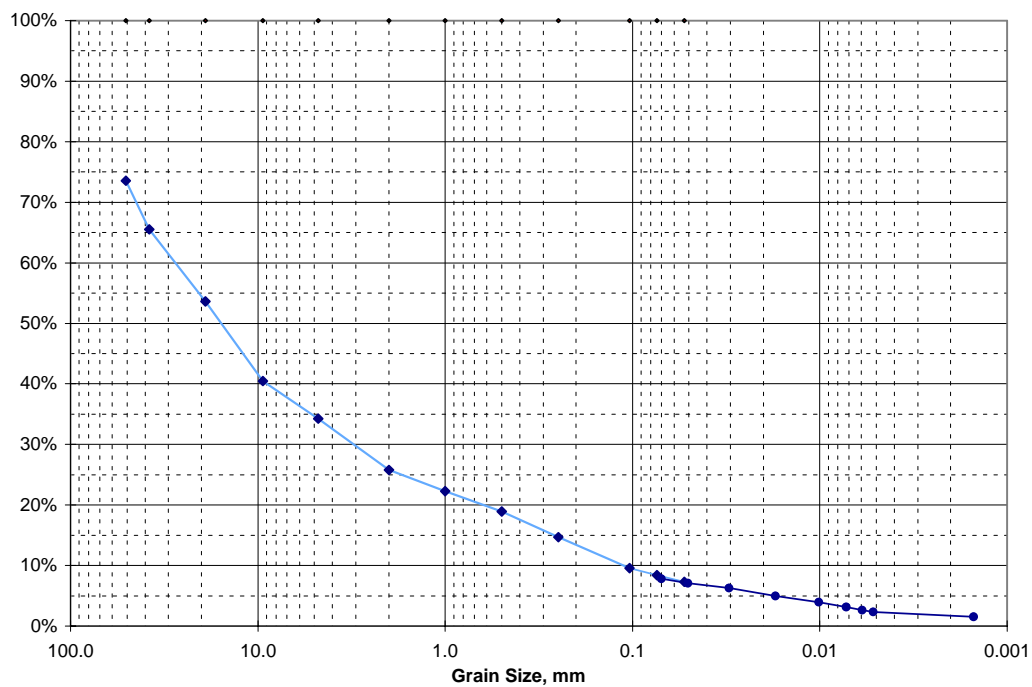
C4689, 96.0-96.5

M.17

Sieve Analysis Data for Sample 98.0-98.5'

Hydrometer

U.S. Std. Sieve Opening in Inches

Grain Size, mm

Fraction <

C4689, 98.0-98.5

Sieve Analysis Data for Sample 99.0-99.5'

C4689, 99.0-99.5

M.19
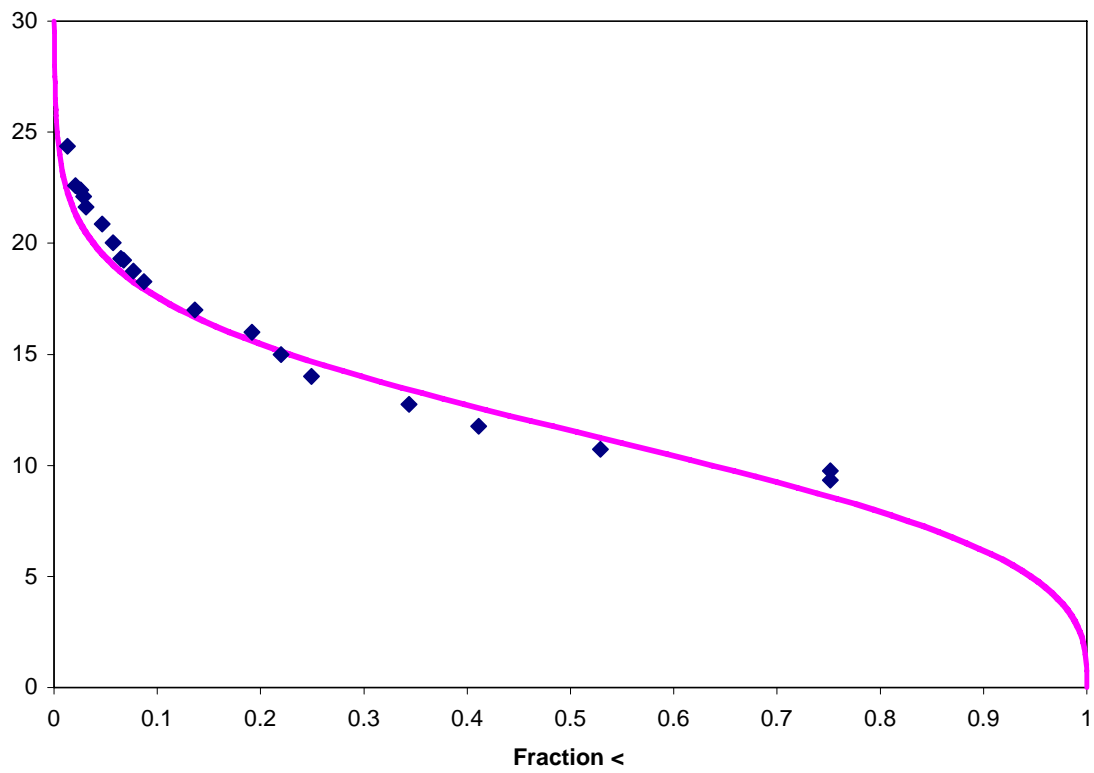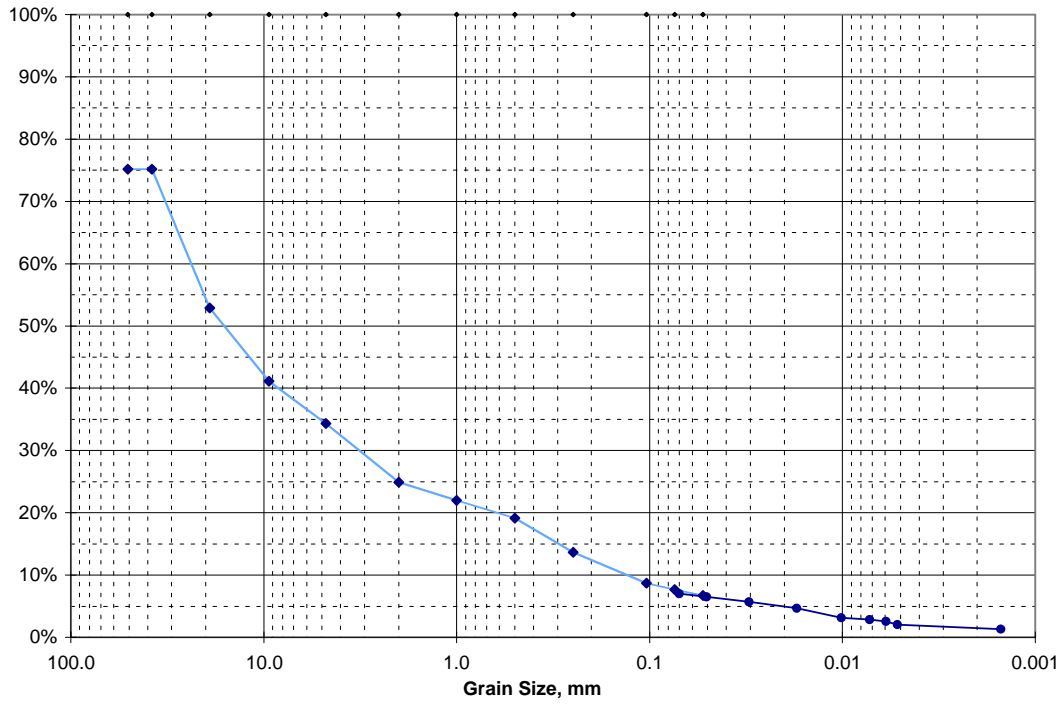
Sieve Analysis Data for Sample 100.5-101.0'
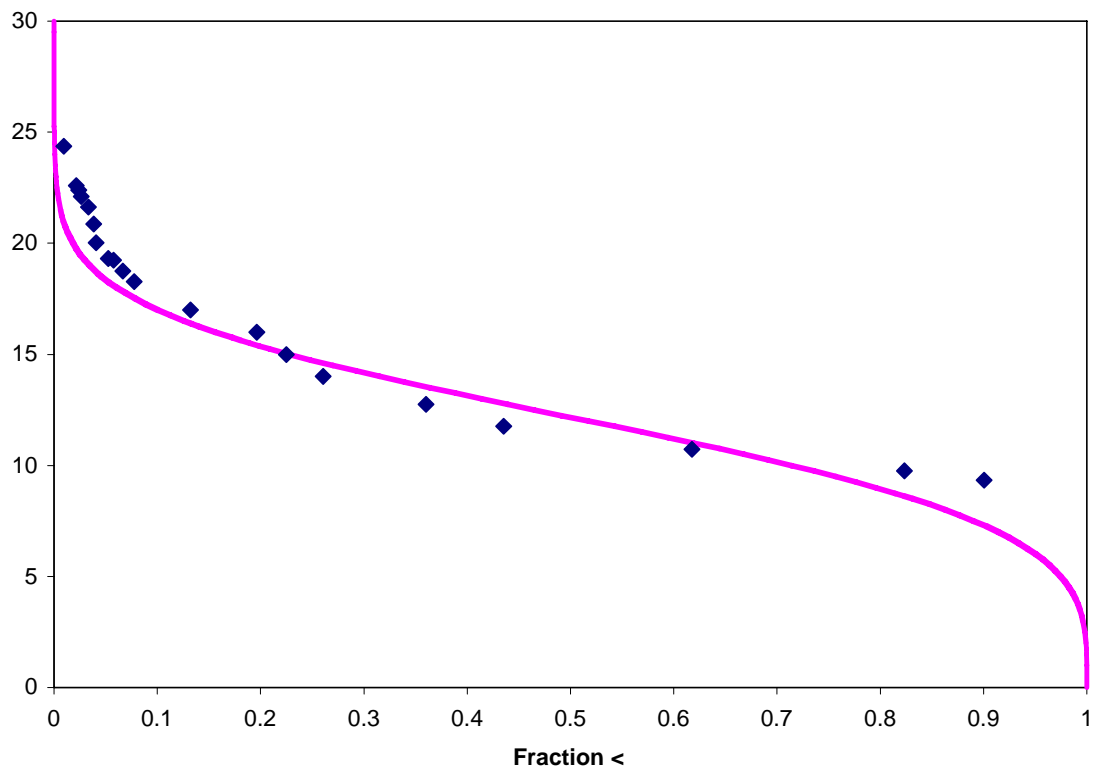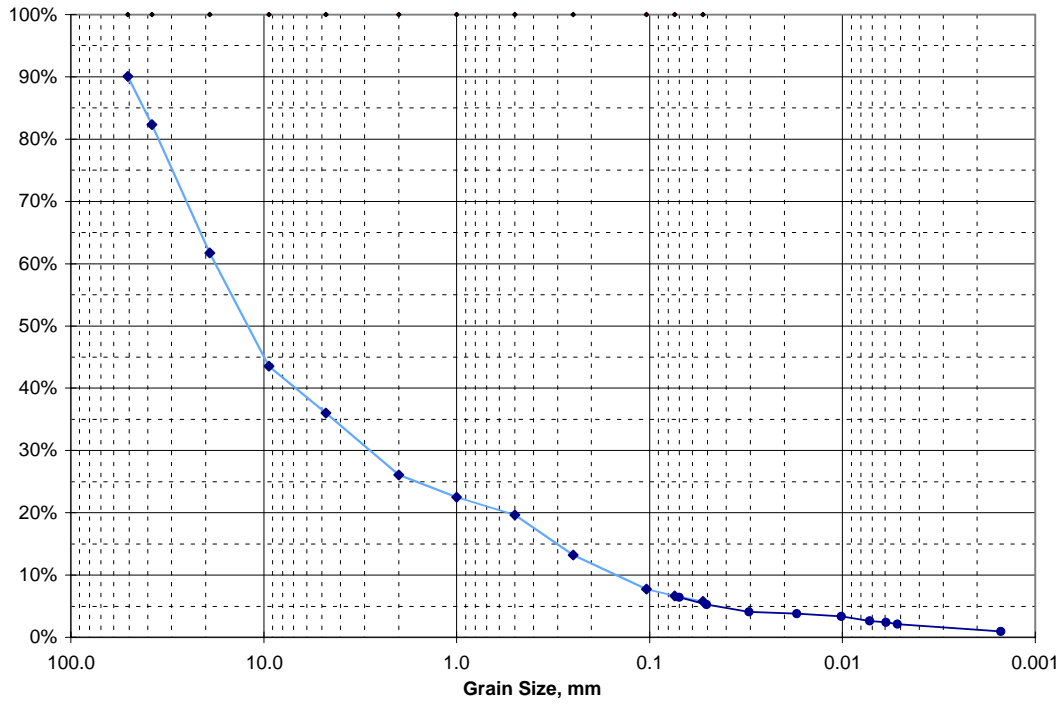
C4689, 100.5-101.0

Sieve Analysis Data for Sample 101.5-102.0

C4689, 101.5-102.0

M.21
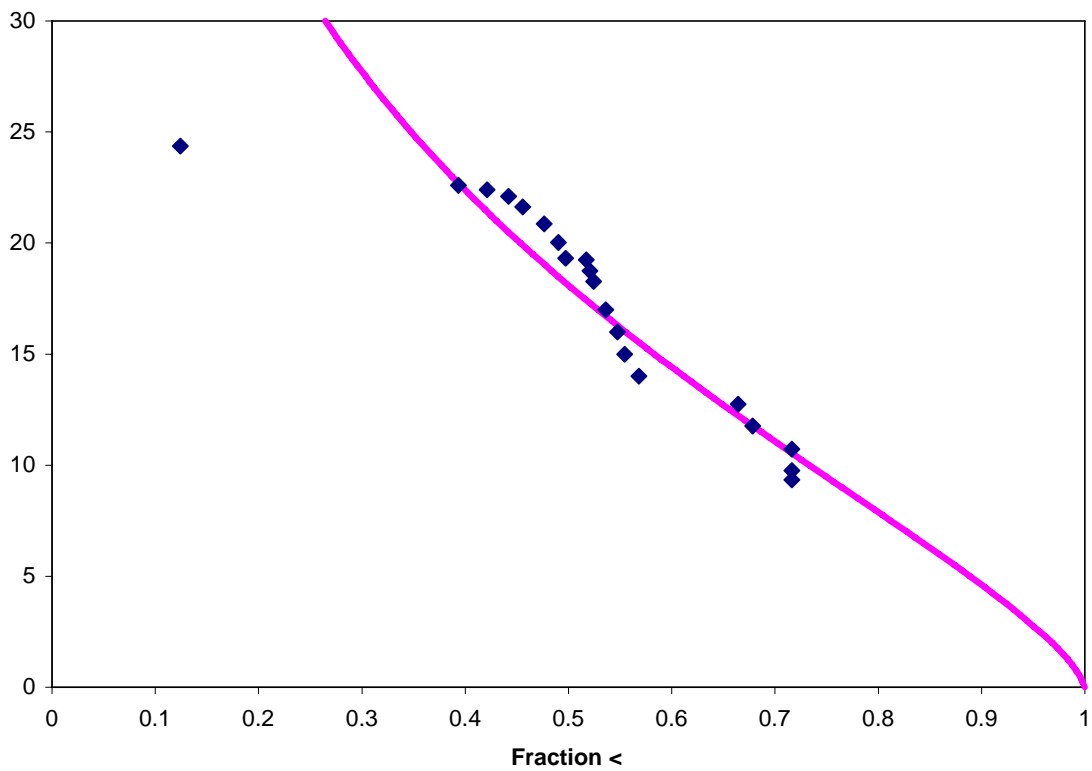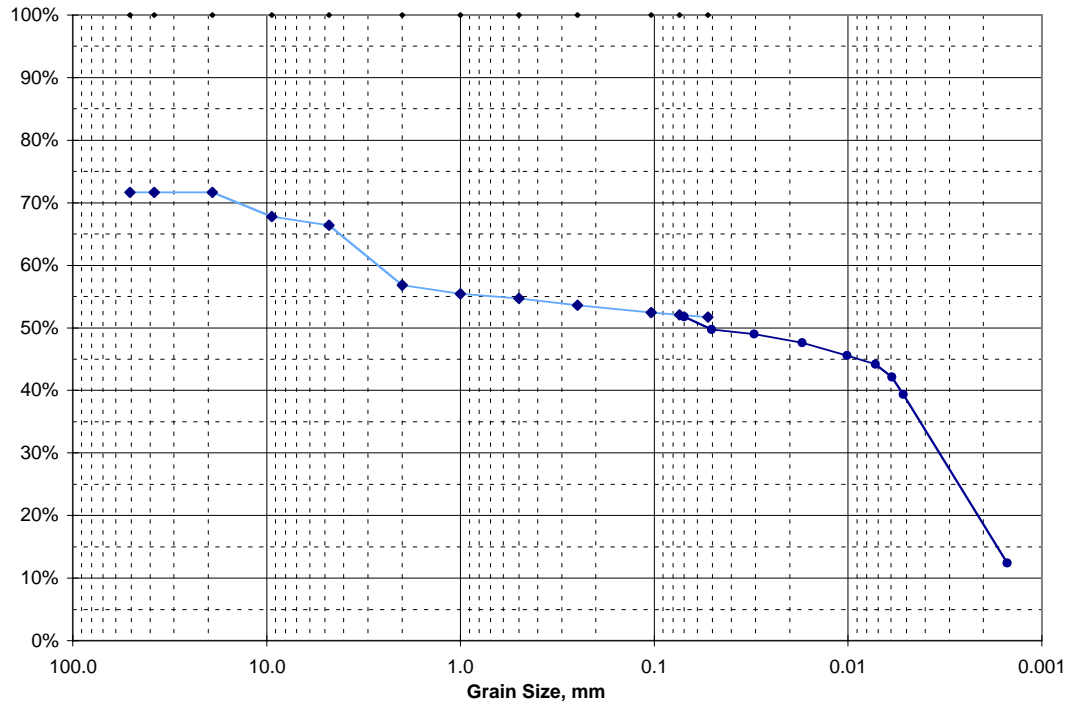
Appendix N

Electromagnetic Borehole Flow Meter Testing in 2002

Appendix N - Electromagnetic Borehole Flow Meter Testing in 2002

This appendix presents two subcontractor-supplied electromagnetic borehole flow meter (EBF) testing reports, each of which contains plots of the collected field data (flow meter profiles in Appendix A and relative hydraulic conductivity plots in Appendix B). In addition to presenting results from the two separate EBF field testing campaigns, general information regarding the test method and analysis approach is provided.

Results of Field Tests with the
Electromagnetic Borehole Flowmeter
At the
100-D Area In Situ Redox Manipulation Barrier Site
Pacific Northwest National Laboratory

by

William R. Waldrop
And
Hubert S. Pearson

March 2002

Quantum Engineering Corporation

112 Tigitsi Lane, Tellico Village

Loudon, Tennessee 37774

Phone (865) 458-0506   FAX (865) 458-0504

Web Site: www.qec-ebf.com

Introduction

Quantum Engineering Corporation (QEC) conducted a flowmeter test of the 100-D Area In Situ Redox Manipulation Barrier Site at the Pacific Northwest National Laboratory (PNNL) . The tests were performed under subcontract to Battelle Institute, the prime contractor for the U.S. Department of Energy. The instrument system used, the Electromagnetic Borehole Flowmeter (EBF), was designed expressly for such tests as performed at the PNNL site (Young and Waldrop, 1989). Data from this procedure provide a cost-effective method to define a profile of hydraulic conductivity throughout the screened or uncased portion of the saturated zone. The QEC team that performs EBF tests are inventors of the instrument system. They have conducted similar tests for a wide range of geohydrology throughout the United States.

Field data were collected in 13 wells at the site during a three-day period in March 2002.   The tests were conducted according to a scope of work developed jointly by staff of QEC and PNNL. This report presents results from the field tests as well as describes the test protocol and the EBF system used.

The Borehole Flowmeter Method

The flowmeter method represents a reasonably simple approach for assessing the relative hydraulic conductivity in porous media or flow through fractured rock at discrete positions in a screened well or uncased borehole. This method is equally effective for evaluating the direction of ambient vertical hydrostatic pressure gradients throughout the depth of a borehole.   The technique involves measuring at arbitrarily selected intervals as water is transmitted through a well under ambient and induced pumping conditions. These data can serve as the basis for computing the relative hydraulic conductivity at each interval.

In principal, the flowmeter method is very straightforward. Consider the test setup for the well shown in Figure 1. When water is pumped into or from the well at a constant rate for an extended time (i.e. typically about 10 minutes), then the water surface level inside the well will adjust until it reaches equilibrium. At that time, water is being induced into (or from) the well at the same rate as that being pumped near the surface. Water is entering or exiting the well horizontally throughout the screened or open interval of the well and flowing vertically within

the well. The objective is to measure the vertical distribution of the horizontal flow into or from the well. The horizontal flow rate at each stratum is indicative of the hydraulic conductivity of those strata as discussed by Molz, et. al. (1990).

Under ideal conditions, the probe is sealed to the wall such that any vertical flow must pass through the recording zone of the meter. Then the flow into or from the well below the meter is recorded as it flows vertically in the well. For some applications, it is not possible to effect a complete seal with the wall and prevent bypass flow. For such cases, it is often desirable, but not essential, to determine the percentage of flow rate bypassing the recording section of the probe and correct the probe readings accordingly.
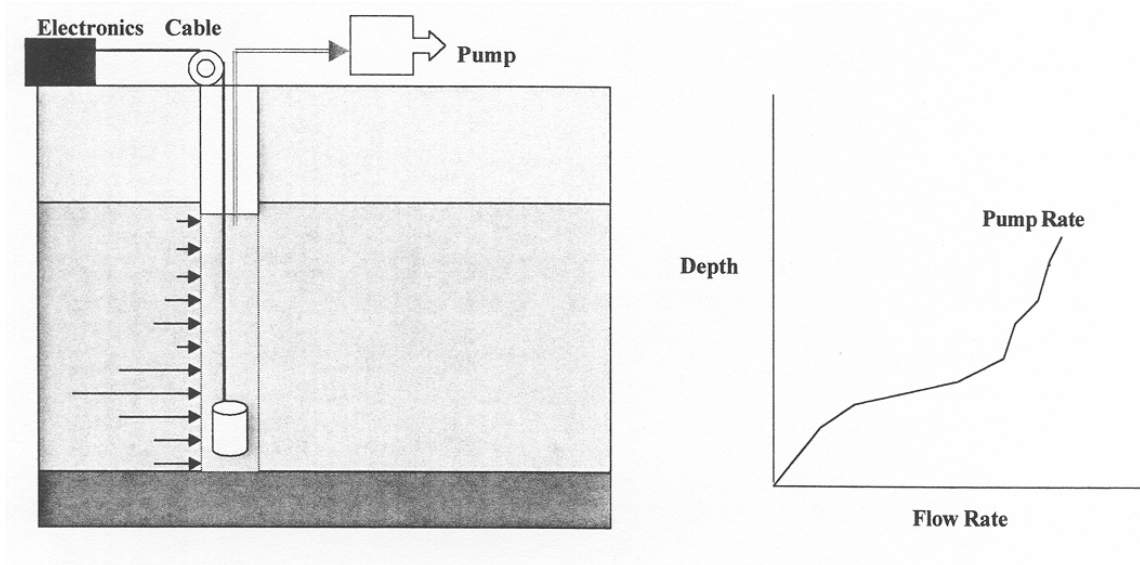
Figure 1. Apparatus and Geometry of a Borehole Flowmeter Test

A flowmeter test for a well is usually initiated by measuring for ambient flow throughout the screened or uncased section of the well. This is typically initiated with the flowmeter at the bottom of the screen where flow rates should be zero. The probe is then raised one increment. After any flow disturbance caused by the probe movement has subsided, the vertical flow at that station is recorded. This process is repeated throughout the entire screened or uncased region. These ambient flows reveal the presence of vertical pressure gradients, positive or negative, between strata, and provide a baseline for analyzing induced flow into the well during pumping.

Once the ambient flow pattern has been recorded, the induced flow test is initiated by pumping into or from the well at a constant rate. The water surface is monitored to determine when equilibrium conditions have been achieved. At that time, the probe is systematically moved vertically with flow rates recorded at predetermined intervals throughout the well screen or uncased region. Data at each depth are displayed on a digital readout and stored in a data file of a portable computer. These tests can be performed with equal accuracy by injecting flow into the well at a constant rate instead of pumping.

Data analysis is also relatively simple. The lateral inflow from each stratum is calculated by successively subtracting the cumulative flow measured at those strata from the cumulative flow recorded at the level immediately below. Hydraulic conductivity can be calculated for those strata by using the Cooper-Jacob formula for horizontal flow to a well. The ratio of local hydraulic conductivity K_i to average K_{ave} for each well is computed using Equation 7 from Molz and Young (1993),

$$K_i / K_{ave} = ((\text{Delta } Q_i - \text{Delta } q_i) / \text{Delta } z) / (Q_{pump} / b) \; ; \; i = 1,2, \dots n$$

where

> Delta Q_i = Flow from the ith layer in the well;
>
> Delta q_i = Ambient flow from the ith layer of the well;
>
> Delta z = ith layer thickness;
>
> Q_{pump} = Flow rate pumped from the well during the induced flow test; and
>
> b = Aquifer thickness.

Additional details are presented in Molz et al. (1994).

The Electromagnetic Borehole Flowmeter

The EBF measures flow using Faraday's Law of Induction. This principal states that the voltage induced by a conductor moving at right angles through a magnetic field is directly proportional to the velocity of the conductor through the field. The flowing water is the conductor, the electromagnet generates the magnetic field, and the electrodes measure the induced voltage. The electronics attached to the electrodes transmit a voltage directly proportional to the velocity of

the water flowing through the interior of the probe. The voltage produced by the water movement through the probe is insensitive to the conductivity of the water as long as the water is conductive.

This method of measuring velocity provides essentially an instantaneous response to changes in flow rates.   Data are typically recorded and averaged over 60 seconds for each data point during a static test of a particular stratum. The total time required to position the probe to a desired depth, allow the flow to settle from the disturbance of movement, record a data point, and document notes is about five minutes.

The external dimension of the downhole probe is designed to fit snugly into a Schedule 40 two-inch diameter pipe. Two probes are available - one with a half-inch inside throat diameter and another with a one-inch throat diameter. The performance specifications of both probes are presented in Table 1.

Table 1: Performance Specifications of the EBF Probes

	½-inch id Probe	**1-inch id Probe**
Minimum Flow	10 mL/min (0.0026 gpm)	40 mL/min (0.011 gpm)
Minimum Velocity	0.131 cm/sec (0.0043 fps)	0.131 cm/sec (0.0043 fps)
Maximum Flow	10 L/min (2.64 gpm)	40 L/min (10.6 gpm)
Maximum Velocity	131 cm/sec (4.3 fps)	131 cm/sec (4.3 fps)

Both probes are designed such that the electromagnets, electrodes and electronic components are fixed in place, tested and then potted with a watertight epoxy. The probes have no moving parts and have smooth exterior surfaces for easy cleaning.

Because the EBF can accurately record extremely low flow rates, it is possible to record ambient flow rates occurring naturally in wells as well as the influx of flows during pumping. The flowmeter measures flow in either direction with equal accuracy.

This new instrument system has proved to be useful in support of environmental groundwater investigations throughout the USA during the seven years that it has been produced commercially. The publications by Young, et al (1998), Molz, et al (1994), Hutchins and Acree (2000) and Molz and Young (1993) provide examples of results from several such applications available in the scientific literature. Examples of data and analysis methods are also presented in the QEC web site at www.qec-ebf.com.

The downhole probe, cable, and aboveground electronics box is shown in Figure 2. The compactness of the system makes it easy to transport, ship and handle in the field.

Figure 2: The Electromagnetic Borehole Flowmeter System

Test Results

Hubert Pearson of QEC, a member of the invention team and experienced in conducting EBF tests, served as test engineer. Vince Vermeul of PNNL assisted with logistics and in conducting these tests. Mr. Vermeul provided guidance for test objectives to assure that test data would be consistent with their needs for defining the hydrogeology at this site.

The flowmeter test was performed with the QEC EBF system using the **one-inch** i.d. probe. This probe was selected because the larger throat diameter creates less bypass flow in wire-wrapped screens where it is not possible to obtain a good seal to the wall. A one-half inch diameter probe was available, but was not needed. Water was pumped at a constant rate to perform the induced flow test for each well.

Calibration of the EBF system was checked prior to this test to assure the accuracy of the test data. Experience has shown that the EBF system is not subject to calibration drift. This is attributable to the design features of the electronics and the fabrication method by which the electronics of the probe are encased in watertight epoxy.

The EBF system produced a linear signal throughout the range of flows tested. Upward flows were designated as positive as the sign convention used throughout all testing. Depths reported are referenced to ground surface. QEC furnished the EBF system and a water level measuring device. PNNL provided a GrundFos RediFlo2 downhole pump and controller, and arranged for collection and disposal of all purgewater. Electric power for the EBF system and the pump was available at the site.

All of the 13 wells tested had been completed with a nominal 6-inch diameter wire-wrapped stainless steel screen. The vertical ribs of this type screen preclude sealing the region between the outside of the EBF probe and the screen to prevent all bypass flow around the recording interior of the flowmeter. Nevertheless, a successful flowmeter test was achieved by blocking a consistent percentage of vertical flow. The relative change in flow rate between vertical stations is what is required to determine the profile of hydraulic conductivity of a well. A rubber collar sized slightly larger than the screen diameter was used to block as much of the flow as possible between the outside of the EBF probe and the screen. An inflatable packer can also be used to block vertical flow around the probe. However, an inflatable packer is more time consuming and requires care to assure that the packer is inflated to the same diameter for each depth.

Ambient tests were performed on five of the 13 wells to establish if ambient flow might be a significant factor in analyzing the pump data. Neither preliminary nor final analysis revealed

any ambient flow rates of significance in any of the wells. Therefore, ambient tests were not performed for the other eight wells. The parameters for the 13 wells tested are presented in Table 2. The bottom of the well shown is where the flowmeter rested on the bottom, probably on silt.

Table 2: Parameters of the Wells Tested

Well No.	Top of Screen (ft)	Bottom of Well (ft)	Pump Rate (gpm)	Pumped Depth to Water (ft)	Drawdown (ft)
199-D4-25	83.9	99	1.47	84.3	-0.65
199-D4-26	85.1	100	1.51	83.77	-0.18
199-D4-31	81.2	96	1.47	88.56	-3.49
199-D4-35	81.3	96.2	1.40	83.93	-0.20
199-D4-62	83.6	107	1.46	83.35	-0.71
199-D4-63	85.0	108	1.46	83.32	-0.68
199-D4-64	84.56	108	1.58	83.23	-0.47
199-D4-65	84.93	109	1.25	83.23	-0.43
199-D4-66	84.09	107	1.40	83.42	-0.47
199-D4-67	84.7	108	1.40	82.96	-0.16
199-D4-68	80.52	110.2	1.40	82.58	-0.04
199-D4-70	81.87	106.8	1.52	82.75	-0.28
199-D4-72	79.92	109.5	1.55	82.14	-0.02

The pumping rates for the pumping tests varied between 1.25 GPM for Well –65 and 1.55 GPM for Well –72. This generally produced a slight drawdown of water surface of less than one foot. This was important, because excess drawdown restricts the length of the screen for flowmeter testing. Well –31 was the exception for a small drawdown. Pumping at a similar rate as the other wells produced a drawdown of 3.49 feet. From the data available to the authors, there appears no apparent reason for this difference.

The data in Table 2 show that the water surface is near or below the top of the screens for all wells. When considering that the downhole pump was placed in the top part of the water column, it is obvious that flowmeter recordings could not be performed throughout the entire well screen for any of the wells due to physical interference between the pump and the probe. However, readings were performed as near to the water surface as possible without raising the pump above the water surface and changing the pump rate.

Profiles of flow rates recorded in each well while pumping are presented in Appendix A. Data generally were recorded at vertical increments of one foot. As anticipated, a significant percentage of bypass flow was observed in the wire-wrapped screens except in the solid joints where it was possible to get a good seal to the wall. The percentage of bypass flow in the screened portion of the well was computed by comparing data recorded immediately above and below a solid joint. The data shown in Appendix A have been adjusted to account for the bypass flow in the screened portion of the well. Significant parameters and features of each well are included in each graph as notes to assist in interpretation. Questionable data points were omitted from the graphs.

The profiles of flow rate for each well were used to compute profiles of relative hydraulic conductivity by the procedure described in a previous section of this report. As requested by staff of PNNL these data were normalized to show the percentage of the total hydraulic conductivity in each one-foot interval. Profiles for each well are presented in Appendix B. These data illustrate the geologic heterogeneity of the 13 wells tested with the EBF.

References

Hutchins, S.R. and S.D. Acree (2000), Ground Water Sampling Bias Observed in Shallow, Conventional Wells, Ground Water Monitoring and Remediation, Vol. 20 (1), pp. 86-93.

Molz, F.J., Oktay Guven, and J.G. Melville, (1990), Measurement of Hydraulic Conductivity Distributions - A Manual of Practice, U.S. Environmental Protection Agency Technical Report, EPA/600/8-90/046.

Molz, F.J., G.K. Boman, S.C. Young, and W.R. Waldrop, (1994), Borehole Flowmeters: Field Application and Data Analysis, Journal of Hydrology No. 163, pp. 347-371.

Molz, F.J. and S.C. Young, (1993), Development and Application of Borehole Flowmeters for Environmental Assessment, The Log Analyst, pp. 13-23, January-February 1993.

Young, S.C., H.E. Julian, H.S. Pearson, F.J. Molz and G.K. Boman, (1998) Application of the Electromagnetic Borehole Flowmeter, U.S. Environmental Protection Agency Research Report EPA/600/R-98/058, August 1998.

Young, S.C. and W.R. Waldrop, (1989), An Electromagnetic Borehole Flowmeter for Measuring Hydraulic Conductivity Variability, Proceedings of the Conference on New Techniques in Groundwater, National Water Well Association, Dallas, Texas.

Appendix A

Profiles of Flow Rates in the Wells Tested

Figure A-1: Profile of Pumped Flow Rate in Well 199-D4-25

Top of Screen at 83.9 Ft.

Depth to Water at 84.3 Ft.

Solid Joint at 89 Ft.

Essentially no flow entered the well below a depth of 96 feet.

Bottom of Well at 99 Ft.

Depth (Ft.)

Flow Rate (GPM)

Figure A-2: Profile of Pumped Flow Rate in Well 199-D4-26

Water Surface at 83.77 feet

Top of Screen at 85.1 feet

Pump Rate = 1.51 GPM

Solid Joint at 90 feet.

Bottom of Well at 100 feet

Depth (Ft.)

Flow Rate (GPM)

N.17

Figure A-3: Profile of Pumped Flow Rate in Well 199-D4-31

Top of Screen at 81.2

Pump Rate = 1.47 GPM

Water Surface at 88.56 Ft.

Essentially no flow entering the well below a depth of 93 feet.

Bottom of Well at 96 Ft.

Depth (Ft.)

Flow Rate (GPM)

Figure A-4: Profile of Pumped Flow Rate in Well 199-D4-35

Top of Screen at 81.3

Pump Rate = 1.4 GPM

Depth to Water at 83.93 feet.

Solid Joint at 91.5 feet.

Bottom of Well at 96.2 feet.

Depth (Ft.)

Flow Rate (GPM)

Figure A-5: Profile of Pumped Flow Rate in Well 199-D4-62

Water Surface at 83.35 feet.
Top of Screen at 83.6 feet
Pump Rate = 1.46 GPM
Solid Joint at 89 feet.
Essentially no flow entered the well below 101 feet.
Bottom of Well at 107 feet

Figure A-6: Profile of Pumped Flow Rate in Well 199-D4-63

Water Surface at 83.3
Top of Screen at 85 feet.
Pump Rate = 1.46 GPM
Essentially no flow below a depth of 106 feet.
Bottom of Well at 108 feet.

N.19

Figure A-7: Profile of Pumped Flow Rate in Well 199-D4-64

Water Surface at 83.23 feet.
Top of Screen at 84.56 feet.
Solid Joint at 90 feet.
Bottom of Well at 108 feet.

Figure A-8: Profile of Pumped Flow Rate in Well 199-D4-65

Water Surface at 83.23 feet
Top of Screen at 84.9 feet.
Pump Rate = 1.25 GPM
Solid Joint at 90 feet.
Bottom of Well at 109 feet.

N.20

Figure A-9: Profile of Pumped Flow Rate in Well 199-D4-66

Water Surface at 83.42 feet.

Top of Screen at 84.09 feet.

Pump Rate = 1.4 GPM

Solid Joint at 89.5 feet.

Flow rates are essentially zero below a depth of 100 feet.

Bottom of Well at 107 feet.

Depth (Ft.)

Flow Rate (GPM)

Figure A-10: Profile of Pumped Flow Rate in Well 199-D4-67

Water Surface at 82.96 feet.

Top of Screen at 84.7 feet.

Pump Rate = 1.4 GPM

Solid Joint at 90 feet.

Essentially no flow below a depth of 99 feet.

Bottom of Well at 108 feet.

Depth (Ft.)

Flow Rate (GPM)

Figure A-11: Profile of Flow Rate in Well 199-D4-68

Top of Screen at 80.52 feet.

Water Surface at 82.58 feet.

Pump Rate = 1.4 GPM

Solid Joint at 91 feet.

Bottom of Well at 110.2 feet

Figure A-12: Profile of Pumped Flow Rate in Well 199-D4-70

Top of Screen at 81.87 feet.
Water Surface at 82.75 feet.

Pump Rate = 1.52 GPM

Solid Joint at 87 feet.

Essentially no flow below a depth of 97 feet.

Bottom of Well at 106.8 feet.
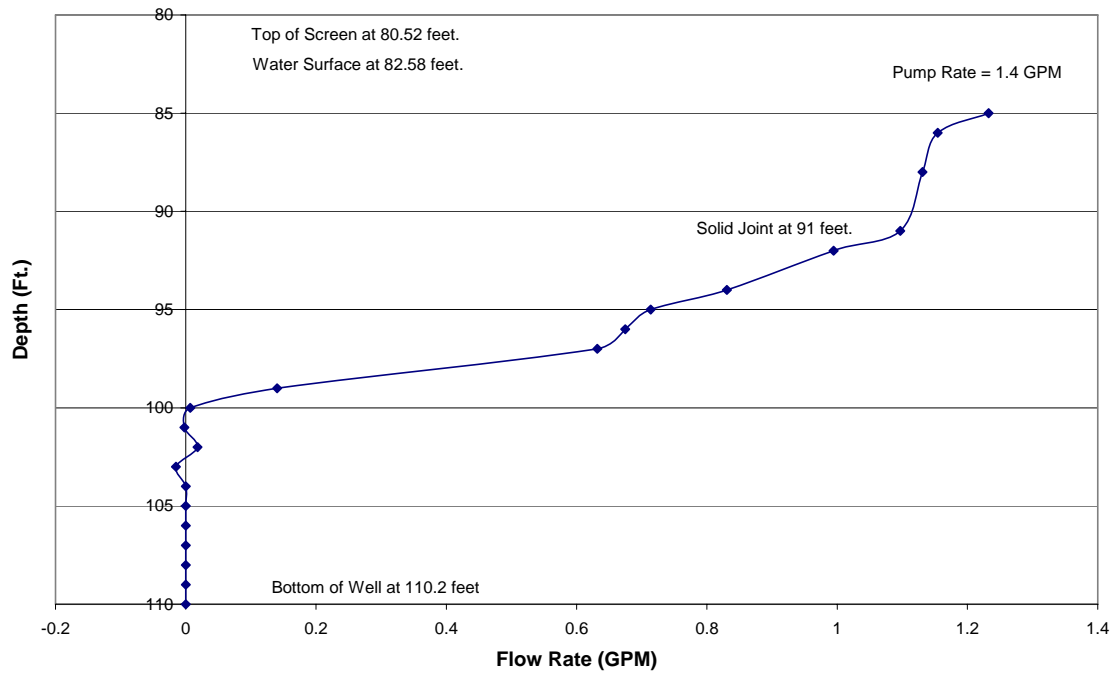
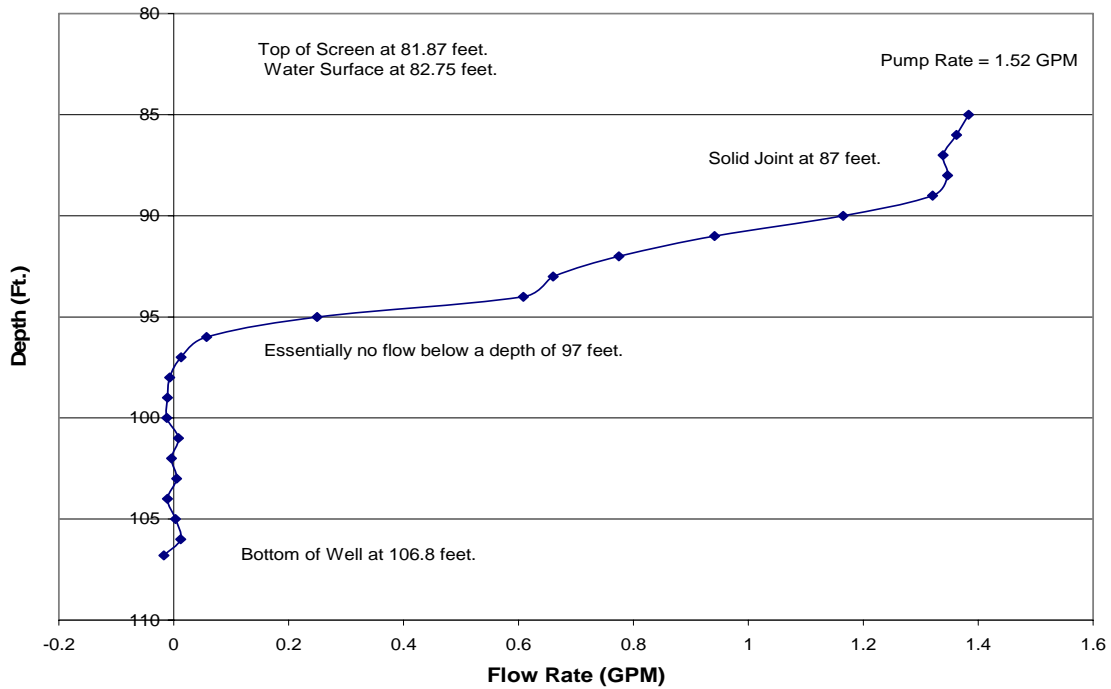**Figure A-13: Profile of Pumped Flow Rate in Well 199-D4-72**
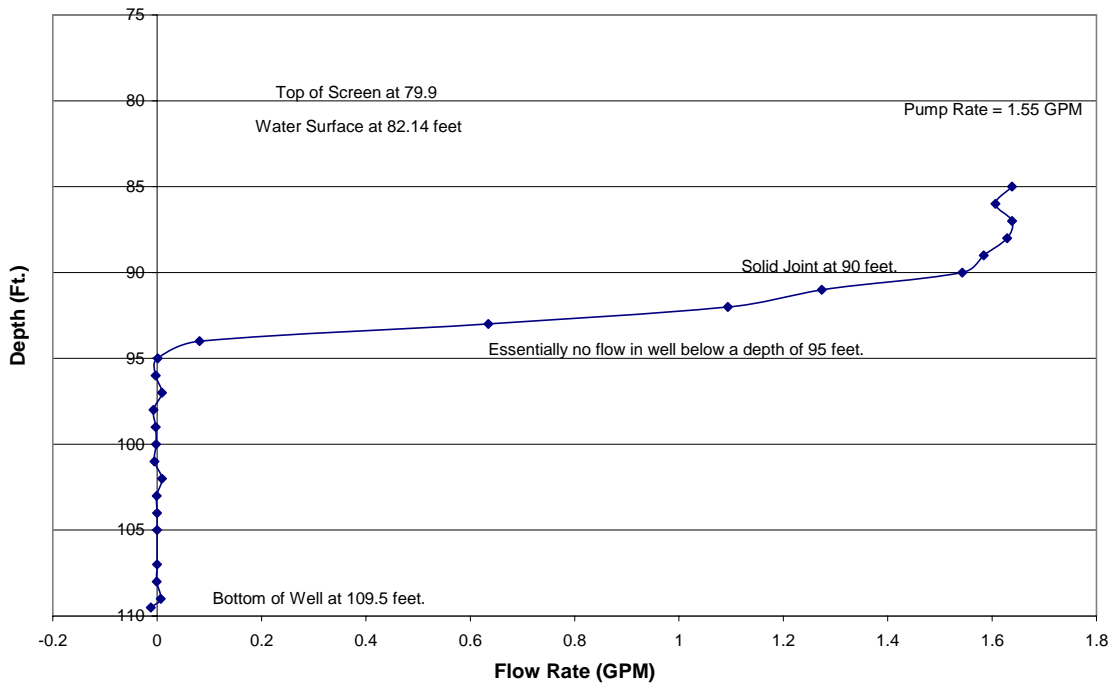
Appendix B

Normalized Distributions of Hydraulic Conductivity

Figure B-1: Normalized Profile of Relative Hydraulic Conductivity for Well 199-D4-25
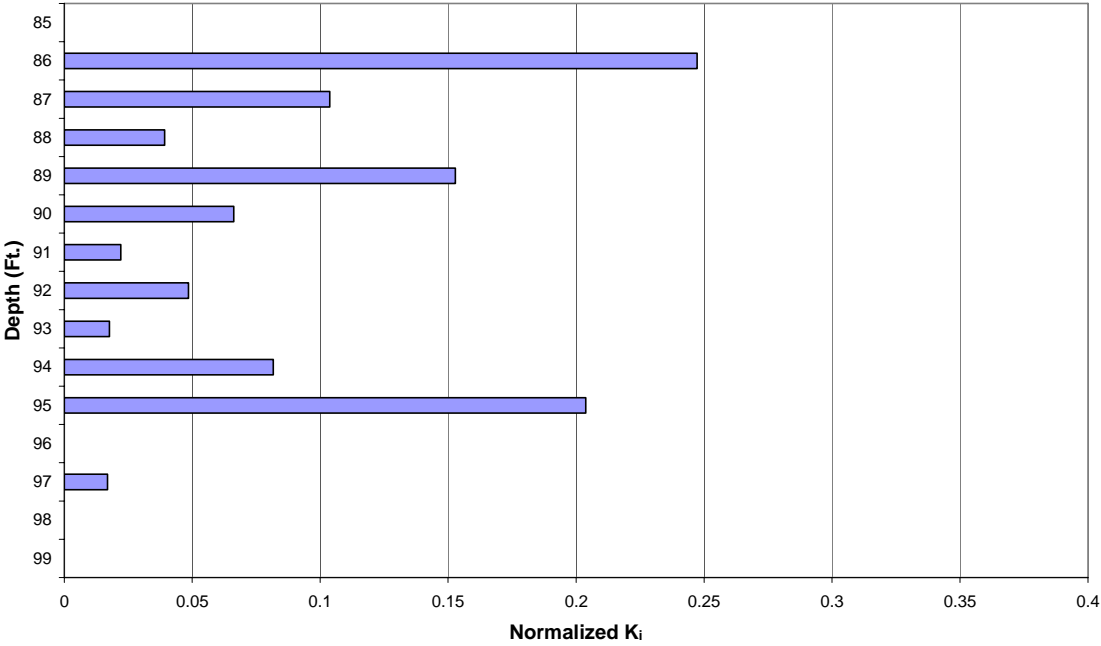
Figure B-2: Normalized Profile of Relative Hydraulic Conductivity for Well 199-D4-26
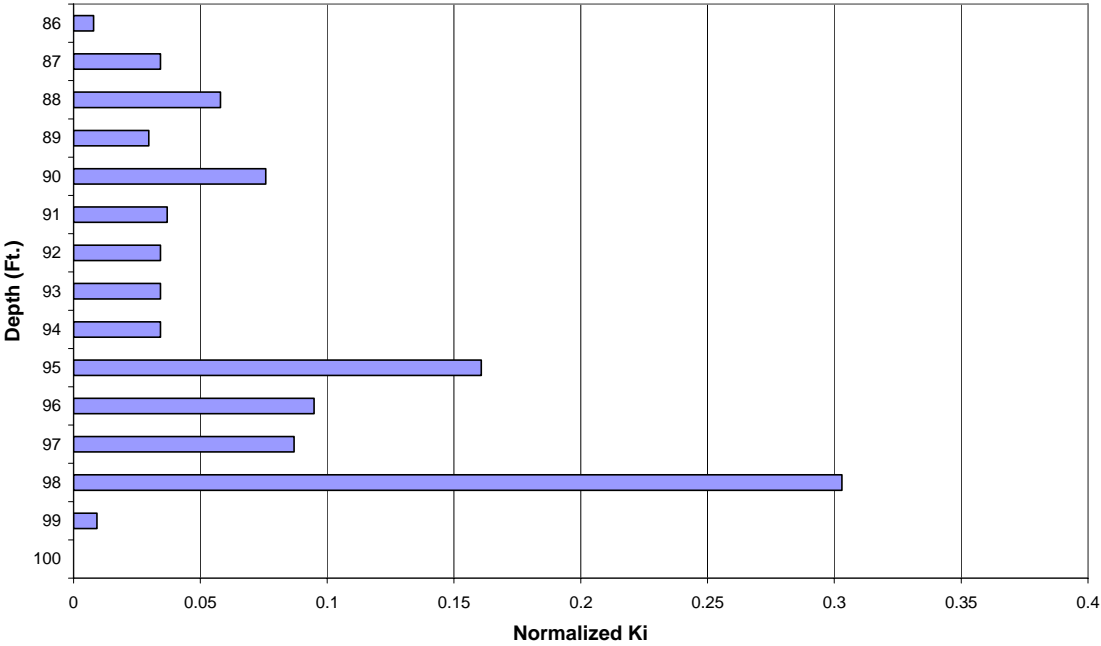
**Figure B-3: Normalized Profile of Relative Hydraulic Conductivity for
Well 199-D4-31**

**Figure B-4: Normalized Profile of Relative Hydraulic Conductivity for
Well 199-D4-35**

**Figure B-5: Normalized Profile of Relative Hydraulic Conductivity for
Well 199-D4-62**

**Figure B-6: Normalized Profile of Relative Hydraulic Conductivity for
Well 199-D4-63**

**Figure B-7: Normalized Profile of Relative Hydraulic Conductivity for
Well 199-D4-64**
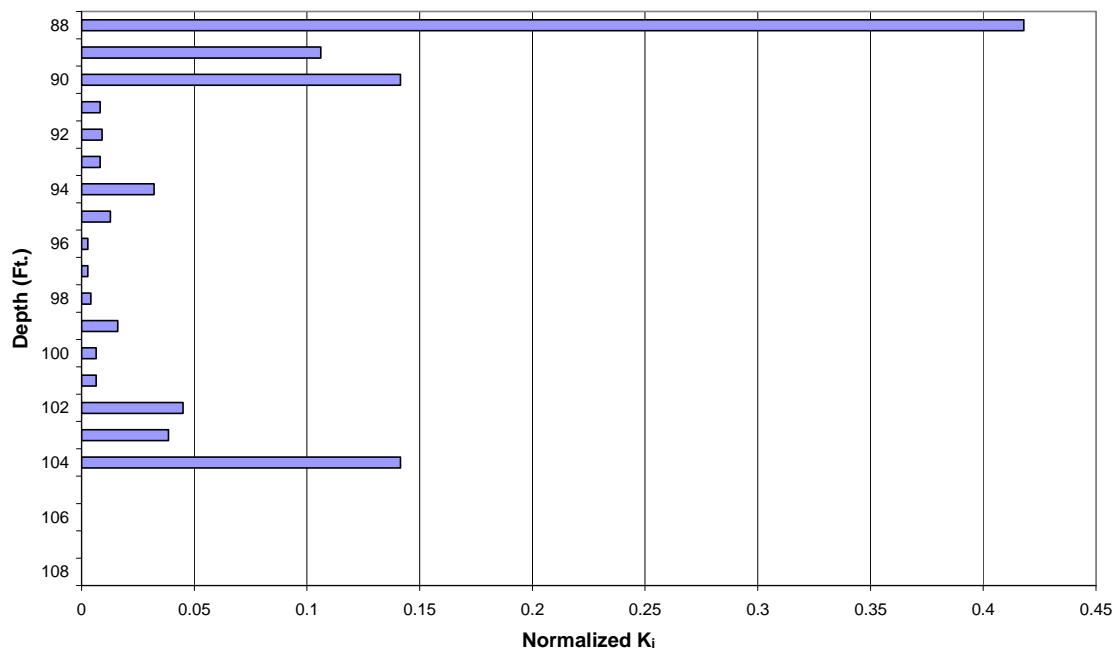
**Figure B-8: Normalized Profile of Relative Hydraulic Conductivity for
Well 199-D4-65**
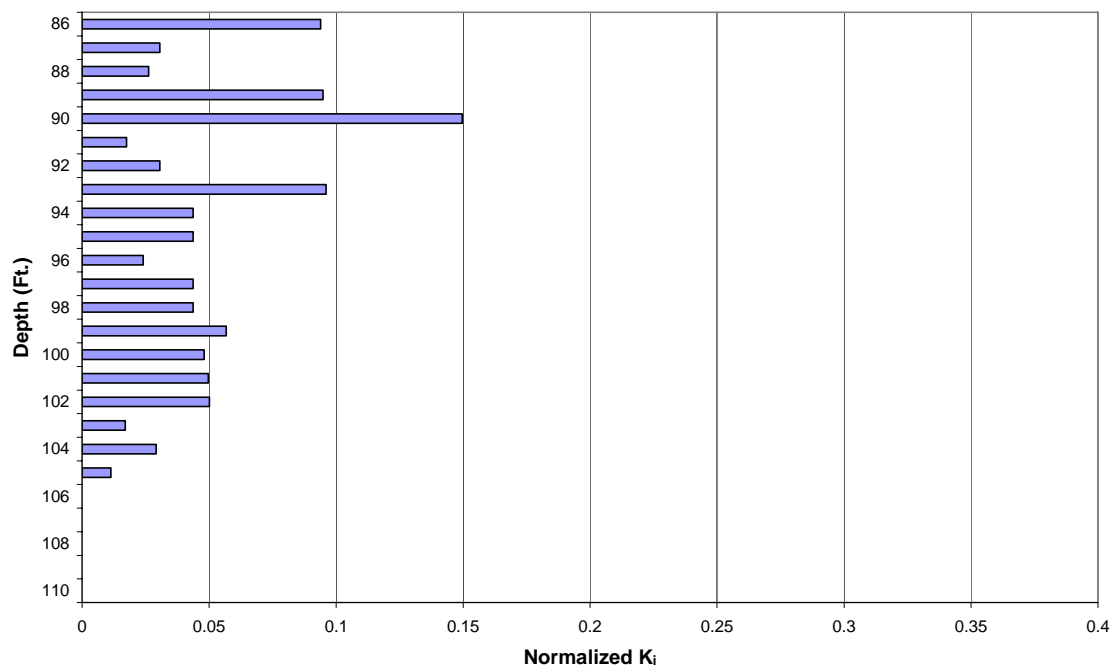
Figure B-9: Normalized Profile of Relative Hydraulic Conductivity for Well 199-D4-66
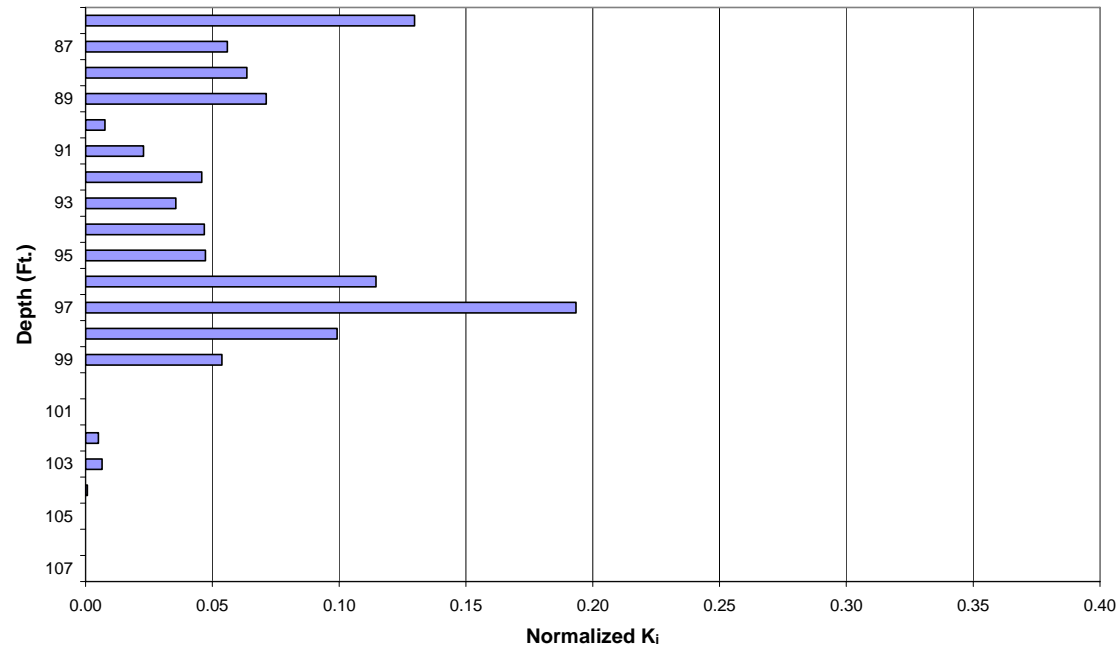
Figure B-10: Normalized Profile of Relative Hydraulic Conductivity for Well 199-D4-67
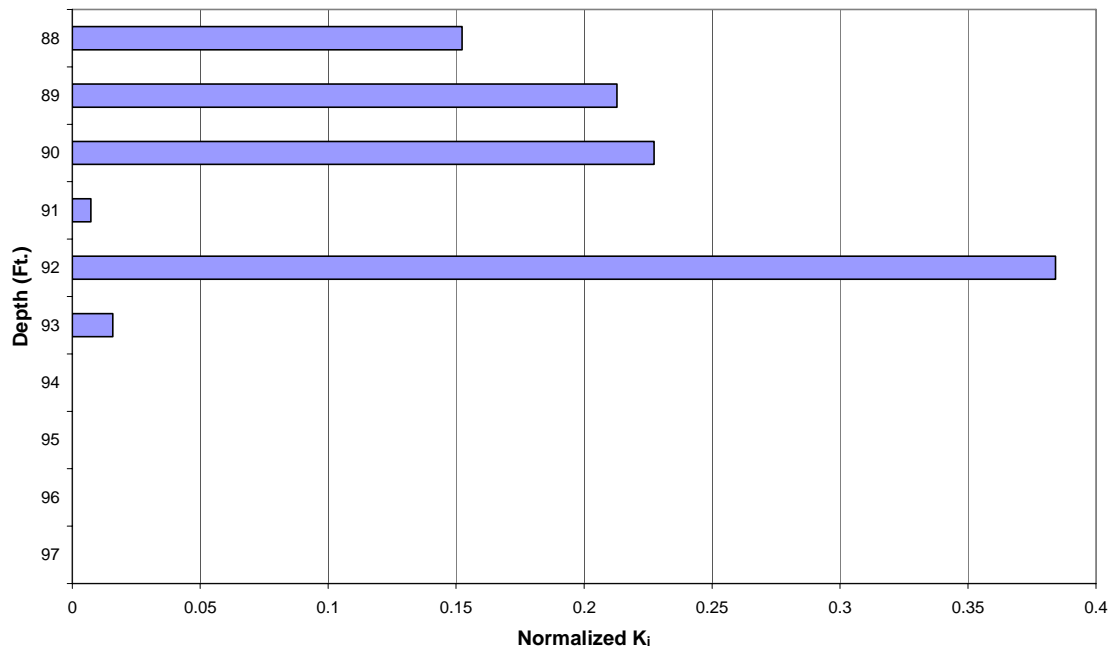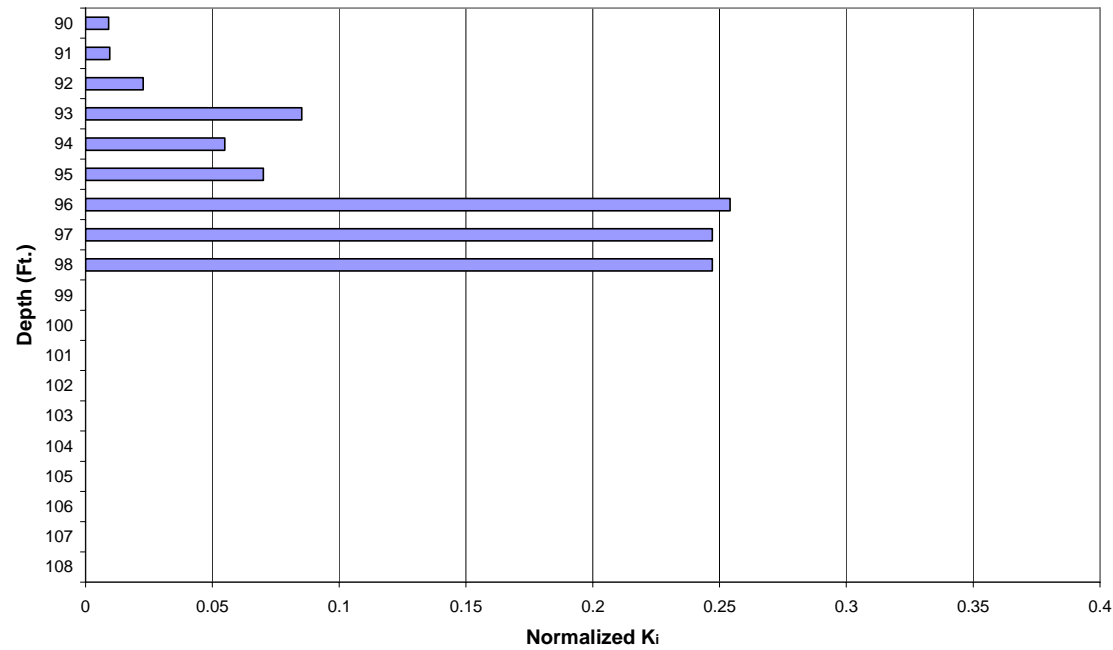
Figure B-11: Normalized Profile of Relative Hydraulic Conductivity for Well 199-D4-68
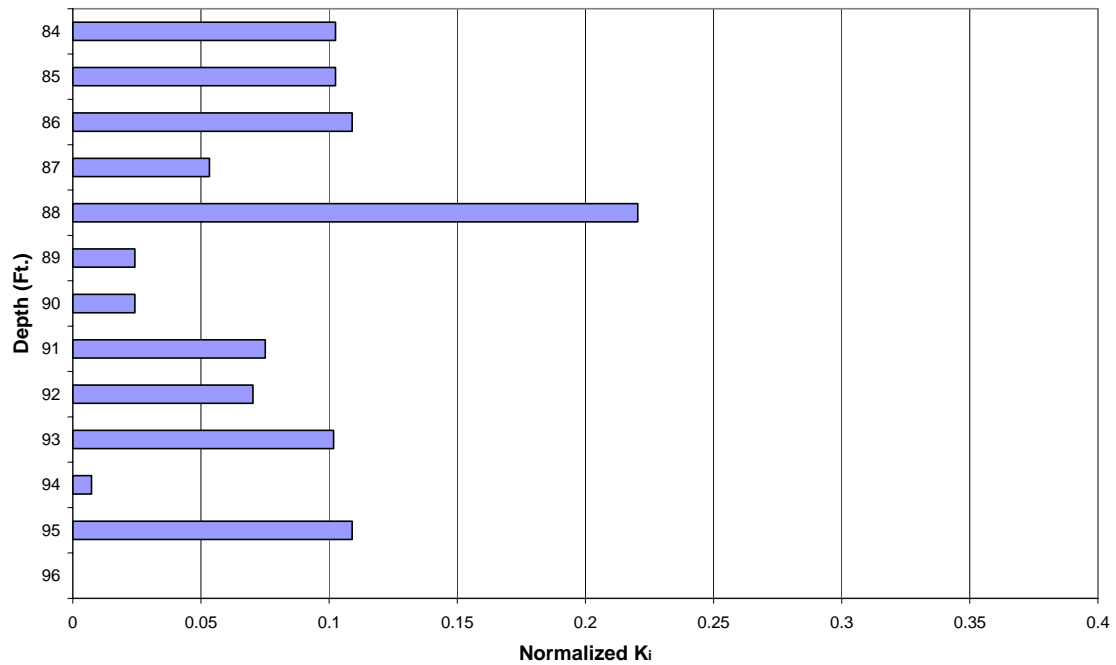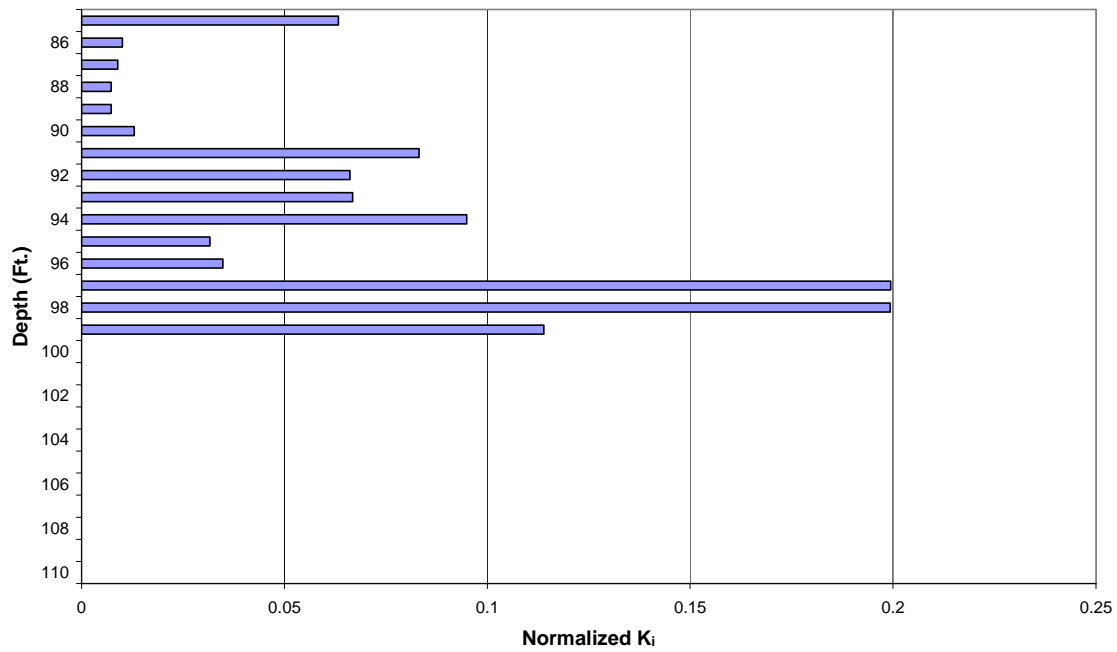

Figure B-12: Normalized Profile of Relative Hydraulic Conductivity for Well 199-D4-70

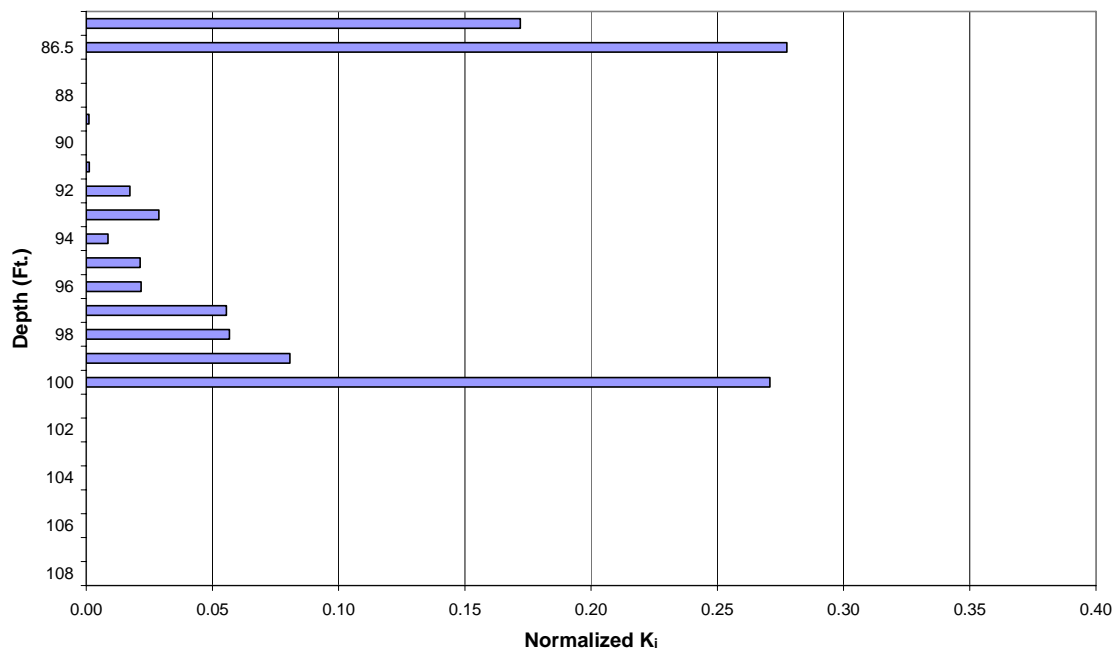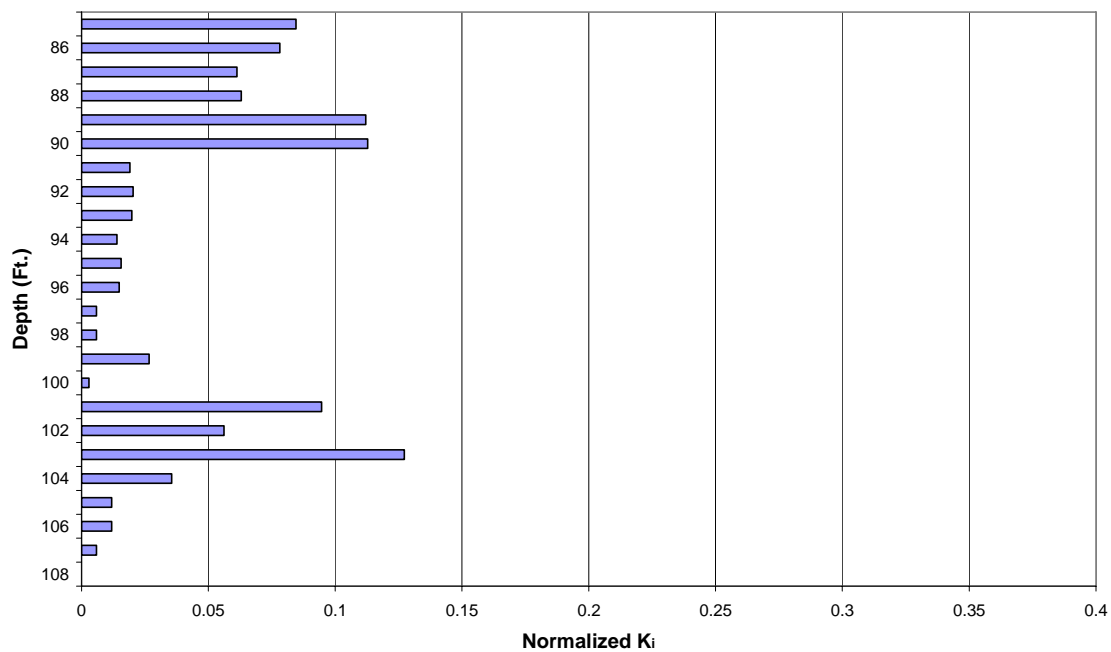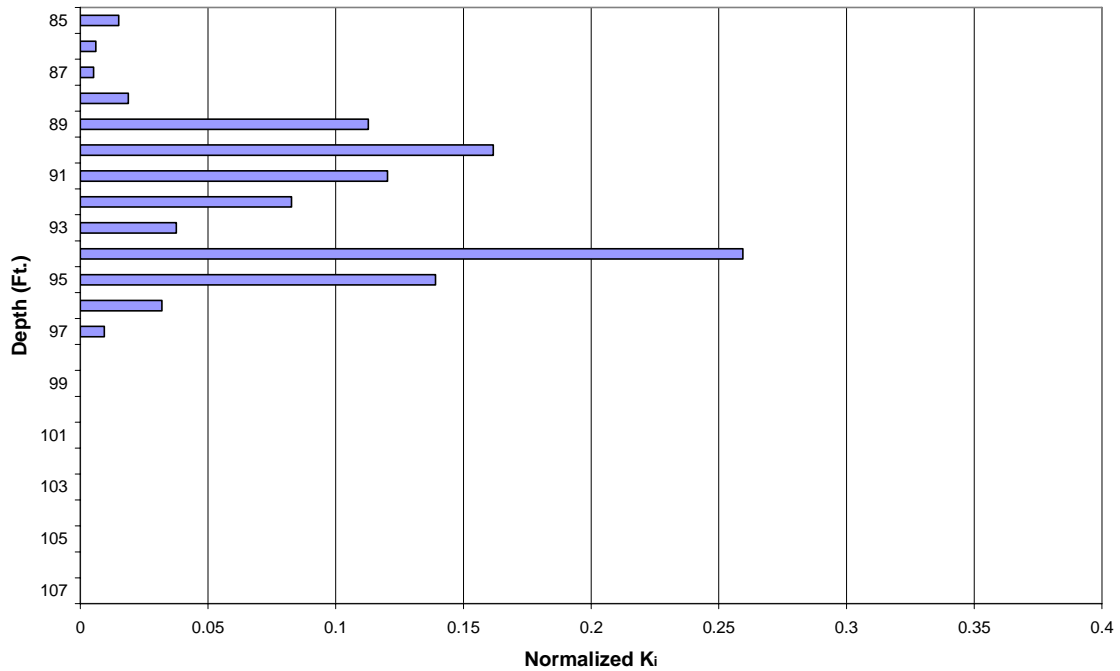**Figure B-13: Normalized Profile of Relative Hydraulic Conductivity for Well 199-D4-72**
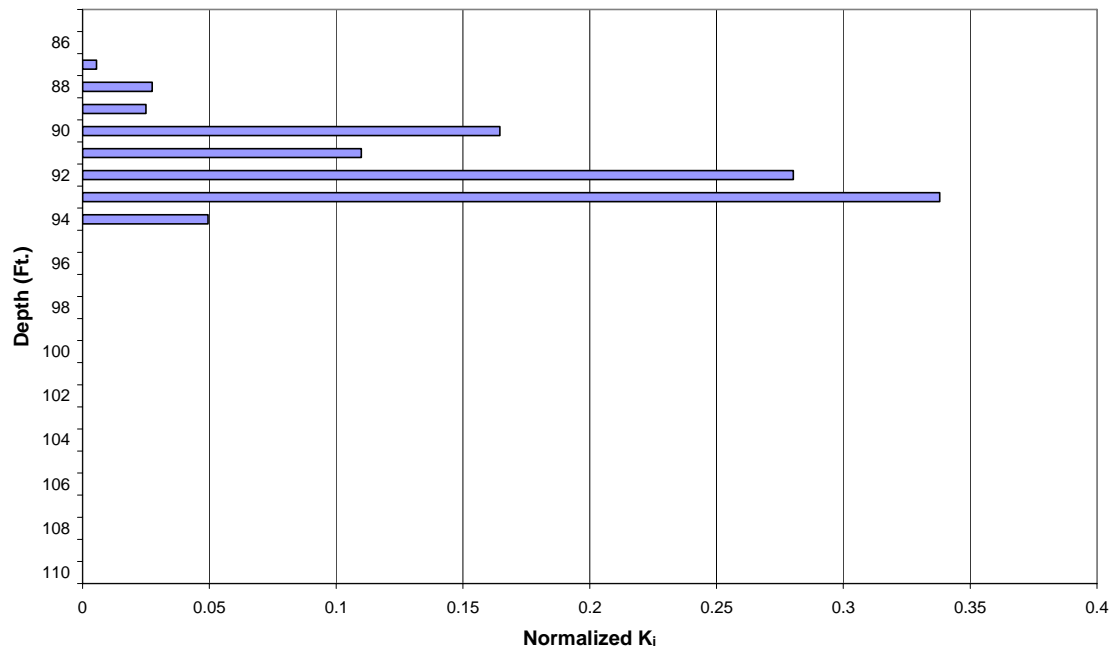
Second Phase of Testing with the
Electromagnetic Borehole Flowmeter
at the
100-D Area In Situ Redox Manipulation Barrier Site
Pacific Northwest National Laboratory

by

William R. Waldrop
And
Hubert S. Pearson

May 2002

Quantum Engineering Corporation

112 Tigitsi Lane, Tellico Village

Loudon, Tennessee 37774

Phone (865) 458-0506   FAX (865) 458-0504

Web Site: www.qec-ebf.com

Introduction

Quantum Engineering Corporation (QEC) conducted a flowmeter test of the 100-D Area In Situ Redox Manipulation Barrier Site at the Pacific Northwest National Laboratory (PNNL). The tests were performed under subcontract to Battelle Institute, the prime contractor for the U.S. Department of Energy. These tests were a continuation of flowmeter tests performed by QEC for Batelle Institute on 11-13 March 2002 in support of a permeable barrier to remediate a groundwater plume contaminated with chromium. The flowmeter data served as the basis for determining the vertical distribution of horizontal hydraulic conductivity along the barrier. These data, along with other geologic data from the site, will be used to determine the potential for reducing the total cost of the barrier installation by reducing the chemical volume and injection labor requirements.

The Electromagnetic Borehole Flowmeter (EBF) was used to perform the test. This instrument system, the method used to collect data, and an explanation of how the data are used to compute a vertical distribution of hydraulic conductivity are described in Waldrop and Pearson (2002). This report presents a description of the previous test performed at PNNL in March 2002. Additional details of the field procedure and data analysis can be found in Molz, et al (1994).

Hubert Pearson of QEC performed the flowmeter test described herein. Mr. Pearson also performed the previous flowmeter test at PNNL using the same instrument system and using similar test procedures. Results of the analysis are presented in a similar format for ease in comparing results from the two test periods. As before, Mr. Pearson was assisted in the field by staff of Battelle Institute. Vince Vermeul of Battelle Institute provided guidance in planning the test program and served as the primary contact.

Test Results

The flowmeter test was performed with the QEC EBF system using the one-inch i.d. probe. This probe was selected because the larger throat diameter creates less bypass flow in wire-wrapped screens where it is not possible to obtain a good seal to the wall. The EBF system produced a linear signal throughout the range of flows tested. Upward flows were designated as positive as

the sign convention used throughout all testing. Depths reported are referenced to ground surface.

QEC furnished the EBF system and a water level measuring device. PNNL provided a GrundFos RediFlo2 downhole pump and controller, and arranged for collection and disposal of all purgewater. Electric power for the EBF system and the pump was available at the site.

Twelve wells were successfully tested. All of the 12 wells had been completed with a nominal 6-inch diameter wire-wrapped stainless steel screen. The vertical ribs of this type screen precluded sealing the region between the outside of the EBF probe and the screen to prevent all bypass flow around the recording interior of the flowmeter. Nevertheless, a successful flowmeter test was achieved by blocking a consistent percentage of vertical flow. The relative change in flow rate between vertical stations is what is required to determine the profile of hydraulic conductivity of a well. A rubber collar sized slightly larger than the screen diameter was used to block as much of the flow as possible between the outside of the EBF probe and the screen.   An inflatable packer can also be used to block vertical flow around the probe. However, an inflatable packer is more time consuming and requires care to assure that the packer is inflated to the same diameter for each depth.

Ambient tests were performed on five wells during the March 2002 test to determine if ambient flow might be a significant factor in analyzing the pump data. Results from these previous tests indicated that ambient flow was likely insignificant and would likely have a negligible effect on the analysis of pumped flow data used to determine the vertical profile of hydraulic conductivity. Therefore, ambient flow rates were not performed during the April test program.

The parameters for the wells tested are presented in Table 1. The bottom of the well shown is where the flowmeter rested on the bottom, probably on silt. All depths have been adjusted to ground level.

Table 1: Parameters of the Wells Tested

Well No.	Static Depth to Water (ft)	Bottom of Well (ft)	Pump Rate (gpm)	Pumped Depth to Water (ft)	Drawdown (ft)
199-D4-07	85.0	95.8	2.9	85.5	-0.5
199-D4-09	85.5	96.8	2.6	85.5	Negligible
199-D4-10	85.5	97.0	2.7	85.9	-0.4
199-D4-11	85.0	96.0	2.8	85.9	-0.9
199-D4-12	85.3	96.7	2.88	85.9	-0.6
199-D4-19	84.38	110.4	1.33	84.7	-0.32
199-D4-21	85.9	97.7	2.7	86.4	-0.5
199-D4-32	85.7	97.3	As low as possible	Constantly increasing	
199-D4-69	84.6	107.8	3.47	85.53	-0.93
199-D4-71	84.3	109.6	1.55	84.5	-0.2
199-D4-73	84.40	110.4	1.48	84.44	-0.04
199-D4-74	83.6	111.0	3.77	84.0	-0.4
199-D4-75	84.1	92.6	1.36	84.26	-0.16

Staff of PNNL using a calibrated bucket and a stopwatch measured the pump rates. The pump rates for the pumping tests varied between 1.33 GPM for Well –19 and 3.77 GPM for Well –74. This generally produced a slight drawdown of water surface of less than one foot. This was important, because excess drawdown restricts the length of the screen for flowmeter testing. Note that Table 1 includes parameters for Well 199-D4-32. It was not possible to perform a pump test on this well because a steady state condition could not be achieved. The water surface was continuously dropping at the lowest pump rate achievable.

The water surface for the wells tested was near or below the top of the screen.. When considering that the downhole pump was placed in the top part of the water column, it is obvious that flowmeter recordings could not be performed throughout the entire well screen for any of the wells due to physical interference between the pump and the probe. However, readings were performed as near to the water surface as possible by raising the pump as near the water surface as possible without changing the pump rate. Data for this restricted zone was estimated by linear interpolation between the uppermost data point considered reliable and the measured pump rate assumed at the water surface.

It was not possible to test all wells originally planned because the test engineer encountered a problem with ground currents. Ground currents are created whenever there is a voltage difference between the grounds at two different locations. Voltage differences are created by the voltage drop across the impedance of the circuits involved, by poor grounding, and by induced voltages such as lightning. Good solid copper grounds with low impedance can help to lower the voltage gradients, but soil itself does not have low impedance and large voltage gradients may result.

It is not unusual to encounter a change in voltage exceeding two volts from the bottom of the well to the water surface. The test engineer measured a difference of 2.5 volts between the bottom and water surface in some wells at this site. Although the EBF is designed to cancel equal noise on the electrodes, the flowmeter responds to microvolts of signal. Therefore, a slight difference in noise encountered between electrodes can distort the microvolts generated by actual groundwater flow.

When ground currents are encountered in the field that disturb EBF readings, they are usually attributable to the operation of heavy machinery nearby. In this case, it appears that the problem was apparently caused by the operation of large pumps in the area.   Usually, the test engineer can isolate the grounds and eliminate the problem. For example, the GrundFos RediFlo2 downhole pump used in performing these tests had a problem probably caused by leakage from one of the power leads to the water. This created local currents (a ground loop) between the pump and the EBF probe. The test engineer eliminated this problem by using a generator to supply power to the EBF system and using local power for the pump.

The problem with ground currents occurred on the third day of testing. Two wells near the injection site, Wells 69 and 74, were tested with no difficulty during the first day prior to pump operation. Wells further from the injection site were successfully tested during the second day. However, the problem with ground currents was encountered on the third day when attempting to test wells near the injection site with the pumps operating.

Mr. Pearson devoted considerable effort in determining the cause of the problem. He tried all combinations of power and grounding with no success. Several factors led him to the conclusion that the problem was associated with ground currents originating from the injection pumps. First of all, the problem did not occur until the pumps began operating. Secondly, testing in various wells revealed that the noise was inversely proportional to the distance from the pumps. Lastly, he compared signals recorded in a solid joint of the SS wire-wrapped screen with data at the entrance and exit to the joint. The data measured in the solid joint indicated a slightly negative flow rate, and the adjacent data points at the entrance and exit to the joint indicated positive flow. This is obviously not possible, but is attributed to the insulating effect of the joint.

Although it was not possible to obtain meaningful data from several wells scheduled for flowmeter testing in the vicinity of the injection pumps, successful tests were performed on Wells 71, 73, and 75. Questionable data points were eliminated from the database for these wells, but enough reliable data were recorded to construct a profile of flow rates in these wells. Flow data for Well 73 between depths of 91 and 101 feet were included as an example of how the ground currents distorted the voltage signals recorded by the EBF. Data from the other wells affected by ground currents were too noisy and showed no reasonable pattern.

Profiles of flow rates recorded in each well while pumping are presented in Appendix A. Data generally were recorded at vertical increments of one foot. As anticipated, a significant percentage of bypass flow was observed in the wire-wrapped screens except in the solid joints where it was possible to get a good seal to the wall. The percentage of bypass flow in the screened portion of the well was computed by comparing data recorded immediately above and below a solid joint. The data shown in Appendix A have been adjusted to account for the bypass flow in the screened portion of the well. Significant parameters and features of each well are included in each graph as notes to assist in interpretation. Questionable data points were omitted from the graphs.

The profiles of flow rate for each well were used to compute profiles of relative hydraulic conductivity by the procedure described in Waldrop and Pearson (2002). As requested by staff of PNNL, these data were normalized to show the percentage of the total hydraulic conductivity

in each one-foot interval. Profiles for each well are presented in Appendix B. These data illustrate the geologic heterogeneity of the 12 wells tested with the EBF.

References

Molz, F.J., G.K. Boman, S.C. Young, and W.R. Waldrop, (1994), <u>Borehole Flowmeters: Field Applications and Data Analysis</u>, Journal of Hydrology, No. 163, pp. 347-371.

Waldrop, William R. and Hubert S. Pearson (2002), <u>Results of Field Tests with the Electromagnetic Borehole Flowmeter at the 100-D Area In Situ Redox Manipulation Barrier Site, Pacific Northwest National Laboratory</u>, Quantum Engineering Corp. Report QEC-T-146.
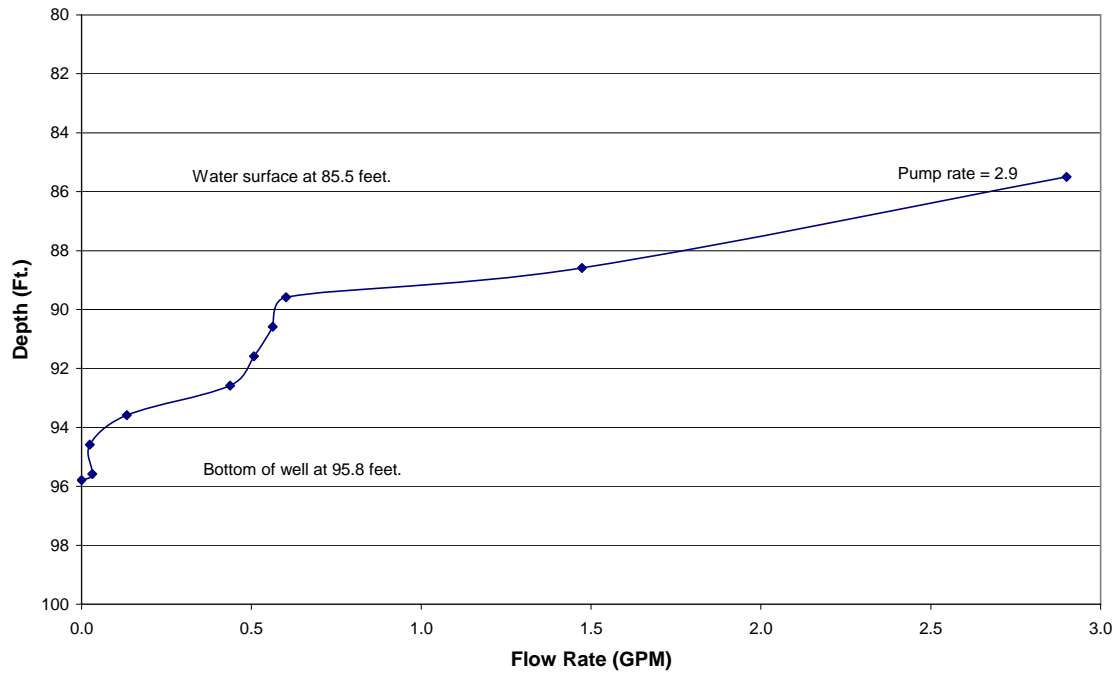
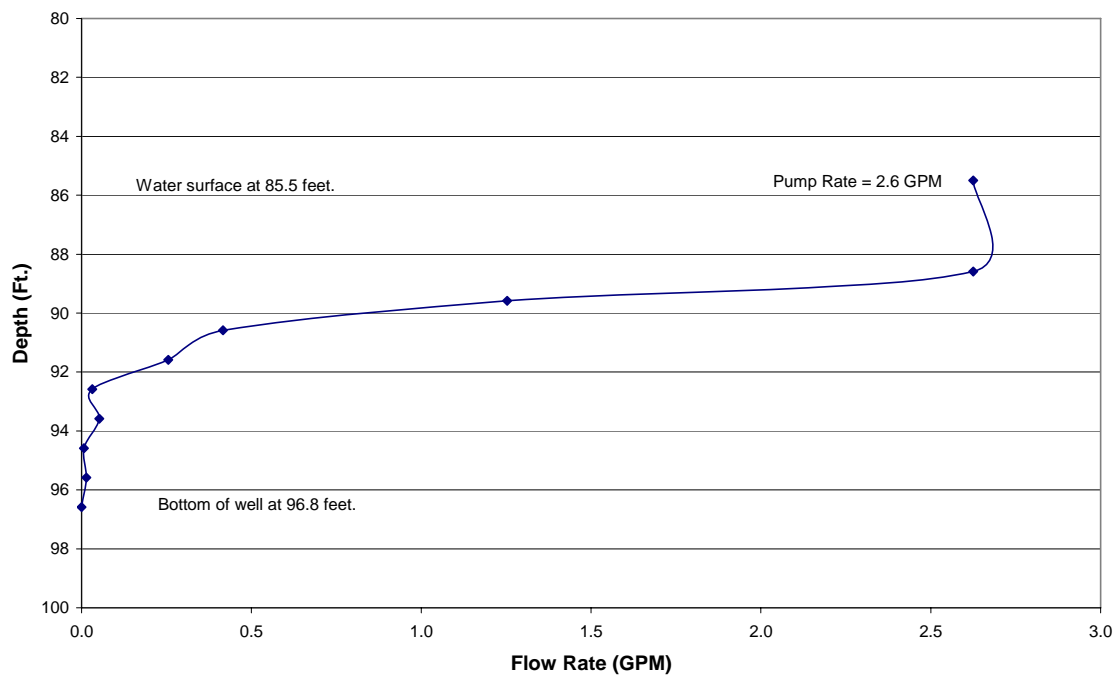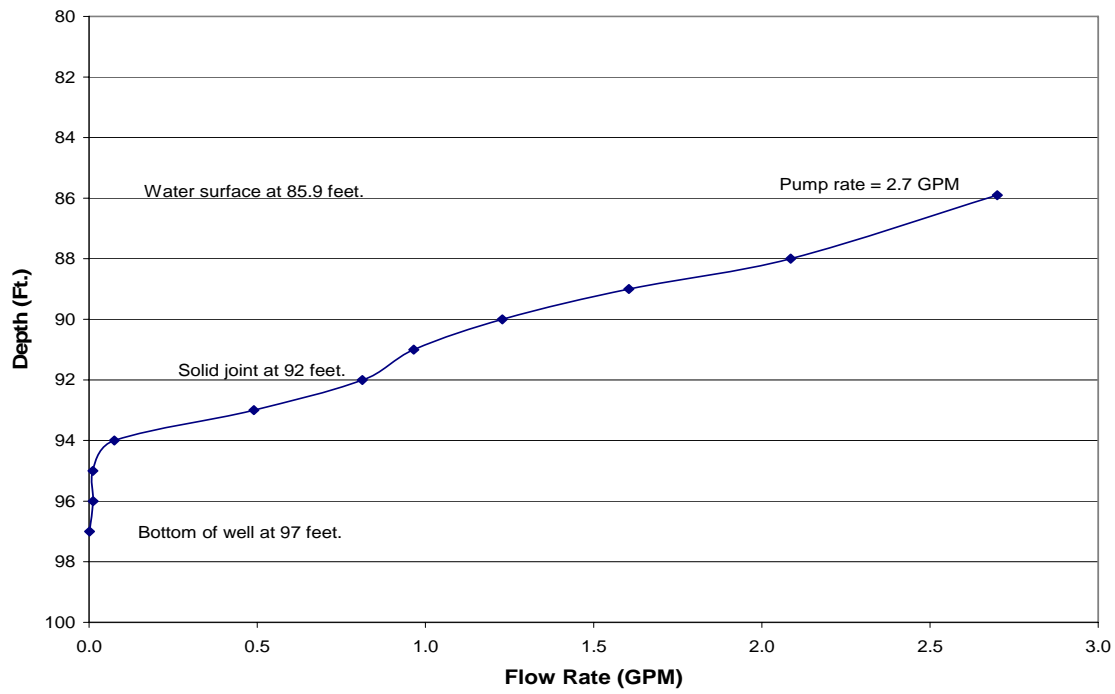# Appendix A

Profiles of Flow Rates in the Wells Tested

Figure A1: Profile of Pumped Flow Rate in Well 199-D4-07

Water surface at 85.5 feet.
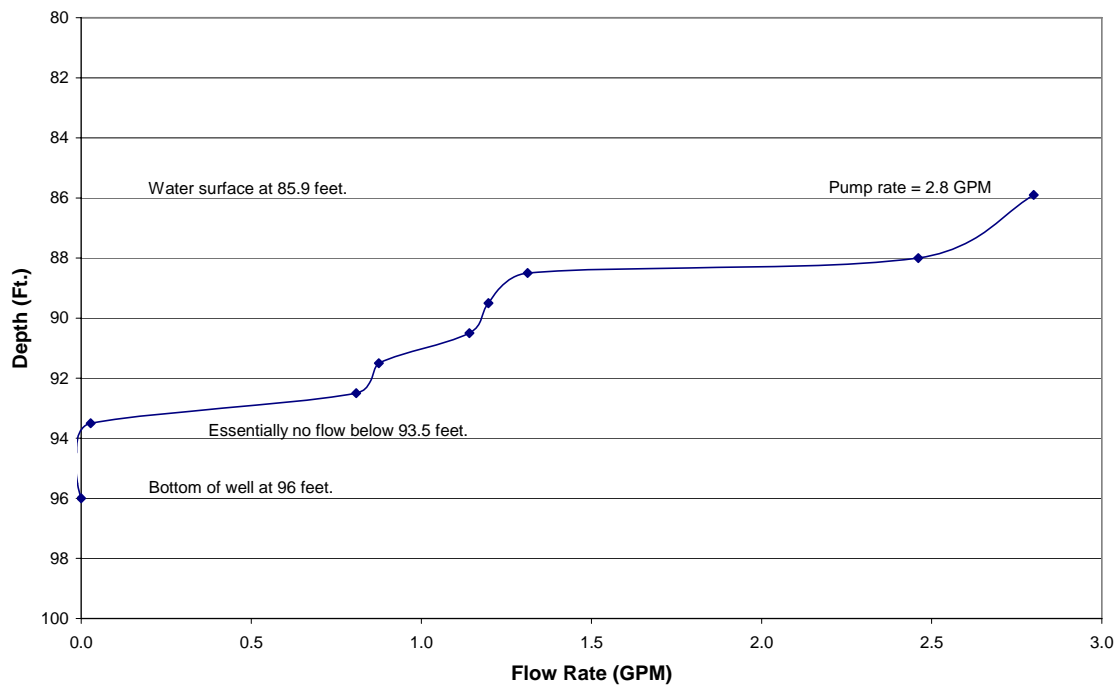
Pump rate = 2.9

Bottom of well at 95.8 feet.

Figure A2: Profile of Pumped Flow Rate in Well 199-D4-09

Water surface at 85.5 feet.

Pump Rate = 2.6 GPM

Bottom of well at 96.8 feet.

Figure A3- Profile of Pumped Flow Rate in Well 199-D4-10

Water surface at 85.9 feet.

Pump rate = 2.7 GPM

Solid joint at 92 feet.

Bottom of well at 97 feet.

Depth (Ft.)

Flow Rate (GPM)

Figure A4- Profile of Pumped Flow Rate in Well 199-D4-11

Water surface at 85.9 feet.

Pump rate = 2.8 GPM

Essentially no flow below 93.5 feet.

Bottom of well at 96 feet.

Depth (Ft.)

Flow Rate (GPM)

N.46

Figure A5 - Profile of Pumped Flow Rate in Well 199-D4-12

Water surface at 85.9 feet.

Pump rate = 2.88 GPM

Essentially no flow below a depth of 94.5 feet.

Bottom of well at 96.7 feet.

Figure A6 - Profile of Pumped Flow Rate in Well 199-D4-19

Water surface at 84.7 feet.

Pump rate = 1.33 GPM

Essentially no flow below a depth of 101.5 feet.

Bottom of well at 110.4 feet.

N.47

Figure A7 - Profile of Pumped Flow Rate in Well 199-D4-21

Pump rate = 2.7 GPM

Water surface at 86.4 feet.

Essentially no flow below a depth of 94 feet.

Bottom of well at 97.7 feet.

Figure A8 - Profile of Pumped Flow Rate in Well 199-D4-69

Pump rate = 3.47 GPM

Water surface at 85.53 feet.

Solid joint at 88.6 feet.

Essentially no flow below a depth of 98.6 feet.

Bottom of well at 107.8 feet.

Figure A9: Profile of Pumped Flow Rate in Well 199-D4-71

Figure A10: Profile of Pumped Flow Rate in Well 199-D4-73
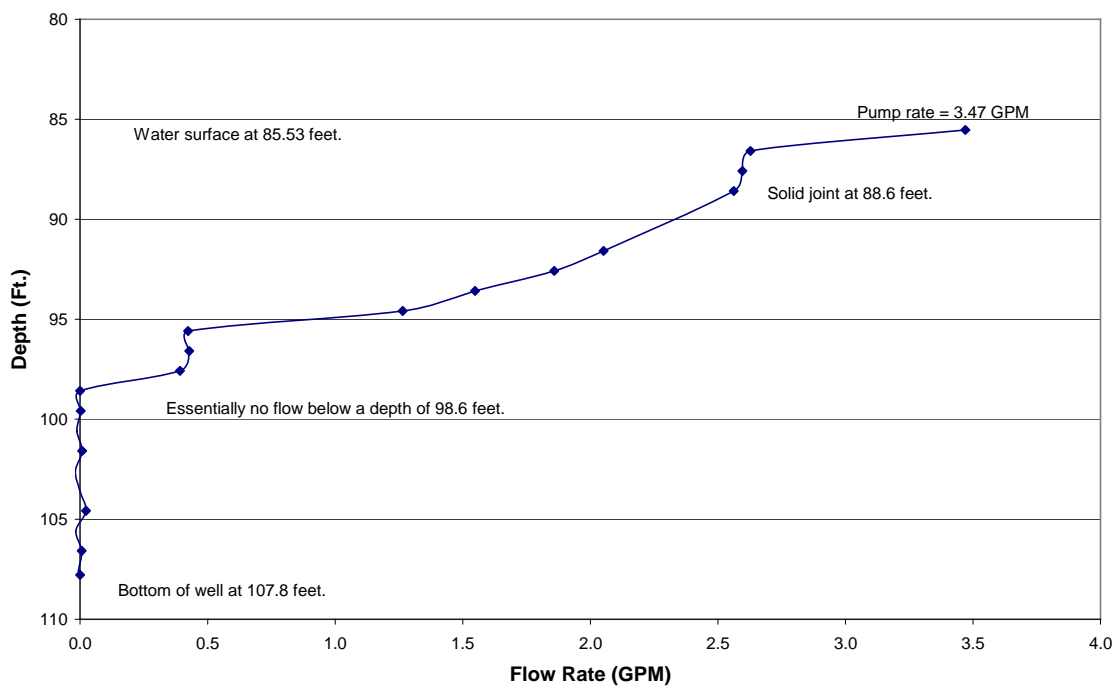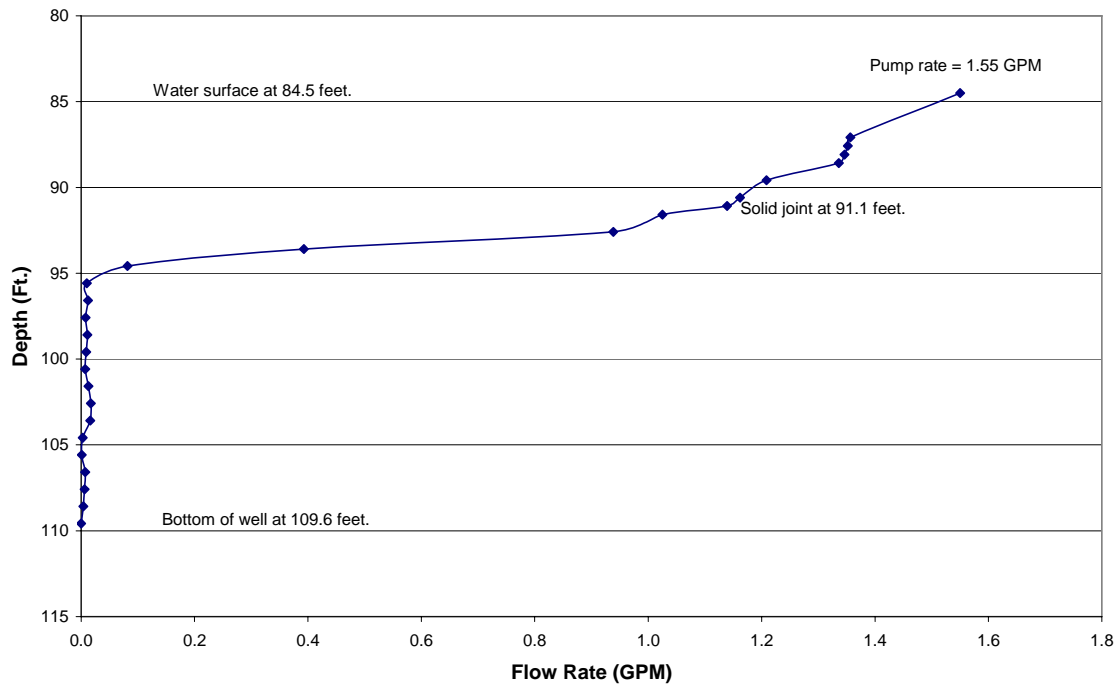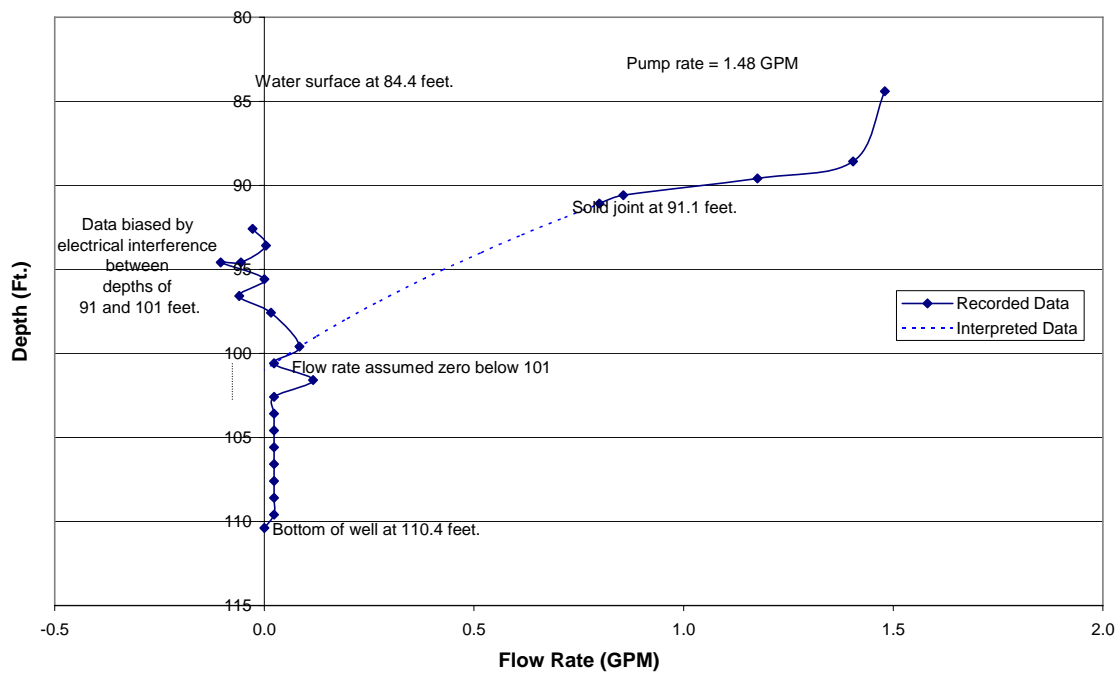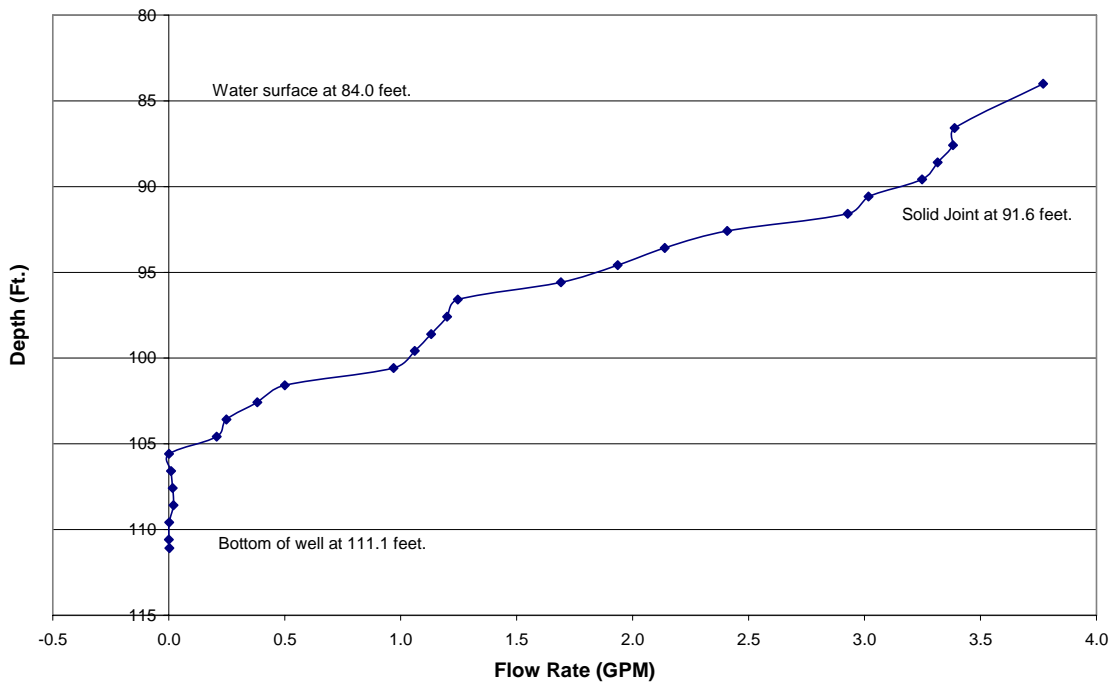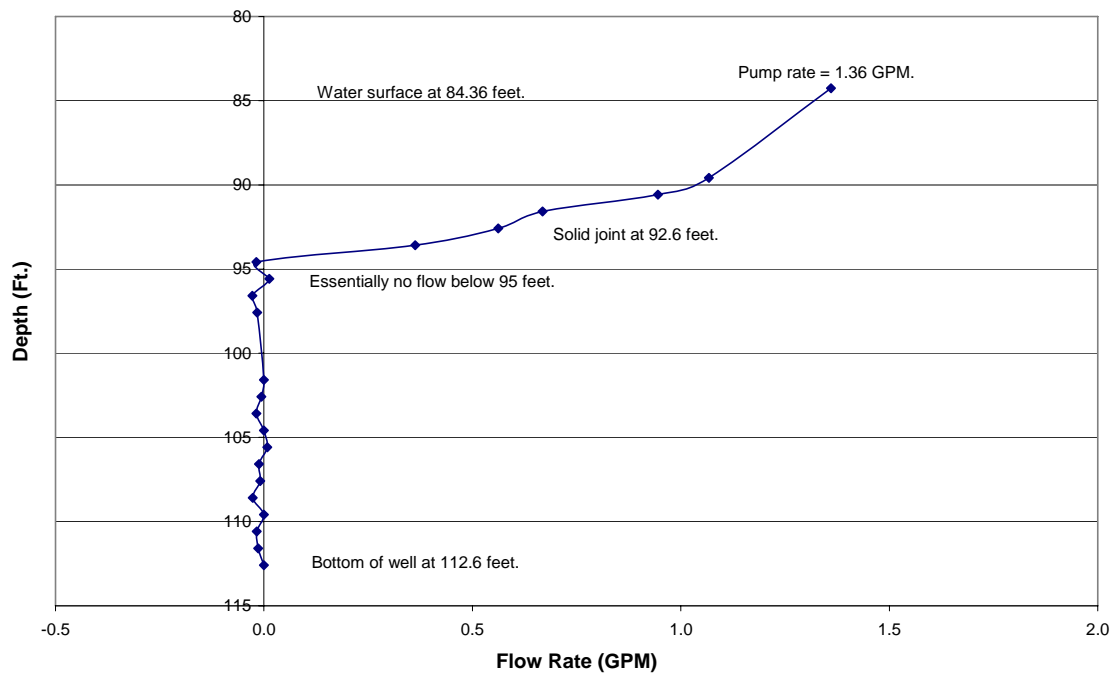
Figure A11: Profile of Pumped Flow Rate in Well 199-D4-74

Water surface at 84.0 feet.

Solid Joint at 91.6 feet.

Bottom of well at 111.1 feet.

Figure A12: Profile of Pumped Flow Rate in Well 199-D4-75

Pump rate = 1.36 GPM.

Water surface at 84.36 feet.

Solid joint at 92.6 feet.

Essentially no flow below 95 feet.

Bottom of well at 112.6 feet.

N.50
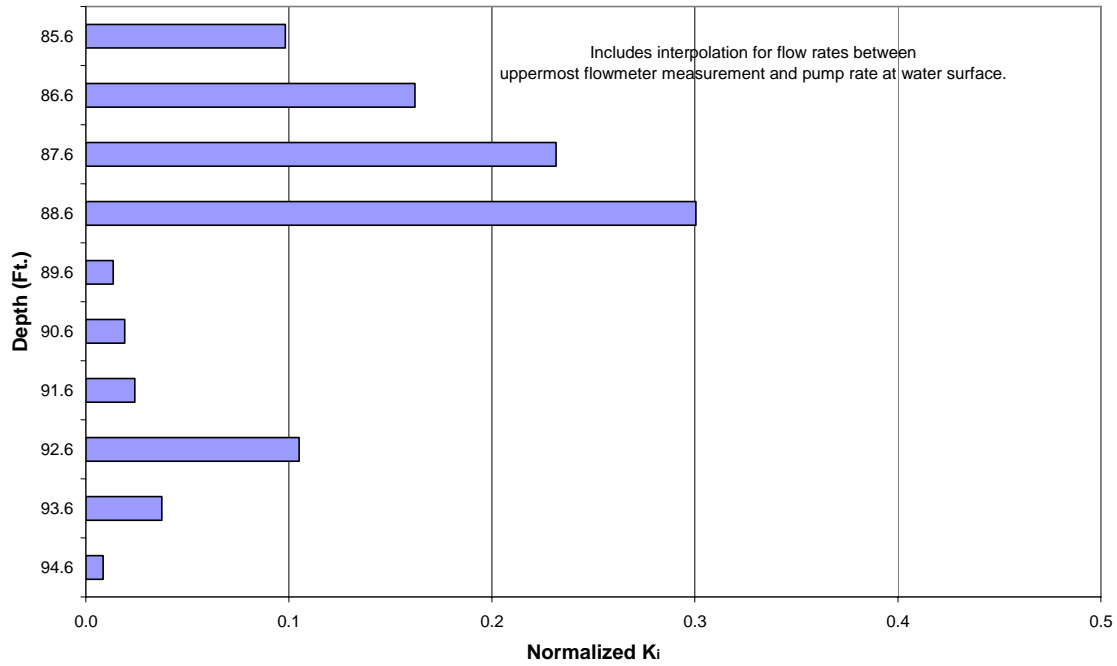
Appendix B

Normalized Distributions of Hydraulic Conductivity

Figure B1: Normalized Profile of Relative Hydraulic Conductivity for Well 199-D4-07

Includes interpolation for flow rates between uppermost flowmeter measurement and pump rate at water surface.

Figure B2: Normalized Profile of Relative Hydraulic Conductivity for Well 199-D4-09

Includes Interpolation for flow rates between uppermost flowmeter measurement and pump rate at water surface.

N.53

**Figure B3- Normalized Profile of Relative Hydraulic Conductivity for
Well 199-D4-10**

Includes interpolation for flow rates between
uppermost flowmeter measurement and pump rate at water surface.

**Figure B4- Normalized Profile of Relative Hydraulic Conductivity for
Well 199-D4-11**

Includes interpolation for flow rates between
uppermost flowmeter measurement and pump rate at water surface.
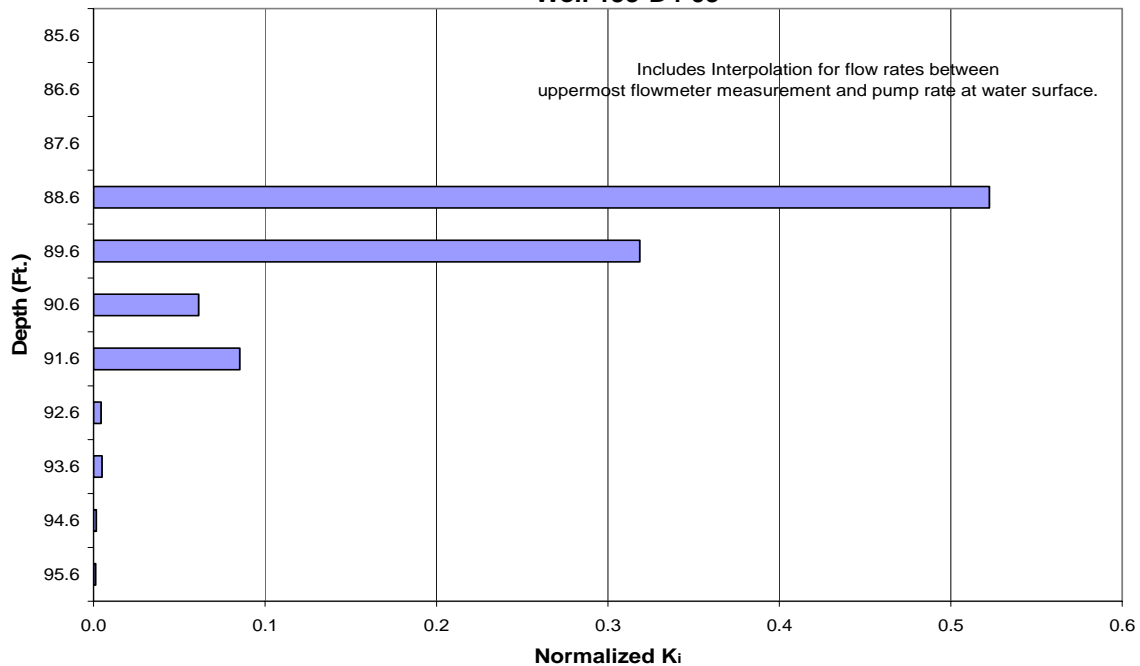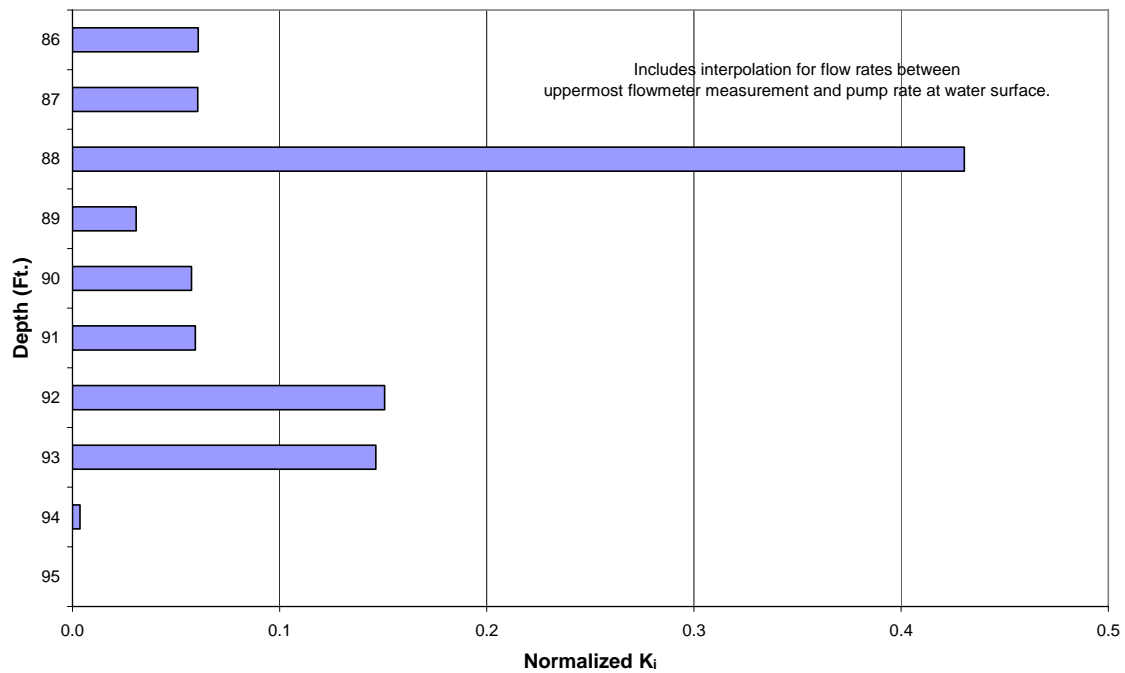
Figure B5 - Normalized Profile of Relative Hydraulic Conductivity in Well 199-D4-12

Includes interpolation for flow rates between uppermost flowmeter measurement and pump rate at water surface.

Figure B6 - Normalized Profile of Relative Hydraulic Conductivity for Well 199-D4-19

Includes interpolation for flow rates between uppermost flowmeter measurement and pump rate at water surface.
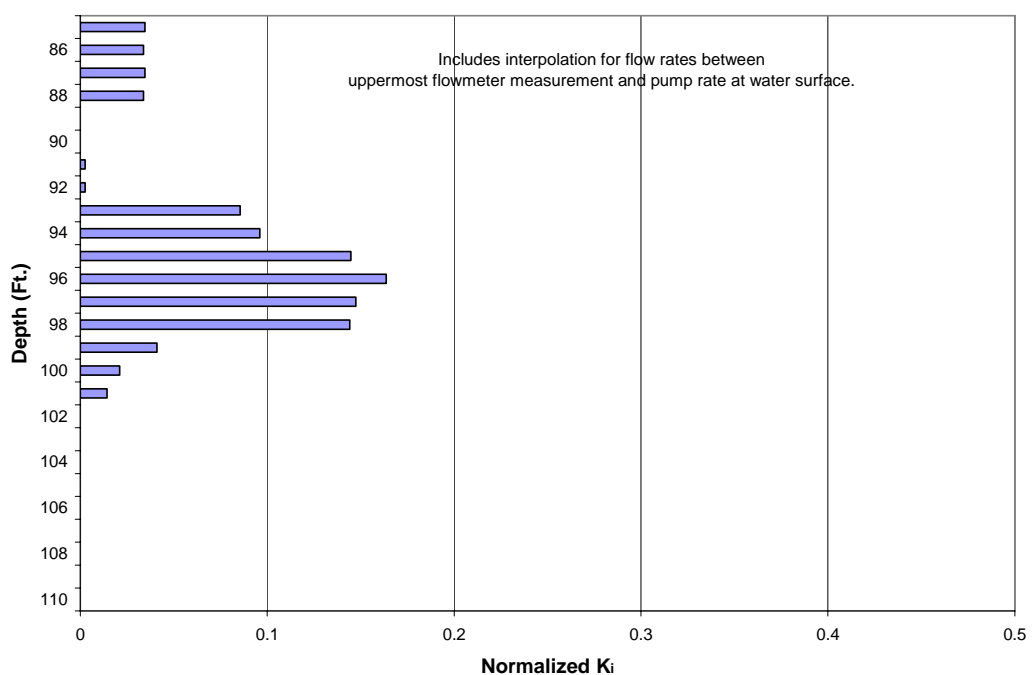
**Figure B7 - Normalized Profile of Relative Hydraulic Conductivity for
Well 199-D4-21**

Includes interpolation for flow rates between
uppermost flowmeter measurement and pump rate at water surface.

**Figure B8: Normalized Profile of Relative Hydraulic Conductivity for
Well 199-D4-69**

Includes interpolation for flow rates between
uppermost flowmeter measurement and pump rate at water surface.

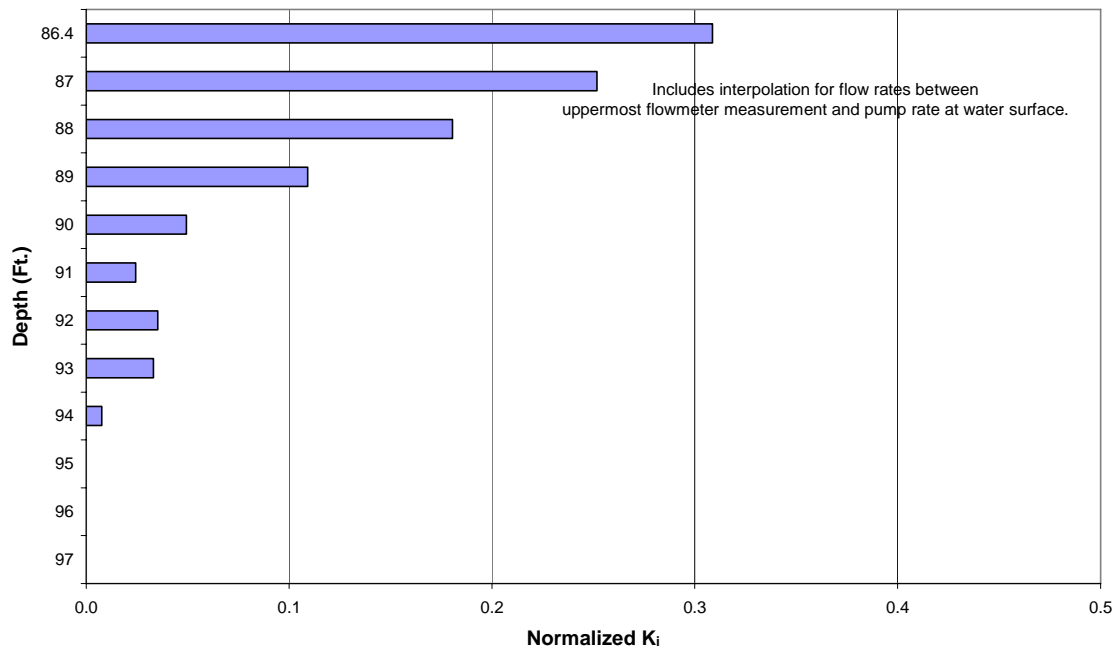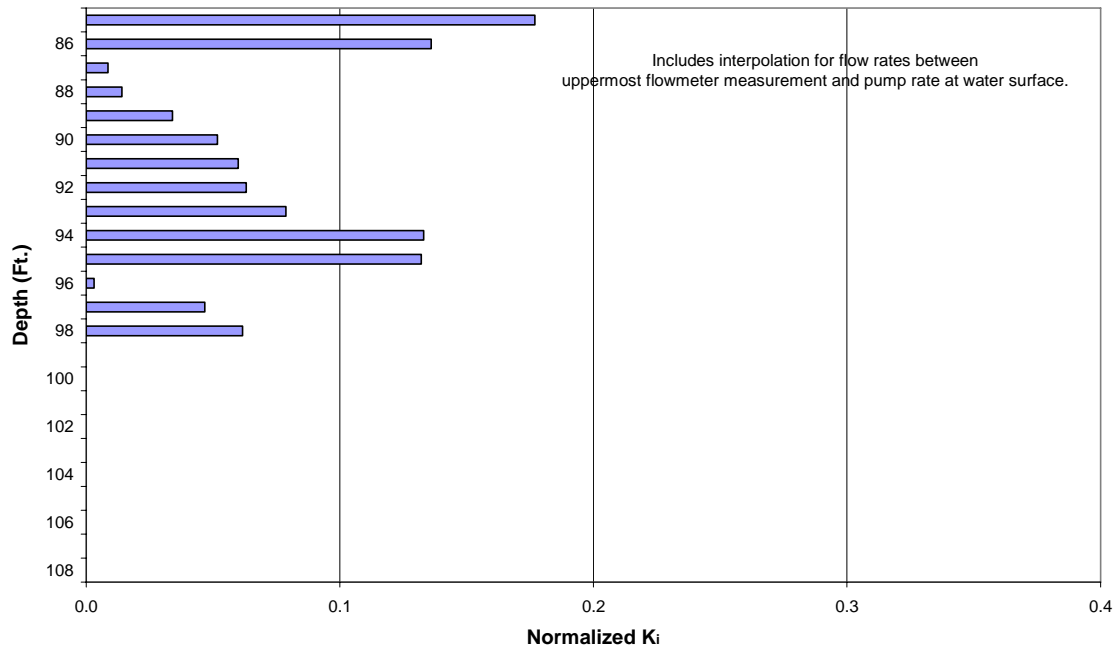**Figure B9: Normalized Profile of Relative Hydraulic Conductivity for Well 199-D4-71**

Includes interpolation for flow rates between
uppermost flowmeter measurement and pump rate at water surface.

Depth (Ft.)

Normalized K$_i$

Figure B10: Normalized Profile of Relative Hydraulic Conductivity for Well 199-D4-73

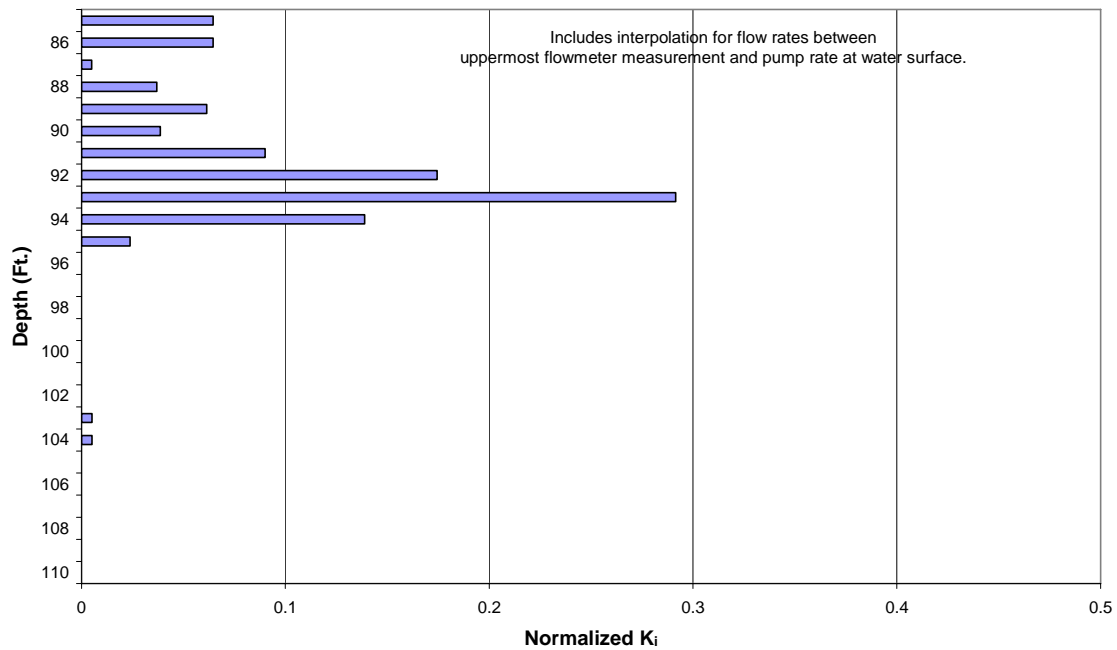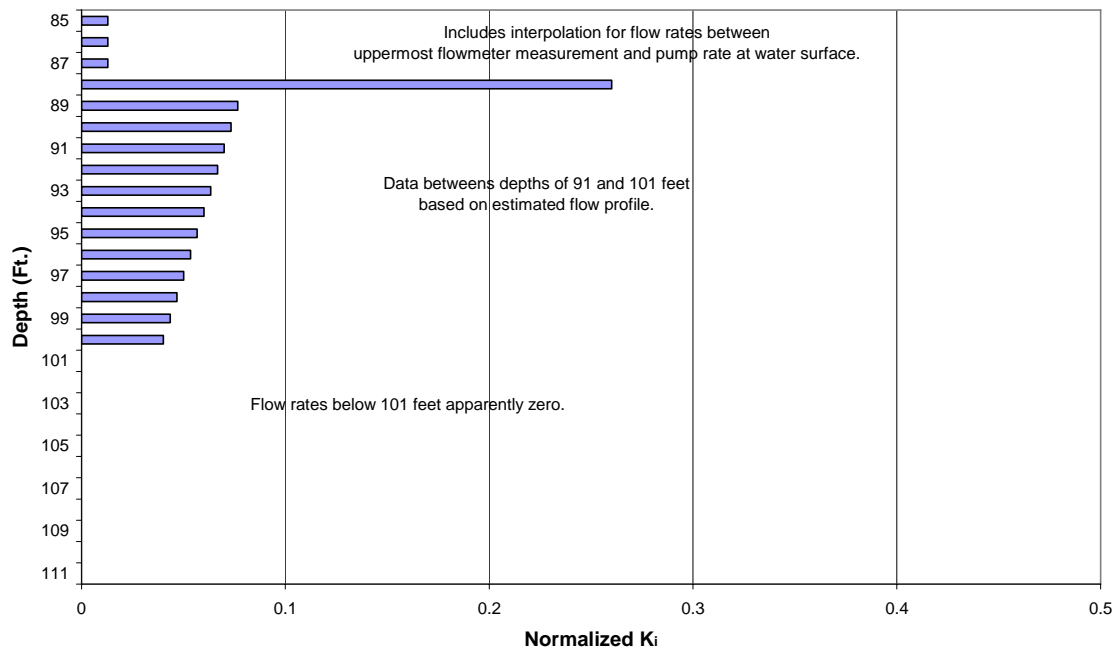Includes interpolation for flow rates between
uppermost flowmeter measurement and pump rate at water surface.

Data betweens depths of 91 and 101 feet
based on estimated flow profile.

Flow rates below 101 feet apparently zero.

Depth (Ft.)

Normalized K$_i$

N.57

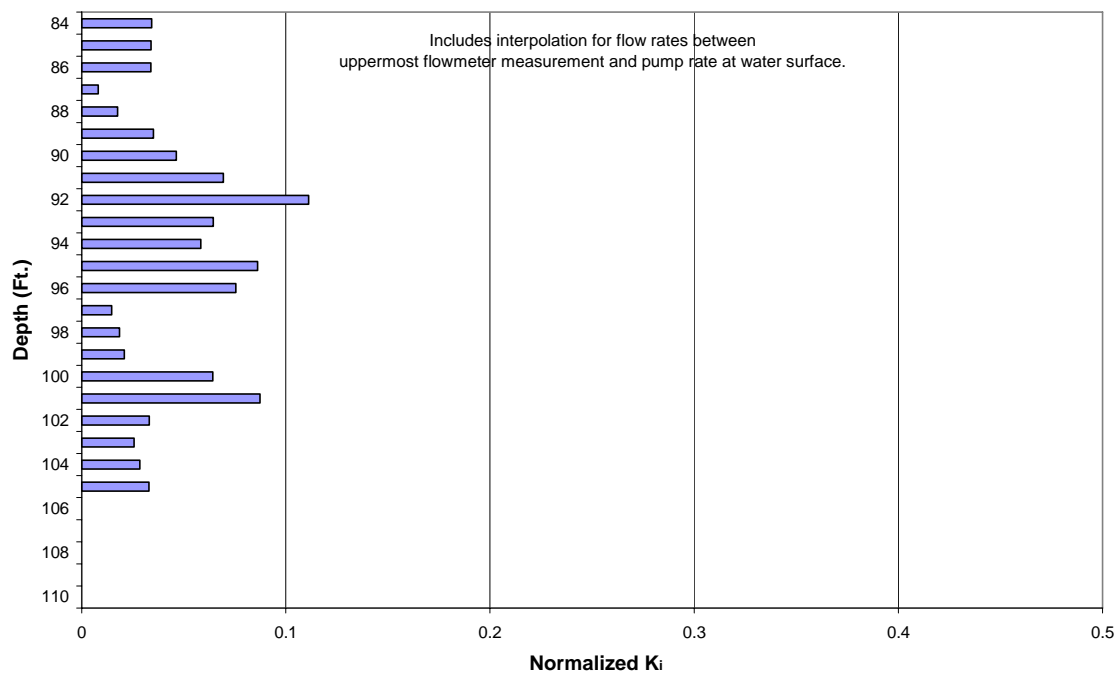**Figure B11: Normalized Profile of Relative Hydraulic Conductivity for Well 199-D4-74**

Includes interpolation for flow rates between
uppermost flowmeter measurement and pump rate at water surface.

Depth (Ft.)

Normalized K$_i$

Figure B12: Normalized Profile of Relative Hydraulic Conductivity for Well 199-D4-75

Includes interpolation for flow rates between
uppermost flowmeter measurement and pump rate at water surface.

Depth (Ft.)

Normalized K$_i$

N.58

Distribution

1   DOE Richland Operations Office

BL Charboneau
JG Morse
KM Thompson
AC Tortoso

Fluor Hanford, Inc.

JV Borghese
TW Fogwell
BH Ford
R Jackson
VG Johnson
SW Petersen
LC Swanson

Washington State Department of Ecology

J Price

5   Pacific Northwest National Laboratory

JE Amonette
BJ Devary
JS Fruchter
TJ Gilmore
Y Liu
JP McKinley
JL Phillips
ML Rockhold
JE Szecsody
VR Vermeul
MD Williams

Distribution will be made by email notification of availability from PNNL publication website
(http://www.pnl.gov/main/publications/).